Journal of Vertebrate Paleontology

ISSN: 0272-4634 (Print) 1937-2809 (Online) Journal homepage: http://www.tandfonline.com/loi/ujvp20

The Morphology of the Thirioux dodos

Leon P. A. M. Claessens, Hanneke J. M. Meijer & Julian P. Hume

To cite this article: Leon P. A. M. Claessens, Hanneke J. M. Meijer & Julian P. Hume (2015) The Morphology of the Thirioux dodos, Journal of Vertebrate Paleontology, 35:sup1, 29-187, DOI: 10.1080/02724634.2015.1121723

To link to this article: http://dx.doi.org/10.1080/02724634.2015.1121723

Published online: 21 Mar 2015.

Society of Vertebrate Paleontology Memoir 15
Journal of Vertebrate Paleontology
Volume 35, Supplement to Number 6: 29–187

THE MORPHOLOGY OF THE THIRIOUX DODOS

LEON P. A. M. CLAESSENS,*[,1,2] HANNEKE J. M. MEIJER,[3,†] and JULIAN P. HUME[4]
[1]Department of Biology, College of the Holy Cross, 1 College Street, Worcester, Massachusetts 01610, U.S.A., lclaesse@holycross.edu;
[2]Department of Geology, Naturalis Biodiversity Center, Darwinweg 2, 2333 CR, Leiden, The Netherlands;
[3]Institut Català de Paleontologia Miquel Crusafont, 08193, Cerdanyola del Vallès, Barcelona, Spain, Hanneke.Meijer@uib.no;
[4]Bird Group, Department of Life Sciences, Natural History Museum, Akeman Street, Tring, Hertfordshire, HP23 6AP, U.K., j.hume@nhm.ac.uk

ABSTRACT—Despite its status as an icon of extinction and relatively recent disappearance, our knowledge of the anatomy of the dodo has been hampered by a scarcity of preserved remains. The handful of dodo relics that survive from collections made prior to the bird's extinction consist solely of cranial and pedal materials, whereas other dodo skeletons preserved in museum collections are incomplete composites, constructed from subfossil skeletal remains discovered since 1865 at the Mare aux Songes locality. Here we describe the skeletal anatomy of two exceptional dodo specimens, collected around 1904 by amateur naturalist Louis Etienne Thirioux in the caves and crevasses surrounding Le Pouce, which have escaped detailed scientific analysis until now. The Port Louis specimen appears to consist of the skeletal remains of a single bird and is essentially complete, whereas the Durban specimen has been constructed from a limited number of birds but contains many bones that appear to be associated. The Port Louis specimen provides the first information regarding relative skeletal proportions of the dodo. Unique skeletal elements that were unknown or never described scientifically before include the patella, tarsal sesamoids, ulnare and radiale, and distal wing phalanges. The anatomy of the Thirioux dodos supports recent reinterpretations of the dodo as a resilient bird that was well adapted to the Mauritian ecosystem.

Citation for this article: Claessens, L. P. A. M., H. J. M. Meijer, and J. P. Hume. 2015. The morphology of the Thirioux dodos; pp. 29–187 in L. P. A. M. Claessens, H. J. M. Meijer, J. P. Hume, and K. F. Rijsdijk (eds.), Anatomy of the Dodo (*Raphus cucullatus* L., 1758): An Osteological Study of the Thirioux Specimens. Society of Vertebrate Paleontology Memoir 15. Journal of Vertebrate Paleontology 35(6, Supplement).

INTRODUCTION

The dodo *Raphus cucullatus* (L., 1758), an extinct giant flightless pigeon once endemic to the island of Mauritius, may arguably be the most widely known animal species to have gone extinct in human history, a true icon of extinction. However, despite its prominence in popular culture, surprisingly little is known of its anatomy and biology. The dodo was extinct by ca. 1693 (Hume, 2006), less than 100 years after the discovery and colonization of Mauritius by the Dutch. Not a single complete specimen of the dodo survives from 17th century collections of living animals, and only a few fragments remain: a single dessicated head, a skull, a beak, and a foot. There are also a few genuine but often contradictory contemporary written accounts and drawings. It was not until the discovery of a mid-Holocene fossil concentration Lagerstätte on Mauritius in 1865, the Mare aux Songes, that scientists, most notably Sir Richard Owen, were able to gain a greater understanding of the dodo's skeletal anatomy by constructing composite, yet incomplete skeletons (Owen, 1866, 1872). Surprisingly, only a few additions to our knowledge of dodo anatomy, paleoecology, and extinction have been made since Owen's studies, a vast library of semipopular works on the dodo notwithstanding. Fossil collection at the Mare aux Songes continued intermittently until the 1930s, but several decades later the site was generally considered to be lost, buried under the newly constructed Mauritian international airport (Hume et al., 2015).

In 2005, a team of scientists fortuitously rediscovered the Mare aux Songes locality during a paleoecological survey of the island. Shortly afterwards, the Dodo Research Programme was founded, a Mauritian-Dutch research initiative aimed at the study of the world of the dodo. Nine years after the site's rediscovery, the Dodo Research Programme has led and directed large, multidisciplinary studies that have produced a wealth of data and are starting to fill in major gaps in our knowledge regarding the Mare aux Songes, the dodo, and Mauritian paleoecology in general (see Rijsdijk et al., 2015).

Unfortunately, associated bones of individual dodo skeletons are not preserved in the Mare aux Songes. Around 1904, Mauritian amateur naturalist Louis Etienne Thirioux discovered two extraordinary dodo skeletons in the caves and crevasses near Le Pouce, Mauritius (Claessens and Hume, 2015). The first of the two specimens is now housed at the Mauritius Institute in Port Louis and represents the only known almost entirely complete dodo skeleton, as well as the only skeleton known composed of bones of a single individual (Fig. 1A). The second specimen, now housed at the Durban Natural Science Museum, South Africa, is a nearly complete partially associated skeleton (Fig. 1B). A third associated dodo skeleton was discovered at a cave in the highland area of Bois Cheri in the south of the island, but it proved too fragmentary to be of morphometric use (Hume, 2012). In contrast, all other known (sub)fossil dodo skeletal material consists of isolated, disarticulated bones of multiple individuals, and skeletal reconstructions are composite and invariably incomplete. Surprisingly, the Thirioux specimens have never received the scientific attention they deserve. The Port Louis skeleton has never been described, and only a brief descriptive note was published on the Durban skeleton nearly a century ago (Chubb, 1919). In this memoir, we describe the anatomy of these exceptional specimens, which exhibit multiple skeletal elements that have never been described or figured before. The Port Louis, and to a lesser extent the Durban, specimen provides information on the relative proportions of the skeleton for a single individual, which cannot be determined with a high degree of accuracy from a composite reconstruction. This memoir is the first major treatise on dodo skeletal anatomy since the works of Strickland and Melville (1848), Owen (1866, 1872), and Newton and Gadow (1893), all of which were based upon incomplete, disassociated, and, with the exception of Strickland and Melville's (1848) description, composite materials. The aim of this article is to provide novel and comprehensive information on the dodo and its anatomy, to facilitate further scientific

*Corresponding author.
†Current address: University Museum of Bergen, Department of Natural History, University of Bergen, Postboks 7800 5007 Bergen, Norway.
Color versions of one or more of the figures in this article can be found online at www.tandfonline.com/ujvp.

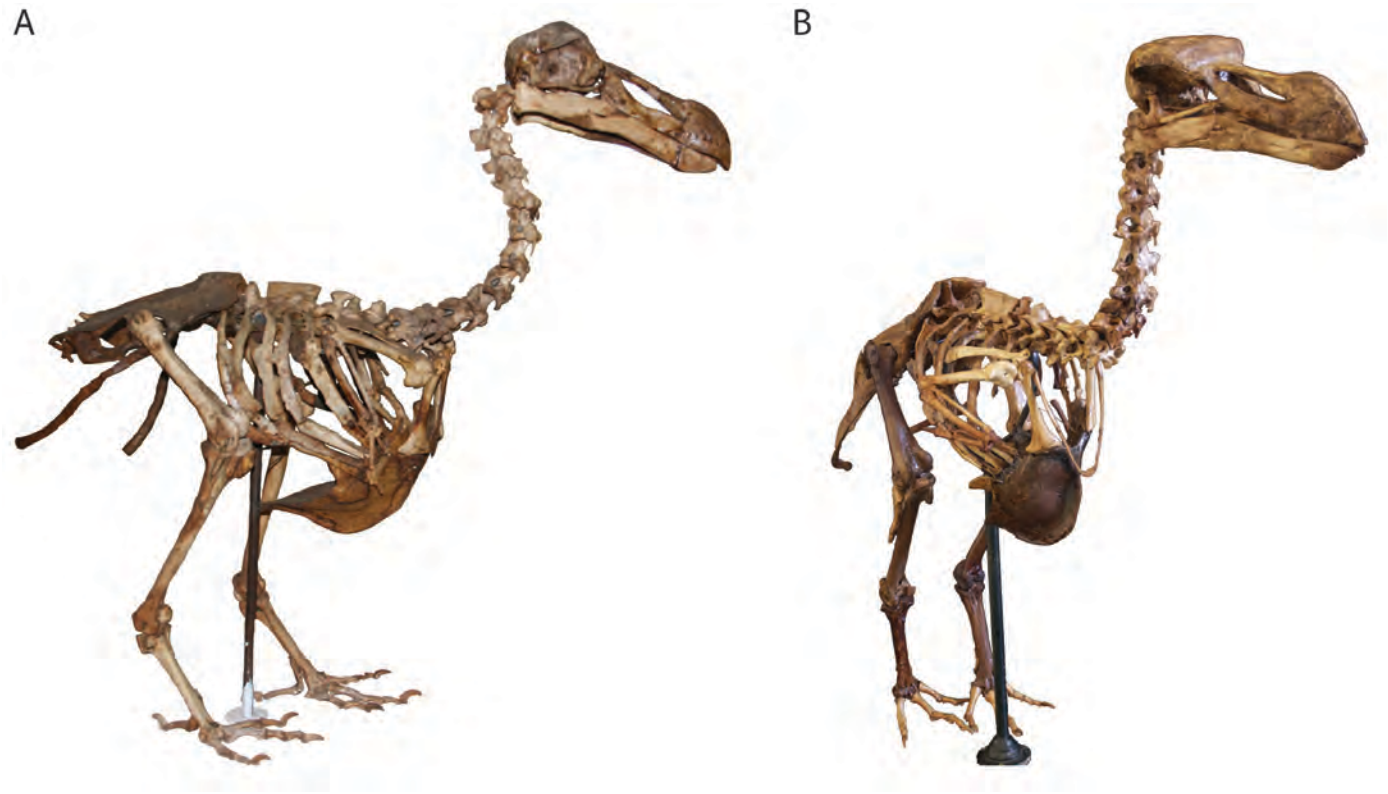

FIGURE 1. Photographs of the mounted Thirioux dodo skeletons. **A**, Port Louis specimen; **B**, Durban specimen (DNSM 2366).

inquiry into the dodo's form, function, and paleobiology, because after more than 300 years since this emblematic bird's extinction, these issues still continue to stimulate heated debate (e.g., Angst and Buffetaut, 2011a, 2011b; Louchart and Mourer-Chauviré, 2011).

Institutional Abbreviations—**DNSM**, Durban Natural Science Museum, Durban, South Africa; **MCZ**, Museum of Comparative Zoology, Harvard University, Cambridge, Massachusetts; **MGL**, Musée Cantonal de Geologie de Lausanne, Lausanne, Switzerland; **MI**, Mauritius Institute, Port Louis, Mauritius; **MNHN**, Musée National d'Histoire Naturelle, Paris, France; **NBC**, Naturalis Biodiversity Center, Leiden, The Netherlands; **NHMUK**, Natural History Museum, London, U.K.; **NMNH**, Smithsonian Institution, Washington, D.C., U.S.A.; **OUM**, Oxford University Museum of Natural History, Oxford, U.K.; **SMF**, Senckenberg Forschungsinstitut und Naturmuseum, Frankfurt, Germany; **UMZC**, University Museum of Zoology, Cambridge, U.K.; **YPM**, Yale Peabody Museum of Natural History, New Haven, Connecticut, U.S.A.; **ZMUC**, Zoological Museum, University of Copenhagen, Copenhagen, Denmark.

Anatomical Abbreviations—See Appendix 1.

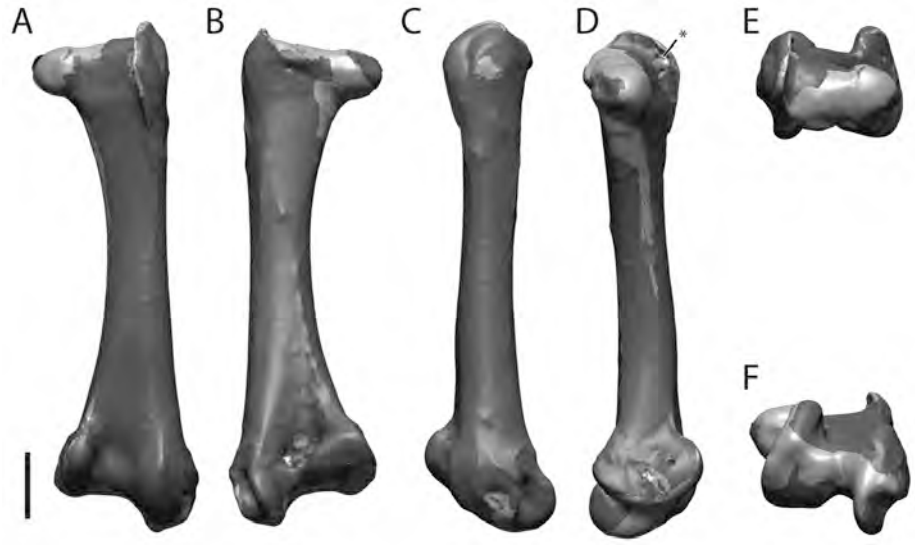

FIGURE 2. 3-D scan image of left femur, Port Louis specimen, highlighting areas of reconstruction in light gray. Most areas of reconstruction or interpolation are located where the laser was (partially) obscured by another bone (proximally the pelvis; distally the tibiotarsus) or by metal mounting wire (e.g., in the fossa poplitea and the epicondylar regions). Scan mesh reconstruction in the gray areas was based on the digital interpolation of point cloud densities less than 100 μm, on-site during the scanning process. All models were rendered as a 'watertight' mesh during scanning, and all vascular and pneumatic foramina were filled in during 3-D editing. An asterisk (*) marks the location of several filled-in pneumatic foramina in the fossa trochanteris. **A**, cranial; **B**, caudal; **C**, lateral; **D**, medial; **E**, proximal; **F**, distal views. Scale bar equals 20 mm.

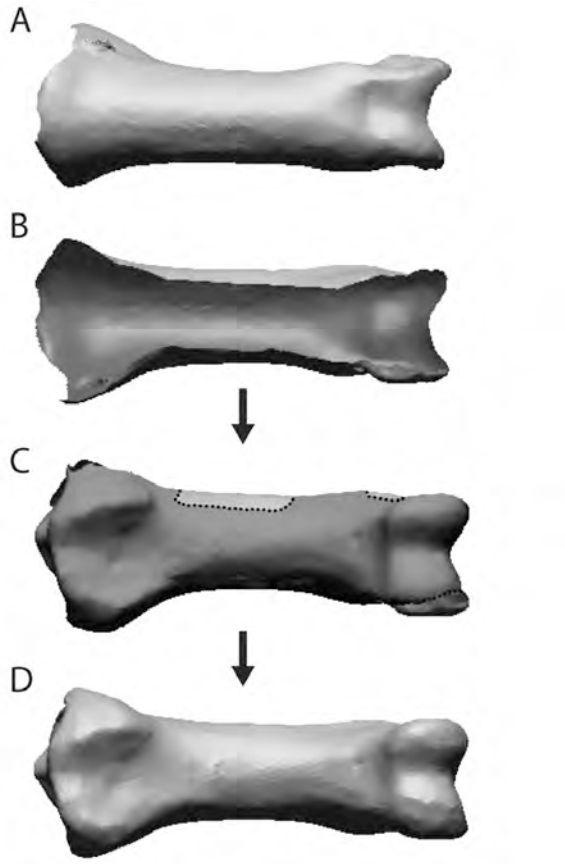

FIGURE 3. Digital reconstruction process for large areas with missing surface data. **A**, pedal phalanx with scanned dorsal surface; **B**, underside of pedal phalanx showing missing plantar surface scan data due to inaccessibility of laser beam; **C**, scan data from another specimen (Oxford dodo pedal phalanx) is isometrically scaled to best fit the missing data; **D**, scan data are merged to form a single mesh.

MATERIALS AND METHODS

Dodo Specimens

Our study includes the Port Louis Thirioux dodo (Mauritius Institute), the Durban Thirioux dodo (DNSM 2366), and the UMZC collection of Thirioux dodo remains (415.KK). The Port Louis Thirioux dodo is formally and permanently reposited in the collections of the Mauritius Institute in Port Louis, but does not have an assigned specimen number. From this point, we refer to the Thirioux dodo skeletons as the Port Louis and the Durban specimens, respectively. Also examined were hundreds of Mare aux Songes subfossil remains from the recent Dodo Research Programme excavations and the MI, NHMUK, UMZC, OUM, MNHN, MCZ, YPM, NMNH, and NBC collections. Historic remains of the head and foot of the dodo, collected prior to the bird's extinction, were examined in the OUM and ZMUC, as well as casts of historic specimens in the NHMUK, UMZC, OUM, MNHN, MCZ, and YPM.

Comparative Materials

The skeletal anatomy of *Raphus cucullatus* was compared with that of its extinct sister species, *Pezophaps solitaria* (Gmelin, 1789) from Rodrigues Island, and that of the closely related extant taxa *Caloenas nicobarica* (L. 1758), *Goura cristata* (Pallas, 1764), *G. victoria* (Fraser, 1844), and *Didunculus strigirostris* (Jardine, 1845), which all form part of the same clade (Shapiro et al., 2001). *Raphus* and *Pezophaps* differ markedly in their much greater size in all skeletal elements from the other taxa examined, so comparisons presented here are based on morphological differences only.

Comparative osteological material examined includes *Caloenas nicobarica* (MCZ 341255; NHMUK S/1985.26.2 F; SMF 10573; SMF 7677; SMF 8475); *Didunculus strigirostris* (MCZ 340353; NHMUK S/1952.3.50 u/s; NHMUK 1875.10.16.6 u/s; SMF 6334/YMH44); *Goura cristata* (YPM 102319; NHMUK 1891.7.20.40 u/s; SMF 1667; SMF 1668; SMF 12469); *Goura victoria* (SMF 6330; NMNH 488755); *Pezophaps solitaria* cranium NHMUK A3505; coracoids NHMUK u/r L and NHMUK u/r R; scapulae NHMUK A1424 R and NHMUK A1424 L; humerus

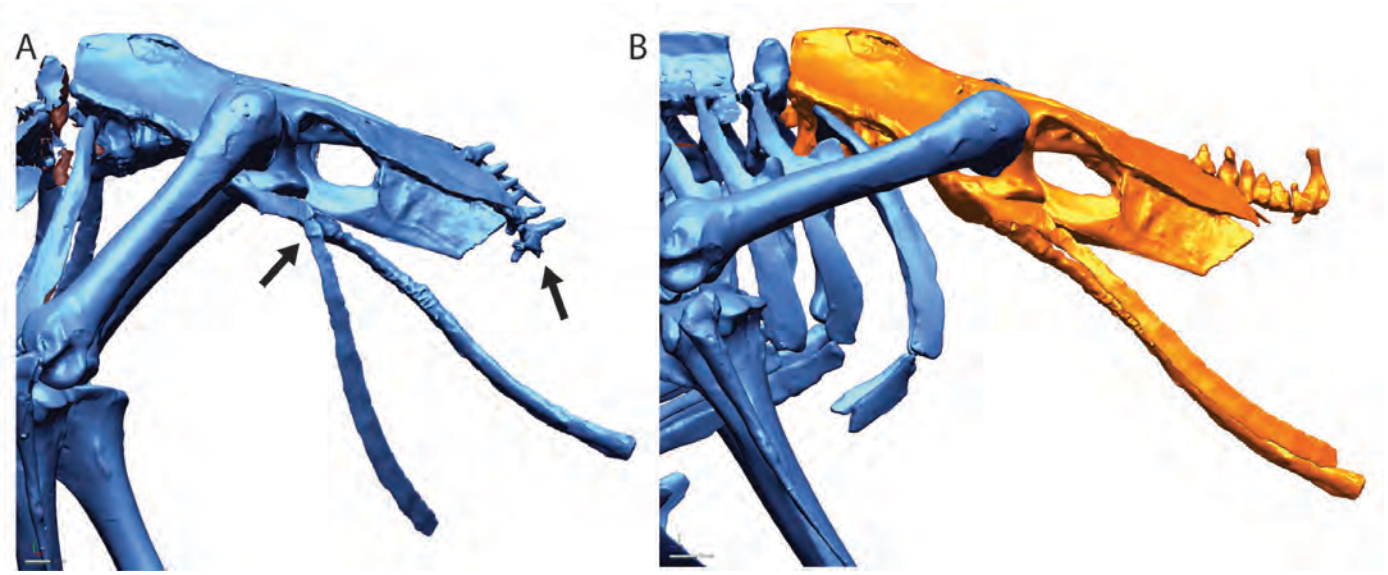

FIGURE 4. Example of digital reconstruction of misaligned regions of the skeletal mount. **A**, lateral view of the 3-D scan of the Port Louis specimen, as mounted in the museum. Note the break in the proximal ramus of the left pubis and the misalignment of the caudal vertebrae and pygostyle (arrows); **B**, 3-D image file after digital reconstruction. The pubis, pygostyle, and caudal vertebrae have been realigned. Note that in this figure, the femur has also been oriented more horizontally, in agreement with *in vivo* data for extant columbids and historic sketches of the dodo.

FIGURE 5. Illustrations of live dodos made in 1601 by J. Laerle in the *Gelderland* ship journal (from Hume, 2003).

NHMUK u/r L; radius NHMUK u/r R; ulna NHMUK A1384; carpometacarpus NHMUK A3506; sternums NHMUK 1373 and NHMUK A3506; pelvis NHMUK A3506; femurs NHMUK A1397 R and NHMUK u/r R; tibiotarsus NHMUK A1403 R; tarsometatarsus NHMUK A3506 R.

Laser Surface Scanning

The Port Louis and Durban Thirioux dodos were each mounted approximately a century ago using a metal framework, with metal wire fastening bones of the ribcage and limbs via small holes that were drilled through the bones. Non-contact laser surface scanning was chosen as the safest method for digitally capturing three-dimensional (3-D) anatomical data without compromising the integrity of the fragile specimens. Three-dimensional digital surface scans were generated with a Konica Minolta Range7 non-contact 3-D laser surface scanner, which was mounted onto a Manfrotto 161MK2B tripod. Each mounted skeleton was placed onto a wooden manual turntable that enabled fine adjustment of the degree of rotation of the specimen, and the height and angle of the 3-D scanner was also adjusted throughout the scanning process to obtain maximal laser access for each skeletal element. During data acquisition, one person controlled scanner focusing, alignment, and data capture, while a second individual manipulated scanner position with the tripod and adjusted the specimen turntable position. The specimens were scanned using the Range7 wide lens at a point-cloud density of approximately 100 μm. The Port Louis Thirioux dodo specimen was scanned on-site at the Mauritius Institute over a period of 3 weeks, in August 2011. The Durban Thirioux dodo specimen was scanned on-site at the Durban Natural Science Museum, using the same three-person team and equipment, over a period of 2 weeks in January 2012. Skull and mandible were taken off the mount in both the Port Louis and Durban specimens, enabling better laser scanner access to obstructed or relatively convoluted areas, including the occipital region of the skull. In addition, cervical vertebrae 1–9 and 11–14, and the left distal wing, of the Durban specimen were taken off the mount, which enabled more extensive scanner access to these bones than in the Mauritius Institute specimen. It was not possible to dismount these bones on the Port Louis skeleton.

TABLE 1. Angles at the hip, knee, and ankle joints as mounted in the museum, and the digitally repositioned scan, using angles determined from extant taxa and Laerle's drawing.

Skeletal element	Port Louis specimen museum mount	Digitally repositioned scan
Femur	50°	20°
Tibiotarsus	75°	60°
Tarsometatarsus	65°	75°

Angle measurements were taken with respect to the ground surface (horizontal).

Digital Processing and Editing of Three-Dimensional Scan Data

Individual raw scan surfaces were aligned with Range7 Rangeviewer software (Konica Minolta) during scan capture. Further scan editing was undertaken with Rapidform XOR (now Geomagic Design X). All initial editing of the raw scan data 3-D mesh was undertaken on-site during raw scan data acquisition, in order to minimize interpretation and maximize accuracy during digital reconstruction of those areas of the skeleton that were inaccessible to the laser scanner (Fig. 2A–F). One person was engaged full-time with scan editing during the scanning process and communicated directly with the two scanner operators regarding the acquisition of surface data. The scan editor visually compared and verified reconstructed surfaces with the actual specimen, and an edited static 3-D model of the mounted skeletons was finished on-site (Pls. PL1, D1).

Segmentation of the more than 100 individual bones per skeleton out of the static 3-D model of each mounted skeleton was undertaken in the months following scan acquisition. The process of separating closely approximated skeletal elements in the static scan occasionally created regions of missing scan data, such as the articular surfaces of joints where bone surfaces touched and the undersides of the pedal phalanges, which were mounted to the skeleton's base. Relatively small regions of missing data were interpolated from the scanned mesh, taking into account photographs of the skeleton and 3-D scan files of bones from the Mare aux Songes.

For larger regions that could not be faithfully reconstructed, scan data from individual skeletal elements from the Mare aux Songes were substituted into the missing regions. Scan data from a plaster cast of the Oxford dodo pedal skeleton (MCZ 341515), a left pes, was scaled to fit the plantar surface of the pedal phalanges of the Thirioux skeletons, which were mounted to a base plate and blocked from view for the Range7 scanner (Fig. 3). This procedure was repeated for the right pes by digitally mirroring the Oxford pedal skeleton in Rapidform.

Segmentation of the vertebral column of the static Port Louis digital model revealed large areas of missing surface scan data on cranial and caudal articular surfaces. Due to the extent of missing surface data in the axial column of the Port Louis skeleton, we decided not to substitute scan data from the Durban specimen here (see Appendices 2 and 3). During segmentation of the static digital model, structures on the mounted skeleton that were damaged and displaced, such as the broken left pubis of the Port Louis specimen, were digitally repaired (Fig. 4A, B), but parts of the skeleton that were missing were not substituted, with the exception of cervical vertebra 10 in the Durban specimen.

Digital Repositioning of the Bones in the Dodo Skeletons

After segmentation of the static digital models of the Port Louis and Durban specimens, the skeleton was digitally reassembled

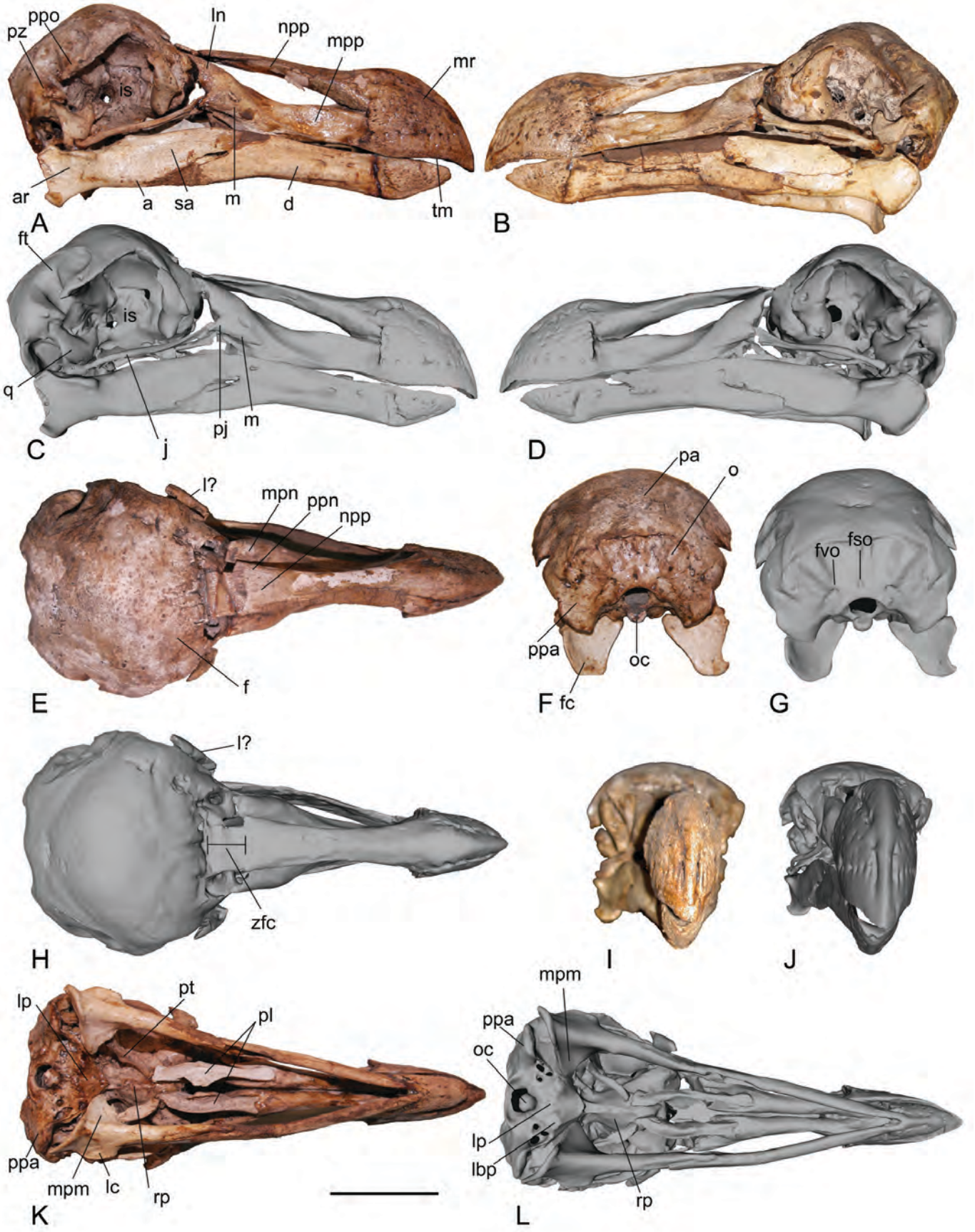

FIGURE 6. The skull of the Port Louis dodo specimen depicted by photographs (**A**, **B**, **E**, **F**, **I**, **K**) and scan data (**C**, **D**, **G**, **H**, **J**, **L**) from the following aspects: **A**, **C**, right lateral; **B**, **D**, left lateral; **E**, **H**, dorsal; **F**, **G**, caudal; **I**, **J** anterior; **K**, **L**, ventral. Anatomical abbreviations as in Appendix 1. Scale bar equals 5 cm.

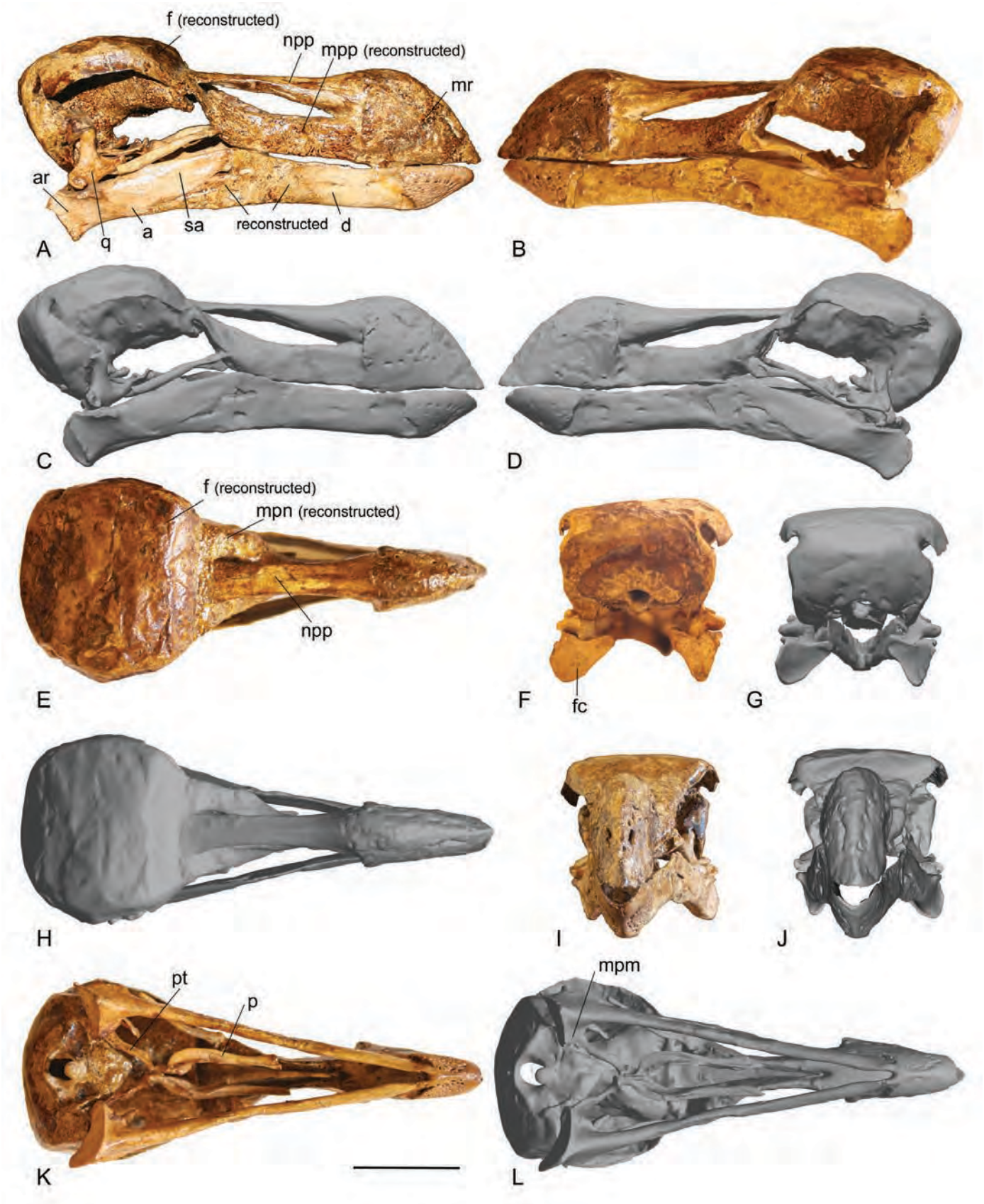

FIGURE 7. The skull of the Durban dodo specimen depicted by photographs (**A**, **B**, **E**, **F**, **I**, **K**) and scan data (**C**, **D**, **G**, **H**, **J**, **L**) from the following aspects: **A**, **C**, right lateral; **B**, **D**, left lateral; **E**, **H**, dorsal; **F**, **G**, caudal; **I**, **J** anterior; **K**, **L**, ventral. Braincase and part of the rostrum have been crudely reconstructed in plaster before 1918 (see also Pl. D4, and Claessens and Hume, 2015). Anatomical abbreviations as in Appendix 1. Scale bar equals 5 cm.

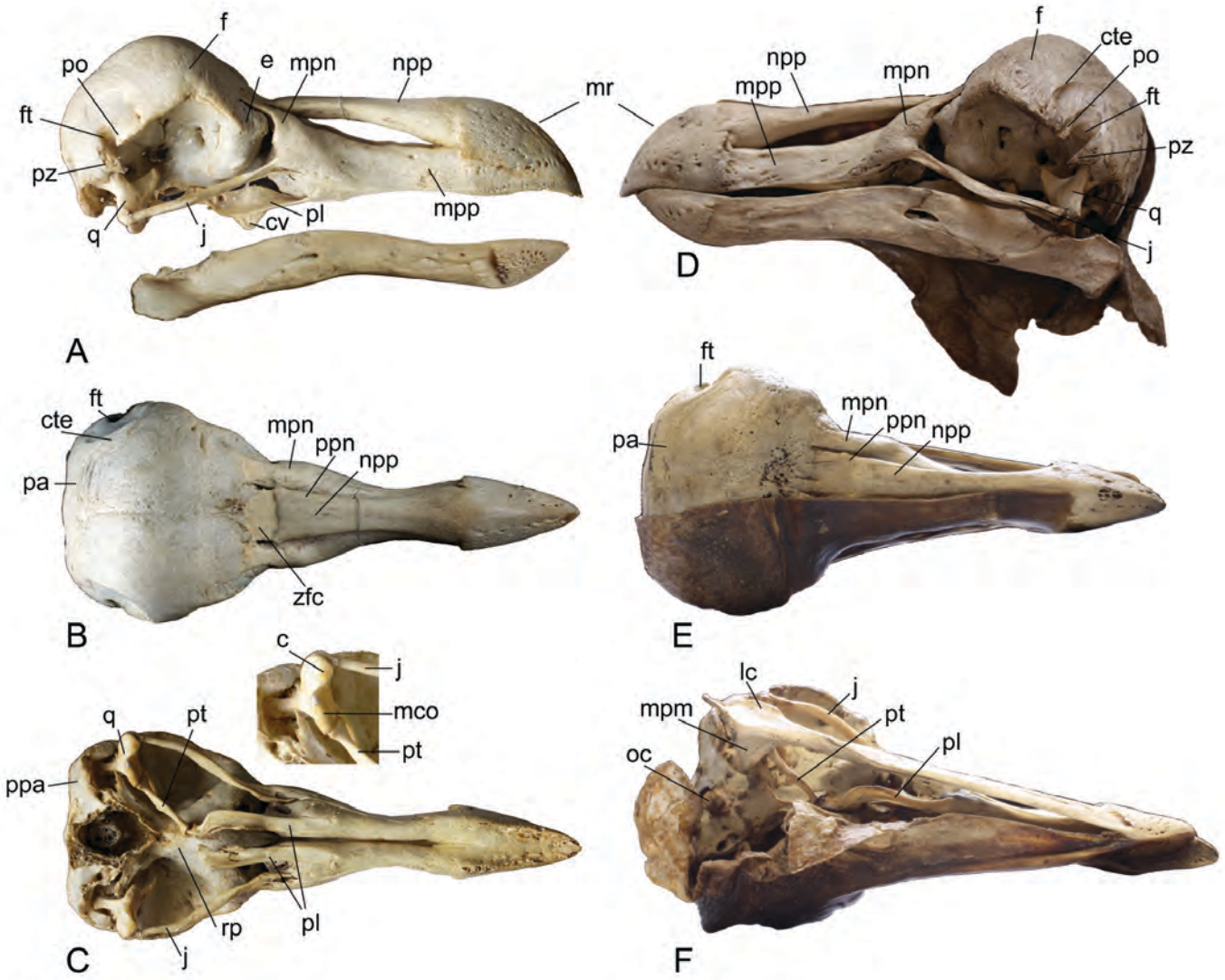

FIGURE 8. Photographs of the skulls of the Copenhagen (**A**–**C**) and Oxford (**D**–**F**) dodo specimens in **A**, right lateral; **D**, left lateral; **B**, **E**, dorsal; and **C**, **F**, ventral views with detail of the quadrato-pterygoid articulation of **C**. Anatomical abbreviations as in Appendix 1.

into a dynamic, anatomically correct digital model (Pls. PL2, PL3, D2, D3), based on joint morphology, comparisons with extant birds, and historic illustrations, especially the Laerle sketches and the Mansur painting, which are the only two depictions known to have been based on observation of living dodos (see, e.g., Hume, 2003, 2006; Parish, 2013). The position of the femur, tibiotarsus, and tarsometatarsus was reconstructed based on the Laerle illustrations (Fig. 5; Table 1), which appear to depict relatively accurate body proportions (see also the other detailed sketches in the Gelderland journal, e.g., Moree, 2001), using the location of the tarsometatarsus as the anchor point, because it is almost entirely outside the dodo's plumage. The Mansur painting of a living dodo (e.g., Hume, 2006) could not be used for the reconstruction of hind limb joint angles, because it is painted in a naïve style and not to scale. Additional information for the assembly of the pes was derived from 3-D scans of a cast of the now-lost British Museum's desiccated dodo foot (MCZ 341509).

Wing anatomy and angles of the elbow and wrist joint of the dodo were reconstructed based on the Laerle and Mansur sketches, which all show extension at the elbow and wrist. Observations of physical 3-D printed models of the skeleton of the Port Louis and Durban specimens further helped guide digital reconstruction of the Port Louis and Durban dodo skeletons.

Measurements

Measurements were taken on the specimens using digital calipers, dial calipers, and rulers, and from the digital scans, which enabled greater access to individual skeletal elements than the fragile skeletal mounts would allow.

Digital measurements were taken using the 'measuring tool' in Rapidform XOR (now Geomagic Design X) and the 'measuring tool' in MeshLab version 1.3.3. (Visual Computing Lab-ISTI-CNR, http://meshlab.sourceforge.net/).

Anatomical Terminology

Anatomical terminology used in this study follows the Nomina Anatomica Avium (Baumel and Witmer, 1993). Terminology for the quadrate is based on Elzanowski and Stidham (2010). Additional sources on avian skeletal anatomical terminology consulted for this memoir are Butendieck (1980) and Livezey and Zusi (2006).

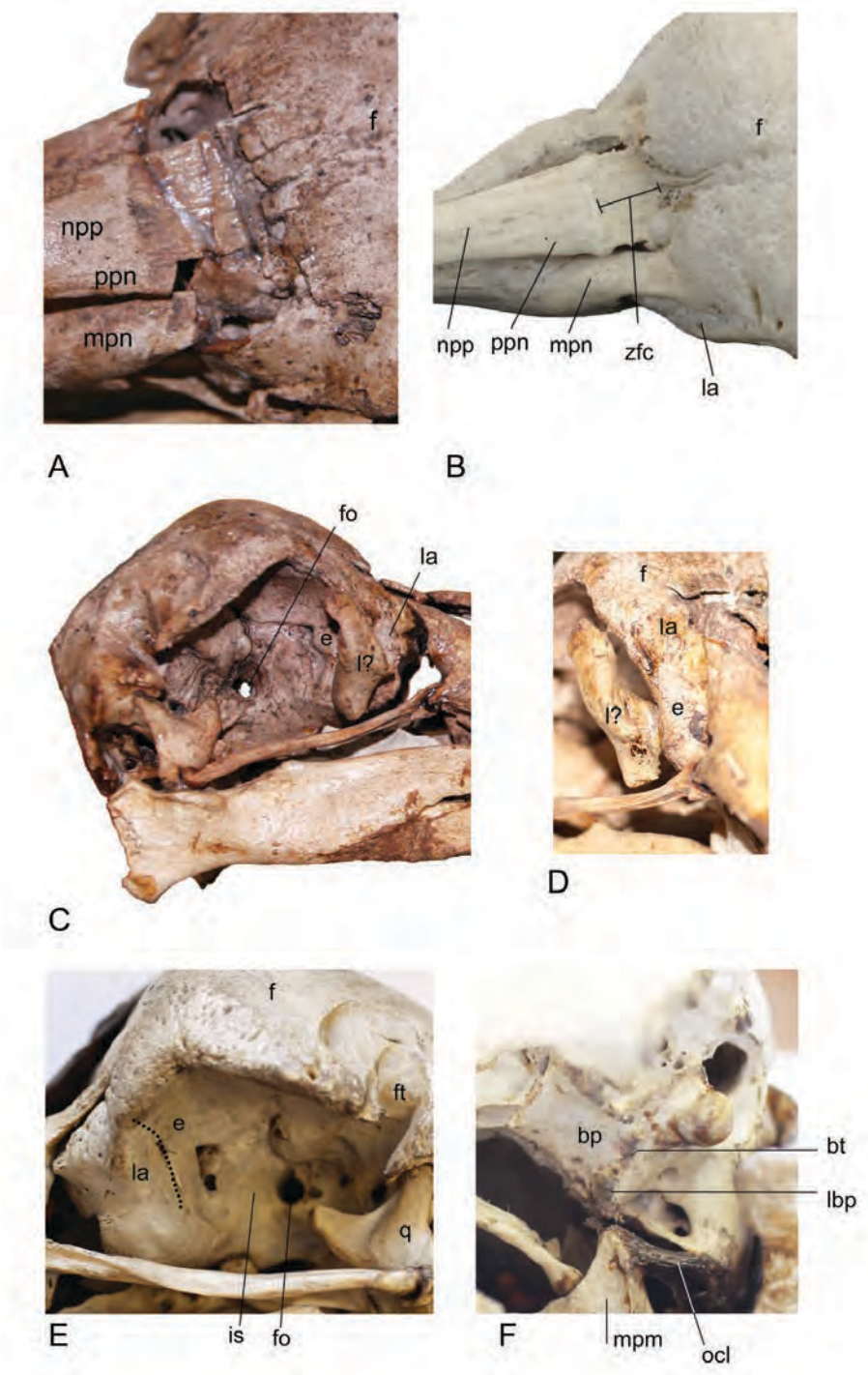

FIGURE 9. Details of dodo skull anatomy. **A**, close-up of nasofrontal hinge of Port Louis specimen; **B**, close-up of nasofrontal hinge of Copenhagen specimen; **C**, lateral view of the orbital region of the Port Louis specimen; **D**, close-up of the lacrimal region of the Port Louis specimen; **E**, close-up of the preorbital region in the Oxford specimen; **F**, close-up of the basitemporal region in the Oxford specimen. Dotted line in **E** denotes presumed border between lacrimal and ethmoid. Note the presence of the occipitomandibular ligament (ocl) connecting the caudal edge of the medial process of the mandible with the paroccipital process in the Oxford specimen (**F**). Anatomical abbreviations as in Appendix 1.

Digital Repository for Scan Data

All digital surface scans generated in this study are reposited in the Aves 3D database (http://Aves3D.org).

DESCRIPTION AND COMPARISONS

Skull and Mandible

Ossa Faciei—The upper bill is elongate and almost twice the length of the cranium, which is relatively short in comparison (Figs. 6–9; Pls. PL4, D4; Table 2). This becomes particularly evident when comparing it with *Pezophaps solitaria* and the closely related pigeons *Caloenas nicobarica, Goura victoria*, and *Didunculus strigirostris* (Fig. 10; Tables 2, A1). The maxilla is higher than wide, similar to the condition observed in *Didunculus* and *Pezophaps*, but unlike that in *Caloenas* and *Goura*. The rostrum maxillae is deep and mediolaterally compressed, and its anterior tip is rounded and hooked ventrally. The rostrum maxillae constitutes the anterior half of the total length of the maxilla, similar to the condition observed in *Pezophaps*, but unlike the condition

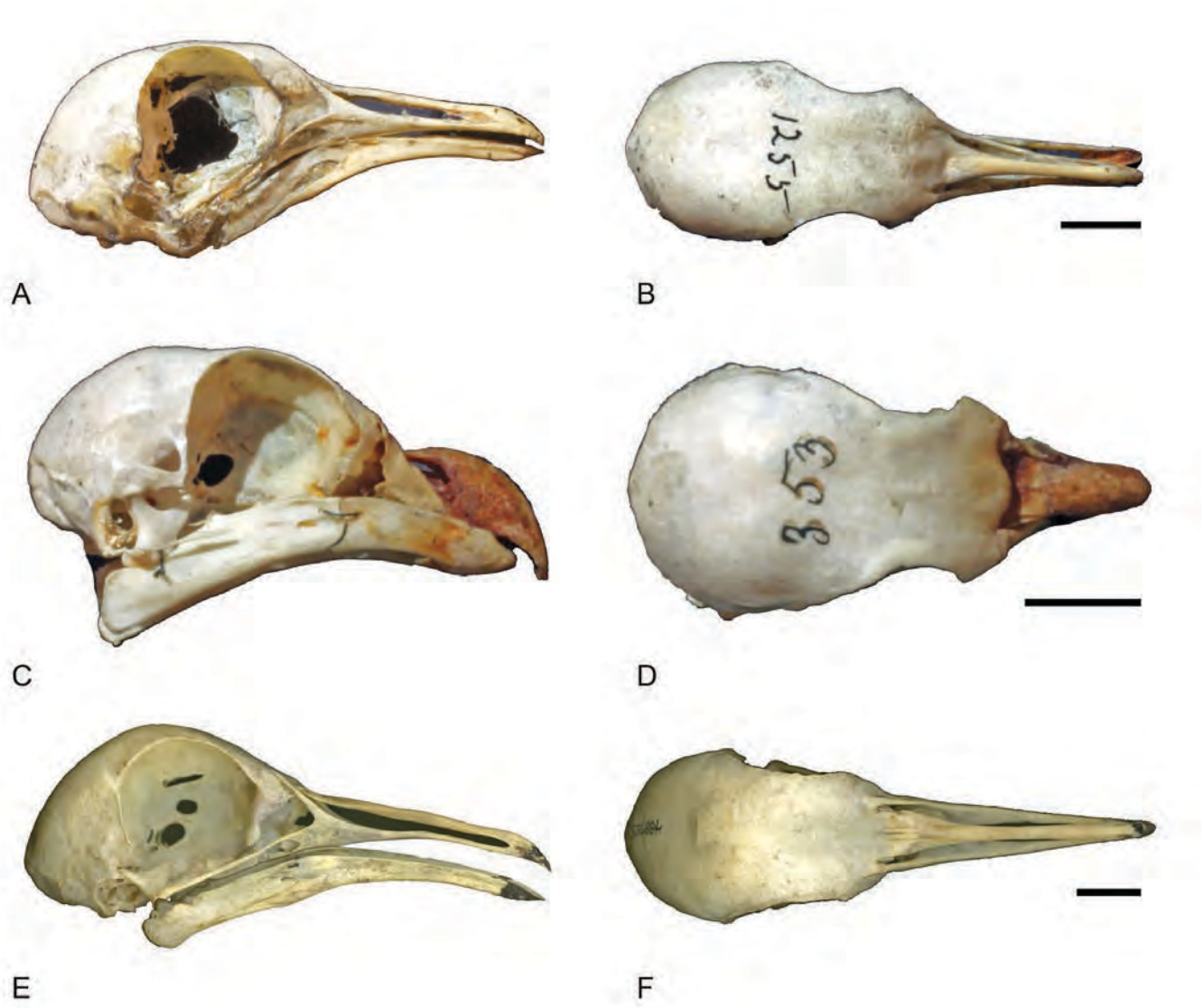

FIGURE 10. Skulls of *Caloenas nicobarica* MCZ 341255 (**A**, **B**), *Didunculus strigirostris* MCZ 340353 (**C**, **D**), and *Goura victoria* NMNH 488755 (**E**, **F**) in right lateral (**A**, **C**, **E**) and dorsal (**B**, **D**, **F**) views. Note that skulls are scaled to the same length to illustrate differences in skull proportions. Scale bars equal 2 cm. A-D courtesy of Museum of Comparative Zoology, Harvard University. © President and Fellows of Harvard College.

TABLE 2. Measurements of the cranium of the Port Louis and Durban dodos (in mm).

Dimension	Port Louis	Durban
Length of skull (from tip of premaxilla to parietal)	217	207*
Length of premaxilla (from tip to nasofrontal hinge, along central axis)	139	126
Length of braincase (from nasofrontal hinge to caudal edge of parietal, along central axis)	84	75*
Length of rostrum premaxillae	62	61
Maximum height of premaxilla	40	39
Maximum width of premaxilla	29	27
Length of naris (diagonally)	75	64
Width across nasofrontal hinge	55	49
Width of cranium at processus postorbitalis	86	—
Width of cranium at fossae temporalis	62	—
Width of cranium at processus zygomaticus	73.5	—
Length of arcus jugalis	57 (L) 58 (R)	68 (L) 45* (R)
Width across processus paroccipitalis	67	—
Length from condylus occipitalis to rostral tip of rostrum parasphenoidalis	27	—
Minimum width of rostrum parasphenoidalis	12	—
Length of rostrum parasphenoidalis (anterior tip of lamina parasphenoidalis to anterior end of rostrum parasphenoidalis)	38	—
Width across the ectethmoids	44	—
Length of pterygoids	27 (L) 25 (R)	27 (L) 27 (R)
Length of palatines	46 (L) 55 (R)	56 (L) 57 (R)

*Value is underestimated due to damage and/or reconstructive work.

in *Caloenas* and *Goura* where it makes up ~18–21% of total maxillary length, or in *Didunculus*, where it constitutes 65% of maxillary length (Table 2). The palatal surface of the rostrum maxillae is deeply concave and bordered by a sharp crista tomialis. The rostrum's outer surface bears several neurovascular foramina. Along the dorsal axis, the foramina join and form large grooves parallel to the longitudinal axis of the maxilla. The premaxilla lies posterior to the rostrum maxillae and constitutes half of the length of the upper bill (Table 2), whereas the maxilla is much reduced and forms the posterior part of the upper jaw and the anterior articulation with the jugal. The premaxilla encloses the large, elongated external naris that extends posterodorsally from the posterior border of the rostrum maxillae at an angle of approximately 25° with the long axis of the upper bill. A similarly elongated naris is observed in *Pezophaps*, as well as in *Caloenas* and *Goura*. In the latter two species, it extends almost along the entire length of the upper bill, in contrast to the condition in *Didunculus*, where the naris is short. There is no ossified septum nasale. The processus frontalis of the premaxilla (Figs. 6A, 7A) is subcircular in cross-section anteriorly, but is flat and narrows towards the cranium. In the Port Louis skeleton, a small layer of historically applied shellac is flaking and peeling and exposes lighter bone underneath (Fig. 6A). A similarly long and narrow processus frontalis of the premaxilla is also seen in *Pezophaps, Caloenas*, and *Goura*, but it is broad and short in *Didunculus*. The posterior half of the processus frontalis of the premaxilla is laterally flanked by the processus premaxillaris of the nasal bone (referred to as 'ento-nasal' by Strickland and Melville, 1848), and faint longitudinal lines are visible that delineate the processus frontalis of the premaxilla from the processus premaxillaris of the nasal (Fig. 9A, B). The processus maxillaris of the nasal (ecto-nasal in Strickland and Melville, 1848) is larger and extends as a broad bar ventrolaterally to synostose with the processus maxillaris of the premaxilla. In the Port Louis specimen (Fig. 6H), the posterior parts of both the processus premaxillaris and processus maxillaris of the nasal are broken off, and the most posterior part of the dorsal bar of the upper bill has been reconstructed from fragments (Fig. 9A). Short longitudinal grooves on the nasal (Fig. 6E) indicate that the processus frontalis of the premaxilla extended posteriorly between the nasals

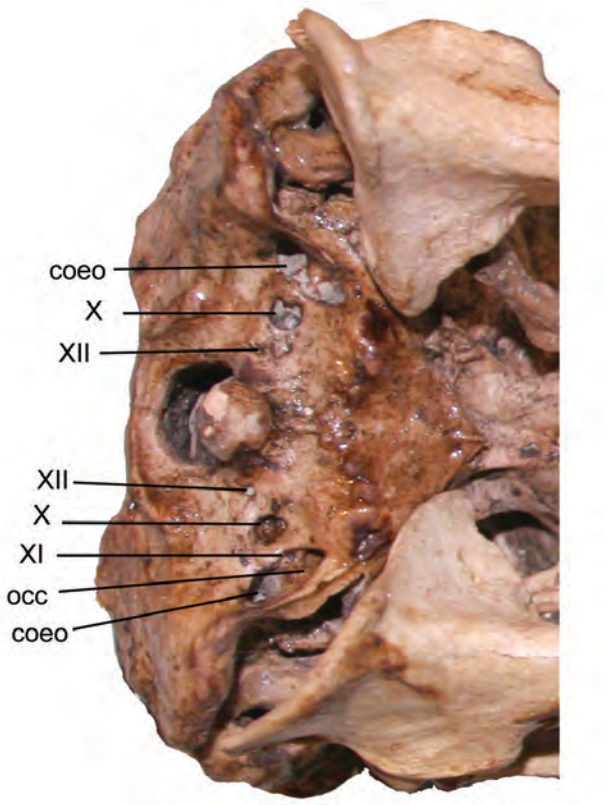

FIGURE 11. Close-up photograph of the base of the skull of the Port Louis specimen, showing the location of cranial nerve foramina.

(Strickland and Melville, 1848:85), a feature more clearly visible in the Oxford specimen (Fig. 8B). In the Durban dodo skull, the processus frontalis of the premaxilla and processus premaxillaris of the nasal are intact, but the frontal bones and the processus

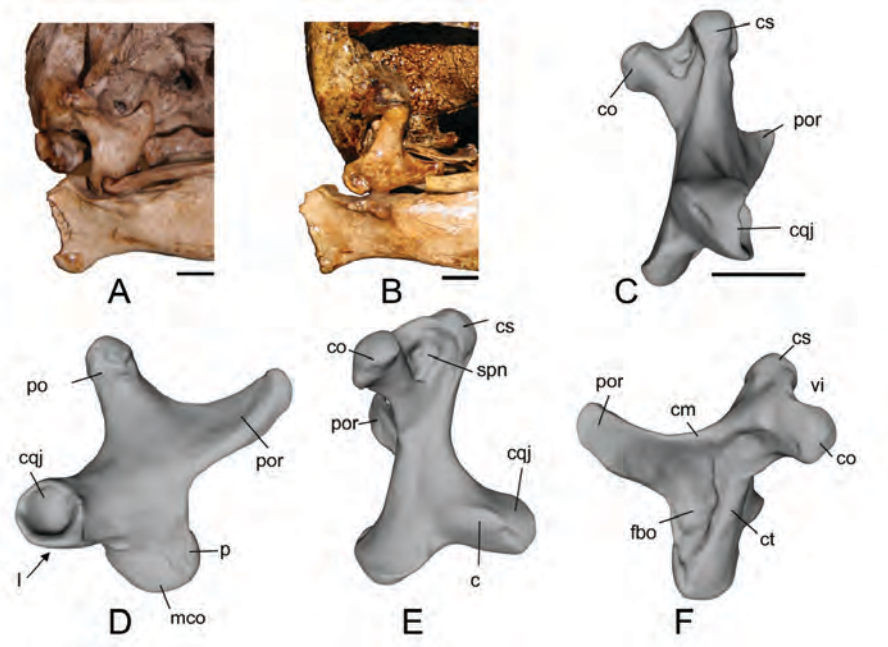

FIGURE 12. Dodo quadrate. **A**, lateral view of Port Louis specimen; **B**, lateral view of Durban specimen (note that quadrate orientation has been incorrectly reconstructed in this specimen); **C**–**F**, 3-D scans of a right quadrate from Mare aux Songes (MAS11-11020) in lateral view (**C**), anterior view (**D**), caudal view (**E**), and medial view (**F**). Scale bars equal 1 cm.

TABLE 3. Measurements of dodo quadrate (MAS11-11020) (in mm).

Length from capitulum squamosum to condylus medialis	32
Length from processus oticus to processus lateralis	32.7
Length across processus oticus (capitular span in Elzanowski and Stidham, 2010)	15.2
Width of condylus medialis	9.8
Width across cotyla quadratojugularis	6.5

maxillare of the nasal are reconstructed. In the Copenhagen and Oxford dodo crania (Fig. 8B, E), the processus frontalis and processus premaxillaris are intact. In the Copenhagen specimen, the processus premaxillaris of the nasal has fully fused with the processus frontalis of the premaxilla, but a suture is visible between the processus premaxillare of the nasal and the processus frontalis of the premaxilla in the Oxford specimen. In *Pezophaps*, the processus premaxillaris of the nasal and the processus frontalis of the premaxilla, as well as the posterior halves of the processus frontalis themselves, appear unfused.

In the dodo, the area of fusion between the nasals and premaxillae is thin and would have allowed considerable flexibility (i.e., kinesis) in the dodo upper jaw. This area, the zona flexoria craniofacialis, is characterized by a striated surface structure as seen on the processus premaxillaris and frontalis in the Port Louis specimen, and in the Oxford and Copenhagen crania (as well as in the cranium MAD 5971; Janoo, 1996). In the Copenhagen specimen (Figs. 8B, 9B), this striated surface is visible on the processus maxillaris of the nasal as well. The zona flexoria craniofacialis measures approximately 1.5 cm in length and is distinct from the more rostral section of the processus frontalis of the premaxilla in terms of the thinness of the bones and the striated structure. In addition to the long zona flexoria craniofacialis, the functional uncoupling of the dorsal and lateral bars of the premaxilla (i.e., a schizorhinal nostril; Bock, 1964) allows movement of the lateral and ventral parts of the premaxilla, whereas the processus frontalis remains stationary. The possession of a schizorhinal nostril is associated with having a rhynchokinetic upper jaw (Bock, 1964), and the kinetics of the dodo premaxilla and feeding behavior are likely to have been complex. Zusi (1984) noted that a kinetic upper premaxilla allows a bird to feed on larger food items, a characteristic beneficial to frugivorous pigeons. The morphology of the dodo nasofrontal region agrees with that of other columbids that are considered to display rhynchokinesis. *Pezophaps* also possesses a schizorhinal nostril and together with *Caloenas* and *Goura* displays a similarly thin nasofrontal region that smoothly fuses with the frontals (Fig. 10). In *Didunculus*, the fusion between the nasals and premaxillae is more abrupt. In both *Caloenas* and *Goura*, the naris extends posteriorly between the processus premaxillare and maxillare of the nasal, similar to the condition in *Raphus* and *Pezophaps*. In *Didunculus*, the naris is short and the processus premaxillare and maxillare fuse posteriorly.

The processus maxillare of the premaxilla is high and laterally compressed immediately posterior to the rostrum maxillae and has a concave lateral surface (Fig. 6A, 8A, D). Posteriorly, the processus maxillare is laterally and dorsally expanded and fused with the maxilla, which forms the posteroventral border of the upper bill. Dorsally, the maxilla is fused with the processus maxillare of the nasal. This structure is complete in the Port Louis specimen (Fig. 6A), but reconstructed in the Durban specimen (Fig. 7A). In ventral view, the two processus maxillares of the premaxilla run parallel to each other, and their inner surfaces form a narrow median palatal cleft. In the dodo, as well as in

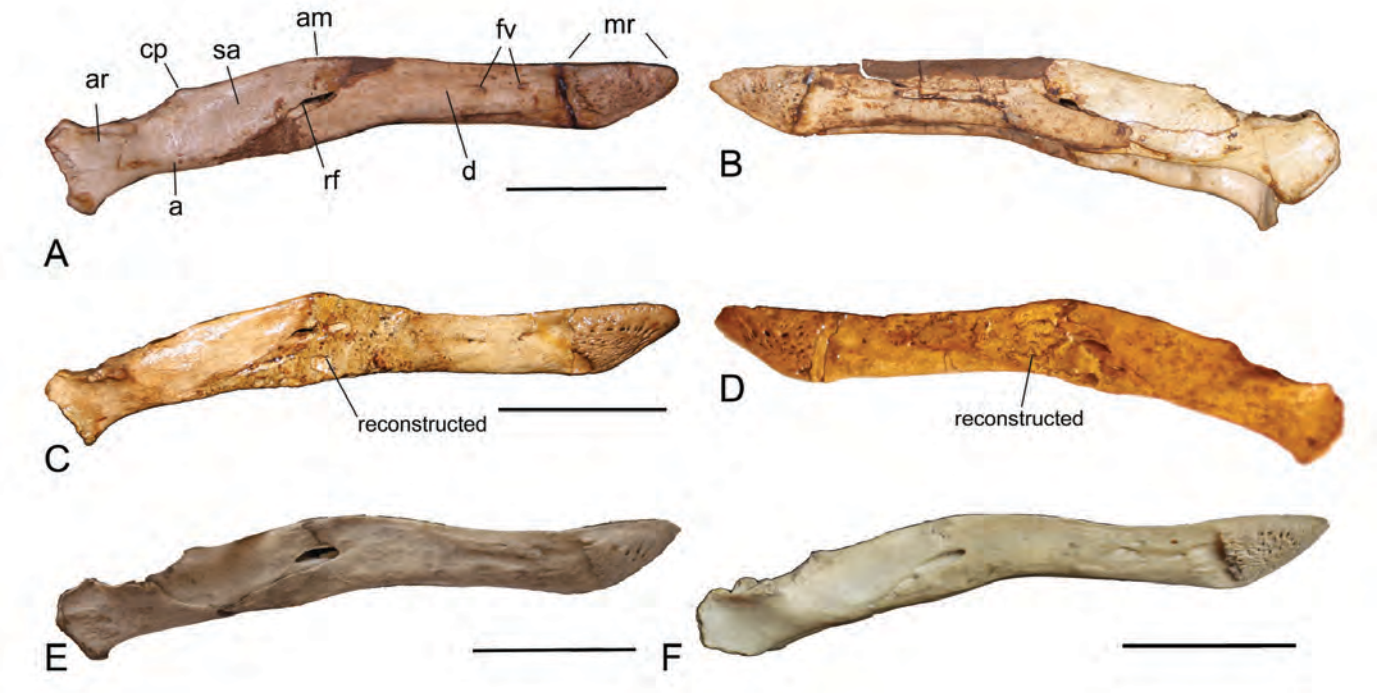

FIGURE 13. Dodo mandibles in lateral view. Port Louis specimen, right (**A**) and left (**B**) sides; Durban specimen, right (**C**) and left (**D**) sides; **E**, Oxford specimen (mirrored image of left side); **F**, Copenhagen specimen, right side. Anatomical abbreviations as in Appendix 1. Scale bars equal 5 cm.

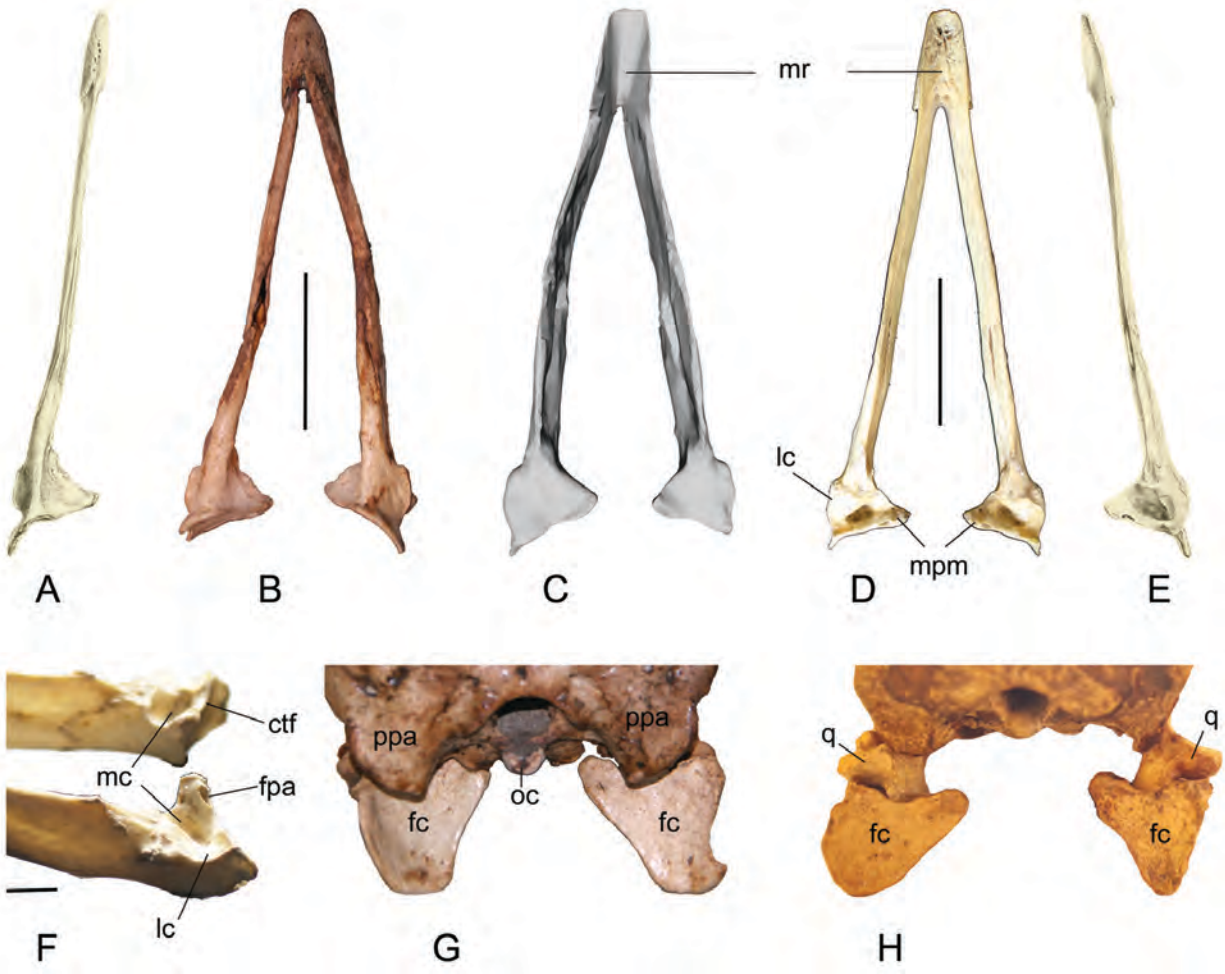

FIGURE 14. Dodo mandibles in ventral (**A**, **B**), dorsal (**C**, **D**, **E**), oblique (**F**), and caudal (**G**, **H**) views. **A**, right mandibular ramus, Oxford specimen, from Strickland and Melville (1848), plate VIII; **B**, Port Louis specimen; **C**, 3-D reconstruction lacking articular surface detail, Durban specimen; **D**, Copenhagen specimen; **E**, right mandibular ramus, Oxford specimen; **F**, detail of the articular mandibular surface, Copenhagen specimen; **G**, fossa caudalis, Port Louis specimen; **H**, fossa caudalis, Durban specimen. Anatomical abbreviations as in Appendix 1. Scale bars equal 5 cm (**A**–**E**, **G**, **H**) and 1 cm (**F**).

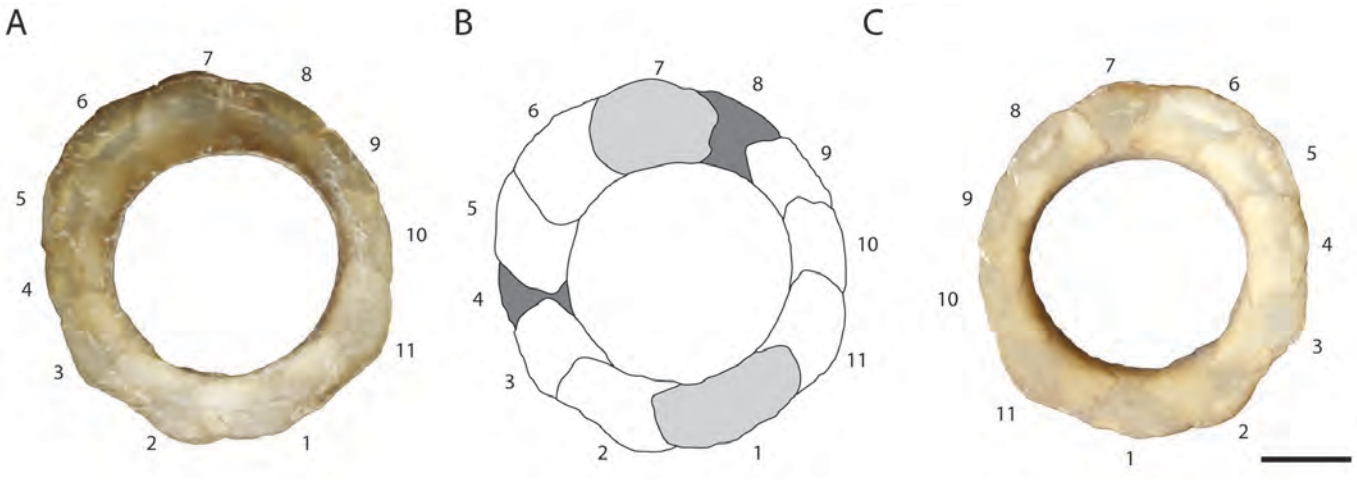

FIGURE 15. Articulated scleral ossicles of the right eye of the Copenhagen dodo. **A**, lateral surface; **B**, outline drawing of the lateral surface, showing the distribution of overplates (light gray; 1, 7) and underplates (dark gray; 4, 8) according to the terminology of Curtis and Miller (1938); **C**, medial surface. Scleral ossicles in **A**–**C** oriented with dorsal (ca. pl. 7) towards the top of the page. Scale bar equals 5 mm.

FIGURE 16. Photographs of the axial skeleton of the Port Louis (**A**, **C**, **E**) and Durban (**B**, **D**, **F**) Thirioux dodos. **A**, **B**, neck and head, right lateral view; **C**, **D**, ribcage, right lateral view; **E**, **F**, caudal vertebrae and pygostyle, oblique top view. Background has been blurred in **A** and **C**.

Pezophaps and *Didunculus*, the processus maxillaris of the nasal, and especially the processus maxillaris of the premaxilla, is stout, but is slender in *Goura* and *Caloenas* (Fig. 10). In *Didunculus*, the processus maxillaris of the premaxilla projects posterodorsally from the rostrum maxillae, whereas it is horizontal in *Caloenas* and *Goura*. The processus jugalis extends posteriorly from the maxilla at roughly mid-length of the processus maxillare of the nasal. Posteriorly, it fuses with the jugal and the quadratojugal to form a slightly sigmoidal bar, linking the maxilla to the quadrate. The jugal projects obliquely posteriad at an angle of 125° with the posterior edge of the maxilla (Figs. 6A, 7A, 8A, D). In the Port Louis specimen (Fig. 6A, B), the jugal is broken from

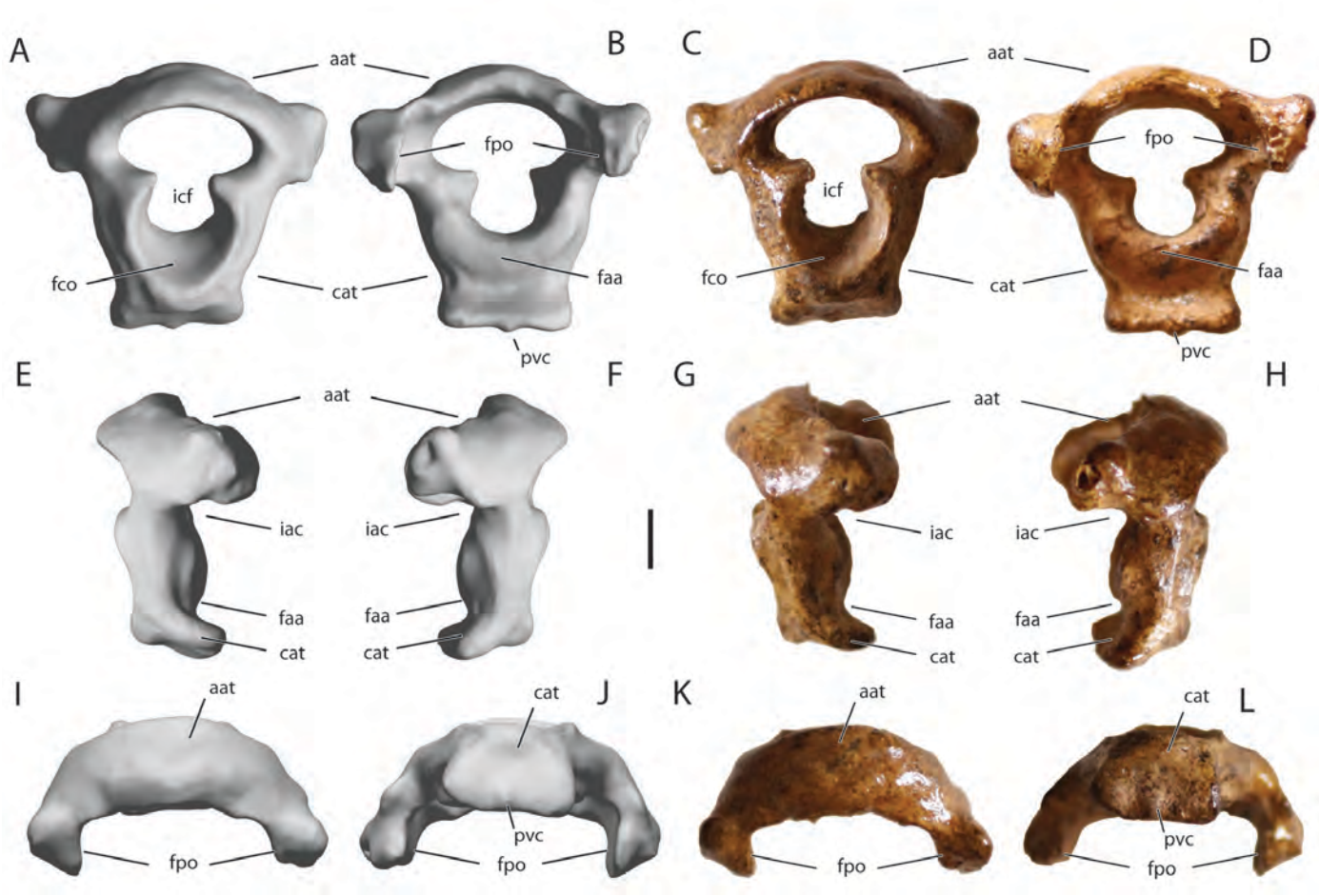

FIGURE 17. Atlas, Durban specimen. 3-D scans (**A**, **B**, **E**, **F**, **I**, **J**) and photographs (**C**, **D**, **G**, **H**, **K**, **L**) in cranial (**A**, **C**), caudal (**B**, **D**), left lateral (**E**, **G**), right lateral (**F**, **H**), dorsal (**I**, **K**), and ventral (**J**, **L**) views. Anatomical abbreviations as in Appendix 1. Scale bar equals 5 mm.

the processus jugalis on both sides. Due to the reconstructed nature of the Durban specimen (Fig. 7A, B), the right processus jugalis is missing, and the right quadratojugal is incomplete (missing its posterior end). The left arcus jugalis (Fig. 7B, D) is more sigmoid than is observed in the Port Louis (Fig. 6A, B), Copenhagen (Fig. 8A), and Oxford (Fig. 8D) skulls, which is likely due to individual variation. The arcus jugalis is relatively longer and more slender in *Caloenas, Goura*, and *Didunculus* (Table 2). The palatine bones (Figs. 6K, L, 7K, L) are slender, dorsoventrally flattened, and curved. They are unfused and articulate posterodorsally with the rostrum parasphenoidalis. The anterior articular surface of the palatine for the maxilla is broad and flat in the Port Louis skull (Fig. 6K, L), but a ventrally directed ridge is present medially in the Durban specimen (Fig. 7K, L). In the Port Louis skull, the palatines are not fused with the processus maxillaris of the premaxilla, whereas they are fused in the Copenhagen (Fig. 8C) and the Oxford (Fig. 8F) specimens. The ventral surface of the palatine is concave, and the lateral rim forms a distinct crest, the crista lateralis, that projects lateroventrally along its lateral side. Medially, the lamella choanalis forms a distinct and medially concave crista ventralis. In lateral view, the ventral rim of the crista ventralis is squared in the Port Louis skull, but less so in the Copenhagen specimen (Fig. 8A). Dorsally, the lamella choanalis has a squared top, similar to the crista ventralis, but is wider anteroposteriorly and might have extended anteriad towards the maxilla. The lamella choanalis is missing from the right palatine in the Port Louis skull. The posterior articular surface, with which it articulates with the rostrum parasphenoidalis and the pterygoid, is flat and wide, but the crista lateralis continues almost to the posterior end. The palatines are relatively longer in *Caloenas, Goura*, and *Didunculus* (Fig. 10). In *Didunculus*, they are relatively straight, curving medially only posteriorly, where they expand dorsally to articulate with the rostrum parasphenoidalis. The palatines are more curved in *Goura* and *Caloenas*. In these taxa, the crista ventralis is also located more posteriorly and has a rostroventrally directed spur.

There is no vomer preserved in the Port Louis specimen (Fig. 6); the rostrum parasphenoidalis that would articulate with the vomer is very short and does not extend beyond the nasofrontal region. However, it appears broken and it cannot be excluded that the rostrum parasphenoidalis may have supported a vomer. The cranium of the Durban specimen has been reconstructed; therefore, it provides no anatomical information. The absence of an ossified vomer is believed to be a derived character in Columbiformes (Cracraft, 1988), although ossified vomers have been recorded in certain species of pigeons (Martin, 1904; Huxley, 1867; Shufeldt, 1901). In the Oxford specimen, Strickland and Melville (1848) described the rostrum parasphenoidalis forming a compressed plate projecting forwards into the inferior nasal fissure, but they refrained from referring to this structure as the vomer. The rostrum parasphenoidalis projects anteriorly of the nasofrontal region in the Oxford and Copenhagen

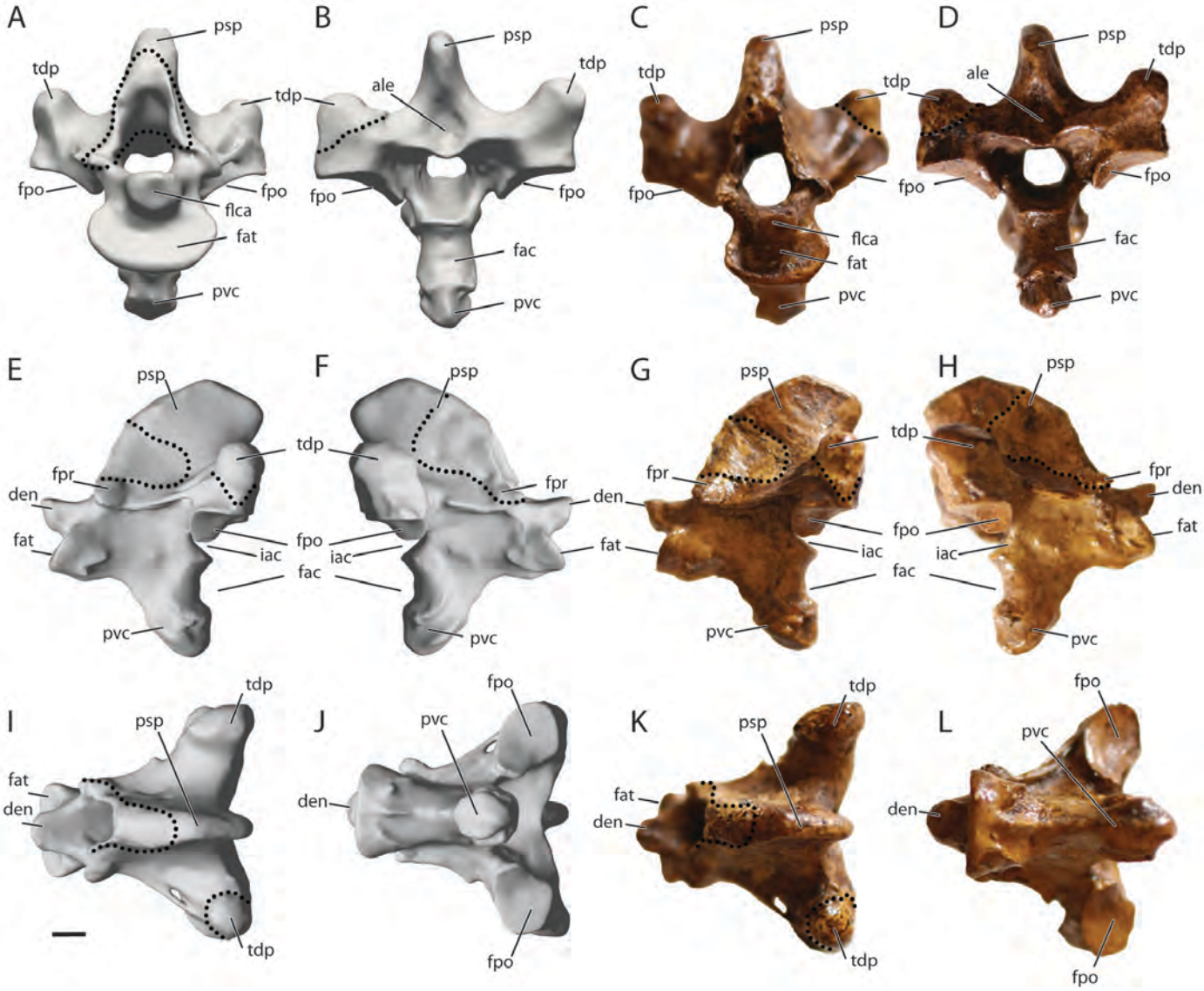

FIGURE 18. Axis, Durban specimen. 3-D scans (**A**, **B**, **E**, **F**, **I**, **J**) and photographs (**C**, **D**, **G**, **H**, **K**, **L**) in cranial (**A**, **C**), caudal (**B**, **D**), left lateral (**E**, **G**), right lateral (**F**, **H**), dorsal (**I**, **K**), and ventral (**J**, **L**) views. A portion of the cranial margin of the processus spinosus, right facies articularis prezygapophysis, and left tuberculum dorsale postzygapophysis have been reconstructed in plaster, as indicated by a stippled line. Anatomical abbreviations as in Appendix 1. Scale bar equals 5 mm.

specimens (Fig. 8C, F; also see Strickland and Melville's pls. VIII and X, fig. 2; note that in the scan of the Port Louis specimen (Figs. 6K, L, 7K, L, 8C, F), this structure is not visible due to digital reconstruction of this region). Janoo (1996) hypothesized that the rostrum parasphenoidalis in the Oxford specimen might be broken and that the absence of an ossified vomer could be artificial, but our examination of the Oxford specimen does not support this interpretation. There is no evidence of a vomer in the Copenhagen dodo. Based on the evidence available, we consider it likely that the dodo did not have an ossified vomer. A vomer is present in *Didunculus* as a laterally compressed vertical plate. In *Goura* and *Caloenas*, as well as in *Pezophaps*, it is a rostrally directed spur.

Cranium—The cranium is slightly wider than it is long (Pls. PL4, D4; Table 2), which is in contrast to the condition observed in *Caloenas, Goura*, and *Didunculus* (Fig. 10; Table A1); but similar to that in *Pezophaps*. The broad and convex frontal bones rise abruptly posteriorly to the nasofrontal region and form a dome with its maximum height above the posterior parts of the orbits. The angle created by the frontals with the premaxilla and nasal at the nasofrontal region (lateral view) is roughly 135°. Several authors (Owen, 1846, 1866; Strickland and Melville, 1848; Janoo, 1996) have remarked on the highly expanded and bulbous frontals as characteristic, even apomorphic for dodos (Janoo, 1996). In contrast, in *Pezophaps*, the frontal region is markedly flat. In lateral aspect, the curvature of the frontals in the Port Louis specimen is less convex than in the Oxford cranium, especially as depicted in Strickland and Melville (1848). The frontal region of the Durban specimen is not preserved and has been reconstructed comparatively inaccurately and extremely flat. Although the frontals are dorsally expanded in *Goura* (albeit to a lesser degree as in *Raphus*), the nasofrontal region slopes gently in both *Goura* and *Caloenas*, whereas it is more angled in *Didunculus*.

Much of the lateral aspect of the cranium is occupied by the orbit. The anterior wall of the orbit is formed by the lacrimal-ectethmoid complex; this complex (see Cracraft, 1968) fuses with

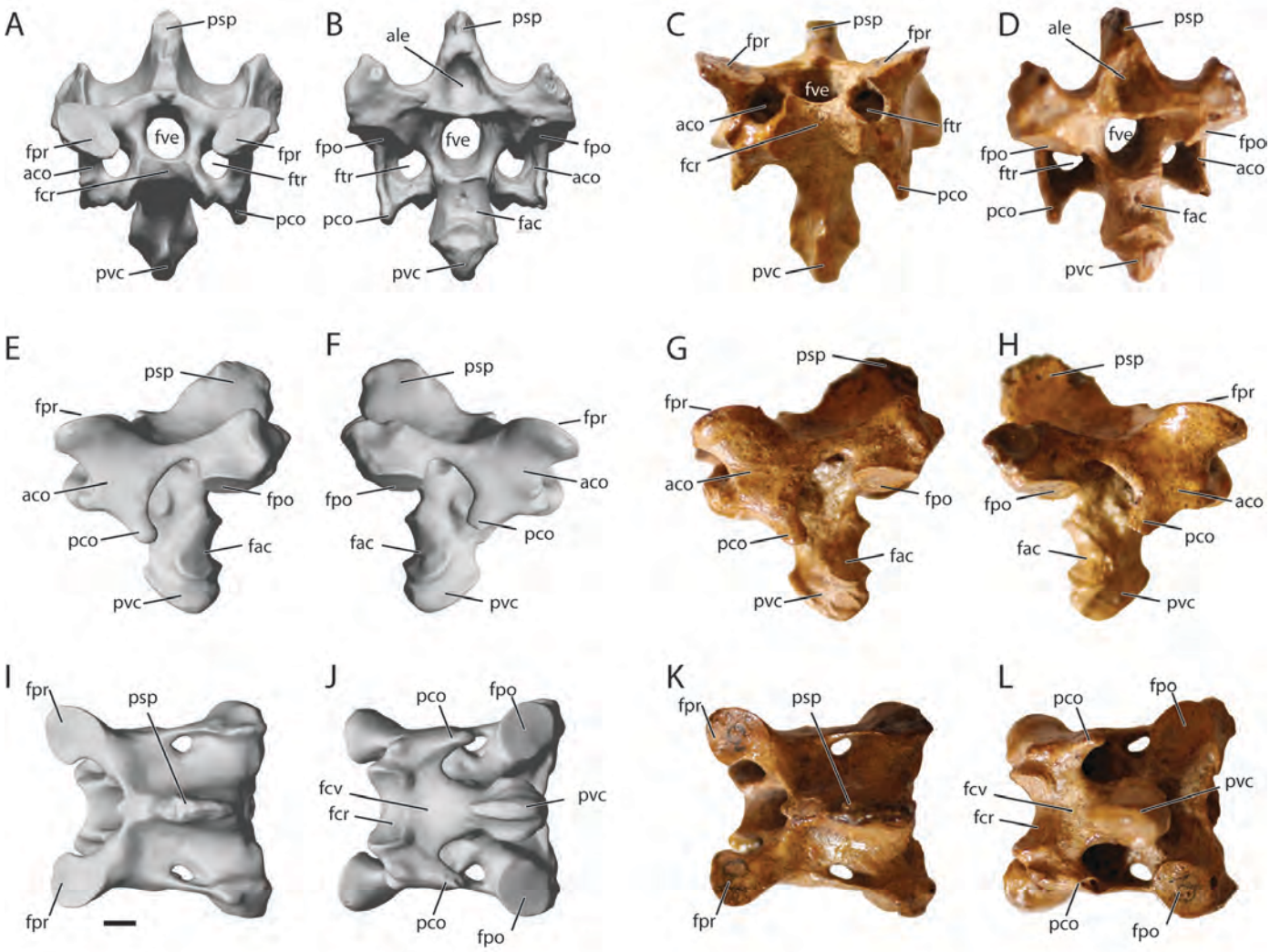

FIGURE 19. Presynsacral (cervical) vertebra 3, Durban specimen. 3-D scans (**A**, **B**, **E**, **F**, **I**, **J**) and photographs (**C**, **D**, **G**, **H**, **K**, **L**) in cranial (**A**, **C**), caudal (**B**, **D**), left lateral (**E**, **G**), right lateral (**F**, **H**), dorsal (**I**, **K**), and ventral (**J**, **L**) views. Anatomical abbreviations as in Appendix 1. Scale bar equals 5 mm.

the frontals dorsally just posterior to the nasofrontal hinge. The lacrimal-ectethmoid complex does not extend anteriorly beyond the nasofrontal region in the Port Louis cranium (Fig. 6A, C), but in the Copenhagen and the Oxford specimens (Fig. 8C, F), it projects more anteriorly along the midline. The lateral part of the lacrimal-ectethmoid complex extends dorsally and is smoothly joined to the nasal just posterior to the nasofrontal region and is in close proximity to the processus maxillaris of the nasal. This is evident in the Copenhagen and Oxford specimens (Fig. 8A, D), and this position could indicate a functional role for the lacrimal-ectethmoid complex, for instance, in support of the nasofrontal region. Ventrally, the lacrimal-ectethmoid complex is bulbous and fuses with the rostrum parasphenoidalis. Because the posterior part of the nasals (where they cross the nasofrontal hinge) is missing in the Port Louis specimen, the interior fossae bulbi olfactorii are visible in dorsal view on both sides of the hinge.

On the lateral rim of both orbits, the Port Louis specimen displays an additional bone (Figs. 6A, B, 9C, D). It is elongated and oriented vertically and follows the curvature of the anterior rim of the orbit. However, this bone is not fused with the rim of the orbit and is artificially attached. In overall size and shape, the extra bone resembles the lacrimal, but its morphology does not fit descriptions of the lacrimal given by various authors (e.g., Strickland and Melville, 1848; Owen, 1866; Cracraft, 1968), who all described the lacrimal being fused to the ectethmoid. Moreover, no mention has been made of separate or additional lacrimals in the dodo. In the closely related extant taxa *Goura, Didunculus*, and *Caloenas*, the lacrimal and ectethmoid are separated dorsally by the foramen orbitonasale mediale. Given the highly autapomorphic nature of the dodo skull, complete separation of the lacrimal from the ectethmoid would not be improbable. In *Pezophaps*, the attachment of the lacrimal to the ectethmoid is reduced to only the ventral-most portion. However, there is no evidence for a separated lacrimal in the Copenhagen skull or the Oxford dodo head, without doubt the most intact specimen, nor are there articular facets on the lateral rim of the orbit to articulate with a separate lacrimal. Therefore, the elements attached to the Port Louis orbital rim are likely not a part of the original Port Louis dodo cranium, and we tentatively interpret them as an additional, unfused set of lacrimals that must have belonged to a different, skeletally

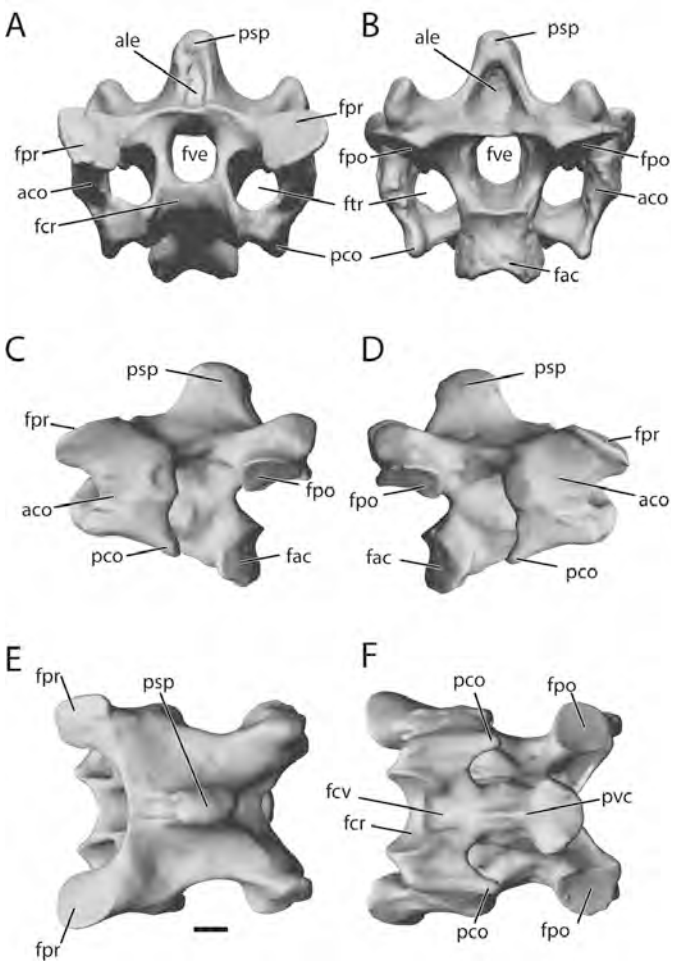

FIGURE 20. 3-D scans of presynsacral (cervical) vertebra 4, Durban specimen. **A**, cranial; **B**, caudal; **C**, left lateral; **D**, right lateral; **E**, dorsal; **F**, ventral views. Anatomical abbreviations as in Appendix 1. Scale bar equals 5 mm.

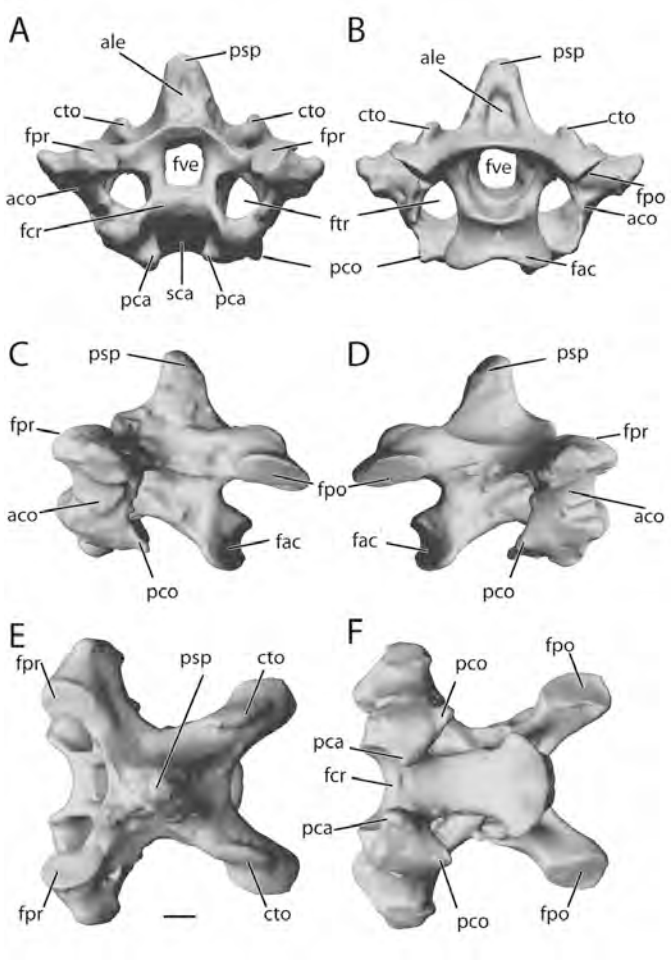

FIGURE 21. 3-D scans of presynsacral (cervical) vertebra 5, Durban specimen. **A**, cranial; **B**, caudal; **C**, left lateral; **D**, right lateral; **E**, dorsal; **F**, ventral views. Anatomical abbreviations as in Appendix 1. Scale bar equals 5 mm.

immature individual that was erroneously incorporated in the skeletal mount in the early 1900s (see also Claessens and Hume, 2015).

The orbits are separated by the ossified septum interorbitale that forms a solid bone wall between the orbits. The foramen opticum is small and circular and is located posteroventrally in the septum. The septum interorbitale is much larger in *Caloenas, Goura*, and *Didunculus*, where it takes up most of the interorbital surface. Although it is mostly ossified, it forms merely a thin sheet of bone in these taxa. The frontal and the alisphenoid form the roof of the orbit. In lateral view, the orbital margin is markedly angled at almost 90°, whereas it is rounded in *Caloenas, Goura*, and *Didunculus*. Posteriorly, the roof of the orbit, formed by the alisphenoid, continues outwards and posteriorly, projecting in a straight line to the processus postorbitalis, which is directed posteriorly. It is broad and triangular and ends in a narrow tip. In *Pezophaps*, the orbital rim is rounded and the processus postorbitalis shorter, albeit directed rostroventrally. In *Caloenas, Goura*, and *Didunculus*, the alisphenoid continues further ventrally, and the processus postorbitalis is directed ventrally or even rostroventrally. The fossa temporalis is deep and narrow, being wider lateromedially than anteroposteriorly. However, a broad extension of the fossa temporalis bordered by a distinct crista temporalis extends dorsally and rostrally of the processus postorbitalis. Medially, the distance between these shallow fossae measures 45 mm. A distinct processus zygomaticus of the squamosal forms the posterior border of the fossa temporalis. It is oriented anteroventrally and extends further ventrally than the processus postorbitalis. In *Caloenas, Goura*, and *Didunculus*, the fossa temporalis is smaller and located further ventrally and laterally, and the crista temporalis is less pronounced and located entirely laterally, rather than extending dorsally as in the dodo. The processus zygomaticus is very small in *Goura* and *Caloenas*, but larger, projecting anteriorly (similar to *Raphus*) and even converging towards the processus postorbitalis in *Didunculus. Pezophaps* displays a wide fossa temporalis with a crista temporalis much thicker than that of *Raphus*; its processus zygomaticus is blunt.

The posterior, downward slope of the skull is dorsally demarcated by the crista nuchalis transversalis (occipital crest in Janoo, 1996). The occipital area is oriented vertically and, in lateral view, forms an angle of ~100° with the parietal region. In posterior view, the occipital area is subelliptical, with no prominentia cerebralis (similar to *Pezophaps*). The surface of the occipital area is rugose, with the central part slightly concave, especially dorsally, and is bordered laterally by the low crista nuchalis transversus. The foramen supraoccipitalis is visible on the midline of the occipital facet. The foramina venae

occipitalis externae are positioned lateral to the foramen supraoccipitalis and open up in grooves that are oriented ventrolaterally. Laterally, the exoccipitals form the processus paroccipitalis (paroccipital in Janoo, 1996; exoccipital in Shufeldt, 1901), ventrally directed, flange-like projections that make up the posterior wall of the cavum tympanicum. The ventral border of the occipital facet is formed by the distinct, semicircular infraoccipital ridge that overhangs the foramen magnum. In the Port Louis specimen, the foramen is rectangular with rounded corners and is deeper than wide. The Oxford dodo shows a foramen magnum that is pointed dorsad and is narrower in the upper half (Owen, 1846). In the Copenhagen dodo, the basicranium is missing. The morphology of the occipital region in the dodo differs markedly from that in *Goura* and *Caloenas* (Fig. 8), where the prominentia cerebralis is well developed (the prominentia cerebralis is only minimally pronounced in *Didunculus*). In *Goura* and *Caloenas*, the occipital region is oriented posteroventrally, whereas in *Raphus, Pezophaps*, and *Didunculus*, the occipital region is more vertical. In all three extant taxa, however, the processus paroccipitalis is less distinct and oriented anteroventrally.

The condylus occipitalis is described by Janoo (1996) as hemispheroidal (also reflected in his measurements in Table 1), but in the Port Louis specimen it is between semicircular and reniform in shape. The lower half is rounded, with the upper half concave and exhibiting a median notch, similar to the condition observed in the Oxford specimen, as well as in *Caloenas, Goura*, and *Didunculus*. Janoo (1996) noted that the position of the condylus occipitalis, which is dorsal of the lamina parasphenoidalis, is in contrast with the usual condition in columbiforms. In the Port Louis specimen, however, the condylus occipitalis appears to originate from the same level as the lamina parasphenoidalis, but projects posteriorly and ventrally from it. In ventral view, the flattened aspect of the occipital facies of the dodo cranium becomes apparent, with the condylus occipitalis in line with the processus paroccipitalis (it is located in line with or posteriorly of the processes paraoccopitalis in extant columbids). On either side of the condylus occipitalis, there is a small opening of the canalis n. hypoglossi (XII; Fig. 11). Lateral to it lies the round foramen n. vagi (X; Fig. 11). Most laterally, on the posterior side of the lamina parasphenoidalis, a cluster of relatively large foramina is situated within an elongated ostium. Most posteriorly is the canalis opthalmicus externus ostium. Rostral to it, at the posterior margin of the lamina parasphenoidalis, lies the ostium canalis carotici. The foramen n. glossopharyngealis (IX; Fig 11) is small and situated posteriorly to the ostium canalis carotici. The lamina parasphenoidalis itself is triangular in shape. Its anterior part is situated lower (i.e., more ventral) than the rest of the ventral surface of the cranium. Anterior of the foramina on the lamina parasphenoidalis are a number of bony processes. These bony protuberances were noticed, but not named, by Strickland and Melville ("scabrous tubercle"; Strickland and Melville, 1848:78) and also Owen ("larger tuberosities"; Owen, 1866:36 and pl. 11, fig. 1). Owen stated that a pair of small tubercles was present between the larger ones in some, but not all, dodo skulls he examined. In the Port Louis specimen (Fig. 6K, L), as well as in the Oxford specimen (Fig. 8F), two sets of bony processes can indeed be distinguished, a pair of small medial ones and a pair of larger lateral ones. The medial ones, the mammillary processus, are rounded, and serve as insertion for cervical muscles and are well developed in taxa with long skulls. The lateral ones, referred to as the lateral basitemporal process by Bock (1960), are lateromedially elongated and mark the insertion for the neck muscles (Merz, 1963; Baumel and Witmer, 1993). In the Oxford specimen, where the articulation with the mandible is preserved in situ, the processus mandibularis of the mandible appears to abut the lateral aspect of the lateral basitemporal process. Such an arrangement would prevent the lower jaw from disarticulating when the bill is opened. This seems to be in agreement with the observation by Bock (1960) that a secondary mandibular articulation could have been present in the dodo.

The ventral surface of the cranium (Figs. 6K, L, 7K, L, 8C, F) displays the large excavations of the orbitotemporal region, separated medially by the rostrum parasphenoidalis. The rostrum parasphenoidalis is constricted near its origin posteriorly, but expands anteriorly to fuse with the lacrimal-ectethmoid complex. The fossae bulbi olfactorii of the ethmoid coalesce laterally with the bulbous ventral expansion of the ectethmoid. In *Caloenas, Goura*, and *Didunculus*, the rostrum parasphenoidalis is much narrower, not exceeding the width of the palatines, and it continues to narrow anteriorly as it meets the ectethmoids. In *Pezophaps*, the rostrum parasphenoidalis is relatively narrow and not constricted as in *Raphus*. Along the midline of the rostrum parasphenoidalis runs a groove that tapers anteriorly. Further anteriorly, the median axis of the rostrum parasphenoidalis is raised into a low medial ridge that separates the articulating surfaces for the palatines and pterygoids. The pterygoid extends anteromedially from the condylus pterygoideus on the quadrate to the posterior end of the palatine beside the rostrum parasphenoidalis. The posterior and anterior ends are expanded and flattened, but in different planes, so that the pterygoid appears twisted along its longitudinal axis. In the Port Louis specimen, a triangular, dorsomedially oriented facies articularis basipterygoidea projects from the middle of the right pterygoid; this expansion is absent from the left pterygoid and likely to have been broken off. In *Caloenas, Goura*, and *Didunculus*, the facies articularis basipterygoidea articulates with a well-developed processus basipterygoideus on the rostrum parasphenoidalis. However, in *Raphus*, as well as in *Pezophaps*, there is a wide space between the pterygoid and the lamina parasphenoidalis (l. basitemporalis), and there is no processus basipterygoideus on the surface of the rostrum parasphenoidalis. Given that the pterygoid-basipterygoid articulation is present in extant columbids, it must be considered lost in the dodo.

Quadrate—In both the Port Louis specimen and the Durban specimen, the quadrate is fixed in place, obscuring the capitulum oticum and capitulum squamosum (Figs. 6A–D, 7A–D, 12; Pls. PL4, D4). Here we augment their description with anatomical information from a complete dodo right quadrate from the Mare aux Songes (MAS11-11020; Fig. 12; Table 3). Note that in the Durban specimen, whose cranium has been heavily reconstructed, the quadrate is rotated ventroposteriorly, so that the pars oticus lies anterior to the pars mandibularis. The dodo quadrate (tympanic in Strickland and Melville, 1848, and Owen, 1866) is 'X'-shaped in anterior view (Fig. 12D), similar to that of extant columbids. The processus orbitalis projects anteromedially from the corpus of the quadrate. It is long and slender with a rounded tip that curves dorsally, leaving the distal half of the rostral surface concave. The ventral margin of the orbital process forms a thickened ridge, the crista orbitalis. In *Caloenas* and *Goura*, the tip is dorsally flattened, giving the processus orbitalis an overall straighter appearance. In *Didunculus*, the processus orbitalis is shorter with a rounded tip. The medial surface of the processus orbitalis is concave and deepens at the base into the fossa basiorbitalis on the medial side of the corpus. Posteriorly, the fossa basiorbitalis is bordered by a thick and broad crista tympanica, which extends from approximately 7 mm below the capitulum oticum ventromedially towards the processus medialis. The Port Louis specimen lacks pneumatic foramina in the fossa basiorbitalis. Most of the ventral portion of the pars mandibularis is taken up by the condylus medialis, which is wide and anteroposteriorly compressed. On the ventromedial margin of the pars mandibularis, and confluent with it, lies the small condylus pterygoideus, which is separated from the condylus medialis by a shallow, 'V'-shaped fossa. The articulation with the pterygoid is visible in the Copenhagen specimen (Fig. 8C). Whereas the condylus medialis with the condylus pterygoideus forms a transversely oriented

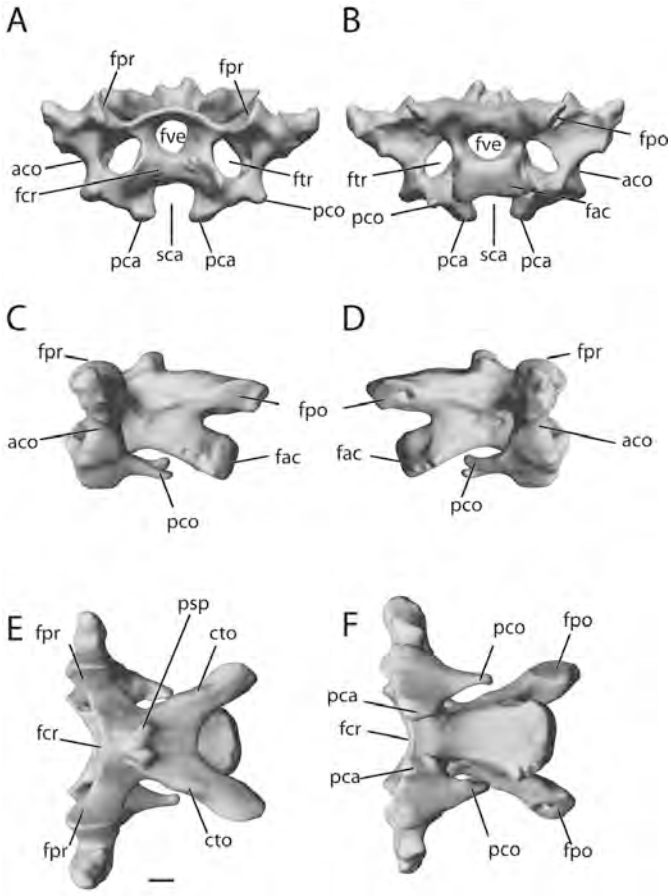

FIGURE 22. 3-D scans of presynsacral (cervical) vertebra 6, Durban specimen. **A**, cranial; **B**, caudal; **C**, left lateral; **D**, right lateral; **E**, dorsal; **F**, ventral views. Anatomical abbreviations as in Appendix 1. Scale bar equals 5 mm.

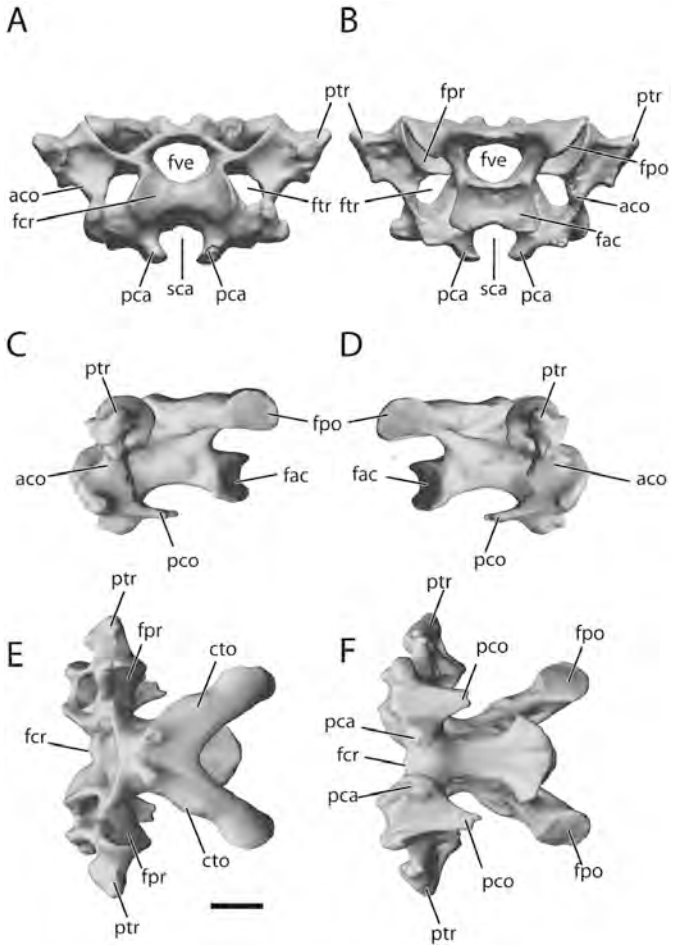

FIGURE 23. 3-D scans of presynsacral (cervical) vertebra 7, Durban specimen. **A**, cranial; **B**, caudal; **C**, left lateral; **D**, right lateral; **E**, dorsal; **F**, ventral views. Anatomical abbreviations as in Appendix 1. Scale bar equals 10 mm.

ridge, the condylus lateralis is a flattened surface on the ventral side of the processus lateralis. The condylus caudalis forms a flattened, rounded surface on the posterior side of the processus lateralis. The cup-shaped cotyla quadratojugularis is pronounced and deep and projects further anteriorly from the processus lateralis than in *Goura* and *Caloenas*. In anterior view, the angle between the processus medialis and the processus lateralis is ~90°, whereas it is larger in *Goura* and *Caloenas*. Posterodorsally, the pars oticus is stout and bears the large capitulum squamosum (laterally) and the slightly smaller capitulum oticum (medially). The capitulum squamosum is oblong and oriented anteroposteriorly and does not overhang the lateral facies of the pars oticus. The capitulum oticum is set posteromedially at an angle of 40° to the long axis of the capitulum squamosum and overhangs the medial facies of the corpus. The capitulum oticum is more globular, but becomes triangular in dorsal view, with the tip directed posteriad. The two capituli are connected by a ridge-like vallecula intercapitularis. Posteroventrally of the vallecula intercapitularis there is a large, rounded, and deep sulcus pneumaticus with several pneumatic foramina; according to Owen (1866), these pneumatic foramina communicate with the tympanic cavity. In *Caloenas, Goura*, or *Didunculus*, the sulcus pneumaticus is only very shallowly indicated, although in the latter two taxa, one or two small foramina were observed on the surface posteroventrally of the incisura intercapitularis.

Mandible—The mandible is gently curved: the posterior half is angled ventrally with respect to the anterior half at approximately 10° (Fig. 13; Pls. PL4, D4; Table 4). In *Caloenas, Goura*, and *Didunculus*, the mandible is angled more strongly (Fig. 10), whereas the curvature of the mandible is reduced in *Raphus* and *Pezophaps*. The mandibular rami are lateromedially thin but dorsoventrally deep, with their greatest depth just posterior to the processus coronoideus. In the Port Louis specimen, in dorsal view, the two rami curve inwards posteriorly of the processus coronoideus (Fig. 14B, C), but in the Copenhagen and Oxford specimens, the rami are straight in dorsal view (Fig. 14A, D, E). This is similar to the condition observed in *Pezophaps, Caloenas, Goura*, and *Didunculus*. At the symphysis mandibulae, the two mandibular rami diverge at an angle of approximately 25° and the apex of the rostrum mandibulae is deep and blunt. The outer surface of the rostrum mandibulae bears the openings of the foveae corpusculorum nervosorum. In both the Port Louis specimen and the Durban specimen, a break is visible posterior to the rugose area of the rostrum mandibulae that marks a unit of the ramphotheca. The anterior half of the mandibular ramus is formed by the mandibular symphysis, which is formed by the symphysis of the anterior parts of the dentary and the splenial. The dentary extends posteriorly from the mandibular symphysis and fuses with the splenial, which lies medially. Two vascular foramina penetrate the lateral side of the ramus, oriented anteroproximally and connected to form a groove on the lingual side of the bone. However, there is doubt regarding the degree of fusion

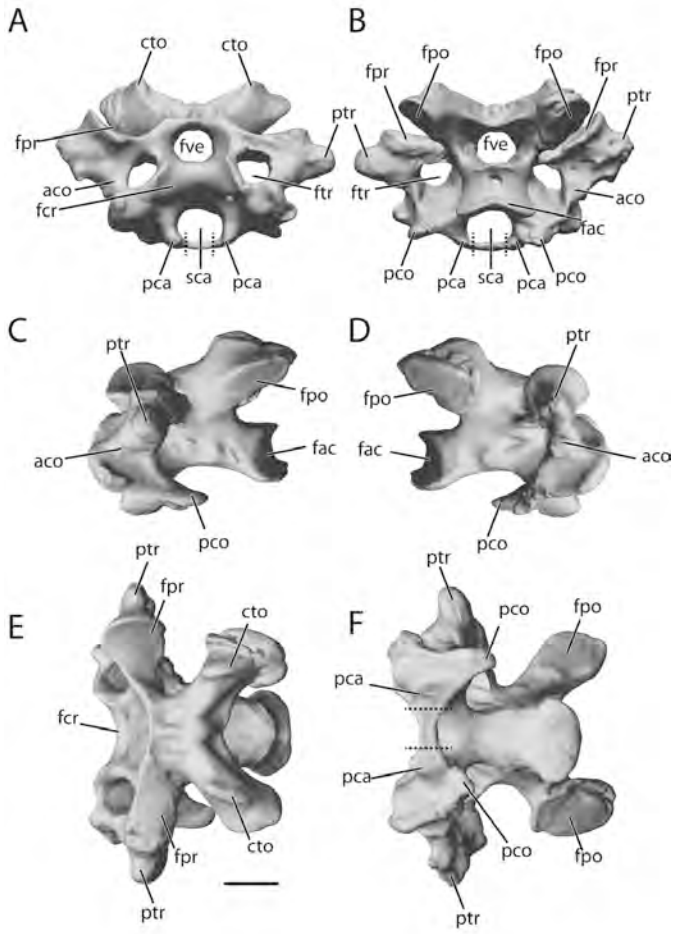

FIGURE 24. 3-D scans of presynsacral (cervical) vertebra 8, Durban specimen. **A**, cranial; **B**, caudal; **C**, left lateral; **D**, right lateral; **E**, dorsal; **F**, ventral views. Dashed lines mark area of incorrect plaster reconstruction enclosing the sulcus caroticus. Anatomical abbreviations as in Appendix 1. Scale bar equals 10 mm.

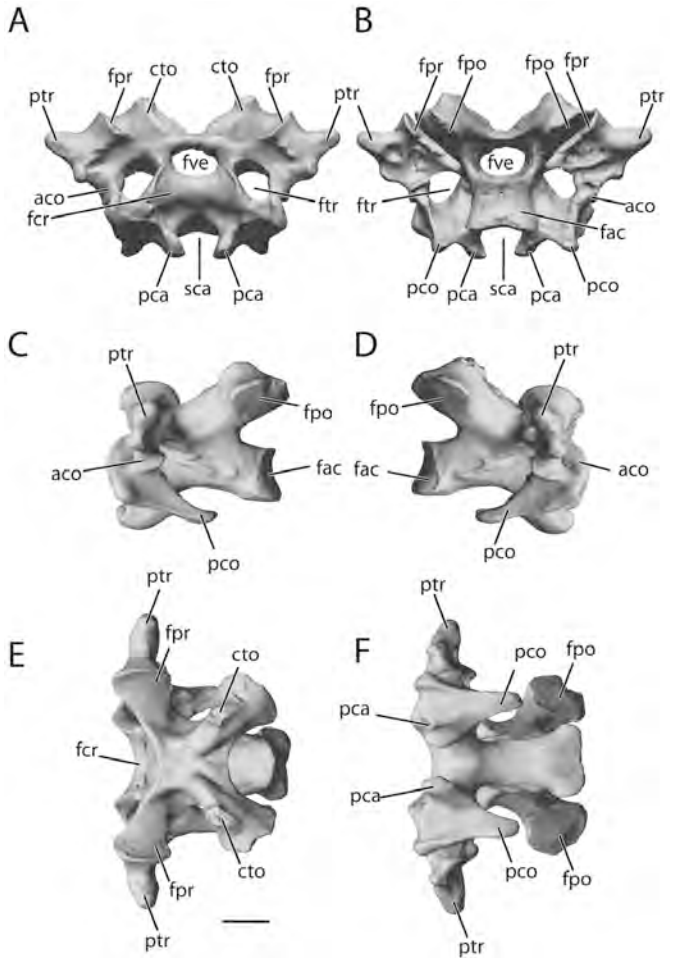

FIGURE 25. 3-D scans of presynsacral (cervical) vertebra 9, Durban specimen. **A**, cranial; **B**, caudal; **C**, left lateral; **D**, right lateral; **E**, dorsal; **F**, ventral views. Anatomical abbreviations as in Appendix 1. Scale bar equals 10 mm.

of the dentary with the splenial. Melville (in Strickland and Melville, 1848:95) stated that the splenial remained distinct, perhaps, to a late period of life, whereas Owen (1866:35) pondered if the splenial was ever distinct at all.

Posteriorly, the dentary, and the closely applied splenial, are forked into an upper and a lower part, with the lower part extending further posteriorly along the ventral edge of the mandibular ramus than on the upper part. The upper part receives the rostral part of the supra-angular; the lower part overlies the angular. In the Port Louis specimen, the sutures between the bones are not fused, and the left ramus has been reconstructed from the separate mandibular elements. The upper part of the dentary appears to be missing in both rami, because the rostral part of the supra-angular extends anteriorly on the dorsal edge of the dentary (compare the Port Louis specimen, Fig. 13A, B, with the Oxford specimen, Fig. 13E). In the Durban specimen, this part of the mandibular ramus has been partially reconstructed (Figs. 7A, B, 13C, D). There is only one mandibular fenestra, the fenestra rostralis mandibulae, located in the bifurcation of the dentary, similar to the condition seen in other columbids. The forked dentary is also observed in *Pezophaps* and extant columbids, although the upper part is missing in *Pezophaps* specimen NHMUK A3505, likely due to its fragile nature. The mandibular fenestra in *Pezophaps, Caloenas*, and *Goura* is distinct and rounded, but the fenestra is more slit-like in *Didunculus* (Fig. 10). The presence of visible sutures in other dodo mandibles, such as the Copenhagen and Oxford specimens (Fig. 13E–F), suggests that the anterior and posterior halves of the dodo mandibular ramus never fully fuse. This agrees with the fossil evidence: anterior and posterior halves of the rami have only been found as separate halves in historic and recent Dodo Research Programme collections. In *Pezophaps*, the two halves of the mandibular ramus also appear incompletely fused.

The posterior part of the mandibular ramus extends from the fenestra rostralis mandibularis to the fossa caudalis. On the lateral surface, the attachment of the adductor mandibulae externus muscle forms a distinct ridge extending posteriorly from the mandibular fenestra, which may be the ventral border of the supra-angular. In the Port Louis specimen, the processus coronoideus, the attachment point for the aponeurosis of the adductor mandibulae externus muscle, is visible as a small yet distinct protuberance on the dorsal edge of the mandible halfway between the angulus mandibulae and the posterior border of the mandible (Fig. 13A, B). It is missing on the right ramus in the Durban specimen (Fig. 13C), but visible on the left ramus (Fig. 13D). The angulus mandibulae is more pronounced in the Durban specimen (Fig. 13C, D), but this appears to be the result

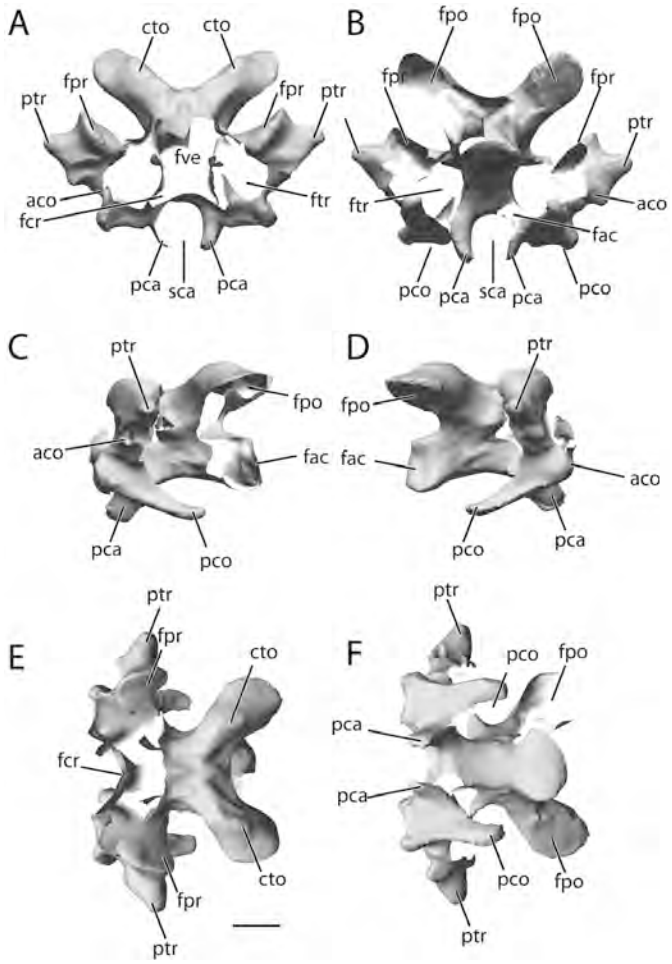

FIGURE 26. 3-D scans of presynsacral (cervical) vertebra 10, Port Louis specimen. Areas where no scan data were captured are translucent. **A**, cranial; **B**, caudal; **C**, left lateral; **D**, right lateral; **E**, dorsal; **F**, ventral views. Anatomical abbreviations as in Appendix 1. Scale bar equals 10 mm.

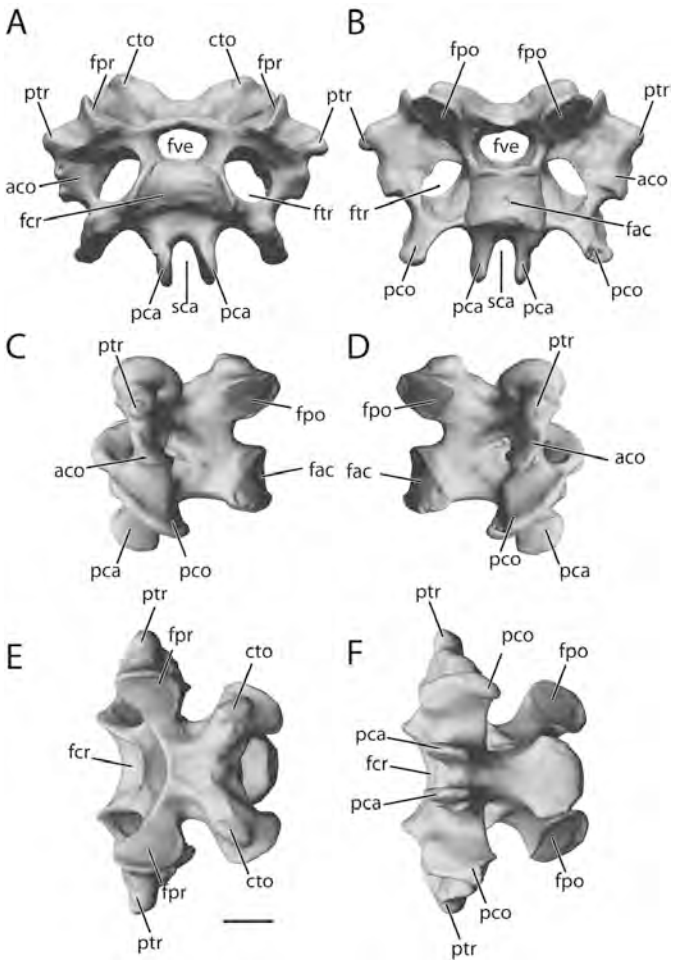

FIGURE 27. 3-D scans of presynsacral (cervical) vertebra 11, Durban specimen. **A**, cranial; **B**, caudal; **C**, left lateral; **D**, right lateral; **E**, dorsal; **F**, ventral views. Anatomical abbreviations as in Appendix 1. Scale bar equals 10 mm.

of restoration. In both rami of the mandible of the Durban specimen, the bone surface around this area is rough and differs from the adjoining areas due to the application of an artificial coating. The processus coronoideus is similarly small in *Goura, Caloenas, Didunculus*, and *Pezophaps*. In the former two species, it is located further posteriorly, whereas it attains a more proximal position in *Didunculus*.

The posterior end of the dodo mandible is significantly expanded medially (Fig. 14). The articular, forming the articulation of the mandible with the quadrate, fuses posteriorly with both the supra-angular and angular, but no suture is visible in adults. Note that in both the Port Louis specimen and the Durban specimen, the mandible has been glued to the cranium and cannot be separated for scanning; thus, inner surface detail has not been captured by the laser beam. The Copenhagen specimen, where the mandible is separate, therefore provides the best representation of the anatomy of the posterior end of the mandible (Fig. 14D, F). The observed flat surface of the cotylae in the 3-D model of the Port Louis specimen mandible (Fig. 14C) is an artifact of the 3-D scanning process. There is no discernible tuberculum pseudotemporale anterior to the fossa articularis quadratica, similar to the condition in *Caloenas* and *Goura*. The fossa articularis quadratica carries two cotylae, the anteroposteriorly oriented cotyla lateralis and the larger transversely oriented cotyla medialis (Fig. 14F), which articulate with the two condylae of the quadrate. The cotyla lateralis overhangs the lateral surface of the mandible and is elongated and slightly concave (see Copenhagen specimen; Figs. 8, 14F). Medially, the processus medialis mandibulae is large and triangular, and its tip is blunt and oriented dorsally. A lateromedially elongated foramen, the foramina pneumaticum articulare, is present on the dorsal surface of the processus medialis mandibulae, The processus medialis mandibulae carries the cotyla medialis, which is large, circular, and deeply excavated. It is posteriorly bordered by an anteroposteriorly narrow, ridge-like crista transversa fossae. The processus medialis mandibulae is similarly strongly developed in *Pezophaps*, but is located more posteriorly with respect to the cotyla lateralis. In *Caloenas* and *Goura*, the processus medialis mandibulae is less pronounced and is located more posteriorly with respect to *Raphus* as well (the posterior end of the mandible was not preserved in the *Didunculus* specimen available). In addition, the crista transversa fossae is broader anteroposteriorly in the latter two taxa. Posteriorly, the mandibular ramus in *Raphus* culminates in a short, ventrally directed processus retroarticularis. The fossa caudalis extends medially from the processus retroarticularis to the posterior surface of the processus mandibulae medialis. It is subtriangular in shape, shallowly concave, and oriented at a downward angle of 45° with respect to

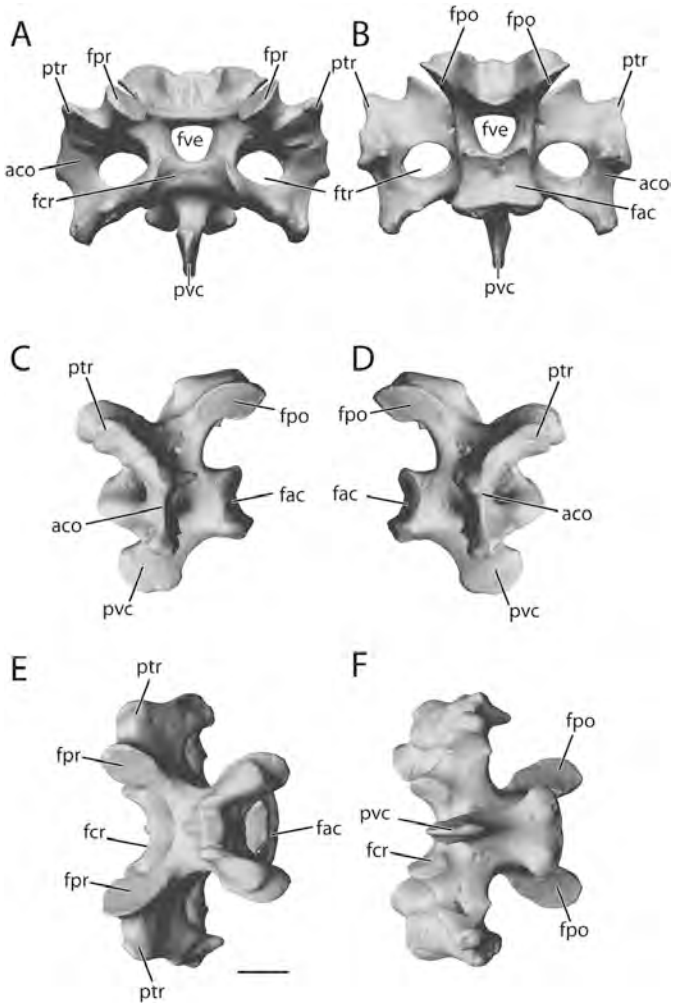

FIGURE 28. 3-D scans of presynsacral (cervical) vertebra 12, Durban specimen. **A**, cranial; **B**, caudal; **C**, left lateral; **D**, right lateral; **E**, dorsal; **F**, ventral views. Anatomical abbreviations as in Appendix 1. Scale bar equals 10 mm.

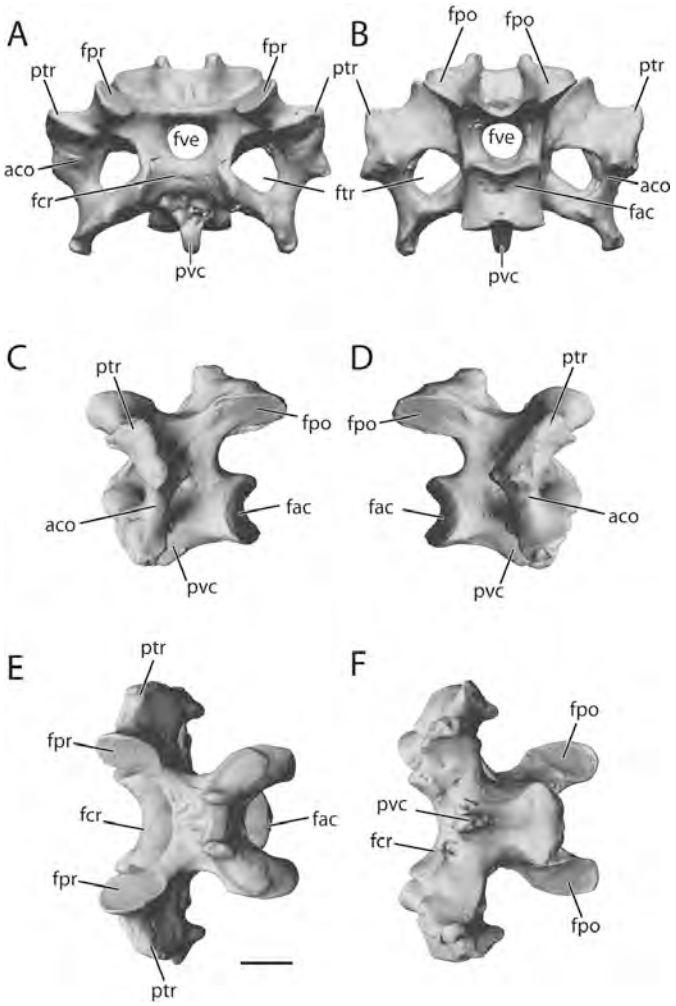

FIGURE 29. 3-D scans of presynsacral (cervical) vertebra 13, Durban specimen. **A**, cranial; **B**, caudal; **C**, left lateral; **D**, right lateral; **E**, dorsal; **F**, ventral views. Anatomical abbreviations as in Appendix 1. Scale bar equals 10 mm.

the long axis of the ramus. *Pezophaps* displays a similarly short processus retroarticularis and a convex fossa caudalis. In *Caloenas* and *Goura*, the processus retroarticularis is short as well, but in contrast to the dodo, the fossa caudalis in these taxa is convex.

Hyobranchial Skeleton—Etienne Thirioux, in his correspondence with Alfred Newton (see also Claessens and Hume, 2015), mentioned the recovery of skeletal remains of the dodo hyoid and even the purported remains of the tongue, which he fixed in alcohol (UMZC Thirioux-Newton correspondences 9 [September 5, 1900], 13 [January 31, 1901], and 17 [November 13, 1901]). However, no remains that could be unambiguously identified as belonging to the hyobranchial skeleton were recovered in the MI, DNSM, and UMZC collections.

Scleral Ossicles—There are no scleral bones preserved with the Durban or Port Louis specimen, and scleral skeletal elements are also not known from the UMZC Thirioux collection. However, they are preserved in the Oxford and Copenhagen dodo skulls. The scleral rings of the Oxford and Copenhagen dodos consist of 11 approximately equal-sized rectangular to trapezoid ossicles, which is a low number of ossicles in comparison with many extant birds, but similar to other columbiforms (e.g., Curtis and Miller, 1938; Lima et al., 2009). *Raphus* exhibits the same unique arrangement of over- and underplates as other columbiforms (Fig. 15A–C).

Axial Skeleton

The axial skeleton of the dodo as revealed by the Port Louis and the Durban specimens (Figs. 16–39; Pls. PL5–PL26, D5–D26; Tables 5–7) consists of 19 presynsacral vertebrae (i.e., 14 cervical, one cervicodorsal, and four thoracic vertebrae, of which the first three are fused into a notarium), approximately 16 synsacral vertebrae, six free caudal vertebrae, and a pygostyle (Fig. 1A, B; 16A–E). There is one elongate cervicodorsal rib (costa cervicodorsalis), four true ribs (costae vertebralis verae) that articulate with the sternum via sternal ribs (costae sternalis), and one additional rib segment on the first synsacral vertebra that articulates indirectly with the sternum through contact between its sternal rib and the sternal rib of the preceding 19th (caudal-most) thoracic vertebra. The ribs in the mounted skeleton each articulate with corresponding fovea costalis tuberculi et capituli. The sternum is large, although slightly comparatively reduced in overall size relative to the sterna of other, much smaller volant columbids, such as *Goura, Caloenas, Didunculus*, or *Columba*.

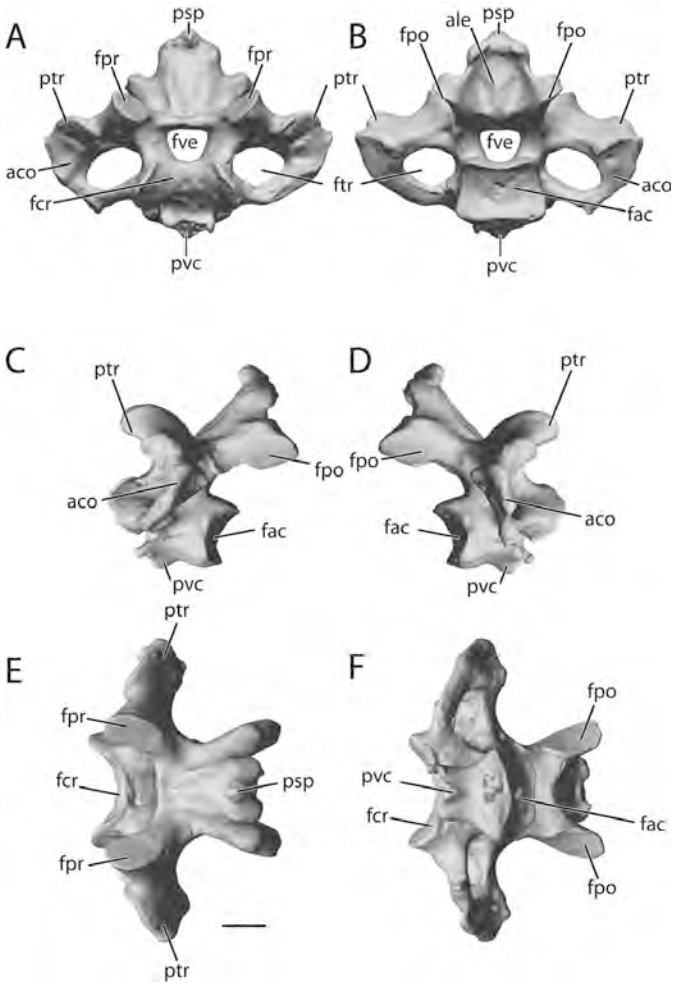

FIGURE 30. 3-D scans of presynsacral (cervical) vertebra 14, Durban specimen. **A**, cranial; **B**, caudal; **C**, left lateral; **D**, right lateral; **E**, dorsal; **F**, ventral views. Anatomical abbreviations as in Appendix 1. Scale bar equals 10 mm.

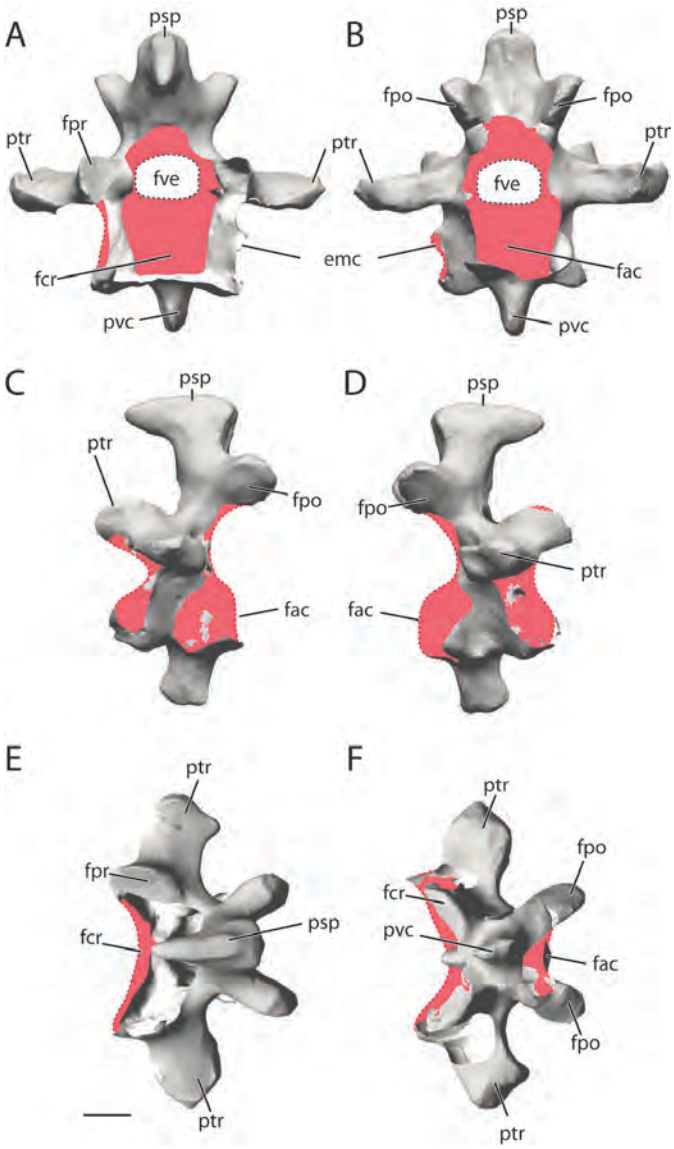

FIGURE 31. 3-D scans of presynsacral (cervicodorsal) vertebra 15, Port Louis specimen. Due to the large amount of missing scan data, especially in the cranial and caudal planes, raw scan data are shown here, superimposed upon a generalized outline. **A**, cranial; **B**, caudal; **C**, left lateral; **D**, right lateral; **E**, dorsal; **F**, ventral views. Anatomical abbreviations as in Appendix 1. Scale bar equals 10 mm.

Atlas—The fossa condyloidea on the cranial surface of the corpus atlantis is deep and rounded and articulates with the condylus occipitalis of the skull (Figs. 16A, B, 17A–L; Pls. PL5, D5). The dorsal margin is incised by the incisura fossae, which provides an opening for the dens of the axis (Fig. 17). The opening for the spinal cord is oval and wide laterally. The ventral surface of the corpus atlantis is rectangular. It is angled caudally and extends underneath the cranioventral margin of the axis. A diminutive processus ventralis corporis (hypapophysis) is present in the caudoventral midline (Fig. 17). The facies articularis axialis possesses a broad and deep sulcus ventrally, demarcated by the caudoventral extension of the corpus atlantis (Fig. 17). The processus articularis caudales are small, face medially, and are positioned high on the arcus atlantis. The atlas also lacks a foramen transversarium.

Axis—The axis articulates with the corpus atlas along a broad oval facies articularis atlantica and the dens. It also articulates with the arcus atlantis via the prezygapophyses (processus articulares craniales). The dens projects cranially from the corpus axis and is positioned dorsal to the facies articularis atlantica. It is robust and its rounded cranial extremity contains a small depression for the ligament connecting to the atlas, the fovea ligamenti collateralis atlantoaxialis (Fig. 18A; Pls. PL5, D5). The facies articularis zygapophyses craniales are small and face laterally. The axis increases in size caudally, and the facies articularis zygapophyses caudales are large, face ventrally, and are slightly curved medially (Fig. 18). Dorsally, each processus articularis caudalis possesses a robust tuberculum dorsalis. The facies articularis caudalis of the corpus axis is heterocoelous and deeper than it is wide. The foramen vertebrale is arched dorsoventrally, with the angle of its floor above the facies articularis caudalis inclined approximately 25° ventrally in comparison with the dorsal margin of the dens and the more cranial part. The neural spine is robust; its caudal margin, and especially its cranial margin, is inclined caudally. A pronounced area ligamentum elastici is present at the base of the processus spinosus on the caudal side. The processus ventralis is deep, and the corpus axis is incised ventrally, which visually adds to the depth of the processus ventralis. A thin lamina extends between the cranial and caudal articular processes. A small, dorsoventrally directed foramen

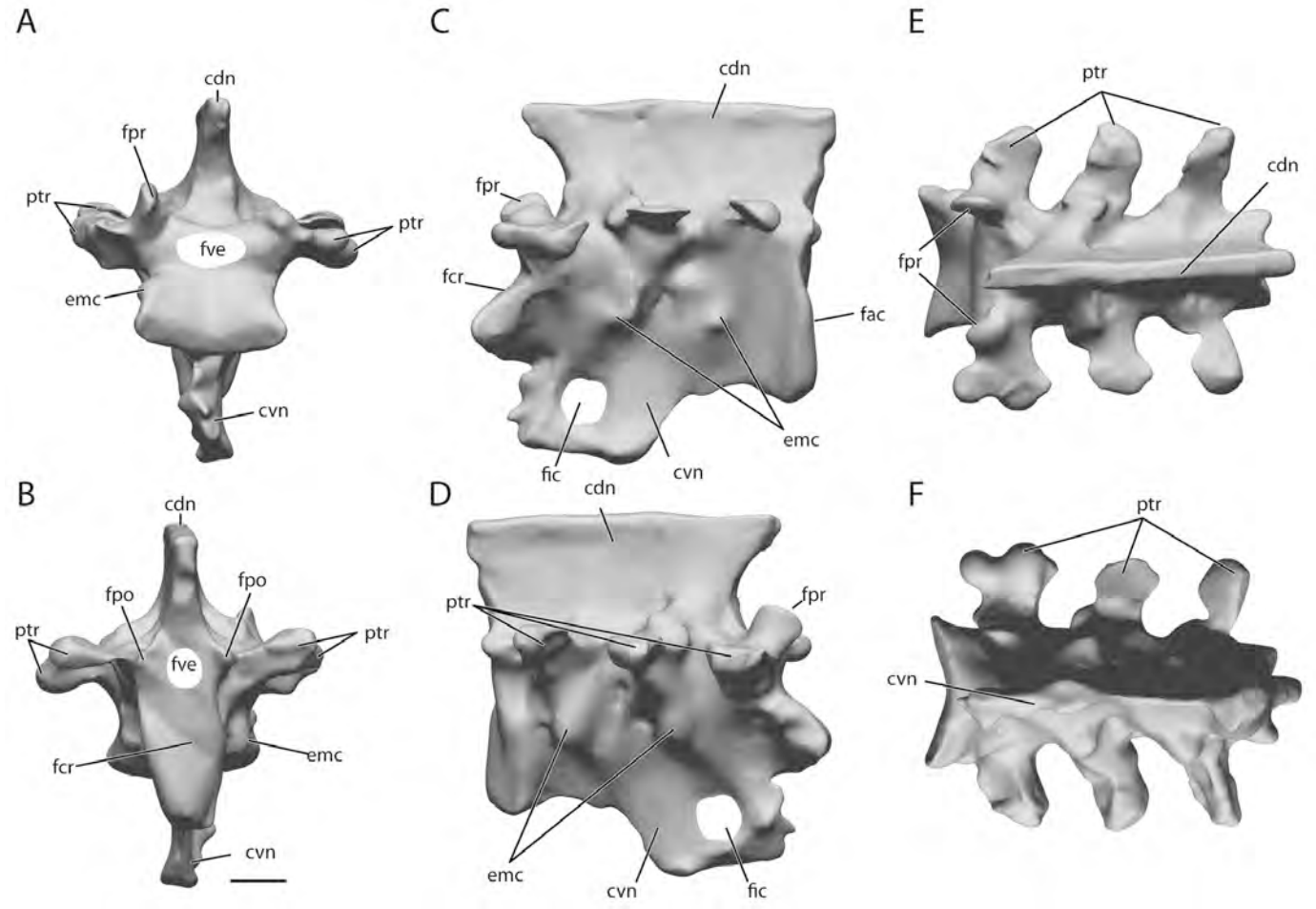

FIGURE 32. 3-D scan reconstruction of the notarium (presynsacral thoracic vertebrae 16–18), Durban specimen. Cranial and caudal articular surfaces have been digitally closed to provide a generalized outline. **A**, cranial; **B**, caudal; **C**, left lateral; **D**, right lateral; **E**, dorsal; **F**, ventral views. Anatomical abbreviations as in Appendix 1. Scale bar equals 10 mm.

transversarium is present laterally between the ansa costotransversaria and the arcus axialis. In the Durban specimen, the left ansa costotransversaria is broken and the lateral margin of the foramen is not preserved.

Presynsacral (Cervical) Vertebra 3—The third cervical vertebra also possesses a large processus ventralis on the corpus vertebrae, which contains a relatively ventrally positioned facies articularis caudalis (Fig. 19; Pls. PL6, D6), similar to the axis. The facies articularis cranialis extends from the cranial onto the ventral side of the corpus vertebrae, which is indicative of a large degree of potential ventral flexion at the C2–C3 joint. The ansae costotransversaria bear a short processus costalis ventral to the processus articulares craniales. The foramina transversaria are large. The facies articularis zygapophyses caudales are large and face dorsomedially. The facies articularis zygapophyses craniales are inclined ventrally. The processus spinosus is relatively short and positioned caudally on the mid-dorsal surface of the arcus vertebrae (neural arch). A pronounced area for the attachment of the ligamentum elastici is present caudally at the base of the processus spinosus. A lamina extends horizontally between the zygapophyseal processes, similar to but slightly more robust than that observed on the axis. Dorsally at mid-length, there is a small circular foramen arcocostalis cranialis, which passes through to the caudal side of the facies articularis cranialis.

Presynsacral (Cervical) Vertebra 4—The fourth cervical vertebra does not have a prominently developed processus ventralis (Fig. 20; Pls. PL6, D6), unlike the axis and the third cervical vertebra, but it has a thin mid-ventral ridge on the ventral surface of the corpus vertebrae. The facies articularis zygapophyses craniales face cranioventrally. The facies articularis cranialis extends along the cranial and ventral margins of the corpus vertebrae, similar to but to a somewhat lesser extent than the third cervical vertebra. It has a relatively deep fovea cranioventralis, indicating a capacity for a relatively high degree of ventral flexion at the C3–C4 joint. Short ossa costalia vera (cervical ribs) are ankylosed to the craniolateral surface of the corpus and arcus vertebra, ventral to the processus articulares craniales. The foramen transversarium is slightly larger than in the third cervical vertebra. A tuberculum caudalis is present on the postzygapophyses. The facies articularis zygapophyses caudales face ventrally and are smaller than the facies articularis zygapophyses craniales. The transverse width of the arcus vertebrae along the postzygapophyses is slightly less than the transverse width at the level of the prezygapophyses. The facies articularis caudalis of the corpus vertebrae is heterocoelous and approximately square in shape. The processus spinosus is short and positioned further caudally on the arcus vertebrae. The cranial

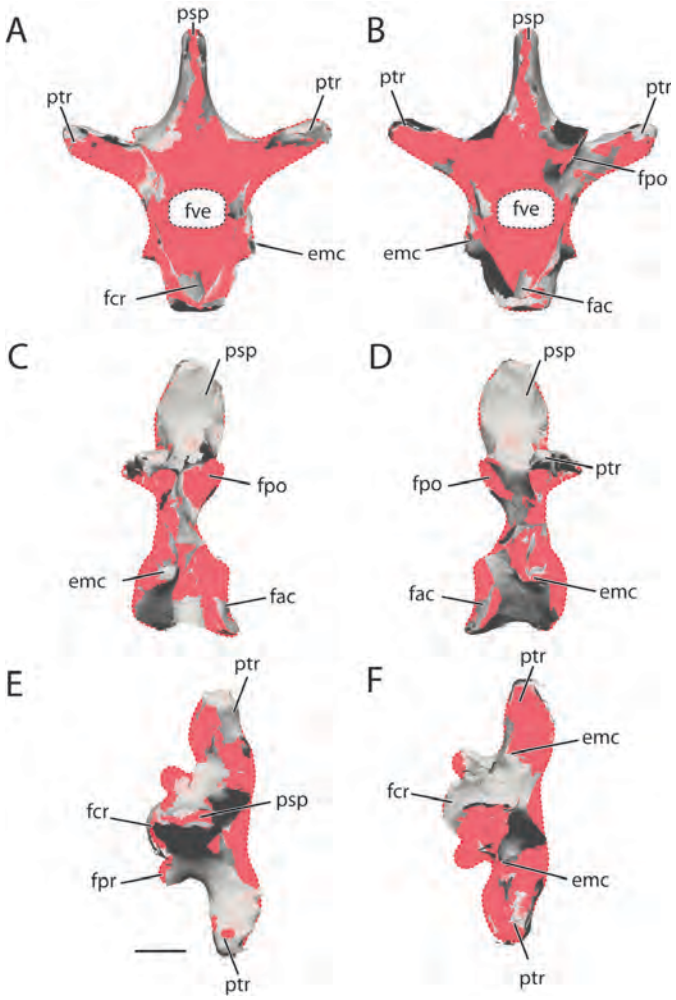

FIGURE 33. 3-D scans of presynsacral (thoracic) vertebra 19, Port Louis specimen. Due to the large amount of missing scan data, especially in the cranial and caudal planes, raw scan data are shown here, superimposed on a generalized outline. **A**, cranial; **B**, caudal; **C**, left lateral; **D**, right lateral; **E**, dorsal; **F**, ventral views. Anatomical abbreviations as in Appendix 1. Scale bar equals 10 mm.

and caudal areas for the ligamentum elastici at the base of the processus spinosus are deep and well developed.

Presynsacral (Cervical) Vertebra 5—The ansae costotransversaria of the fifth cervical vertebra extend laterally beyond the prezygapophyseal articular facets (Fig. 21; Pls. PL7, D7). The foramen transversarium is slightly larger than in the preceding vertebrae. The processus spinosus is narrow and relatively short and is positioned in the middle of the arcus vertebrae. A shallow depression for the ligamentum elastici is present cranially at the base of the processus spinosus, whereas the caudal area ligamentum elastici is deep. The facies articularis cranialis extends along the cranial and ventral surfaces. Cranioventrally, the facies articularis corpus vertebrae is bordered by two processus carotici that border a relatively shallow sulcus caroticus. The facies articularis zygapophyses craniales are relatively small and inclined craniomedially. The postzygapophyses are elongated caudally and extend beyond the corpus vertebrae and facies articularis caudalis corpus vertebrae. A low crista transversarium obliqua is present on the dorsal surface of the postzygapophyses. The facies articularis zygapophyses caudales face ventrally and are elongate craniocaudally. The facies articularis caudalis is wider than high, unlike in the preceding vertebrae (C3, C4), in which it is deeper than it is wide. Similar to the preceding vertebrae, the facies articularis caudalis is heterocoelous.

Presynsacral (Cervical) Vertebra 6—The corpus of the sixth cervical vertebra is longer than that of cervical vertebrae 3–5 (Figs. 16A, B, 22; Pls. PL7, D7). The processus costalis extends further caudad than in the preceding vertebrae and is more than half the length of the corpus, whereas it is less than half the length of the corpus in cervical vertebrae 3–5. The foramen transversarium is approximately equal in diameter to that of the preceding fifth cervical vertebra. The facies articularis cranialis is wide and low and is positioned mostly on the cranial surface of the corpus vertebrae. A shallow fovea cranioventralis is present on the ventral surface. The processus carotici extend further ventrally than in the preceding vertebra. The processus transversi extend laterally well beyond the prezygapophyseal articular facets, which are directed dorsomedially. The processus transversi possess a deep dorsal sulcus flanked by a large dorsolateral tubercle. Rather than a single midline processus spinosus, two low dorsal contralateral tubercles are present on the arcus vertebrae. The postzygapophyses extend far caudally and have a low crista transversarium obliqua on their dorsal surface. The facies articularis zygapophyses caudales are directed ventromedially.

Raphus differs from *Pezophaps* in the zygapophysis cranialis being directed further laterally and laterally more expanded, less pointed, and in having the sulcus on the processus transversus being deeper; otherwise they are similar. *Raphus* differs from *Caloenas, Didunculus*, and *Goura* in being less elongate, with the zygapophysis cranialis directed further laterally, and the facies articularis caudalis being more expanded.

Presynsacral (Cervical) Vertebra 7—The seventh cervical vertebra (Fig. 23; Pls. PL8, D8) is relatively similar in overall morphology to the sixth. The facies articularis cranialis is wide and slightly taller than that of the sixth cervical vertebra. The fovea cranioventralis is located partially on the cranial surface, rather than solely on the ventral surface of the corpus. The cranial margin of the arcus vertebrae is set slightly further caudally than in the preceding cervical vertebrae, and the facies articularis cranialis extends from the cranial surface of the corpus vertebrae onto the floor of the foramen vertebrale. Together with the orientation of the prezygapophyseal articular facets, this seems to indicate a change in the angle at which the neck was held at rest, marking the start of cervical dorsal flexion leading up to the trunk. Similar to the sixth cervical, the ventral extremities of the processus carotici are inclined medially, and the sulcus caroticus resembles a ventrally open canal. Furthermore, and as also exhibited in the sixth cervical vertebra, the transverse width of the seventh cervical is greatest along the prezygapophyses, and the transversi processus extend well beyond the facies articularis zygapophyses craniales, which are directed dorsomedially. Dorsal on the arcus vertebrae, slightly cranial to the midpoint of the corpus, two low contralateral tubercles are present, rather than a single midline processus spinosus. The postzygapophyses extend beyond the caudal margin of the corpus, and the postzygapophyseal articular facets are directed ventromedially. The facies articularis caudalis is wide and heterocoelous.

Presynsacral (Cervical) Vertebra 8—The eighth cervical vertebra (Fig. 24; Pls. PL8, D8) is slightly broader and slightly more robust than the seventh. The processus transversi extend further laterally than the postzygapophyses, similar to the seventh cervical, but the facies articularis zygapophyses craniales of the eight cervical are larger and extend further than in the seventh cervical vertebra. The facies articularis zygapophyses craniales are directed dorsomedially, but are less medially inclined than the sixth and seventh cervical vertebrae. The ansa costotransversarium is robust, and the dorsal tubercle of the processus is lower in position than in the seventh cervical vertebra (i.e., mid-height

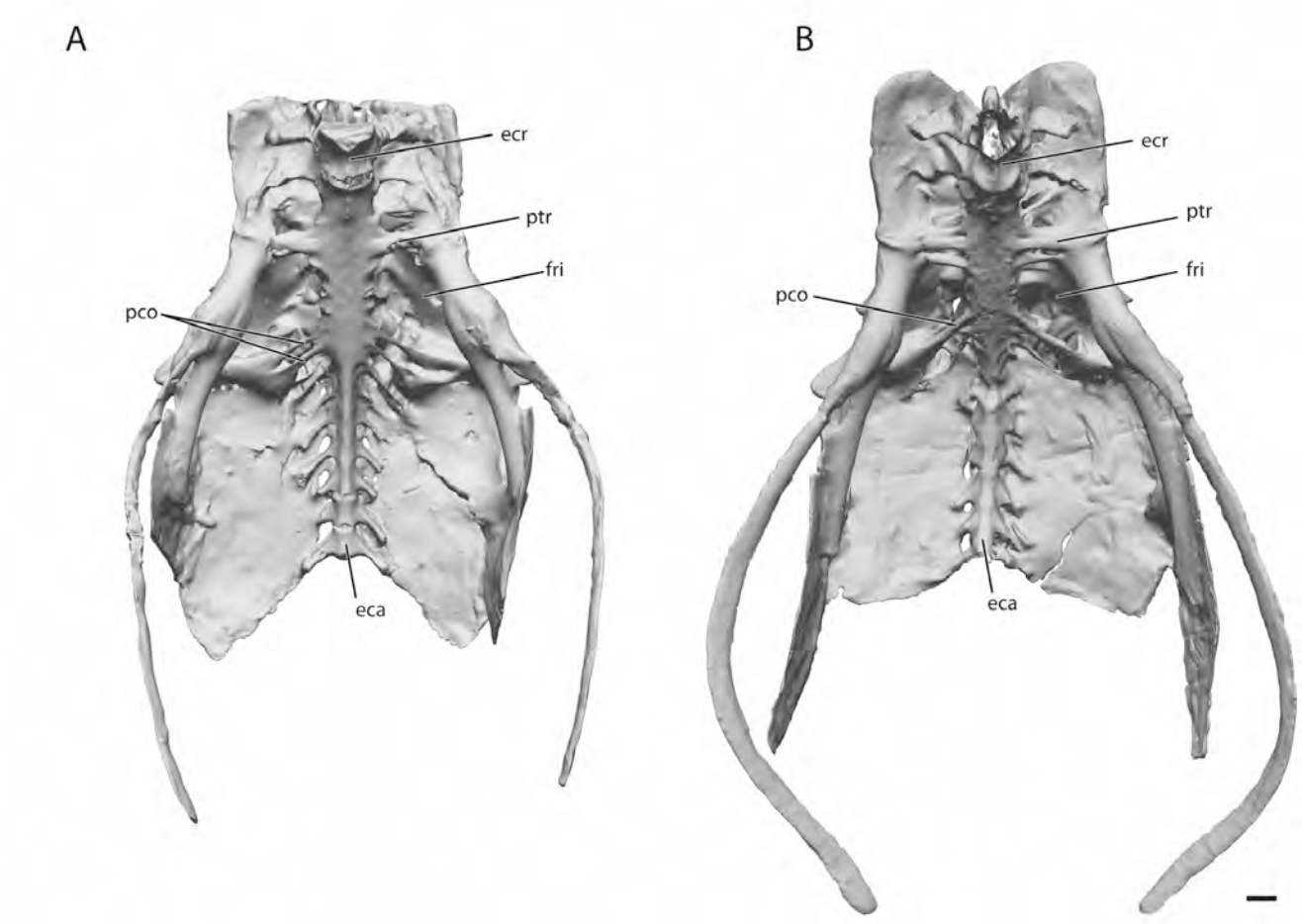

FIGURE 34. 3-D scans of the pelvis in ventral view of the Port Louis (**A**) and Durban (**B**) specimens, showing details of the synsacrum. Anatomical abbreviations as in Appendix 1. Scale bar equals 1 cm.

of the ventromedially inclined facies articularis zygapophyses craniales). The foramen transversarium is approximately equal in size to that of the preceding cervical vertebrae. The cranial margin of the arcus vertebrae is set further caudally than in the seventh cervical vertebra, and the facies articularis extends slightly onto the floor of the foramen vertebrale, indicating capacity for dorsal flexion at this location and change in orientation of the cervical vertebral column toward the subhorizontal vertebral orientation in the trunk. There is a low mid-ventral ridge on the dorsal surface of the arcus vertebrae, flanked by two fossae that are bordered by two low lateral ridges. The postzygapophyses carry a low tubercle or ridge on their dorsal surface. In the Durban specimen, the processus carotici connect in the midline; however, this connection is the result of artificial infilling that has been added between the distal extremities of the processus carotici. There is no indication that these processes actually connected in the specimen, and they do not connect in the ventral midline of the eighth cervical vertebra of the Port Louis specimen. The left ansa costotransversarium and left processus transversus of the eighth cervical of the Durban specimen also have been reconstructed, and the facies articularis zygapophyses craniales are missing. The right postzygapophysis of the Durban specimen is pathological and appears to have experienced additional ossification and ventral displacement of the right facies articularis zygapophyses caudales. The facies articularis caudalis of the eighth cervical vertebra is broader than it is deep, but more square than in the preceding cervical vertebrae.

Presynsacral (Cervical) Vertebra 9—The ninth cervical vertebra (Fig. 25; Pls. PL9, D9) is again slightly more robust than the eighth. The processus transversi extend further laterally than the postzygapophyses. The facies articularis zygapophyses craniales are inclined ventromedially. The ansa costotransversarium is robust, and the processus costalis is more than half the length of the corpus. The dorsal tubercles of the prezygapophyses are positioned at approximately mid-height of the dorsomedially facing prezygapophyseal articular facets, similar to the eighth cervical vertebra. The foramen transversarium is slightly larger than that of the preceding cervical vertebrae. The cranial margin of the arcus vertebrae is positioned slightly more caudally than the facies articularis cranialis. The facies articularis cranialis extends onto the floor of the foramen vertebrale, indicating capacity for a large degree of dorsal flexion at the C8–C9 joint, similar to the preceding two cervical vertebral joints. There is no processus spinosus on the arcus vertebrae. The postzygapophyses carry a distinct tubercle or ridge on their dorsal surface. The articular surface of the postzygapophyses is nearly circular and inclined ventromedially. The processus carotici extend ventrally and curve medially: the sulcus caroticus is open ventrally and semicircular in the Durban specimen, but is enclosed by a thin ventral lamina in the Port Louis specimen. The facies articularis caudalis of the ninth cervical vertebra is only slightly broader than it is deep, similar to the preceding vertebra.

Presynsacral (Cervical) Vertebra 10—The 10th cervical vertebra (Fig. 26; Pl. PL9) was discarded from the Durban specimen

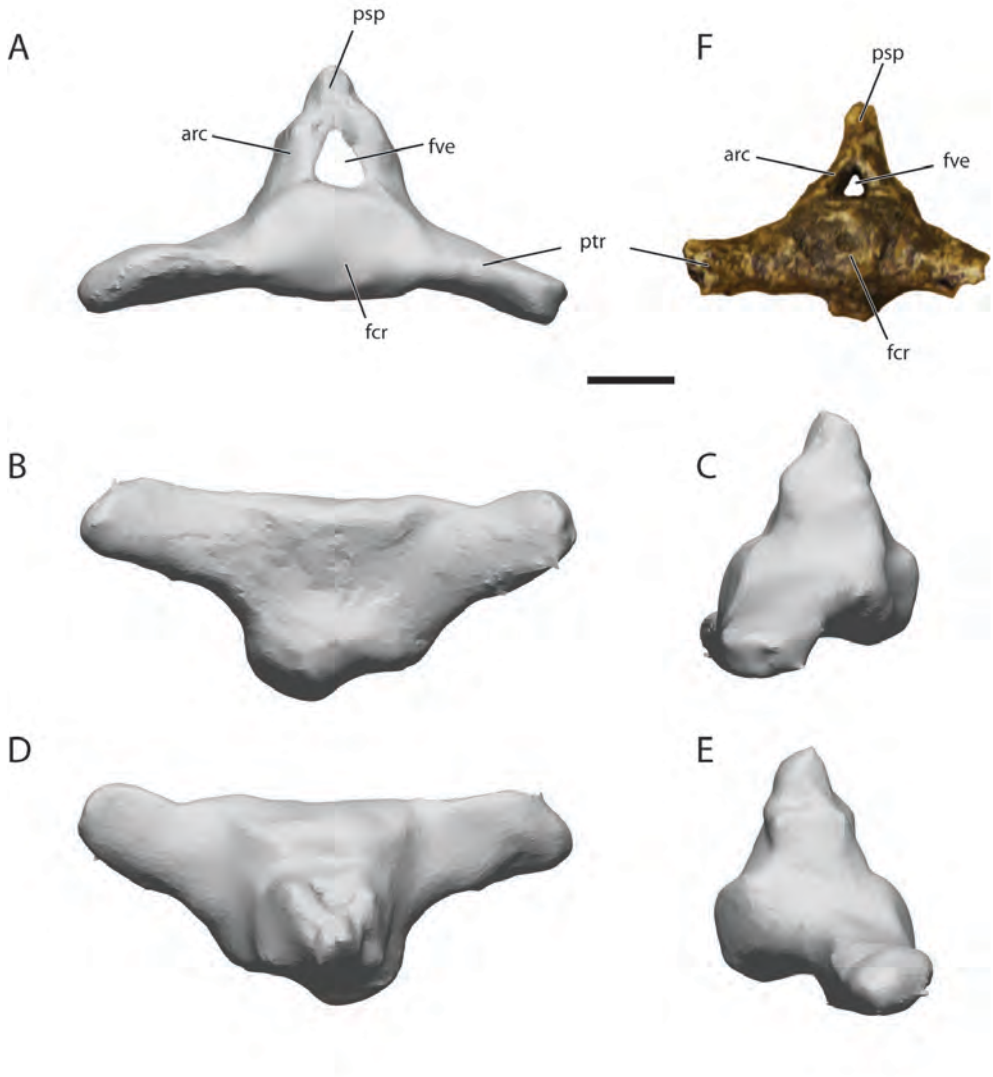

FIGURE 35. 3-D scans of the first free caudal vertebra of the Port Louis specimen (**A**–**E**) in **A**, cranial (facies articularis cranialis digitally reconstructed); **B**, ventral; **C**, left lateral; **D**, dorsal; and **E**, right lateral views; **F**, photograph of cranial facies of free caudal vertebra from the UMZC Thirioux collection (UMZC 415.KK), distal processus transversi broken. Anatomical abbreviations as in Appendix 1. Scale bar equals 5 mm.

early in the 20th century (see Claessens and Hume, 2015), but is present in the Port Louis specimen. The 10th cervical vertebra is quite similar in general morphology to the ninth. The processus costales are longer in C10 of the Port Louis specimen than in C9. The processus transversi extend further laterally than the postzygapophyses. The facies articularis zygapophyses craniales are directed dorsomedially. The ansa costotransversarium is robust. The dorsolateral tubercle of the processus transversus is positioned at approximately mid-height of the ventromedially inclined prezygapophyseal articular facets, similar to the eighth and ninth cervical vertebrae. The cranial margin of the arcus vertebrae is positioned slightly more caudal than the facies articularis. The facies articularis cranialis extends onto the floor of the foramen vertebrale, indicative of the capacity for a large degree of dorsal flexion at the C9–C10 joint. Similar to the preceding cervical vertebrae, there is no processus spinosus. The postzygapophyses carry a distinct tubercle or ridge on their dorsal surface. The articular surface of the postzygapophyses is nearly circular and inclined ventromedially. The processus carotici extend ventrally and curve medially. The sulcus caroticus is open ventrally and is semicircular. The facies articularis caudalis of the eighth cervical vertebra is slightly broader than it is deep, similar to the eighth and ninth cervical vertebrae.

Presynsacral (Cervical) Vertebra 11—The 11th cervical vertebra (Fig. 27; Pls. PL10, D10) is more robust than the preceding 9th and 10th vertebrae. Similar to the preceding vertebrae, the processus transversi extend further laterally than the postzygapophyses. The facies articularis zygapophyses craniales are directed dorsomedially. The ansa costotransversarium is more robust than in the preceding vertebrae. The processus costalis is stout and approximately half the length of the corpus vertebrae. The tubercles of the processus transversus are positioned more laterally than dorsally and are positioned at approximately bottom-height of the facies articularis zygapophyses craniales. The foramen transversarium is larger than that of the preceding vertebrae. The cranial margin of the arcus vertebrae is positioned further caudally than the facies articularis cranialis. The facies articularis cranialis extends from the cranioventral surface of the

FIGURE 36. 3-D scans of right cervicodorsal (I), thoracic (II–V), and synsacral (VI) vertebral ribs, Port Louis specimen. **A**, lateral view; **B**, proximal articular view; **C**, cranial view. Anatomical abbreviations as in Appendix 1. Obstructed portions of the proximal and distal articular facets digitally reconstructed. Scale bar equals 10 mm.

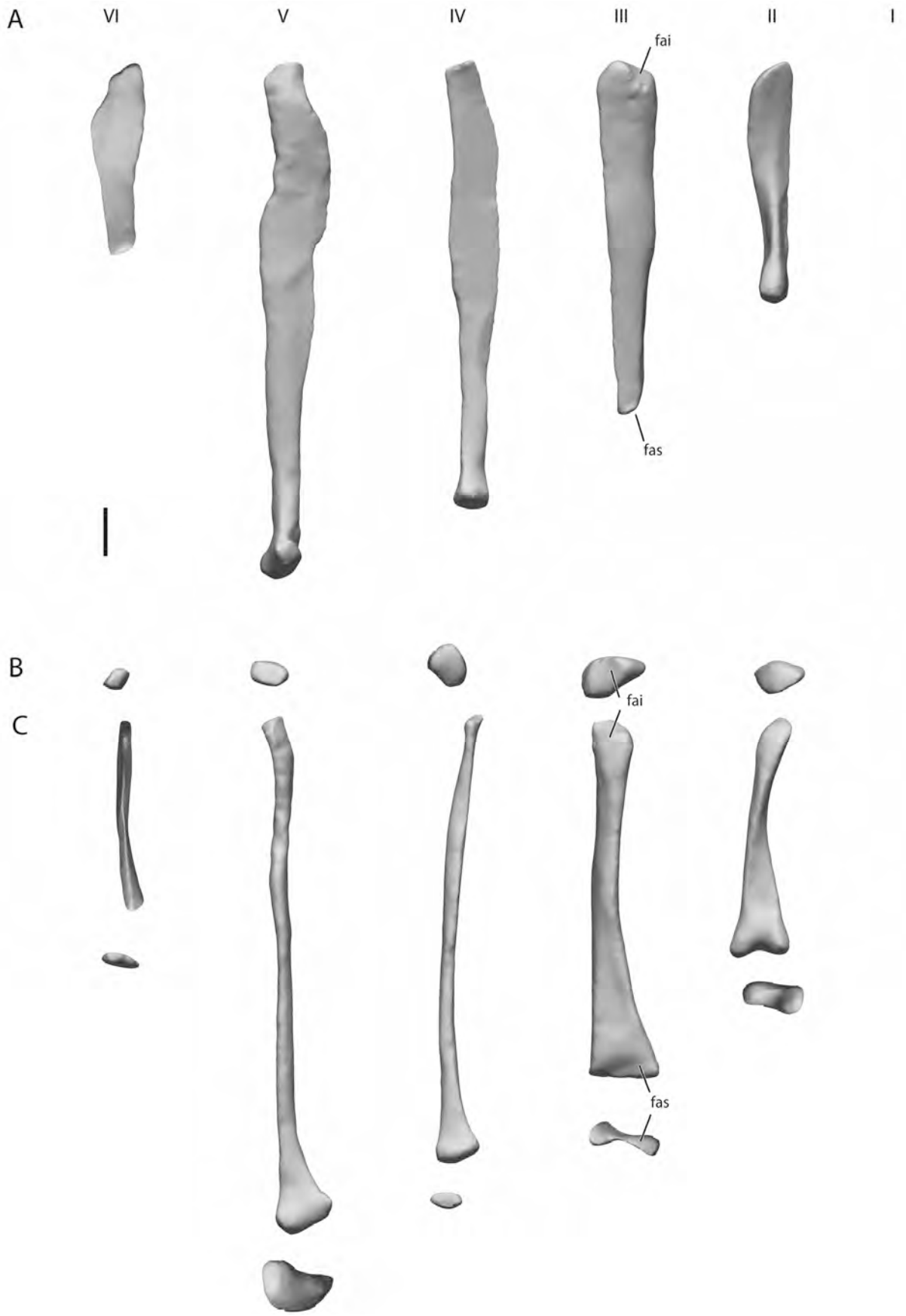

FIGURE 37. 3-D scans of right thoracic (II–V) and synsacral (VI) sternal ribs, Port Louis specimen. **A**, lateral view; **B**, proximal articular view; **C**, cranial view and distal articular view. Anatomical abbreviations as in Appendix 1. Obstructed portions of the proximal and distal articular facets digitally reconstructed. Scale bar equals 1 cm.

FIGURE 38. Photographs of the sternum and nearby skeletal elements. **A**, left lateral view, Port Louis specimen; **B**, right lateral view, Durban specimen; **C**, close-up of margo costalis sterni, left lateral view, Port Louis specimen; **D**, close-up of margo costalis sterni, right lateral view, Durban specimen; **E**, cranial view, Port Louis specimen; **F**, cranial view, Durban specimen.

FIGURE 39. 3-D scan images of the sternum of the Port Louis specimen. **A**, cranial view; **B**, caudal view; **C**, dorsal view; **D**, ventral view; **E**, left lateral view; **F**, right lateral view. Anatomical abbreviations as in Appendix 1. Scale bar equals 20 mm.

TABLE 4. Measurements of the dodo mandible (in mm).

Dimension	Port Louis	Durban
Length of ramus from tip of rostrum mandibulae to fossa caudalis	188 (L) 182 (R)	186 (L) 184 (R)
Maximum height of ramus (at angulus mandibulae)	25 (L) 24 (R)	23 (L) 28 (R)
Length of rostrum mandibulae along ventral side	29	30
Width of mandible across fossae caudalis	71	78
Depth of fossa caudalis	27 (L) 26 (R)	23 (L) 23 (R)
Width of fossa caudalis	32 (L) 29 (R)	29 (L) 26 (R)

corpus to the floor of the foramen vertebrale, indicating the capacity for a relatively large degree of dorsiflexion as well as ventral flexion. A distinct fovea cranioventralis is present immediately caudoventral to the facies articularis cranialis, cranial to the processus carotici. The processus carotici are positioned closer together than in the preceding cervical vertebrae and their ventral extremities do not curve medially; instead, they extend straight ventrally. The sulcus caroticus does not have a ventral bony margin and there is no processus spinosus. The postzygapophyses carry a distinct tubercle on their dorsal surface. The articular surface of the postzygapophyses is nearly circular and is directed ventromedially. The facies articularis caudalis of the 11th cervical vertebra is large and only slightly broader than it is deep, similar to the preceding vertebrae.

Presynsacral (Cervical) Vertebra 12—The processus transversi of the 12th cervical vertebra (Fig. 28; Pls. PL10, D10)

TABLE 5. Measurements of the vertebral column (in mm).

	Port Louis		Durban	
Vertebra	Length	Width	Length	Width
V1	9	26	7	24
V2	36	34	28	35
V3	34	37	26	31
V4	33	30	30	34
V5	41	44	30	44
V6	40	53	34	56
V7	35	56	35	54
V8	30	55	35	55
V9	30	53	37	61
V10	34	58	—	—
V11	35	53	38	56
V12	35	54	30	52
V13	33	58	31	54
V14	38	59	28	65
V15	36	61	31	54
Notarium (V16, 17, 18)	45	60	53	48
V19	10	50	21	57
V20 (first synsacral vertebra)		53		55
Free caudal vertebrae and pygostyle (combined)	51	27	38	25

extend further laterally than the postzygapophyses, similar to the preceding vertebrae. The facies articularis zygapophyses craniales are directed dorsomedially. The ansa costotransversarium is very robust, similar to the 11th cervical vertebra, lacks a processus costalis, and its ventral margin is even thicker than in the preceding vertebra. The tubercles of the transverse processes are positioned laterally at approximately mid- to bottom-height of the facies articularis zygapophyses craniales. The foramen transversarium is large. The cranial margin of the arcus vertebrae is positioned further caudally than the facies articularis, which extends over the cranial and cranioventral surfaces of the corpus, but not significantly onto the floor of the foramen vertebrale. A distinct fovea cranioventralis is present immediately caudal to the facies articularis cranialis, but cranial to the midline processus ventralis. There are no processus carotici or sulcus carotici. There is no processus spinosus, but the postzygapophyses are elevated with respect to the prezygapophyses, which gives some height to the caudal margin of the arcus vertebrae. The postzygapophyses carry a low crista transversarium obliqua on the dorsal surface. The articular surface of the postzygapophyses is nearly circular and faces ventromedially. The facies articularis caudalis of the 12th cervical vertebra is large and only slightly broader than it is deep, similar to the preceding vertebra.

Presynsacral (Cervical) Vertebra 13—The 13th cervical vertebra (Fig. 29; Pls. PL11, D11) is similar in overall morphology to the 12th vertebra. The processus transversi extend further laterally than the postzygapophyses. The ansa costotransversarium is robust with thick ventral margins and lacks a processus costalis. The processus transversi are positioned laterally at approximately bottom-height of the facies articularis zygapophyses craniales. The foramen transversarium is large. The cranial margin of the arcus vertebrae is positioned further caudally than the facies articularis, which in the 13th vertebra is confined to the cranial surface of the corpus. It has a shallow fovea cranioventralis. There are no processus carotici or sulci carotici. There is no processus spinosus, but the postzygapophyses are elevated with respect to the prezygapophyses, similar to the 12th cervical vertebra, which gives some depth to the caudal margin of the arcus vertebrae. A low ridge or tubercle is present at the base of each postzygapophysis, caudally on the arcus vertebrae. The articular surface of the postzygapophyses is nearly circular and is directed ventromedially. The facies articularis caudalis of the 13th vertebra is large and only slightly broader than it is deep, similar to the preceding vertebra.

TABLE 6. Measurements of the ribs (in mm).

Rib	Port Louis R	Port Louis L	Durban R	Durban L
Cervicodorsal rib I (C15)	65	63	64	93
Vertebral rib II (T16)	97	86	90	88
Sternal rib II (T16)	44	45	53	44
Vertebral rib III (T17)	93	93	85	90
Sternal rib III (T17)	67	59	66	61
Vertebral rib IV (T18)	94	90	74	91
Sternal rib IV (T18)	87	86	81	71
Vertebral rib V (T19)	88	90	83	99
Sternal rib V (T19)	103	96	77	79
Vertebral rib VI (V20)	98	93	100	88
Sternal rib II (V20)	34	36	37	28

TABLE 7. Measurements of the sternum (in mm).

Specimen	Length (along midline)	Width at lateral trabecula
Port Louis	170	109
Durban	159	116

Presynsacral (Cervical) Vertebra 14—The 14th presynsacral (Fig. 30; Pls. PL11, D11) is the last vertebra of the cervical series (Fig. 16A, B). The cranial margin of the arcus vertebrae is positioned slightly further caudally than the cranial margin of the facies articularis cranialis, but the caudal margin of the arcus vertebrae extends well beyond the facies articularis caudalis. The caudal margin of the arcus vertebrae is elevated and forms a processus spinosus with a broad base. The processus transversus and ansa costotransversarium extend laterally well beyond the ventromedially inclined articular facets of the prezygapophyses. The ansa costotransversarium is robust and encloses a wide foramen transversarium. The facies articularis cranialis is large and approximately twice as wide as it is deep. A shallow fovea cranioventralis is present. The facies articularis caudalis is broad and tall. The postzygapophyseal articular facets are directed ventromedially at an angle that is greater than 45° with the horizontal, and are inclined more obliquely than the facies articularis zygapophyses caudales of the preceding vertebrae, possibly indicating a greater degree of mobility in the sagittal plane. *Raphus* differs from *Caloenas, Didunculus*, and *Goura* in the processus spinosus being more pronounced with more dorsal projection, the processus transversus being wider and more square-shaped when viewed dorsally, and the processus ventralis being more prominent.

Presynsacral (Cervicodorsal) Vertebra 15—The 15th presynsacral (Fig. 31; Pls. PL12, D12) is the first vertebra having fovea costalis tuberculi et capituli for the articulation of separate, elongate vertebral ribs (costae vertebrales). However, because these ribs are not connected via a sternal rib to the sternum, it is not a thoracic vertebra, but is instead considered a transitional (cervical) vertebra, termed a cervicodorsal (e.g., Fürbringer, 1888;

TABLE 8. Measurements of the coracoid (in mm).

Specimen	Length	Mid-shaft width
Port Louis R	95	8
Port Louis L	94	8
Durban R	87	8
Durban L	89	8

TABLE 9. Measurements of the scapula (in mm).

Specimen	Length	Mid-shaft width
Port Louis R	97	6
Port Louis L	92	7
Durban R	93	6
Durban L	93	7

Gadow, 1933). The 15th presynsacral vertebra has a large processus spinosus, with a large, cranially directed processus dorsalis (Fig. 31). The facies articularis zygapophyses craniales are directed dorsomedially. The processus transversus is stout, and the fovea costalis (diapophysis) is situated on its lateroventral surface for articulation of the tuberculum costale of the vertebral rib (costa vertebralis). The eminentia costolateralis (parapophysis) is positioned on the mid-ventral margin of the corpus for articulation with the capitulum costae of the rib. The facies articularis cranialis is wide. A rectangular processus ventralis is present on the ventral surface of the corpus vertebrae (Fig. 31A–D, F). The facies articularis caudalis is wide and relatively deep, similar to the caudal-most cervical vertebrae. The facies articularis zygapophyses caudales are relatively round and are directed ventromedially.

Presynsacral (Thoracic) Vertebrae 16–18 (Notarium)—The 16th, 17th, and 18th presynsacral vertebra make up the notarium (Fig. 32; Pls. PL12, D12). Presynsacral vertebrae 16–18 are 'true' thoracic vertebrae, because they articulate with vertebral ribs that connect with the sternum via sternal ribs. The notarium is characterized by a broad crista spinosa dorsalis notarii, which is the product of the fusion of the processus spinosi of all three thoracic vertebrae. The dorsal margin of the crista spinosa has been reconstructed in the Port Louis specimen, but is intact in the Durban specimen. The cranial margin of the crista spinosa is inclined cranially. The individual fovea costalis tuberculi are positioned on relatively robust processus transversi that are not fused into a single crista lateralis. The eminentia costalis is positioned ventral to the processus transversum, at the base of the arcus notarii, for all three fused vertebrae. The corpus notarii is laterally compressed and more triangular in shape cranially. Ventral to the corpus notarii a large crista ventralis notarii is present, which is the product of the fusion of the ventral processes of the notarial vertebrae. The processus ventralis of presynsacral vertebra 17 is the longest, and it is partially separated from the processus ventralis of presynsacral vertebra 16 by a round opening (fenestra intercristalis). The processus ventrales of both presynsacral 16 and presynsacral 17 are directed cranially. In the Durban specimen, the processus ventralis of the 18th presynsacral is very small and restricted to the cranioventral margin of the corpus vertebrae. It is not fused into the crista ventralis with the other ventral processes. The ventral process of the ultimate notarial vertebra is variably developed in isolated notaria recovered from the Mare aux Songes, and occasionally it does fuse with the crista ventralis (e.g., Owen, 1866). The facies articularis zygapophyses caudales are large, round, and inclined ventromedially.

Presynsacral (Thoracic) Vertebra 19—The 19th presynsacral vertebra (Fig. 33; Pls. PL13, D13) is also called the prepelvic or intermediate (thoracic) vertebra because of its position between the notarium and the synsacrum. The processus spinosus of the 19th presynsacral vertebra is tall and straight in the Port Louis specimen, and slightly expanded dorsally in the Durban specimen. The processus transversus is robust, and ventrolaterally it carries the fovea costalis tuberculi for articulation with the tuberculum costae. The eminentia costalis for articulation with the capitulum costae is positioned at the base of the arcus vertebrae. There is no processus ventralis, unlike in the notarial vertebrae. The facies articularis cranialis is wide and relatively deep. The facies articularis caudalis is also wider than it is deep, but more rectangular in shape than the facies articularis cranialis. The facies articularis zygapophyses craniales are directed dorsomedially, and the facies articularis zygapophyses caudales are directed ventrolaterally.

TABLE 10. Measurements of the furcula (in mm).

Specimen	Length (along midline)	Width between dorsal ends
Port Louis	97	55
Durban	103	80

TABLE 11. Measurements of the humerus (in mm).

Specimen	Length	Dorsoventral width of proximal extremity	Mid-shaft dorsoventral width	Distal dorsoventral width
Port Louis R	107	35	10	22
Port Louis L	106	35	9.5	22
Durban R	106	35	10	22
Durban L	105.5	34	9.5	21.5

Synsacrum—The synsacrum (Fig. 34; Pls. PL14, D14) consists of approximately 16 vertebrae, which are of thoracic, sacral, and caudal developmental origins (e.g., Gegenbaur, 1871). The cranial-most synsacral vertebra (20) is thoracic in origin and retains the general morphology of the preceding thoracic vertebra. Along the caudal margin of the corpus of the 20th vertebra, there is a clear line of fusion with the other vertebrae of the synsacrum (Fig. 34A, B). The processus transversi of the 20th vertebra are robust and articulate with a vertebral rib. The ribs of vertebral segment 20 articulate with the sternum indirectly (costae completae spuriae), via articulation with the sternal rib of the preceding vertebral segment (19). Between the first synsacral vertebra (vertebra 20) and the first 'true' sacral vertebra (27), there are (approximately) six vertebral segments. The second synsacral vertebra (21) is probably also of thoracic origin. It is associated with a fused vertebral rib in the Durban specimen (see also Chubb, 1919), but in the Port Louis specimen the processus transversi of segment 21 are fused to the interior wall of the ilium. The third and/or fourth synsacral vertebrae (22 and 23) have robust processus transversi, positioned cranial to the renal fossa (fossa renalis, pars ischiadica), that buttress the inside of the ala preacetabularis ilii. Vertebral segments 24–26 lack robust processus transversi. Vertebral segment 27 can be identified as the first 'true' sacral vertebra based on the caudally inclined processus costalis that extends toward the acetabulum. In the Durban specimen, only vertebral segment 27 has a well-developed processus costalis, whereas in the Port Louis specimen a distinct processus costalis is also present in vertebral segment 28. Seven synsacral caudal vertebrae (29–36) are positioned caudal to vertebral segment 28. The size of the corpus vertebrae of the individual vertebral segments that make up the synsacrum is comparable to that of the presynsacral thoracic vertebra in the cranial segments, but starts diminishing rapidly after the fourth synsacral (23).

Caudal Vertebrae and Pygostyle—There are six free caudal vertebrae (vertebrae caudalis liberae) and a pygostyle preserved in the Durban and Port Louis specimens (Figs. 16D, E, 35; Pls. PL15, D15). The free caudal vertebrae are approximately triangular in shape, with distinct processus transversi, most elongate on the sixth; all directed slightly caudad, and with a pronounced processus spinosus, extending further dorsally on the first three vertebrae. The pygostyle is flattened proximally but rounded towards the distal end, with a broad basis pygostyli.

FIGURE 40. Photographs of the pectoral region. **A**, cranial view, Port Louis specimen; **B**, cranial view, Durban specimen; **C**, left scapula and coracoid, oblique craniodorsal view, Port Louis specimen; **D**, left lateral view, Durban specimen; **E**, left scapula in lateral view, Durban specimen.

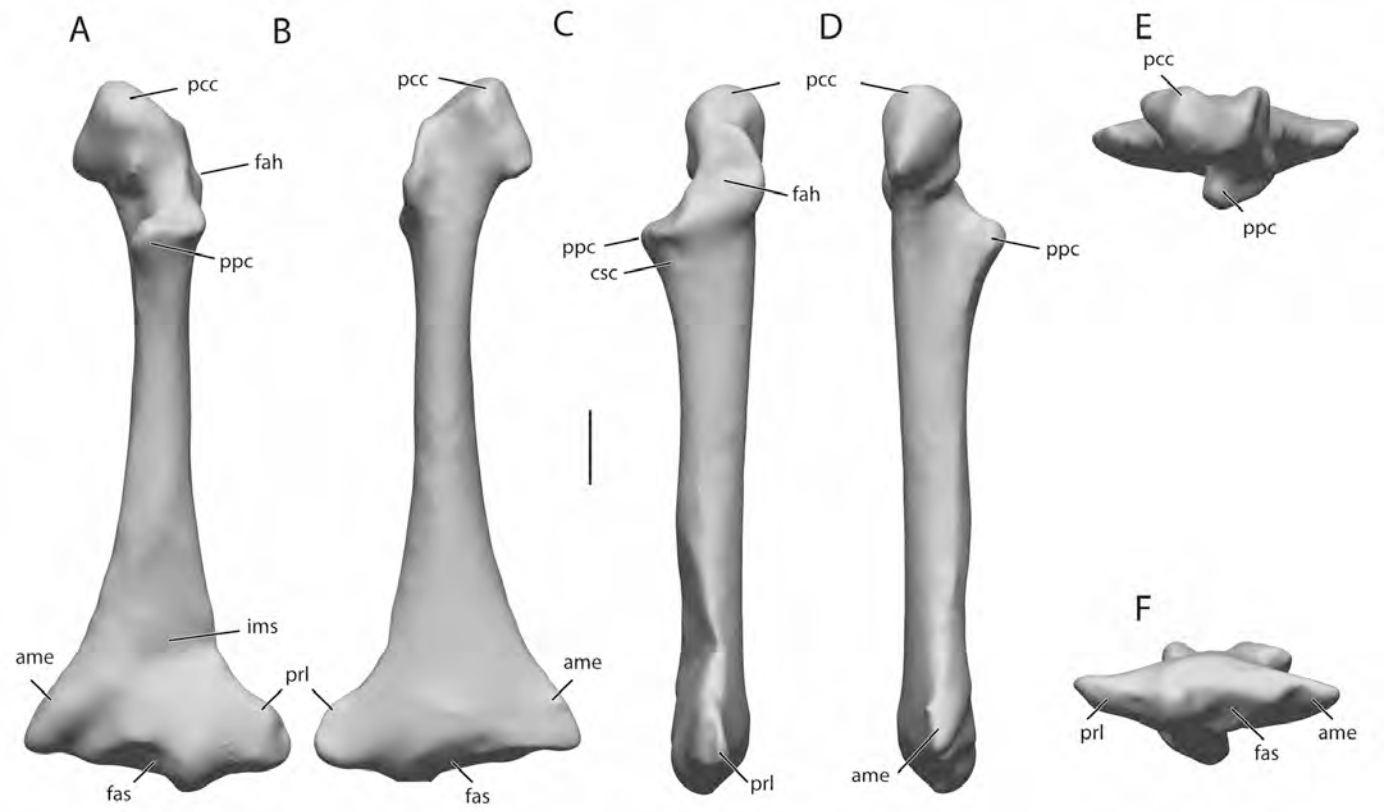

FIGURE 41. 3-D scans of right coracoid, Port Louis specimen. **A**, dorsal; **B**, ventral; **C**, lateral; **D**, medial; **E**, proximal; **F**, distal views. Anatomical abbreviations as in Appendix 1. Scale bar equals 10 mm.

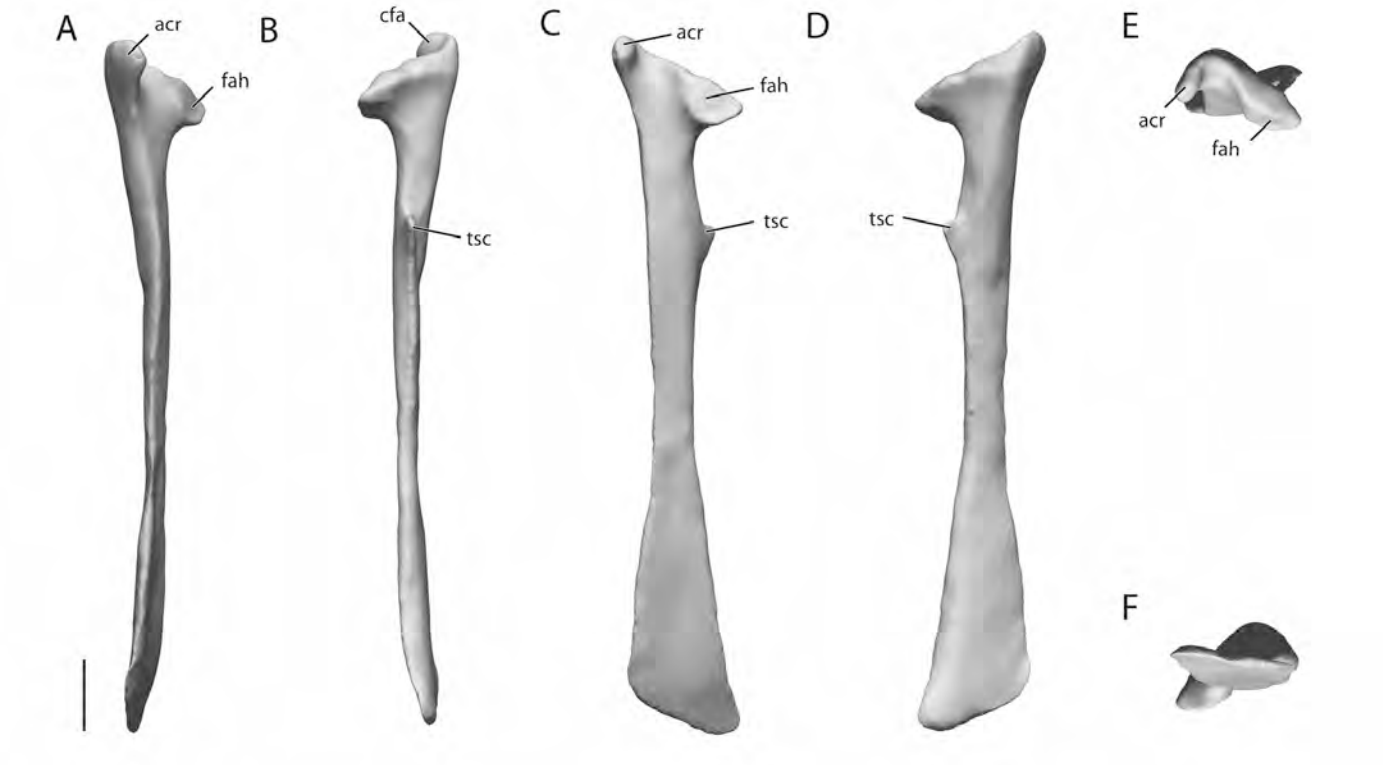

FIGURE 42. 3-D scans of right scapula, Port Louis specimen. **A**, dorsal; **B**, ventral; **C**, lateral; **D**, medial; **E**, cranial; **F**, caudal views. Anatomical abbreviations as in Appendix 1. Scale bar equals 10 mm.

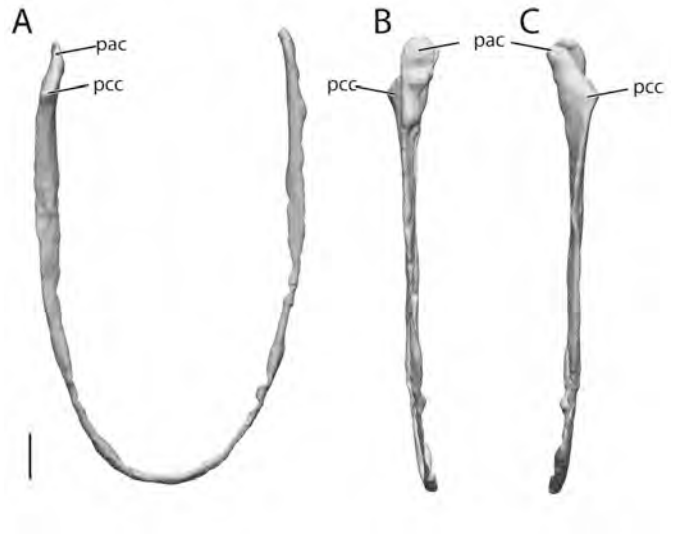

FIGURE 43. 3-D scans of the clavicles (furcula), Port Louis specimen. **A**, cranial surface; **B**, left lateral surface; **C**, right lateral surface. Anatomical abbreviations as in Appendix 1. Scale bar equals 10 mm.

Vertebral Ribs—Cervical vertebral ribs are ankylosed to the corpus and arcus vertebrae in presynsacral (cervical) vertebrae 3–13 (Figs. 16–29; Pls. PL16–21, D16–21; Table 6). A thin, elongate vertebral rib that does not articulate with a sternal rib is present on presynsacral vertebra 15, the last prenotarial vertebra (Fig. 31). Vertebral ribs that articulate with the sternum (costae verae) are present on the notarial vertebrae (16, 17, and 18) and on the last presynsacral vertebra (19) (Figs. 16C, D, 36). A long vertebral rib is also present on the first synsacral vertebra (vertebra 20, developmentally of thoracic origin) (Fig. 16C, D). The second synsacral vertebra (21) of the Durban specimen carries articular facets (diapophysis and parapophysis) for a vertebral rib, and Chubb (1919) mentioned the presence of a small rib on the right side. The capitulum et tuberculum costae are oriented subvertically and are separated by a broad incisura capitulotubercularis. Wide processus uncinati are present on the vertebral ribs of presynsacral vertebral segments 16–19.

Sternal Ribs—The sternal ribs are stout and broad and increase in length caudally (Figs. 16C, D, 37; Pls. PL22–26, D22–26; Table 6). Four sternal ribs articulate with the sternum, namely, the sternal ribs of presynsacral (notarial) vertebral segments 16, 17, and 18 and the sternal rib for presynsacral vertebral segment 19. The vertebral rib of vertebra 20, which is the first synsacral vertebra (developmentally of thoracic origin) articulates with a sternal rib that does not articulate directly with the sternum, but that articulates distally with the sternal rib for vertebral segment 19. The proximal extremity of the each sternal rib is broad craniocaudally and articulates with the distal vertebral rib. The distal sternal ribs for vertebral segments 16–19 are wide transversely and articulate with the sternal processus articularis costales via two convex cotyles.

Sternum—The sternum of the dodo (Figs. 16C, D, 38, 39; Pls. PL27, D27; Tables 7, A2) provides extensive skeletal covering of the ventral body wall, but is reduced in relative size compared with volant columbiforms. The sternum of *Raphus* is approximately equal in length to the synsacrum, which is shorter than the relative length of the sternum in volant pigeons such as *Goura, Caloenas, Didunculus*, and *Columba*. The sternum of *Raphus* differs from that of *Caloenas, Didunculus*, and *Goura* in being comparatively broader, but less long and narrow; in these taxa, the sternum is a quarter to a third longer than the synsacrum. The carina sterni of *Raphus* is significantly reduced in size, and the depth to length ratio of the sternum is only about a quarter of the depth to length ratio of volant columbids (e.g., *Goura, Caloenas, Dicunculus*, and *Columba*). There is also no cranially projected apex carinae, unlike volant columbids. Instead, the carina sterni gently slopes caudad and reaches its greatest depth at approximately 60% of its length. The carina sterni of *Raphus* is also less deep than that of *Pezophaps*, which retains a modest apex carinae as well (see Hume and Steel, 2013). In lateral view, the sulcus articularis coracoideus and sulcus carinae are less deeply excavated in *Raphus* than in *Pezophaps*. In cranial view, a rostrum sterni is absent; instead, the sulcus carinae forms a shallow triangle extending to the apex carinae (absent in *Pezophaps*) and the sulcus medianus sterni is more deeply excavated than in *Pezophaps*. There are a few pneumatic foramina in the incisurae intercostales, and the foramen pneumaticum is relatively indistinct and divided into two small foramina. A large pneumatic foramen is also present on the midline craniodorsal surface of the sternum, whereas other foramina are the result of holes made by wiring the distal end of the sternum to the mount. The highly pneumatic sternum is relatively thick in cross-section compared with volant columbids (Fig. 39). There are four processus costales for articulation with bicotylar sternal ribs on the margo costalis sterni. The processus craniolaterales are short and stout with a distinct oval pit. They are directed laterally and are reduced in comparison with *Caloenas, Didunculus*, and *Goura*. The trabecula lateralis, positioned immediately caudal to the processus costalis, is short, directed dorsad, and much reduced in comparison with the other columbiform genera examined. There are no trabeculae intermediae or fenestrae mediales. The margo caudalis is pointed, not bifurcated, and narrower than in *Pezophaps* (but generally wider than in *Pezophaps* at the level of the margo costalis). The left and right sulci articularis coracoideus do not overlap in the ventral midline, but are widely separated, unlike volant columbids, where the left and right sulci overlap.

There has been loss to the sternum of both the Durban and the Port Louis specimens, and reconstruction has been undertaken on each. The cranial and lateral margins of the Port Louis sternum are original, but portions of the sternal carina and caudal corpus sterni have been reconstructed or covered in plaster. It is not possible to determine visually whether significant portions of bone underlie the areas reconstructed with plaster (as is the case in, for instance, the mandible of the Durban specimen). In the Durban specimen, the left and right trabeculae laterales and the caudal third of the sternum have been reconstructed in plaster. The reconstructed portions of the sternum match the morphology of the sternum of Mare aux Songes *Raphus* specimens (e.g., NHMUK PVA9040; NHMUK 1370; YPM 111118).

Pectoral Girdle

The three skeletal elements that make up the pectoral girdle of *Raphus*, namely, the scapula, coracoid, and clavicle (furcula) are separate and unfused in both the Port Louis and the Durban Thirioux specimens (Figs. 1A, B, 40–44; Pls. PL27–29, D27–29; Tables 8–10).The skeletal elements of the pectoral girdle are also usually recovered separately from the Mare aux Songes, although occasional fusion of the scapula and coracoid (e.g., NHMUK 1351; AMNH FR 3852), or scapula, coracoid, and clavicle (furcula), has been observed (e.g., NHMUK A1341). Fusion of the scapula and coracoid is unknown in *Pezophaps* or other volant columbiforms.

Coracoid—The coracoid of *Raphus* is more gracile than that of volant columbids and much less robust than in *Pezophaps* and less wide, especially in the shaft (Figs. 40, 41; Pls. PL28, D28; Tables 8, A3). Its minimum transverse width to length ratio (ca. 0.25) is less than half that of *Goura, Caloenas, Didunculus*,

FIGURE 44. Photographs of the wing skeleton, Thirioux skeletons. **A**, Port Louis specimen, right wing; **B**, Port Louis specimen, left wing; **C**, Durban specimen, right wing; **D**, Durban specimen, left wing. Anatomical abbreviations as in Appendix 1.

or *Columba*, and slightly less than in *Pezophaps*. Coracoid length is less than two-thirds of synsacral length in the Thirioux specimens, whereas it is generally greater than three-quarters of synsacral length in *Goura, Caloenas, Didunculus*, or *Columba*. In dorsal aspect, the facies articularis humeralis is directed more ventrally than in *Pezophaps*. The sulcus m. supracoracoidei is more deeply excavated and exhibits more pneumatic foramina than in *Pezophaps*. The impressio ligamenti acrocoracohumeralis of *Raphus* is more deeply incised, and the impressio m. sternocoracoidei is less deeply excavated than in *Pezophaps* and also exhibits more pneumatic foramina. In *Pezophaps*, the processus acrocoracoideus is more sharply pointed and directed less medially than in *Raphus*. The facies articularis humeralis is elongate and oval to semicircular in shape. The cotyla scapularis is deeply excavated and oval, and the processus acrocoracoideus is rounded and distinct. *Raphus* differs from

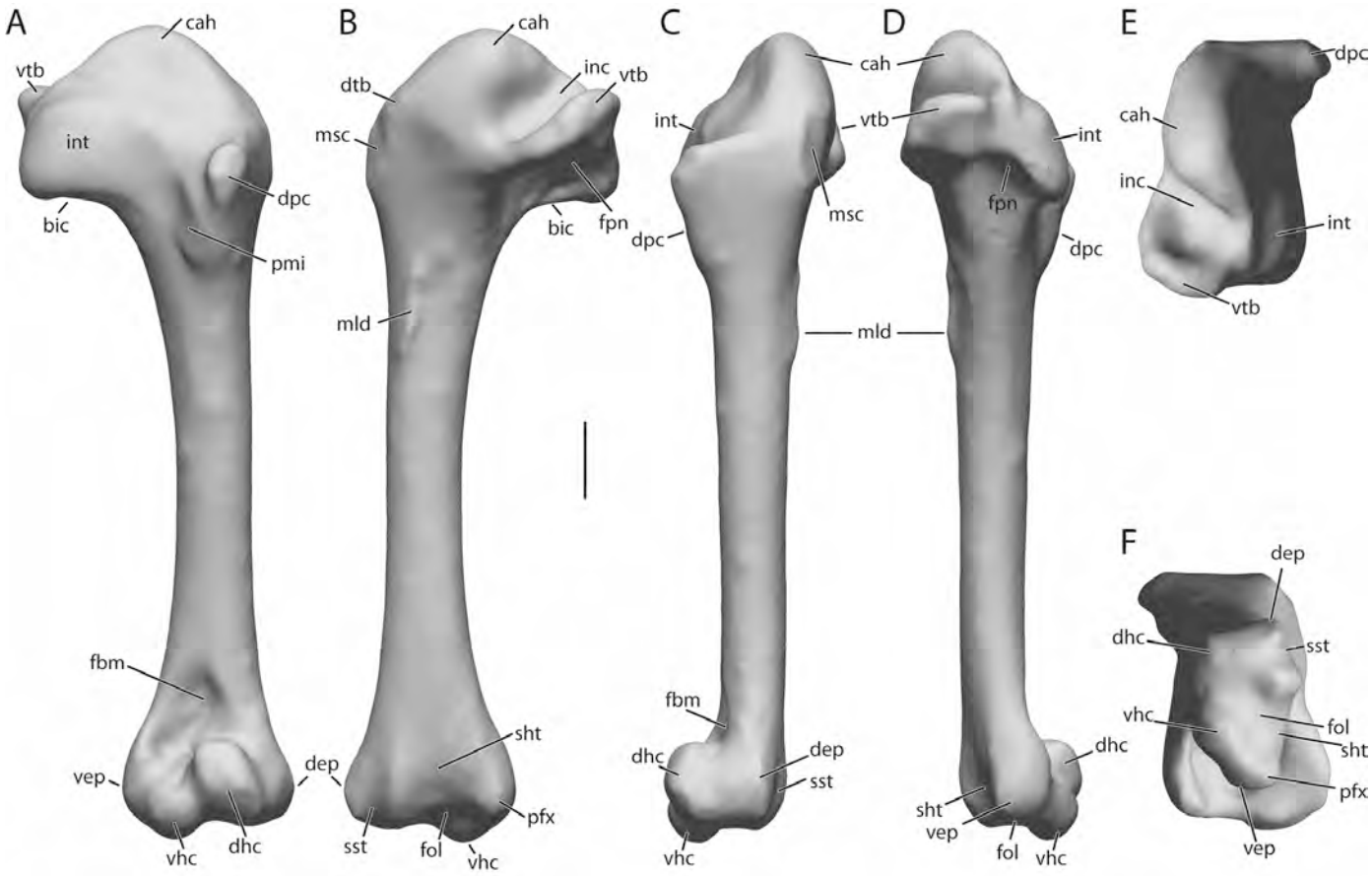

FIGURE 45. 3-D scans of left humerus, Port Louis specimen. **A**, cranial; **B**, caudal; **C**, dorsal; **D**, ventral; **E**, proximal; **F**, distal views. Anatomical abbreviations as in Appendix 1. Scale bar equals 10 mm.

Goura in the processus acrocoracoideus being less bulbous and in having less medial extension of the facies articularis clavicularis. The processus procoracoideus is large but less developed than in volant columbids. It differs from that of *Caloenas* and *Didunculus* by being situated further proximad and extending further dorsad, and it extends less medially than in *Pezophaps*.

On the dorsal surface of the distal end of the coracoid, the facies articularis sternalis is more deeply excavated and extends further proximad than in *Pezophaps*. The angulus medialis is less distinct, with no lateral expansion. The angulus medialis is triangular, extending medially to an equal distance as the processus acrocoracoideus, and the angle between processus lateralis and the facies articularis sterni is obtuse. The distinct processus lateralis is angled sharply from the facies articularis sternalis at approximately 45°; a small ridge is situated on the ventral surface at the distal end where it connects to the sternum. It is less pronounced and with much less lateral extension than in *Caloenas* and *Didunculus*. The relative transverse width of the sternal extremity of the coracoid in *Raphus*, which is around a third of total coracoid length, is approximately equal to those of other volant columbids. The angle between the coracoid and the scapula is more obtuse than that observed in volant pigeons. In specimens where the coracoid and scapula are fused (e.g., NHMUK A1341; NHMUK A1351), the angle between both pectoral girdle elements is approximately 110°.

Scapula—The scapula is elongate and blade-like (Figs. 40, 42; Pls. PL29, D29; Table 9). It is relatively short in comparison with that of volant columbids and less robust than in *Pezophaps*, especially in the shaft. In the Thirioux specimens, scapular length is only slightly more than half of synsacral length, whereas scapular length is approximately equal to synsacral length in volant columbids (e.g., *Goura, Caloenas, Didunculus, Columba*). The facies costalis is concave, and the facies lateralis is convex. The scapular blade increases in dorsoventral width toward the extremitas caudalis, which is blade-like and directed ventrally and terminates in a blunt point. The scapula of *Raphus* differs from that of *Caloenas* and *Didunculus* in having the proximal end much more expanded with a deeper central sulcus. It is most similar to that of *Goura* except that the facies lateralis is shallower, less excavated. The margo dorsalis is less straight than in *Didunculus*, and the extremitas caudalis is much less expanded than in *Pezophaps*. At approximately one-third of scapular length, a pronounced cranially directed tuberculum scapulae is present along the ventral margin of the scapula (Fig. 40A, B), which is also present in *Didunculus, Goura, Caloenas*, and *Pezophaps*, but variable in size in *Pezophaps*. The acromion is oval and directed craniodorsally, and the facies articularis humeralis is relatively flat and semicircular (Fig. 39A, D). There is a deep sulcus between the two, and a small pneumatic foramen is present on the lateral surface of the scapula, at the base of the acromion. The facies articularis humeralis is more circular in *Raphus* than in *Pezophaps, Goura*, and *Caloenas*. In *Raphus*, the excavation between acromion and facies articularis humeralis is shallower, contains less pneumatic foramina, and the shaft is straighter and lacks a ridge on the dorsal surface distal to proximal end compared with *Pezophaps*. Moreover, in *Raphus*, the shaft is straighter and lacks a ridge on the dorsal surface distal to proximal end.

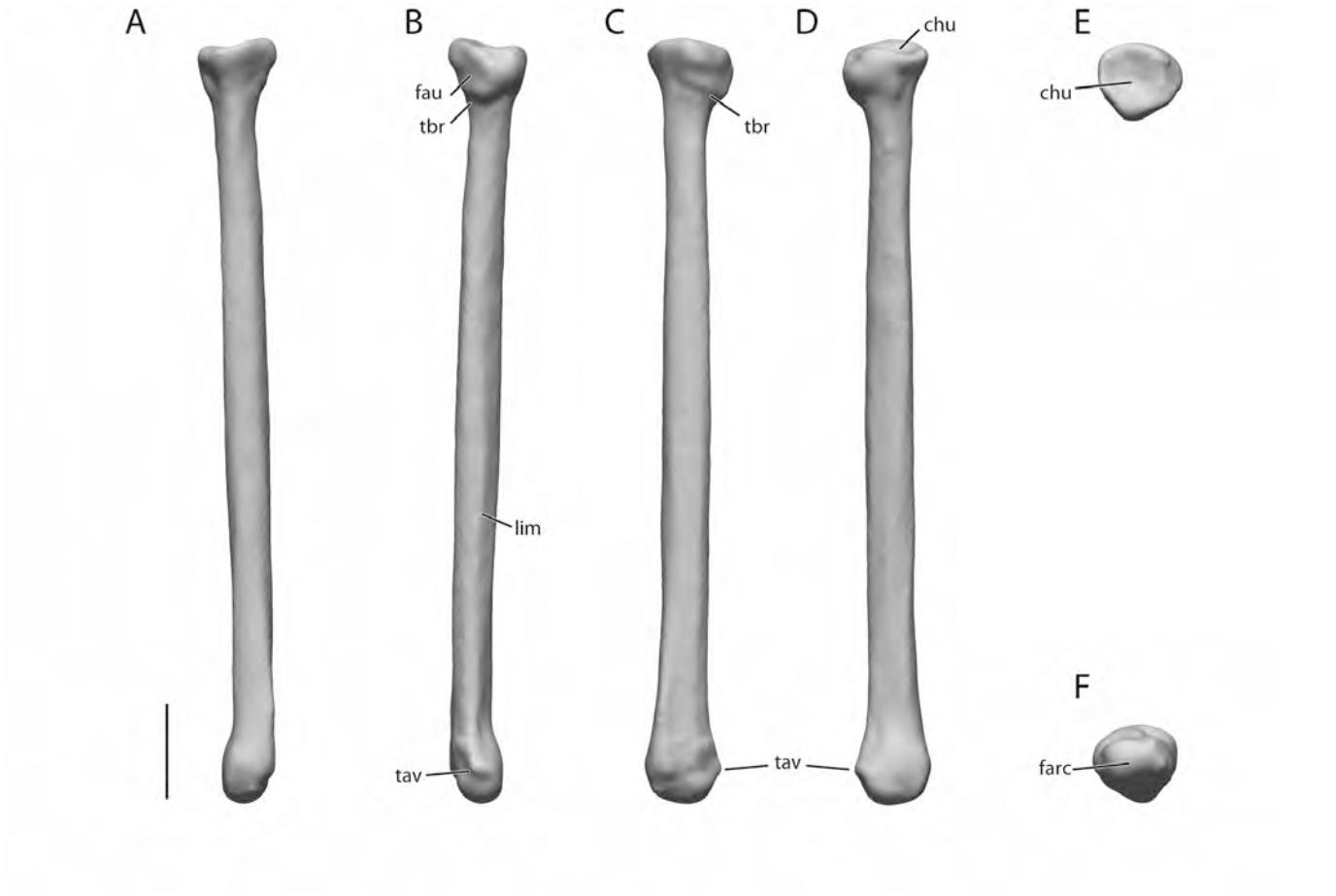

FIGURE 46. 3-D scans of left radius, Durban specimen. **A**, cranial; **B**, caudal; **C**, dorsal; **D**, ventral; **E**, proximal; **F**, distal views. Anatomical abbreviations as in Appendix 1. Scale bar equals 10 mm.

Clavicles/Furcula—The clavicles of the Port Louis skeleton are fused in the ventral midline into a slender 'U'-shaped furcula (Figs. 40, 43; Pls. PL27, D27), similar to the anatomy observed in, for instance, *Goura, Caloenas, Didunculus*, and *Columba*, although the furculae of both specimens have had some reconstruction at the apex. The clavicles of the Port Louis skeleton are slightly longer than the coracoids and lack a ventral apophysis or hypocleideum. The apex of the fused clavicles of the Durban specimen appears to have been extensively reconstructed; it has been rendered slightly more elongate and acute than the Port Louis specimen. The processus articularis claviculae is elongate craniocaudally and has a more caudally positioned processus acromialis and a more cranially positioned processus acrocoracoideus. Several Mare aux Songes specimens are known that have separate, unfused clavicles (e.g., NHMUK A1351; NHMUK PVA9040), and it appears that the presence or absence of midline clavicular fusion in *Raphus* varied intraspecifically. In *Pezophaps*, the presence or absence of clavicular fusion also appears to have varied intraspecifically (J. Parish, unpubl. data). The juvenile skeleton of both *Raphus* and *Pezophaps* is unknown, so the possibility exists that unfused clavicles may belong to young individuals.

Wing Skeleton

The pectoral limb skeleton of *Raphus* (Figs. 44–52; Pls. PL30–35, D30–35; Tables 11–17) is greatly reduced in size compared with that of extant volant columbids (Tables A4–A7), especially the antebrachium, but there has been no loss of skeletal components.

Humerus—The humeri of both Thirioux specimens possess a relatively straight shaft with a nearly cylindrical cross-section at mid-length, similar to dodo humeri recovered from the Mare aux Songes. In cranial view, the proximal end exhibits great dorsoventral expansion and is bulbous; the crista bicipitalis is angled at almost 90° from the shaft, with a distinct hook directed caudad (Figs. 44A–D, 45A–F; Pls. PL30, D30; Table 11, A4). The caput humeri is offset from the main axis of the diaphysis. The proximal apex of the caput humeri is positioned slightly lower than the ventral border of the diaphysis and is inclined medially (Fig. 45B–E). The crista deltapectoralis is triangular in shape, with its proximal margin perpendicular to the shaft and its distal margin merging smoothly with the shaft. In caudal view, the tuberculum dorsale is prominent and directed laterally and has a large insertion area for the m. supracoracoideus. The tuberculum ventrale is well developed and directed slightly ventrally. A deeply excavated incisura capitis separates the tuberculum ventrale from the caput humeri. The fossa pneumotricipitalis contains a large, single pneumatic foramen. A ridge runs proximodistad, increasing in height from the base of the crista bicipitalis, terminating at about one-third of the shaft on the facies caudalis. In cranial view, the impressio coracobrachialis and sulcus ligamentum transversus are shallow; the sulcus n. coracobrachialis is absent.

The distal extremity of the humerus has a well-developed, obliquely inclined condylus dorsalis that is more elongate and extends further proximally than that of the condylus ventralis,

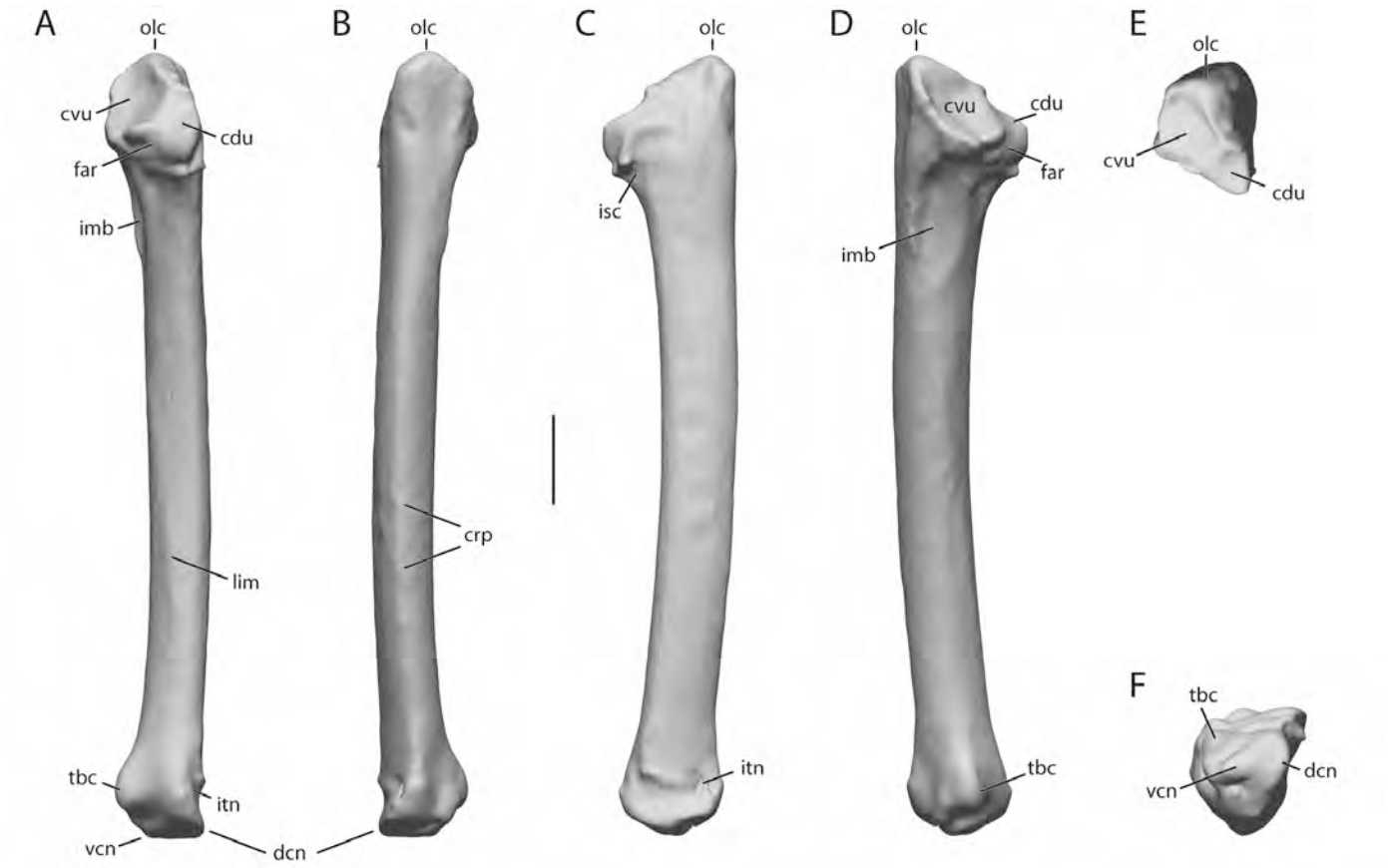

FIGURE 47. 3-D scans of left ulna, Durban specimen. **A**, cranial; **B**, caudal; **C**, dorsal; **D**, ventral; **E**, proximal; **F**, distal views. Anatomical abbreviations as in Appendix 1. Scale bar equals 10 mm.

which is rounded (Fig. 45A–D, F). The processus flexorius is weakly developed and does not extend distally beyond the condylus dorsalis. The distal humeral margin between the condylus ventralis and the epicondylus ventralis slopes proximoventrally, and the fossa m. brachialis is extensive and deeply excavated (Fig. 45A, C). Caudally, the sulcus humerotricipitalis is wide and deep, whereas the more distal sulcus scapulotricipitalis is narrower and shallow, extending from the caudal surface to the ventral surface (Fig. 45B–D, F). The humeri of both Thirioux dodos exhibit a minor degree of laterality, with the right humerus being slightly longer and more robust in both specimens.

The humerus of *Raphus* is overall much less robust and less expanded at proximal and distal ends than in *Pezophaps*. In caudal view, the tuberculum ventrale is directed more ventrally, creating a wider incisura capitis. The fossa pneumotricipitalis is much shallower and less excavated. The crista bicipitalis is more square-shaped, forming an almost right angle to the shaft, and the caput humeri is less inflated and sharper, less rounded. The crista deltopectoralis is more pointed, directed more cranially, and the margo caudalis is more clearly defined with a small ridge. The sulcus scapulotricipitalis and sulcus humerotricipitalis are less excavated, and the processus flexorius is directed less caudally. In cranial view, the tuberculum dorsale is sharper, much more pronounced and directed more cranially, whereas the impressio coracobrachialis is shallower, especially distal to the tuberculum dorsale. The fossa m. brachialis is much less clearly defined and shallower, with a small fossa on the adjacent dorsal surface situated more proximad.

In caudal view, *Raphus* differs from *Caloenas, Didunculus*, and *Goura* in having the crista deltopectoralis more rounded and less triangular, the crista bicipitalis more square, and the incisura capitis wider. The fossa pneumotricipitalis is deeper, with large pneumatic foramina. There is a more distinct ridge for the attachment of the m. latissimus dorsi on the facies caudalis just above mid-shaft, and a pneumatic foramen is present proximal to the sulcus humerotricipitalis. In cranial view, the fossa m. brachialis extends further proximad, and the processus supracondylaris dorsalis is absent.

Radius—The radius of *Raphus* is slightly more robust than in extant volant columbiforms, but more gracile than in *Pezophaps*. Similar to other skeletal limb elements, the radius shows evidence for laterality, with a slightly greater robusticity observed in right side elements than in left side elements. The radius is slender and straight, with slightly expanded proximal and distal ends (Figs. 44A–D, 46A–F; Pls. PL31, D31; Tables 12, A5). The radius is shorter than the humerus, unlike extant volant pigeons, in which the length of the antebrachium exceeds the length of the upper arm. The proximal extremity of the radius is rounded and concave where it articulates with the humerus (Fig. 46E). A small, flat articular surface for the ulna is situated immediately distal to the cotylus humeralis on the ventrocaudal radial surface (Fig. 46B, C). In ventral aspect and distally of the facies articularis ulnaris lies the tuberculum bicipitale radii for the m. biceps brachii. The linea intermuscularis extends along the ventral surface, connecting with the tuberculum aponeurosis ventralis

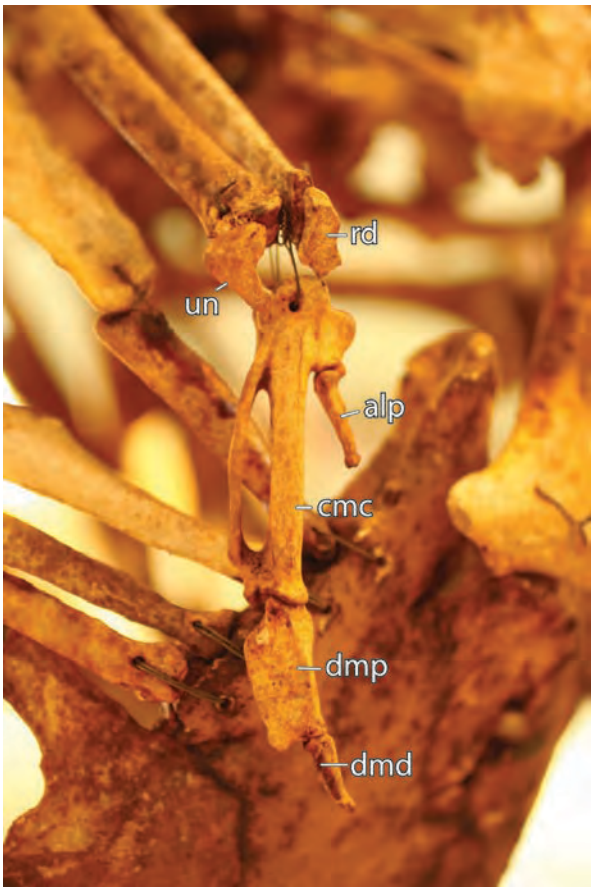

FIGURE 48. Photograph of the distal part of the right wing of the Port Louis dodo skeleton. Anatomical abbreviations as in Appendix 1.

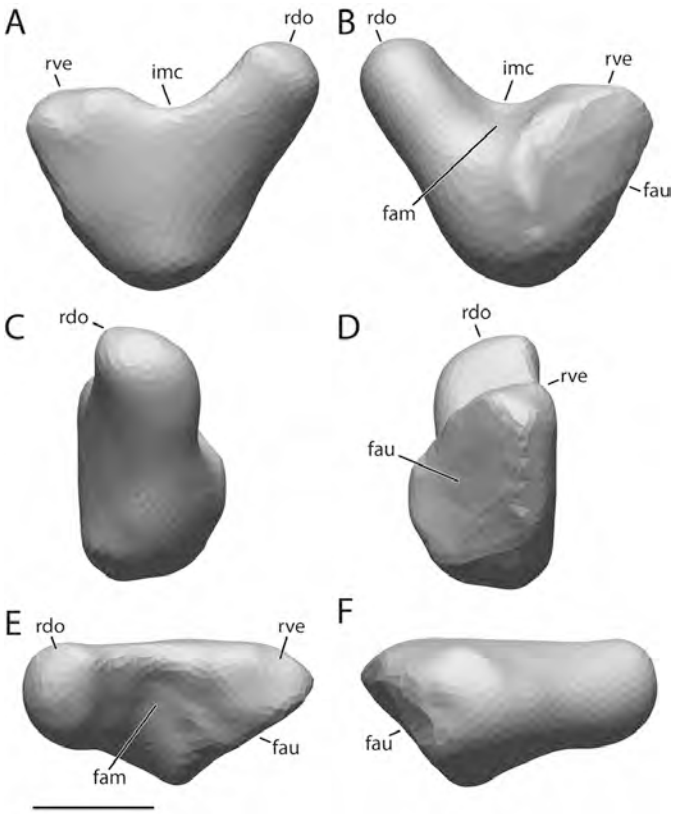

FIGURE 49. 3-D scans of right ulnare, Port Louis specimen. **A**, cranial; **B**, caudal; **C**, dorsal; **D**, ventral; **E**, proximal; **F**, distal views. Anatomical abbreviations as in Appendix 1. Scale bar equals 5 mm.

(Fig. 46B). The distal extremity is flattened dorsoventrally and is inclined cranially, and the facies articularis radiocarpalis is clearly defined with a distinct ridge (Fig. 46A–D, F). In dorsal aspect, the facies articularis ulnaris is distinct and projects dorsad above the cotyla humeralis. The linea intermuscularis extends from the tuberculum bicipitale radii to the distal end, connecting with the wide and deep sulcus tendinosa.

In comparison with *Pezophaps*, the tuberculum bicipitale radii is more pronounced in *Raphus*, whereas the tuberculum aponeurosis ventralis is less sharp and more rounded. The facies articularis radiocarpalis is more distinct and more rounded than in *Pezophaps*, and in the ventral aspect on the proximal end, the cotyla humeralis is bordered with distinct ridges. On the distal end, the depressio ligamentosa is less deeply excavated in *Raphus* than in *Pezophaps*.

Raphus differs from *Caloenas* and *Didunculus* in the shaft being much more expanded and the depressio ligamenti being shallower. It differs from *Goura* in the shaft being straighter, with the distal end less expanded.

Ulna—The ulna is a slightly curved, moderately robust bone in both Thirioux specimens (Figs. 44A–D, 47A–F; Pls. PL32, D32; Table 13). It is approximately 25% shorter than the humerus, unlike volant columbiforms, in which it is longer than the humerus. The humerus is slightly longer than the radius, due to the proximal extension of the facies articularis radii and olecranon, similar to other columbiforms (see Tables 11–13; A5–A7). In ventral aspect, six papillae remigales caudales are evenly distributed over the margo caudalis for the insertion of the secondary feathers (Fig. 47B, C). A

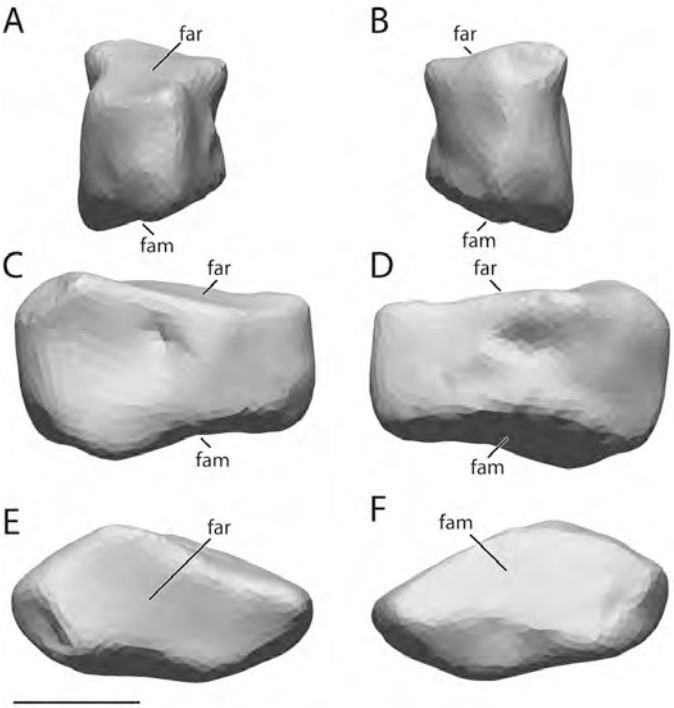

FIGURE 50. 3-D scans of right radiale, Port Louis specimen. **A**, cranial; **B**, caudal; **C**, dorsal; **D**, ventral; **E**, proximal; **F**, distal views. Anatomical abbreviations as in Appendix 1. Scale bar equals 5 mm.

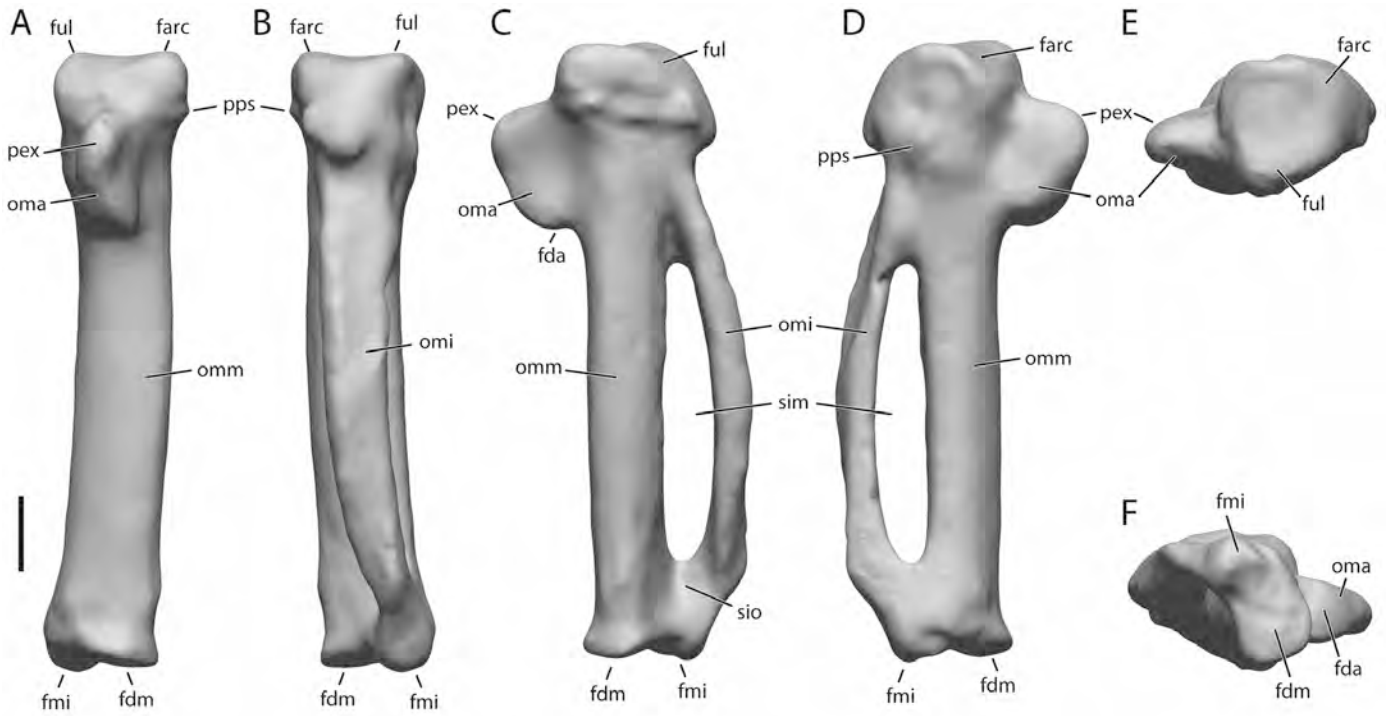

FIGURE 51. 3-D scans of left carpometacarpus, Durban specimen. **A**, cranial; **B**, caudal; **C**, dorsal; **D**, ventral; **E**, proximal; **F**, distal views. Anatomical abbreviations as in Appendix 1. Scale bar equals 10 mm.

deep, oval-shaped impressio brachialis, for the insertion of the m. brachialis, is present on the proximal dorsal surface of the ulna (Fig. 47B). The olecranon is low and blunt. The depressio radialis is deep and oval-shaped, and the sulcus intercondylus is deeply incised. On the proximal joint surface, a cotyla ventralis is present, as well as a clearly defined cotyla dorsalis (Fig. 47D, E). The cotyla ventralis is smaller and shallower than the cotyla dorsalis. The distal ventral and dorsal condyles of the ulna are convex and are separated by a shallow sulcus. In dorsal aspect, the processus cotylaris dorsalis is square, with a small, but deep impressio scapulotricipitis. The incisura radialis is deep and bordered ventrally by a small ridge. The incisura tendinosa is short but clearly defined, and the incisura tuberculum carpalis is deeply excavated with small pneumatic foramina.

In ventral aspect, the ulna in *Raphus* is overall less robust and the shaft more curved than in *Pezophaps*. The olecranon is sharper, directed more proximad, and the crista intercotylaris is more extensive and directed more dorsad. The impressio brachialis is also more deeply excavated. On the distal end, the depressio radialis is less deeply excavated, and the tuberculum carpale is situated further distad. In dorsal aspect, the processus cotylaris dorsalis is situated further distad, the impressio scapulotricipitis is much less excavated, and the condylus dorsalis ulnaris extends further than the condylus ventralis ulnaris.

The ulna of *Raphus* differs from *Caloenas, Didunculus*, and *Goura* in the processus cotylariis dorsalis being less sharp and more rounded. The papillae remigales caudales are less pronounced in *Raphus*, and the impressio brachialis is deeper and more extensive.

Ulnare—The dodo ulnare has not been described previously (the carpal bones figured by Owen in his 1866 monograph were inferred from general pigeon anatomy). The ulnare is known only from the Port Louis Thirioux specimen, in which it has been preserved on both sides (Figs. 44A, B, 48, 49A–F; Pl. PL33), but is lacking in the Durban Thirioux specimen (Fig. 44C, D). The ulnare resembles that of volant columbids in general form. The dorsal ramus is larger than the ventral ramus (Fig. 49A, B), and both rami are separated by the metacarpal incision (Fig. 49A, B, D). The articular surface for the ulna on the ventral surface of the small ramus is slightly concave (Fig. 49B, E).

Radiale—The dodo radiale has never been described. The radiale is present in both wings of the Port Louis specimen and both wings of the Durban specimen. A single radiale is also present in the assemblage of disarticulated remains that Thirioux sent to Cambridge University after 1904 (UMZC 415.KK). The radiale is a relatively rectangular bone with a slightly concave facies articularis for the radius (Fig. 50A, C, E; Pls. PL33, D33) and a slightly concave facies articularis for the carpometacarpus (Fig. 50B, D). It resembles the radiale of volant columbids in general shape.

Carpometacarpus—The carpometacarpus of the dodo is relatively short in comparison with those of volant columbids, such as *Caloenas, Goura*, and *Didunculus*. On the proximal ventral surface, a large, semirectangular, and blunt processus extensorius is present, which bears the articulation for the phalanx digitalis alulare on its distal margin (Figs. 44A, B, 49A, B, 51A–F; Pls. PL34, D34; Tables 14, A7); the processus pisiformis is small but distinct (Fig. 50A–C). The sulcus interosseus is deeply incised and bordered by small ridges on the os metacarpale majus (Fig. 50A, C). In dorsal aspect, the fossa supratrochlearis is shallow, whereas the sulcus tendineus is short but bordered by a raised ridge. The os metacarpale majus is robust and approximately rounded in cross-section, and the os metacarpale minus is broad and craniocaudally flattened, connecting to the caudal surface on the proximal end (Fig. 50A–C). It is offset from the os

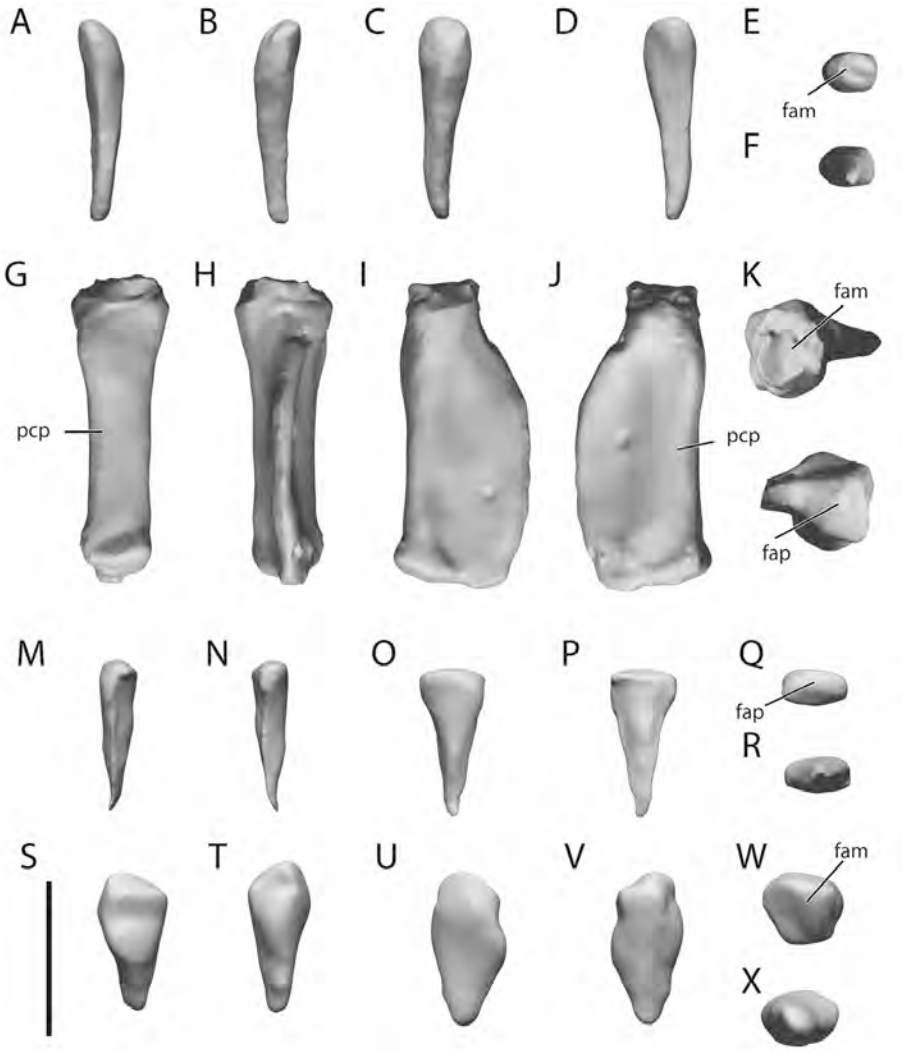

FIGURE 52. 3-D scans of wing phalanges. Left phalanx digiti alulae, Port Louis specimen (**A**–**F**), left phalanx proximalis digiti majoris, Durban specimen (**G**–**L**), right phalanx distalis digiti majoris, Port Louis specimen (**M**–**R**), and right phalanx digiti minoris, Durban specimen (**S**–**X**) in cranial (**A**, **G**, **M**, **S**), caudal (**B**, **H**, **N**, **T**), dorsal (**C**, **I**, **O**, **U**), ventral (**D**, **J**, **P**, **V**), proximal (**E**, **K**, **Q**, **W**), and distal (**F**, **L**, **R**, **X**) views. Anatomical abbreviations as in Appendix 1. Scale bar equals 10 mm.

metacarpale majus and connects caudoventrally at the distal end with equal ventral extension as the os metacarpale majus, and the small processus alularis forms a distinct lip.

The carpometacarpus of *Raphus* differs from *Pezophaps* in being generally more robust, especially on the proximal end. In ventral aspect, the os metacarpale majus is straighter, and the os metacarpale minus is narrower, with a less right-angled turn proximally. The processus pisiformis of *Raphus* is also less distinct. In dorsal aspect, the fossa supratrochlearis is more deeply incised, the sulcus tendineus is less extensive and less distinct, and the sulcus interosseus is more deeply excavated. Unlike *Pezophaps* (Hume and Steel, 2013), the dodo does not exhibit impact callous on the processus extensorius.

Raphus differs from *Caloenas* and *Didunculus* in the processus extensorius being more rounded and directed less cranially. The processus pisiformis is less distinct. It is similar to that of *Goura* except that the proximal and distal ends are less robust, and it lacks the impact callous on the processus extensorius, which is visible in all specimens examined of *Goura* (see also *Pezophaps*).

Wing Phalanges—The phalanges of the dodo wing have never been described. Newton and Gadow (1893) figured the first phalanx of the phalanx digitalis majoris, and Chubb (1919) noted the presence of the phalanx digiti alulae and the phalanx digiti minoris in the Durban specimen, but the morphology of these phalanges was not described in either publication. All other wing phalanges have remained undescribed until now. Although neither of the two Thirioux specimens has a wing that contains all digital phalanges (see Tables 15–17; Fig. 44A–D; Pls. PL35, D35), the right wings of both specimens are most complete; in the Port Louis specimen (Fig. 48), it is missing only the phalanx digiti minoris, and in the Durban specimen (Fig. 44C), only the phalanx digiti alulae. The wing phalanges of *Raphus* differ from those of *Caloenas, Didunculus*, and *Goura* in having comparatively less caudal expansion but are otherwise similar in general morphology. The phalanx digitalis alula is almost a third of the length of the carpometacarpus. It articulates with the processus alularis on the distal border of the processus extensorius of the carpometacarpus. It is broader proximally and tapers to a blunt point distally (Figs. 44A, B, 48, 52). The phalanx proximalis digiti majoris is broad and less than half the length of the carpometacarpus in the Thirioux specimens. The phalanx distalis digiti majoris is almost two-thirds of the length of the first phalanx, is broader proximally, and tapers to a point (Figs. 44A–D, 48, 52). The phalanx digiti minoris, preserved only in the right wing of the Durban specimen, is more than half the length of the phalanx proximalis digiti majoris. It is relatively deeper than the phalanx digiti alulae and the phalanx distalis digiti majoris and tapers to a blunt point distally (Fig. 44C).

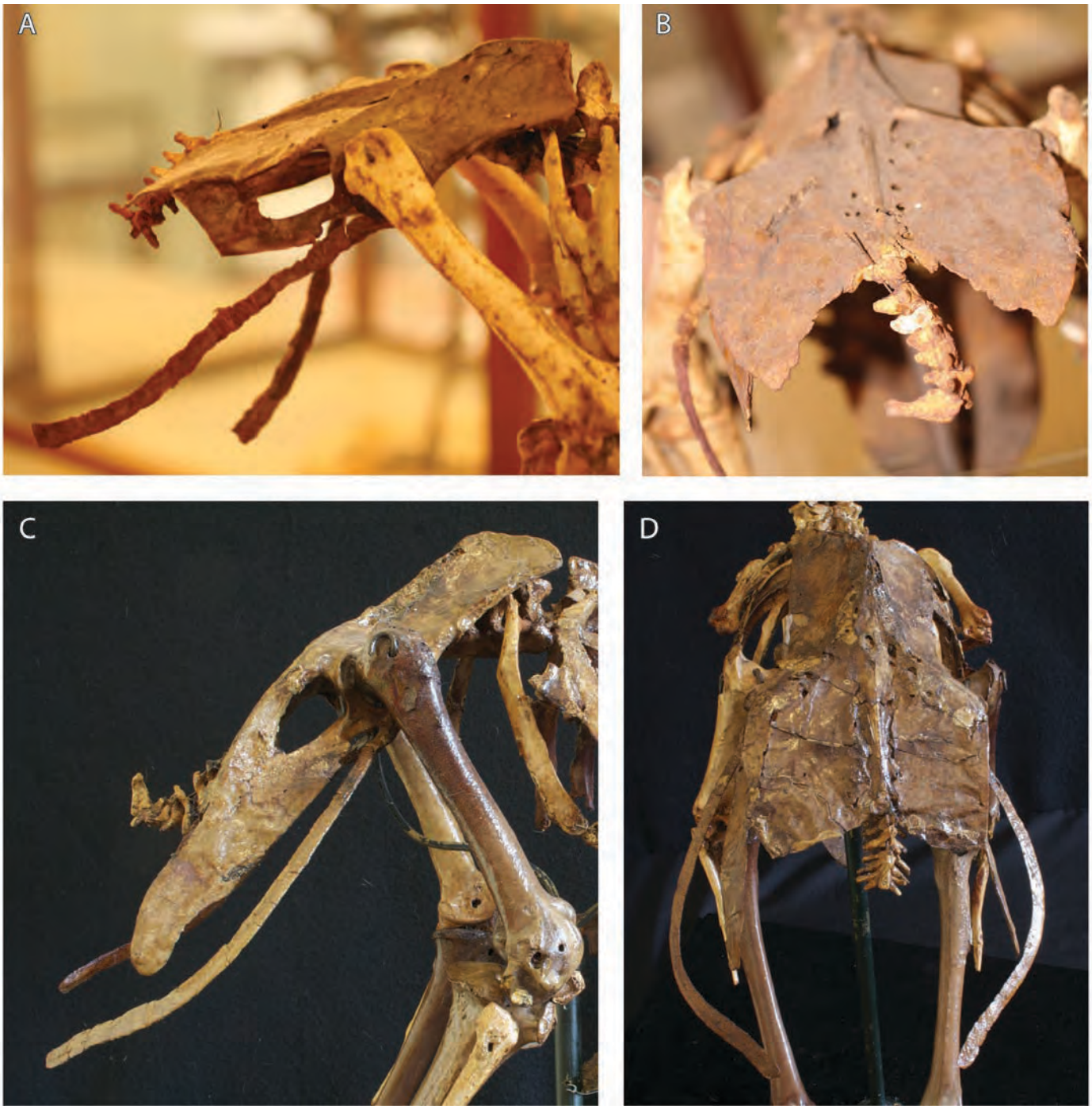

FIGURE 53. Photographs of the pelves of the Port Louis (**A**, **B**) and Durban (**C**, **D**) dodos in **A**, **C**, right lateral and **B**, **D**, dorsal views. Processus terminalis ischii and distal scapus pubis of the Durban dodo are covered in a thick coating of shellac and may have been partially reconstructed.

A separate phalanx digiti minoris has also been preserved in the UMZC collections (415.KK; see Claessens and Hume, 2015: fig. 6B), which displays a more typical anatomy for this element compared with other columbids, such as a distinct caudomedially directed hook. Whether the phalanx digiti minoris preserved with the Durban skeleton is unusually robust and reduced distally, or whether the separate phalanx digiti minoris from Thirioux's collection belongs to the preserved remains of a different bird species, cannot be determined with certainty at this stage.

Pelvic Girdle

Pelvis—There is a slight possibility based on the aberrant coloration of the pelvis in the Port Louis dodo that it may belong to a different individual. The dark brown coloration, as compared with the light tan of the other skeletal elements, appears to be markedly similar to dodo material collected from the Mare aux Songes. However, the internal coloration exposed by a recent breakage to the scapus pubis is of a lighter coloration, similar to the rest of the skeleton. It is possible that the pelvis has become discolored since excavation, or that it was stained a different

TABLE 12. Measurements of the radius (in mm).

Specimen	Length	Dorsoventral width of proximal extremity	Mid-shaft dorsoventral width	Distal dorsoventral width
Port Louis R	76	8	5.5	10
Port Louis L	76	7.5	4	9
Durban R	78	—	5	—
Durban L	78	8	5	9

color due to differential depositional factors, but its loss, if this turns out to be the case, seems surprising considering the excellent preservation of the rest of the skeleton. The postacetabular portion of the pelvis of *Raphus* is wide and the ala postacetabularis ilii is slightly convex dorsally (Figs. 53, 54; Pls. PL14, D14; Table 18), whereas the preacetabular portion of the pelvis is narrower and the ala preacetabularis ilii is concave but inclined ventrolaterally (Fig. 54A–F). Although the pelvis of *Raphus* may appear exceptionally wide at first glance, its general shape and maximum width as a function of synsacral length falls within the same range (ca. 75–84%) as many substantially smaller extant pigeon taxa; the pelvis of *Pezophaps* is comparatively narrower than the pelvis of *Raphus* (e.g., Martin, 1904). The alae postacetabulares ilii of *Raphus* have a sharp, clearly defined division that forms a distinct ridge cranially. The sulcus antitrochantericus is shallower than in *Pezophaps*, and the crista spinosa synsacri is less distinct. In lateral view, the crista iliaca dorsalis is more pronounced than in *Pezophaps* and forms a distinct raised ridge; the foramen ilioischiadicum is comparatively smaller, whereas the corpus ischii is more excavated. The foramen intervertebrale is also smaller in *Raphus* than in *Pezophaps*. In cranial view, the extremitas cranialis synsacri is wider, and the facies articularis femoralis is more pronounced than in *Pezophaps*. The postacetabular portion of the pelvis in *Raphus* is slightly longer than the preacetabular portion. The foramen acetabuli is large and circular. The antitrochanter extends out laterally from the caudodorsal margin of the acetabulum, and its articular surface is oval in shape. The ischium extends further caudad than in other columbids, and the ala ischii of *Raphus* extends beyond the distal margin of the ilium for nearly half of its length (Fig. 54A, B, E, F). The foramen ilioischiadicum is oval and elongate. It is almost half the length of the ala ischii and positioned caudal to the acetabulum.

The pelvis of *Raphus* differs from that of *Caloenas, Didunculus*, and *Goura* in being comparatively wider, with the crista spinosa synsacri being less distinct. The cranial edge of the ala postacetabularis ilii extends less cranially than in *Caloenas, Didunculus*, and *Goura*. In lateral view, the crista iliaca dorsalis forms a distinct ridge, and it differs further from that of *Didunculus* in having the crista iliaca dorsalis enclosed and not open and pneumatic.

The scapus pubis is long and narrow. The scapus is not fused with the ventrocaudal margin of the ala ischii, and the foramen obturatum is open and confluent with the spatium ischiopubicum (fenestra ischiopubicum). The scapus pubis bows out laterally from the corpus pubis and extends further laterally than the ala ischii at mid-length. The caudal portion of the scapus pubis and the apex pubis is angled medially, and the contralateral apices are approximated more closely than the processus terminalis ischii (Fig. 54A, B). A processus pectinealis is absent, similar to other columbids. There are approximately 16 synsacral vertebrae (Fig. 34), and a more detailed description of the synsacrum is provided in the Axial Skeleton section of Description and Comparisons.

The pelvis of the Port Louis specimen has been damaged relatively recently, and the caudal portions of the ala ischii, pubis, and spina dorsolateralis ischii have been broken off (see also Claessens and Hume, 2015). The base of the scapus pubis appears to have been reconstructed and reattached to the corpus pubis during the original mounting of the specimen, and the lesser degree of curvature of the scapus pubis of the Port Louis specimen may be due to the combination of the earlier reconstruction effort and recent damage. The broad curvature and large caudad extent of the scapus pubis and ala ischii of the Durban specimen are similar to the condition observed in another rare complete pelves derived from the Mare aux Songes that is part of the second, composite *Raphus* skeletal mount on display at the Mauritius Institute in Port Louis (The Milne-Edwards unregistered specimen; see Claessens and Hume, 2015).

TABLE 13. Measurements of the ulna (in mm).

Specimen	Length	Mid-shaft dorsoventral width
Port Louis R	85	8
Port Louis L	85	8
Durban R	86	7
Durban L	87	7

TABLE 14. Measurements of the carpometacarpus (in mm).

Specimen	Length	Mid-shaft dorsoventral width
Port Louis R	44	10
Port Louis L	44	10
Durban R	42	10
Durban L	40	11

Hind Limb Skeleton

Femur—The femur of *Raphus* is robust and comparatively straight (Figs. 55, 56; Pls. PL36, D36; Table 19, A8a). It lacks the slight caudolateral deflection of the distal femur of extant columbids such as *Caloenas, Didunculus*, and *Columba*, but has a dorsoventral curvature on the distal half of the shaft. The caput femoris has its proximal margin at the same level as the facies articularis antitrochanterica. In cranial view, the trochanter femoris forms a sharp ridge that is directed medially and concave laterally, and several variably sized pneumatic foramina are present in the fossa trochanteris. Caudally, the impressiones obturatoriae are distinct and form a connecting ridge. The linea intermuscularis cranialis is distinct, extending across the facies cranialis and joining the proximal edge of sulcus patellaris. The sulcus patellaris and sulcus intercondylaris are deeply incised and wide, the impressio ligamenti collateralis lateralis and fovea tendineus m. tibialis cranialis deeply excavated, the latter situated almost

TABLE 15. Wing digits preserved in each specimen.

Specimen	Wing digit preserved			
	Alular phalanx	Phalanx digiti majoris I	Phalanx digiti majoris II	Phalanx digiti minoris
Port Louis R	Preserved	Preserved	Preserved	—
Port Louis L	Preserved	Preserved	—	—
Durban R	—	Preserved	Preserved	Preserved
Durban L	—	Preserved	—	—

TABLE 16. Measurements of the phalanges digiti majoris (in mm).

Specimen	Length	Mid-shaft width	Mid-shaft height
Phalanx proximalis digiti majoris			
Port Louis R	18	7	4
Port Louis L	18	7	4
Durban R	19	8	4
Durban L	19	8	4
Phalanx distalis digiti majoris			
Port Louis R	11	5	3
Durban R	13	5	3

equally distad. In caudal view, the fossa poplitea is deeply excavated and possesses multiple small pneumatic foramina. The linea intermuscularis caudalis is distinct and connects with an extensive, deeply excavated impressio ansae m. iliofibularis. The condylus lateralis has a large, caudally directed ridge, extending much further than the condylus medialis. The condylus medialis is somewhat broader and extends medially and cranially. The trochlea fibularis and crista fibularis are well developed (Fig. 56B, C, F). The crista supracondylaris medialis is bordered by a small ridge, and the impressio ligamentium cruciati cranialis is deep, forming a circular pit. The epicondylus lateralis and medialis are weakly developed. The epicondylus lateralis is a relatively sharp ridge that extends relatively further distad in comparison with other columbids such as *Caloenas, Didunculus*, and *Columba. Raphus* further differs from *Didunculus* in being comparatively more robust, less straight, the sulcus patellaris being comparatively less wide, and the crista trochanteris being more pronounced. It differs from *Goura* in the condylus medialis being more pronounced and the linea intermuscularis caudalis being less distinct.

The femur of *Raphus* is comparatively much more robust than that of *Pezophaps*, especially on the proximal and distal ends. In caudal aspect, the trochanter femoris is shorter with less proximal extension, the facies articularis acetabularis is more bulbous and less flattened, and the fossa poplitea is less extensive but more deeply excavated. In cranial aspect, the crista trochanteris is more ridge-like and extends further distad, the impressions iliotrochantericae is more distinct and broader with more pneumatic foramina, and the sulcus patellaris is shallower. The fovea ligamenti capitis is less excavated, the condylus medialis is more distinct and extends further cranially, and the condylus lateralis is more expanded and extends further laterally.

Patella—The patella is preserved in both the Durban and Port Louis specimens, and a separate patella is also present in the Cambridge Thirioux collection (UMZC 415.KK). In the mounted Durban and Port Louis skeletons, the patellae have been positioned with metal wire on the proximal joint surface of the tibiotarsi in what appears to be an inverted position (Fig. 55A–D). The patella of *Raphus*, the sesamoid of the combined tendon for the m. femorotibialis and m. iliotibialis, is a semilunar-shaped disc, with deep, caudoventrally positioned indentations or cotyles for contact with the condylus lateralis and medialis femoris along the sulcus patellaris (Figs. 56A, 57A–G; Pls. PL37, D37). The margin of the lateral cotyle is more upright than that of the medial condyle, a shape that corresponds to the more upright slope of the cranial surface of the condylus lateralis femoris (Fig. 57B, D, E). There is no prominent impression for the m. ambiens. The texture of the patella is relatively rugose and porous, similar to that of the ankle sesamoid, which is likely reflective of its genesis as an intramembranous sesamoid ossification. A similar-shaped patella is also found in *Pezophaps* (e.g., NHMUK A3505; NHMUK A3506). A patella is also known in other columbids that we have used in our analysis, such as *Goura*, although the disc-like anatomy and presence of deeply excavated cotyles for the femoral condyles as in *Raphus* is not observed in these taxa, a feature that may be related to differences in size and body mass. Because the proximal articular facet of the tibiotarsus is fully formed, the element identified here as the patella is unlikely to represent an unfused portion of the crista cnemialis.

TABLE 17. Measurements of the phalanx digiti alulae (in mm).

Specimen	Length	Mid-shaft width
Port Louis R	15	4
Port Louis L	15	4

Tibiotarsus—The tibiotarsus is the longest skeletal element of the hind limb (Fig. 55, 58; Pls. PL38, D38; Table 20). In comparison, it is slightly more robust than the tibiotarsus of smaller extant columbids (Table A9). In cranial aspect, the crista cnemialis cranialis is approximately triangular in lateral view, with virtually no proximal extension (Fig. 58C–F). Its proximal margin is thick, whereas its distal margin is narrower. The facies gastrocnemialis is rugose, extensive, and deeply excavated and situated on the proximomedial surface (Fig. 58A, D). The crista cnemialis lateralis is shorter and stouter than the crista cnemialis cranialis and, together with the latter, demarcates the sulcus intercnemialis for the m. extensor digitorum longus; the sulcus intercnemialis is deep with small foramen pneumaticum. The crista fibularis extends along the proximal third of the lateral surface of the shaft, whereas the linea muscularis fibularis extends further distally along the lateral margin of the shaft (Fig. 58C). In caudal aspect, the crista patellaris forms a distinct ridge with a slight hook. The facies articularis lateralis is rounded and overlies a deeply excavated fossa flexoria. The impressio ligamenti collateralis medialis forms a small, rugose ridge, and the crista fibularis is short with shallow sulcus. The incisura intercondylaris is deep. A ridge on the facies cranialis runs from the crista cnemialis cranialis to the sulcus extensorius. The well-defined, deeply excavated sulcus extensorius is bridged by a high pons supratendineus (Fig. 58A). The pons supratendineus is offset medially and oriented ventromedially and creates a deep, circular distal opening of the canalis extensorius. Both the sulcus extensorius and the distal opening of the canalis extensorius are located slightly medial to the center of the shaft. The tuberositas retinaculum extensoris medialis is distinct and elongate and is separated from the condylus medialis by a distance approximately equal to the depth of the condylus medialis, whereas the tuberositas retinaculum extensoris lateralis extensorium forms a wide, raised tuberosity; a small foramen is situated immediately laterad to it. The width of the distal condyles is narrower caudally than cranially, and the depth of the condylus medialis is greater than the caudal width of the condyles (see also Worthy, 2001).

The tuberculum retinaculi m. fibularis forms a double ridge on the lateral surface of the shaft, and the sulcus m. fibularis is deep with a single foramen pneumaticum. The epicondylus medialis is distinct, and the tuberositas popliteus exhibits distinct raised ridges, whereas the epicondylus lateralis is indistinct. The trochlea cartilaginis tibialis is wide and shallow.

The tibiotarsus of *Raphus* is comparatively more robust than that of *Pezophaps*, especially at the proximal and distal ends. In caudal aspect, the crista patellaris is less sharp, more square, the fossa flexoria is less deeply excavated, and the facies articularis lateralis is wider, less bulbous. The crista fibularis is larger, extending further distad, and the epicondylus lateralis is more distinct. In cranial aspect, the crista cnemialis cranialis is more pointed proximally, the pons supratendineus is located more medially, the sulcus extensorius is deeper, and the condylus medialis and condylus lateralis are much larger.

The tibiotarsus of *Raphus* differs from those of *Caloenas, Didunculus*, and *Goura* in the sulcus intercnemialis being

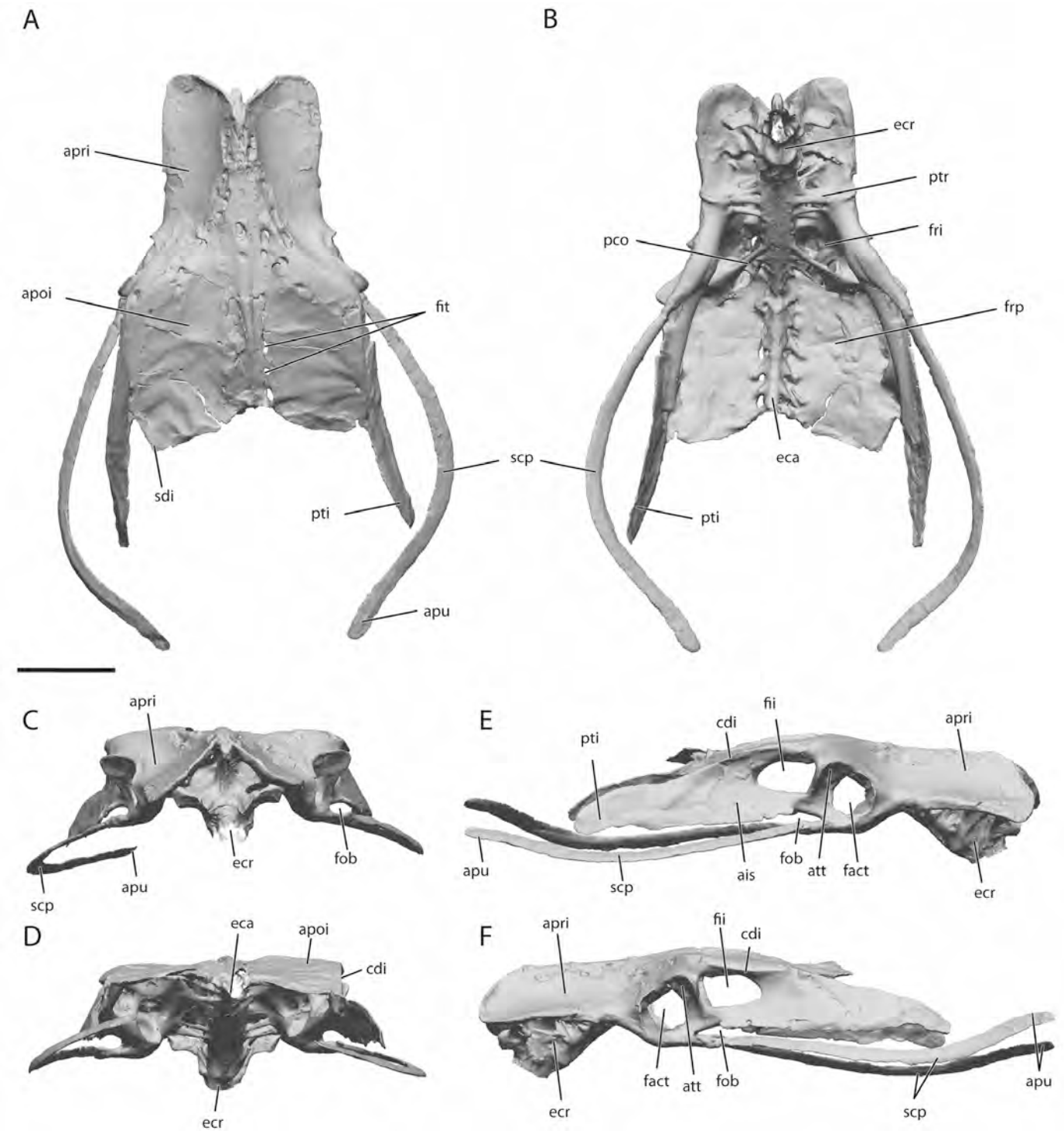

FIGURE 54. 3-D scan images of the pelvis of the Durban dodo specimen in **A**, dorsal; **B**, ventral; **C**, cranial; **D**, caudal; **E**, right lateral; and **F**, left lateral views. Anatomical abbreviations as in Appendix 1. Scale bar equals 50 mm. Processus terminalis ischii and distal scapus pubis are covered in a thick coating of shellac and may have been partially reconstructed.

shallower, and the pons supratendineus being situated further proximad.

Fibula—The Port Louis specimen preserves a complete left fibula (Figs. 55, 59; Pls. PL39, D39; Table 21). The fibula of *Raphus* is known from multiple specimens from the Mare aux Songes, but the thin spina fibulae, which tapers to a thin point distally, is frequently broken and missing its distal extremity. The left fibula of the Port Louis specimen preserves the complete spina fibulae, which is approximately two-thirds of the length of the tibiotarsus (Fig. 55). Owen (1866) also figured a fibula with a largely complete, thin, tapering spina fibulae. However, this figured specimen is marginally shorter than half of the tibiotarsus figured in juxtaposition, and barely a third of tibiotarsus length in Owen's (1866) skeletal reconstruction, underscoring the difficulty of obtaining

TABLE 18. Measurements of the pelvis (in mm).

Specimen	Length (along midline)	Length including pubis	Acetabular width	Width at proximal end	Maximum width at distal end
Port Louis	152*	267*	87	77	124
Durban	160	282	89	78	130

*Value is underestimated due to damage.

accurate relative skeletal proportions from composite specimens. This further highlights the importance of the Thirioux specimens. The caput fibulae is laterally compressed and wide craniocaudally. It is angular when viewed cranially and straight when viewed proximally. In cranial view, the fibula is deflected medially for 30% of its length following the contour of the tibiotarsus, before deflecting laterally for the remaining length. The proximal facies articularis femoralis articulates with the trochlea fibularis of the femur. On the craniomedial surface, a thin and craniocaudally elongate articular surface for the tibia is present (facies articularis tibialis). The fossa poplitea is shallow. The crista articularis tibialis extends along the upper half of the medial surface of the corpus fibulae. The tubercle for the iliofibularis muscle is situated on the caudomedial surface, approximately one-third of the length of the fibula below the caput fibulae (Fig. 59).

The fibula of *Raphus* differs from that of *Pezophaps* in being less robust, with the proximal head less expanded. In dorsal view, the caput fibulae of *Raphus* is more triangular, but otherwise they are similar. *Raphus* differs from *Caloenas* and *Didunculus* in having the proximal end more square in lateral view, whereas in *Goura* the caput fibulae is comparatively wider.

Intertarsal Sesamoid—A large semilunar-shaped sesamoid bone is preserved mounted in the ankle region of both limbs of the Durban and the Port Louis Thirioux specimens (Figs. 60, 61; Pls. PL37, D37), and a similar isolated sesamoid is also known from the Cambridge Thirioux collection (UMZC 415.KK). We interpret this bone as an intertarsal sesamoid, in agreement with the original interpretation of this skeletal element on the mounted skeleton. The intertarsal sesamoid closely fits the trochlea cartilaginis tibialis. In *Pezophaps*, a similar intertarsal sesamoid is also known (e.g., NHMUK A3505; NMHUK A3506). The intertarsal sesamoid is laterally compressed, elongate, and its texture is rugose and porous (Figs. 58, 60). In addition to *Raphus* and *Pezophaps*, similarly shaped tarsal sesamoids are also known in other columbids.

Tarsometatarsus—The tarsometatarsus of *Raphus* (Figs. 55, 62; Pls. PL40, D40; Table 22) is very robust, especially in shaft width and depth, in comparison with other columbids, including *Pezophaps* (Table A10). The cotyla medialis is larger and deeper than the cotyla lateralis. Dorsally, both cotyles are separated by a well-developed eminentia intercondylaris (Fig. 61A, E). In dorsal aspect, the cotyla lateralis has a less distinct ridge, the fossa infracotylaris dorsalis is less deeply excavated, and the foramen vasculare distale is larger and more deeply excavated than in *Pezophaps*. The hypotarsus is large and robust, but maintains the typical columbid monocanaliculate configuration (Mayr, 2015). The hypotarsus has a medially placed single canal that encloses the tendons for the flexor digitorum longus (FDL) muscle. Laterally of the canal for the FDL lies a marked, open sulcus for the tendons of the flexor hallucis longus (FHL) muscle. This sulcus is closed in *Didunculus* and *Goura*, but open in *Caloenas*. Plantarly lie the sulci for the tendons of the m. flexor perforans digit 2 (FP2) and the m. flexor perforans et perforates digiti II (FPP2) (Fig. 62B, E). The crista medialis FDL is strongly developed, increasing the total dorsoplantar depth of the ankle joint by more than 40%. In *Raphus*, the crista medialis hypotarsi extends further plantad, the crista medianoplantaris extends further distad, and the fossa metatarsi I is larger, more distinct, and situated further proximad than in *Pezophaps*. The crista lateralis hypotarsi is extremely large, comparatively much larger than in *Pezophaps*, with a much smaller single crista intermedia hypotarsi enclosing a single sulcus hypotarsi. Prominent intermuscular lines extend down the ventral surface of the tarsometatarsal diaphysis. The fossa metatarsi I is positioned on the plantarmedial margin of the diaphysis, approximately two-thirds down from the proximal extremity of the tarsometatarsus (Fig. 62B, C), similar to *Caloenas* and *Didunculus*. The dodo tarsometatarsus differs from those of *Caloenas* and *Didunculus* in the cotyla lateralis and cotyla medialis being deeper, and the fossa metatarsi I being also deeper with a more pronounced lip. The metatarsal condyles are well developed and separated, more so than in *Caloenas* and *Didunculus*. The tarsometatarsus differs from *Goura* in being overall less elongate and deeper in the shaft, the sulcus extensorius being shallower, the foramen vasculare distale being larger and set deeper, and the crista medialis hypotarsi extending further distad. The trochlea metatarsi III extends furthest distally and has a distinct midline sulcus (Fig. 62A–D, F), whereas the trochlea metatarsi IV is the shortest and oriented ventrolaterally (Fig. 61F). The trochlea metatarsi II extends nearly as far distally as the trochlea for the third metatarsus. The trochleae metatarsorum II and III are both inclined medially.

Metatarsal I (Hallux)—The first metatarsus is a short, robust bone that articulates proximally with an approximately oval articular facet (the fossa metatarsi I) on the caudomedial surface of the tarsometatarsus (Fig. 63; Pls. PL40, D40; Table 23). The articular facet is comparatively flat and projects distinctly medially of the shaft margin. The facies medialis of metatarsus I is slightly convex, and the facies lateralis is concave and spirally wound (Fig. 63A–D). The lateral tubercle is large and relatively more robust than that of closely related volant columbids such as *Goura, Caloenas*, and *Didunculus*, and it is also stouter than in *Pezophaps*. The medial tubercle is less well developed and projects medially slightly proximal to the trochlea metatarsi I. The trochlea is broad and nearly cylindrical (Fig. 62A, B, F).

Pedal Phalanges—The anatomy of the pedal phalanges of the foot of *Raphus* is well known thanks to the preservation of the left pes of the Oxford specimen, which has been described in detail in several early accounts of dodo anatomy (e.g., Owen, 1846; Strickland and Melville, 1848). Both Thirioux specimens preserve a complete pes for each limb (Figs. 55, 60, 64; Pls. PL41–46, D41–46; Table 24). Due to obstruction of the plantar surface of the pedal phalanges by the wooden base plates on which the Durban and Port Louis skeletons were mounted, these surfaces were not accessible to the laser scanner beam, and all plantar surfaces of the Thirioux dodo pedal phalanges were reconstructed using scaled and, if necessary, mirrored 3-D scans of a cast of the Oxford pes (see Materials and Methods). The pedal phalangeal formula for the dodo is 2-3-4-5, similar to extant columbids. The first phalanx of digit 1 (P I-1) is elongate and relatively broad in comparison with the other pedal phalanges, as in all columbids. It is relatively long, but shorter than pedal phalanges II-1 and III-1. The cotyla articularis is wide and shallow. The flexor and extensor fossae on the distal plantar and dorsal surfaces are comparatively shallow. The shape of the distal trochlea is trapezoid due to the oblique orientation of the medial and lateral distal walls; a deep depression for the collateral ligament (fovea ligamentum collateralis) is present in the obliquely inclined lateral and medial surfaces (Figs. 60, 64). The ungual phalanx of the hallux (P I-2) is approximately half the length of P I-1, curved, and has a relatively average-sized tuberculum flexorium, similar to other columbids.

The first phalanx of digit II (P II-1) is approximately equal in length to P III-1. Its diaphysis is more rounded than P I-1. The cotyla articularis of P II-1 has a deep plantar incision for the flexor tendons of the foot, and the lateral portion of the tuberculum flexorium is larger and extends further plantad than the

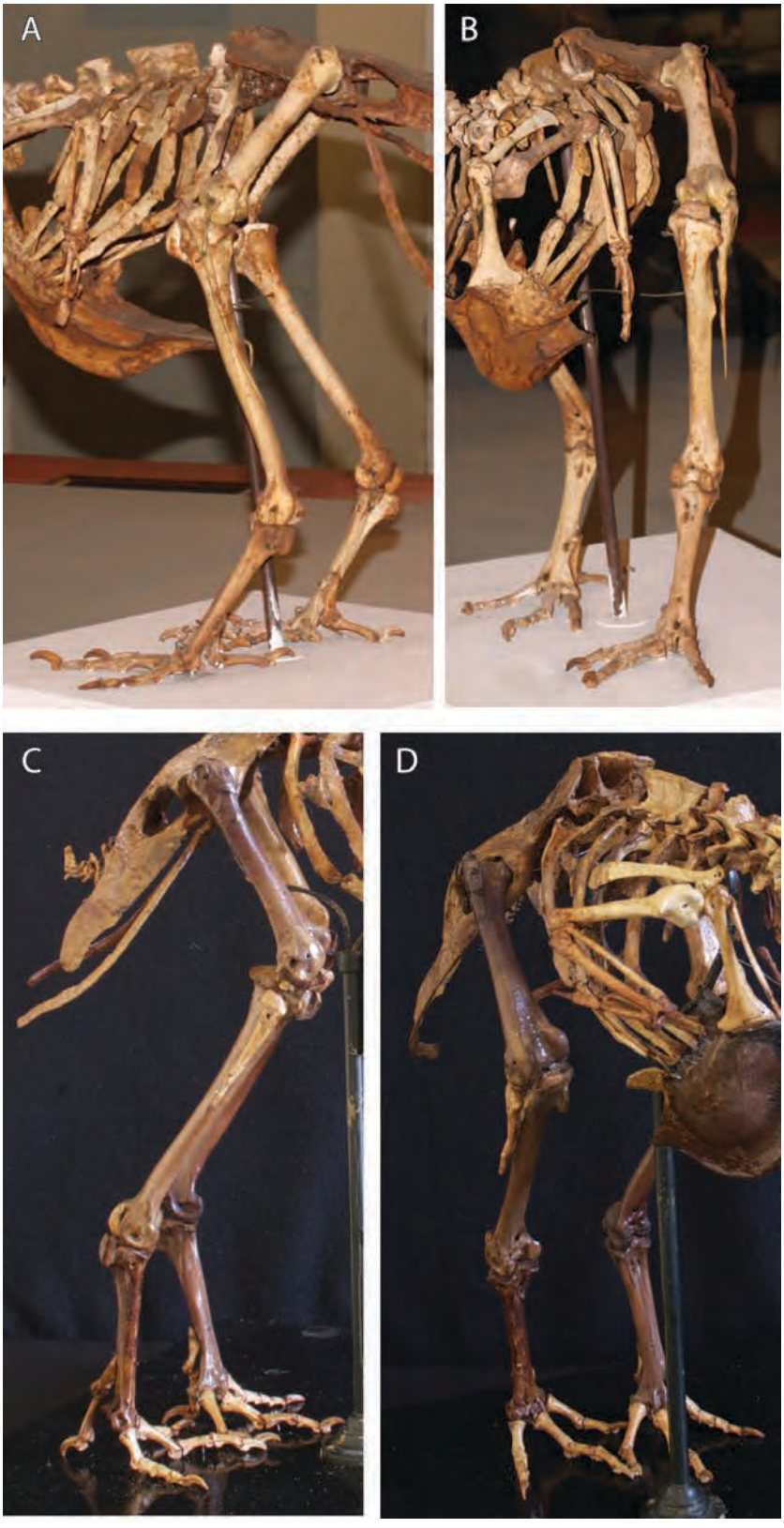

FIGURE 55. Photographs of the hind limb of the Port Louis (**A**, **B**) and the Durban (**C**, **D**) dodos in **A**, left lateral view; **B**, **D**, cranial view; and **C**, right lateral view.

medial portion. Distally, the trochlea articularis has a deep groove and the fovea articularis collateralis is well developed. P II-2 is comparatively short and also has a proximoventral incision for the flexor tendons running below the cotyla articularis. The phalangeal ungual for digit II (P II-3) is similar in its general morphology to ungual P I-2 and the other pedal unguals.

The tuberculum extensorium of the first phalanx of digit III (P III-1) is well developed and extends proximally. The

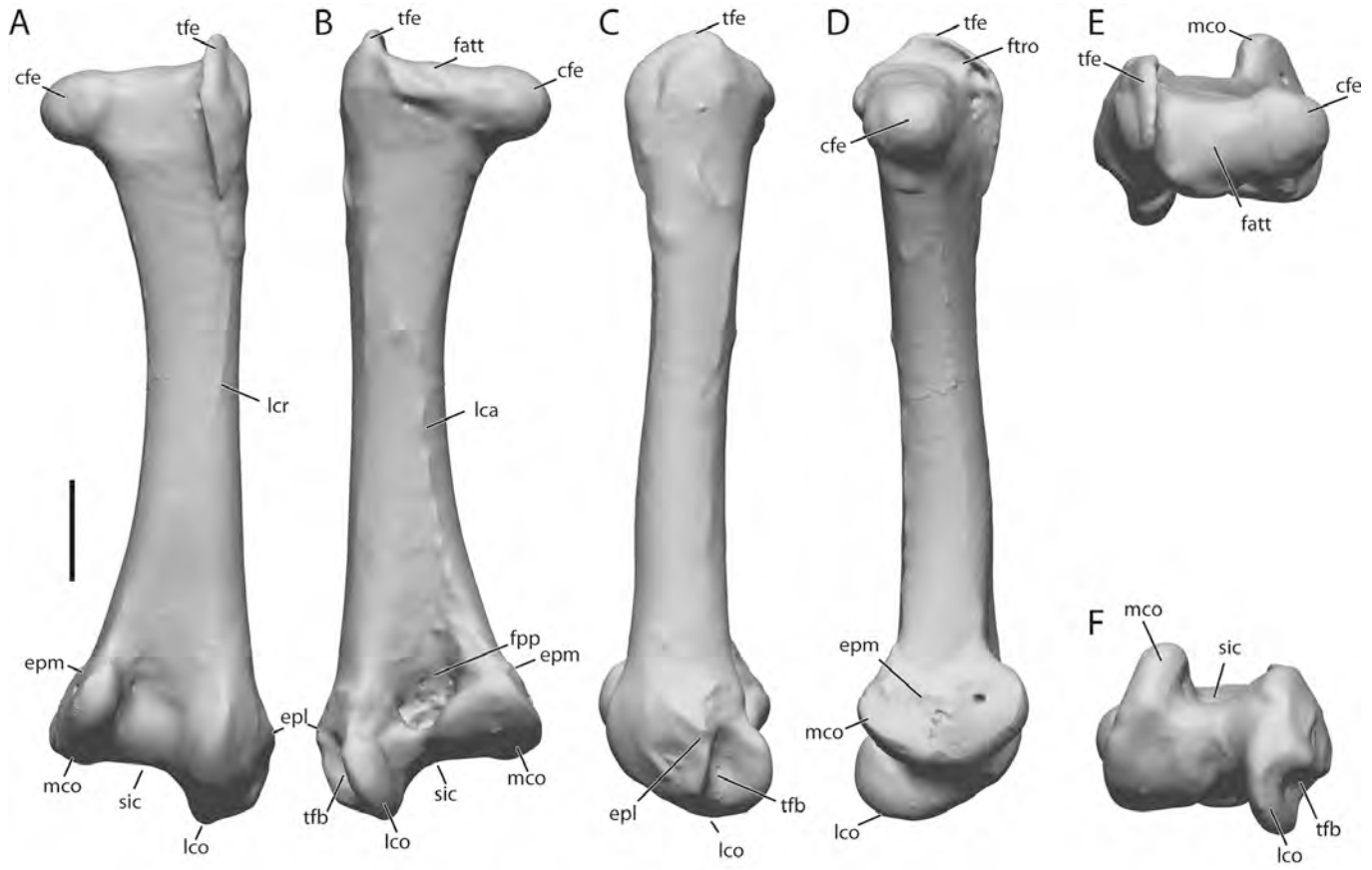

FIGURE 56. 3-D scan images of left femur, Port Louis specimen. **A**, cranial; **B**, caudal; **C**, lateral; **D**, medial; **E**, proximal; **F**, distal views. Anatomical abbreviations as in Appendix 1. Scale bar equals 20 mm.

cotyla articularis of P II-1 is divided into two by a raised, dorsoplantar ridge, which corresponds to the sulcus on trochlea metatarsi III of the tarsometatarsus. Thus, the trochlea metatarsi III–cotyla articularis III-1 joint was more hinge-like and had fewer degrees of freedom than the tarsometatarsal-phalangeal joint of digits I and II, but was also likely able to withstand greater loads. Distally, the trochlea articularis of P III-1 has a deep groove, which corresponds to a similarly subdivided cotylar surface for P III-2. Phalanx III-2 is curved plantad. The trochlea of P III-2 also has a groove, which is most prominent on the plantar surface of the trochlea. Phalanx III-3 is similar in general morphology to P III-2 but only about half as long. The ungual of digit III (P III-4) is similar in general morphology to the other unguals of the foot.

The first phalanx of digit IV is only about two-thirds the length of the first phalanx of digits I–III. Similar to P III-1, it has a dorsoplantar ridge that divides the cotyla articularis into a lateral and a medial depression, and a tuberculum extensorium that extends proximally. Phalanges IV-2, IV-3, and IV-4 are progressively shorter but maintain the subdivision of the trochlea articularis, especially on the plantar surface, and possess associated dorsoplantar cotylar ridges. The ungual of digit IV is smaller than, but similar in morphology to, the unguals of the other digits (Figs. 55, 60, 64).

DISCUSSION

The Port Louis and Durban dodo specimens collected by Louis Etienne Thirioux provide a wealth of new information on dodo anatomy, which we hope this memoir will help make available to a wider audience more than a century after Thirioux's discoveries. The head of the dodo is one of the most apomorphic parts of its anatomy, together with its large body size and the reduction of the wing. Beyond this, the skeletal anatomy of this giant, flightless pigeon is remarkably similar to that of extant volant columbids of much smaller size.

Skull and Mandible

The Port Louis dodo specimen possesses the best-preserved fossil dodo skull in the world. The skull of the Durban specimen is incomplete and has undergone significant restorative work, and cranial material from historic and recent Mare aux Songes collections includes only a few almost complete but unassociated crania and damaged fragments. The dodo's skull is very different from the 'pigeon' model. With its robust morphology and premaxillary rostrum with a distinctly hooked bill tip, it is not surprising that many early systematists included the dodo with the

TABLE 19. Measurements of the femur (in mm).

Specimen	Length	Lateromedial mid-shaft width
Port Louis R	154	18
Port Louis L	152	19
Durban R	152	18
Durban L	151	18

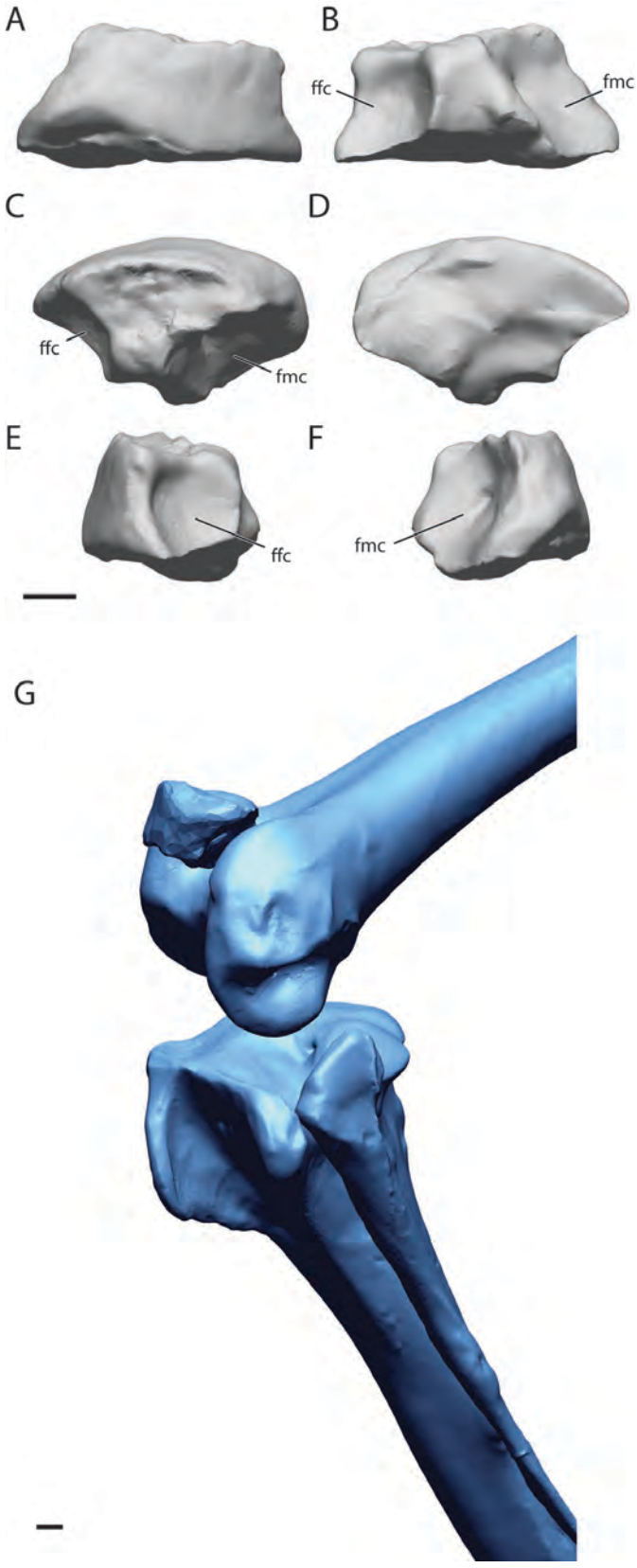

FIGURE 57. 3-D scan images of left patella, Port Louis specimen. **A**, cranial; **B**, caudal; **C**, dorsal; **D**, ventral; **E**, lateral; **F**, medial views; **G**, oblique view of left patella in articulation in sulcus patellaris femoris. Anatomical abbreviations as in Appendix 1. Scale bars equal 5 mm.

birds of prey or vultures (e.g., Blainville, 1830; La Fresnaye, 1839; Owen, 1846; see Parish, 2013, for an overview). In comparison with closely related columbiforms such as *Caloenas, Goura*, or *Didunculus*, the evolutionary transformations of the dodo skull involved a shortening of the cranium and an expansion of the frontals, an elongation and heightening of the premaxilla and mandible, a flattening of the occipital region, and a shift of the occipital condyle to a more caudal position on the base of the skull. The presence of visible sutures in the Port Louis dodo mandible suggests that the anterior and caudal halves never fully fused, an observation that is supported by other complete dodo mandibles and the frequent fossil occurrence of mandible halves, all separated at the point of the suture. Furthermore, the wide nasofrontal hinge, the uncoupling of the dorsal and lateral bars of the premaxilla (i.e., a schizorhinal nostril), and the probable presence of a mandibular brace indicate that the skull was highly kinetic and adapted to withstand high force loads. Although in-depth biomechanical analysis is needed to properly elucidate dodo jaw kinetics and feeding behavior, the dodo jaw morphology is indicative of a diet that included hard food items such as seeds and invertebrates, possibly including crabs.

The only contemporary record of the diet of the dodo is from a Dutch sailor, who noted in 1634 that the dodo fed on 'raw fruit' (see Servaas, 1887). Owen (1866) hypothesized that the dodo's massive jaw enabled it to feed on animal matter, and Hachisuka (1953) was the first to speculate that the dodo might have fed on crustaceans and molluscs, which could also augment a largely herbivorous diet with extra protein in times of breeding, as in other Mascarene columbids (see Hume, 2011).

Although C_3 plants likely made up most of the dodo's diet (Rijsdijk et al., 2009), its massive beak, kinetic skull, and secondary mandibular articulation indicate that land crabs and hard-shelled terrestrial mollusks could have formed an part of the dodo's diet, possibly seasonally. Land crabs have become virtually extinct in the Mascarenes (Hume, 2005), but large numbers, including the huge Coconut Crab *Birgus latro* (L. 1767), formerly inhabited the islands (Leguat, 1708; Hume, 2005; Cheke and Hume, 2008). The massive premaxillary rostrum with a large, hooked bill may also have been an adaptation for combat during the breeding season (see Hume and Steel, 2013). A kinetic nasofrontal hinge and a schizorhinal nostril are present in some columbids (Bock, 1964; Zusi, 1984), but the indications for a mandibular brace are a departure from the typical columbid Bauplan and are testament to the dodo's derived nature and unique adaptive pathway.

Axial Skeleton

Presynsacral Axial Anatomy—There has been debate and confusion regarding the structure of the axial skeleton of *Raphus*, based upon the different interpretations of disassociated Mare aux Songes remains (see Owen, 1866, 1872; Newton and Newton, 1868; Newton and Gadow, 1893; Martin, 1904; Chubb, 1919). The Thirioux specimens help resolve this conundrum, although alteration of the vertebral column in the Durban specimen (see Claessens and Hume, 2015) does complicate the interpretation of presynsacral vertebral anatomy in the Thirioux specimens. The presynsacral vertebral column of the Port Louis specimen appears to derive from a single bird, without additions, removals, or substitutions.

Owen (1866) provided the earliest reconstruction of the complete dodo skeleton, in which he imagined the dodo as a portly bird; Owen had fitted the newly discovered skeletal remains within the 1626 'Edwards dodo' painting by Savery. Owen's (1866) reconstruction featured 19 presynsacral vertebrae, namely, 12 cervical, two cervicodorsal, and five thoracic vertebrae (or, in Owen's terminology, 12 cervical and seven dorsal vertebrae; see Owen, 1872). Owen's (1866) reconstruction featured no less than seven vertebral

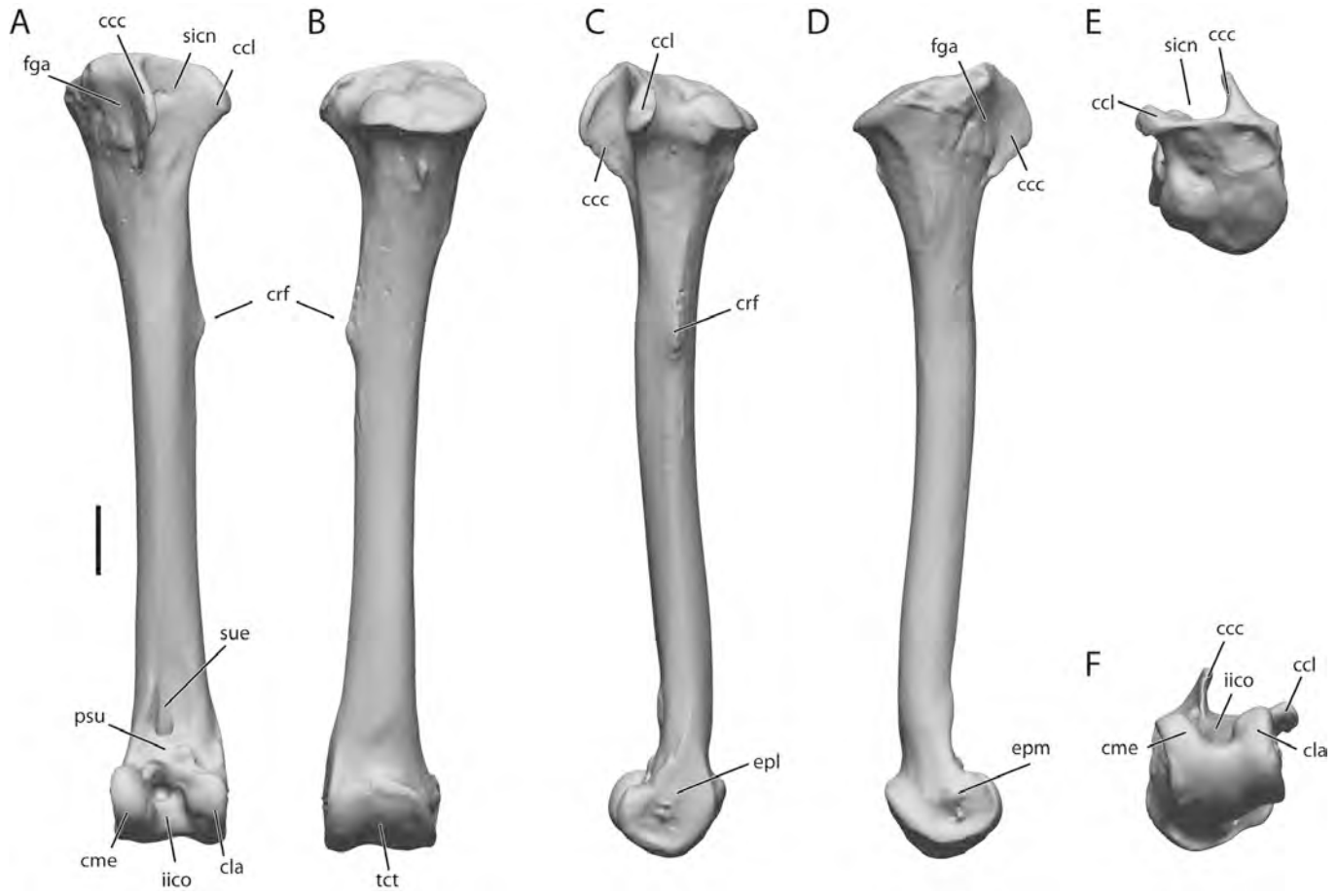

FIGURE 58. 3-D scan images of left tibiotarsus, Port Louis specimen. **A**, cranial; **B**, caudal; **C**, lateral; **D**, medial; **E**, proximal; **F**, distal views. Anatomical abbreviations as in Appendix 1. Scale bar equals 20 mm.

ribs, including five that articulated with the margo costalis of the sternum via a sternal rib.

Newton and Newton (1868) critiqued the fact that Owen (1866) did not provide an explicit vertebral count in the written portion of his monograph and further disagreed with his interpretation of the number of sternal rib articulations for *Raphus*. Newton and Newton (1868) also mentioned perceived inaccuracies in the composition of the vertebral column of *Didunculus strigirostris* as illustrated in Owen (1866). In a revised and refined dodo reconstruction, Owen (1872) decreased the number of costae completae verae, but also argued that providing an exact determination of vertebral segments in the dodo would always be ambiguous if based on skeletal reconstruction from disassociated remains. Newton and Gadow (1893) revisited the subject of dodo axial anatomy nearly two decades later, with a further critique of Owen's (1866, 1872) interpretation of the composition of the presynsacral vertebral column. The exchange regarding the correct interpretation of the presynsacral axial skeleton between Alfred Newton and Richard Owen (Newton and Newton, 1868; Newton and Gadow, 1893; Owen, 1872) was rather heated, and it seems that Newton's arguments were put forward rather rashly and deliberately, and not with much careful skeletal examination. Thus, it is tempting to speculate that discord regarding the 'hijacking' by Owen of the dodo bones intended for Newton may have stood at the basis of Newton's critique (see Hume et al., 2009).

The complete axial skeleton preserved in the Port Louis specimen differs from all interpretations put forward previously (Newton and Newton, 1868; Newton and Gadow, 1893; Owen, 1866, 1872). The correct presynsacral vertebral count for the Thirioux dodos is 19, similar to that tentatively proposed by Owen, but dissimilar to that proposed by Newton and Newton (1868) and Newton and Gadow (1893). However, there are two more cervical, only a single cervicodorsal vertebra, and only four thoracic vertebrae, different from Owen's (1866, 1872) interpretation. The Port Louis specimen has 14 cervical vertebrae: an atlas (C1), axis (C2), and a further 12 cervical vertebrae with no free ribs (C3–C14), followed by one 'cervicodorsal' vertebra with an elongate vertebral rib that does not have a sternal rib component or connection to the breastbone (C15). The four remaining presynsacral (thoracic) vertebrae consist of a notarium, formed through the fusion of presynsacral vertebrae 16, 17, and 18, and a free thoracic vertebra for presynsacral segment 19. There are four costae verae, associated with presynsacral vertebral segments 16–19, which have vertebral followed by sternal ribs that articulate directly with the sternum. There is one costa verae

TABLE 20. Measurements of the tibiotarsus (in mm).

Specimen	Length	Mid-shaft DV width
Port Louis R	218	15
Port Louis L	218	17
Durban R	212	15
Durban L	212	15

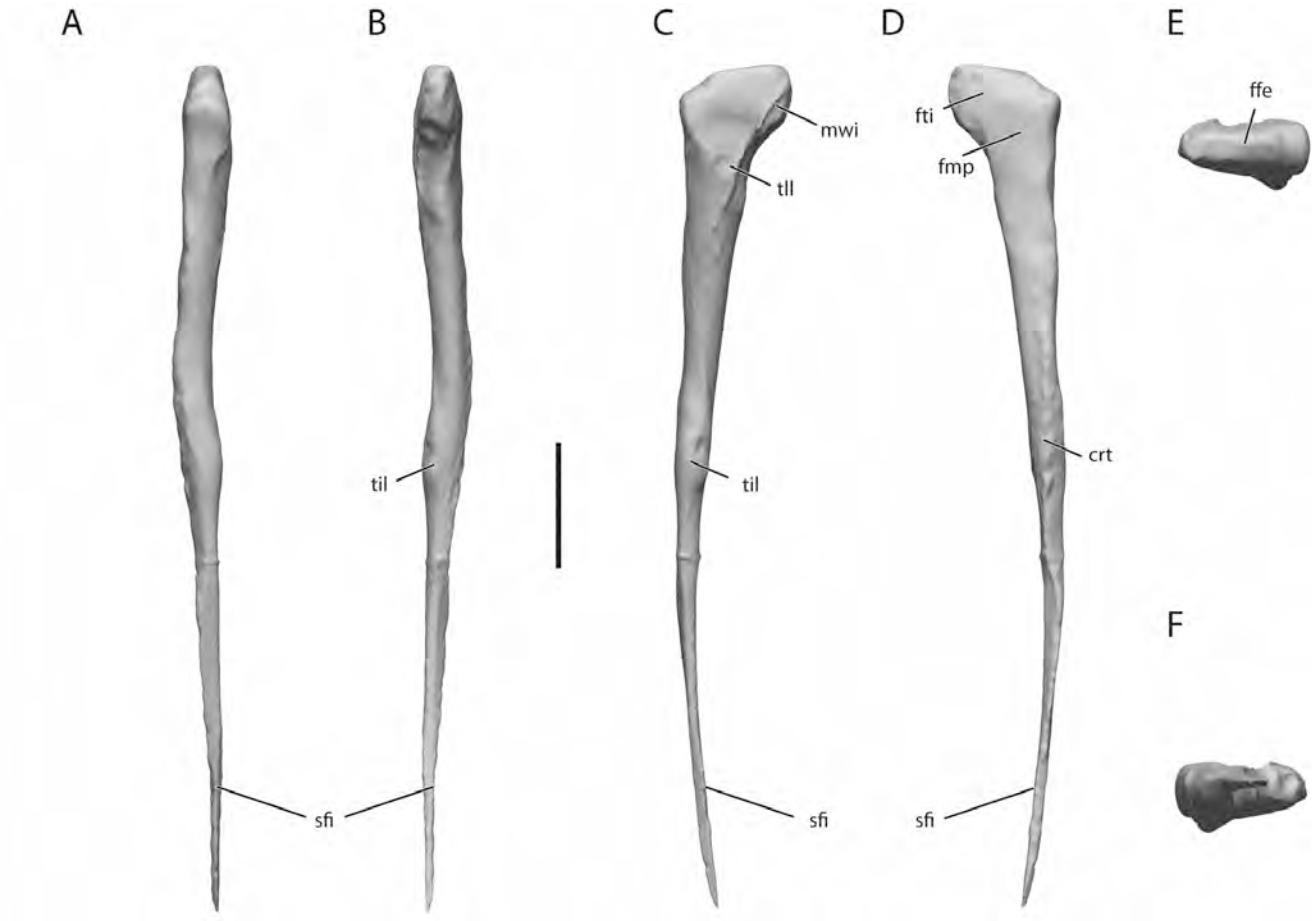

FIGURE 59. 3-D scan images of left fibula, Port Louis specimen. **A**, cranial; **B**, caudal; **C**, lateral; **D**, medial; **E**, proximal; **F**, distal views. Anatomical abbreviations as in Appendix 1. Scale bar equals 20 mm.

spuriae, in which the sternal rib articulates with the preceding sternal rib segment, rather than the sternum, namely, on the first synsacral vertebra.

The structure of the presynsacral axial skeleton of the Durban specimen was similar to that of the Port Louis specimen before alterations were made to the specimen after Thirioux's death and transport of the specimen to Durban (see Claessens and Hume, 2015). Thus, it appears that a composition of the presynsacral vertebral column of the dodo may have consisted of 14 cervical, one cervicodorsal, and four thoracic vertebrae. Yet, it is also important to note that presynsacral, synsacral, and caudal vertebral counts vary intraspecifically in almost all birds, including columbids such as *Goura* and *Columba* (Claessens, pers. observ.; Fürbringer, 1888; Martin, 1904). Thus, establishing an absolute, fixed, and immutable vertebral count for *Raphus* (e.g., Newton and Gadow, 1893), or any bird for that matter, is likely impossible considering the inherent plasticity of vertebral development in birds. Minor deviations from the total vertebral number as well as the borders between different axial regions as observed in the Thirioux specimens is certainly possible in the light of intraspecific variation.

Structure and Function of the Neck—The area ligamentum elastici on the caudal base of the processus spinosus of the axis and of the cranial and caudal bases of the processus spinosus of C3 is large and deep in *Raphus*. In *Didunculus* and *Columba*, the area ligamentum elastici is much less prominent, and it also appears less developed in *Pezophaps*, although the area ligamentum elastici in *Caloenas* appears more equal in development to that in *Raphus*. A comparatively greater development of areas of attachment for cervical and occipital ligaments and muscles in *Raphus* would certainly appear to make sense from a biomechanical perspective, considering the much longer (and thus heavier) skull and more robust rostrum of the dodo. Preservation of the entire cervical vertebral column of the Port Louis specimen enabled an analysis of ventral and dorsal mobility of the neck skeleton of *Raphus*. Taking the point when there is no longer any overlap between the zygapophyseal facets or, if encountered sooner, the moment when portions of adjacent vertebrae collide at the maximum range of flexion, it is apparent that the neck of the dodo was likely capable of significant dorsiflexion and ventriflexion (Fig. 65).

TABLE 21. Measurements of the fibula (in mm).

Specimen	Length	Mid-shaft craniocaudal width
Port Louis R	94*	7
Port Louis L	141	6
Durban R	80*	7
Durban L	102*	9

*Value underestimated due to damage to the specimen.

FIGURE 60. Photographs of the lower leg of the Port Louis specimen. **A**, left oblique caudal view; **B**, oblique dorsal view, left leg; **C**, dorsal view, left leg. All scale bars equal 5 cm.

The Wing Skeleton

The length of the wing of *Raphus* is strongly reduced relative to total body length when compared with extant volant pigeons. Humeral length in the Thirioux dodos is less than half of total pelvic (synsacral) length, whereas humeral length is nearly equal to synsacral length in closely related large volant columbids such as *Goura* and *Caloenas*. Whereas the antebrachium (radius + ulna) is longer than the humerus in volant columbiforms, as is the autopodium (carpals, carpometacarpals, and phalanges), the antebrachium and autopodium are both shorter than the humerus in *Raphus*. The length proportions of the wing (humerus to radius + radiale to carpometacarpus + phalanx proximalis digiti majoris + phalanx distalis digit majoris = approximately 41%:31%:28%) are very different from volant columbids (e.g., 29%:32%:39% in *Caloenas* MCZ 341255). This

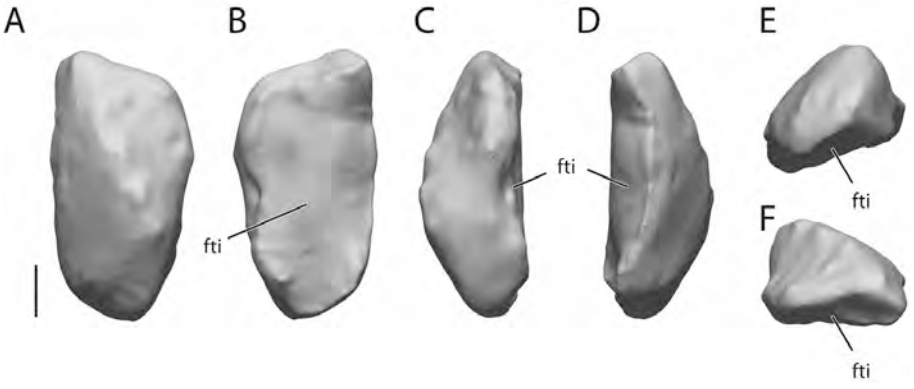

FIGURE 61. 3-D scan images of the intertarsal sesamoid, Port Louis specimen. **A**, cranial; **B**, caudal; **C**, lateral; **D**, medial; **E**, proximal; **F**, distal surfaces. Anatomical abbreviations as in Appendix 1. Scale bar equals 5 mm.

TABLE 22. Measurements of the tarsometatarsus (in mm).

Specimen	Length	Mid-shaft lateromedial width
Port Louis R	123	15
Port Louis L	123	15
Durban R	134	16
Durban L	133	16

accords with the progressive shortening of the wing from the distal to the proximal bony elements in flightless birds (Livezey, 1995). Total wing length of the dodo is only approximately two-thirds greater than synsacral length, whereas it is generally more than four times synsacral length in *Caloenas*.

In the humerus, the distal margin of the crista bicipitalis is nearly perpendicular to the humeral diaphysis, an angle that is more acute than that observed in *Goura, Caloenas, Didunculus*, and *Pezophaps*. The length from the caput humeri to the distal edge of the crista bicipitalis of *Raphus* is less than 25% of total humeral length. This area extends further distally in smaller, volant pigeons such as *Caloenas* and *Didunculus* (approximately 30–35% of total humeral length), but this is likely an artifact of size and allometric growth, because the relative length of the proximal extremity of the humerus of *Raphus* is similar to that in *Goura* and *Pezophaps*. The crista deltopectoralis is well developed in both Thirioux specimens, as is the crista bicipitalis, but compared with smaller volant pigeons, e.g., *Caloenas*, they are shorter. The proximal margin of the crista deltopectoralis is nearly perpendicular to the diaphysis, yet inclined slightly distally. In *Caloenas* and *Didunculus*, the proximal margin of the crista deltopectoralis is slightly inclined proximally. A well-developed ridge for the insertion of the m. latissimus dorsi is present on the proximocaudal surface of the diaphysis in *Raphus* (Fig. 45B–D), which is slightly less prominent in *Goura, Caloenas*, and *Didunculus*. However, our examination shows that this ridge is equally well developed in many *Pezophaps* specimens. The degree of laterality observed is similar to that in extant pigeons, which possess slightly longer and more robust skeletal elements on the right side of the body, as well as to that observed in a large morphometric study of Mare Aux Songes remains (Van Heteren et al., 2014; Johnston and Janiga, 1995).

Apart from the minor difference in robusticity of the antebrachial bones of *Raphus* and other volant columbids, and the inverse length relationship between upper arm and antebrachium, the morphology of the radius in *Raphus* is generally similar to that of closely related columbids such as *Goura* and *Caloenas*. There are no apparent distinct morphological features related to the extended position in which the dodo wing was held at rest. However, considering the large range of motion of the elbow joint of volant pigeons, which flex the elbow during terrestrial locomotion and during the upstroke, and maximally extend the wing during downstroke (Alexander, 2002), the greater extension that the elbow joint in *Raphus* is maintained in certainly falls within the range of motion that the elbow joint experiences in volant columbiforms.

In the ulna, the anatomy of the facies articularis radii is similar to that of volant columbids. Similar to the radius, the ulna is

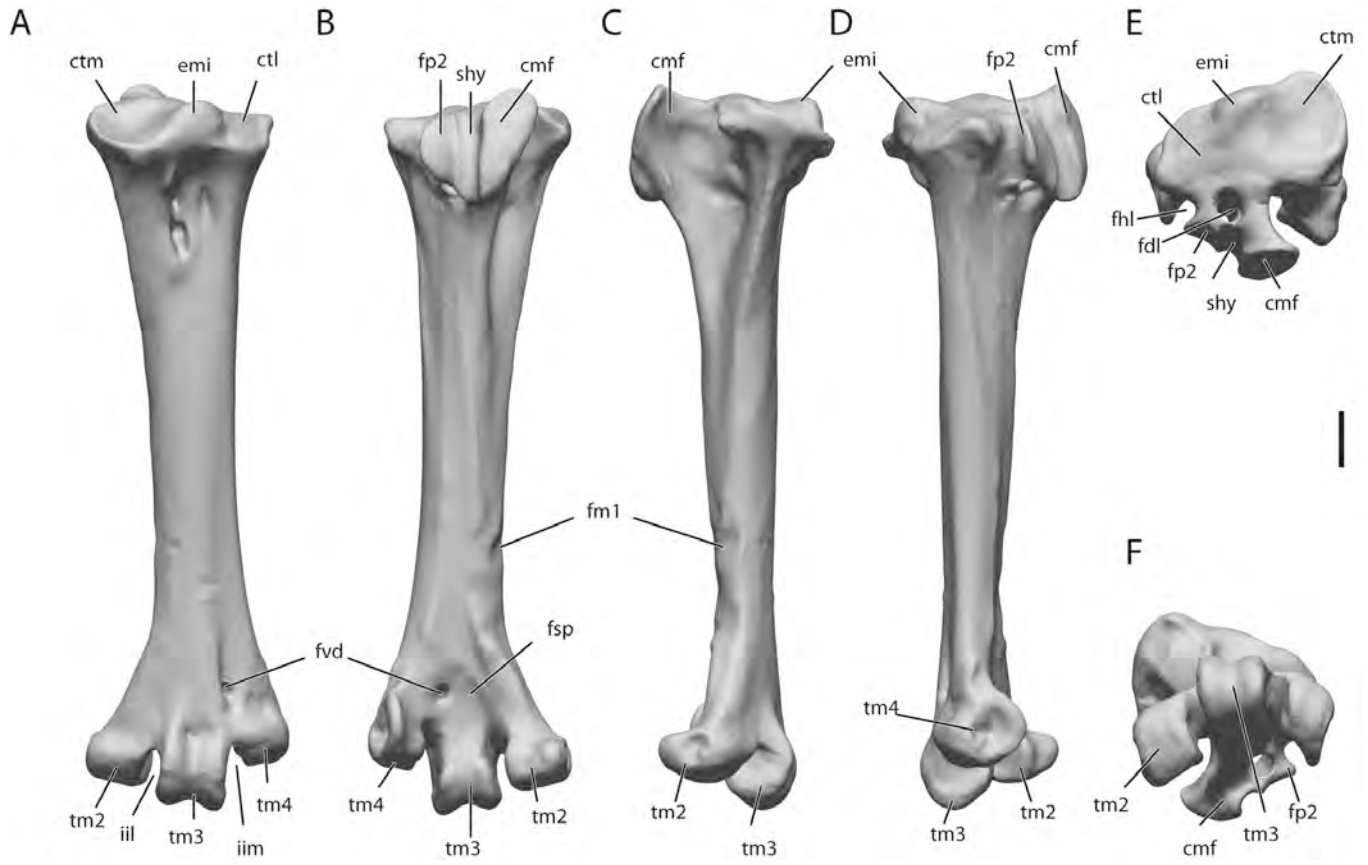

FIGURE 62. 3-D scan images of the left tarsometatarsus, Port Louis specimen. **A**, dorsal; **B**, plantar; **C**, lateral; **D**, medial; **E**, proximal; **F**, distal views. Anatomical abbreviations as in Appendix 1. Scale bar equals 10 mm.

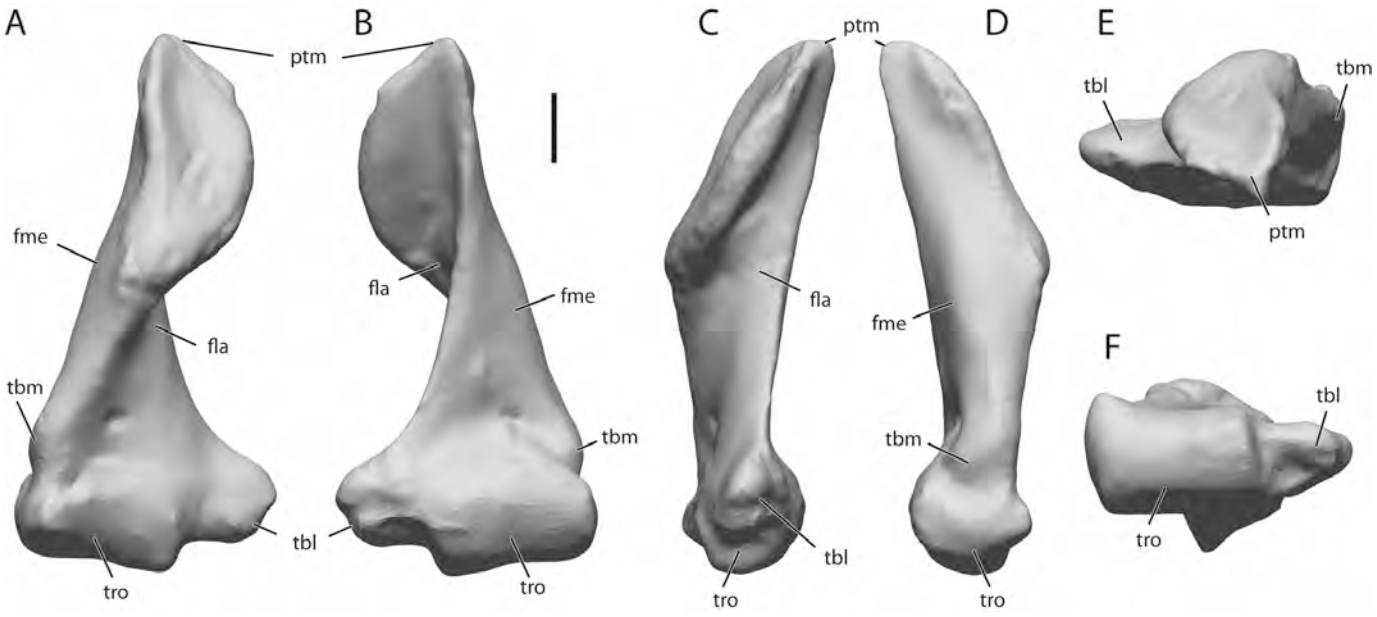

FIGURE 63. 3-D scan images of left metatarsus I, Port Louis specimen. **A**, dorsal; **B**, plantar; **C**, lateral; **D**, medial; **E**, proximal; **F**, distal views. Anatomical abbreviations as in Appendix 1. Scale bar equals 5 mm.

slightly more robust than in volant pigeons, although less robust than in *Pezophaps*. The ulnae of the Thirioux specimens, although less curved than in volant pigeons, are not as straight as the Mare aux Songes specimen described by Owen (1866), but there does appear to be some variation in ulnar curvature in other specimens recovered from this fossil locality. The proximal shaft of the ulnae of the Thirioux specimens is fairly curved, whereas the distal shaft is somewhat straighter.

Judging from the few images known that were drawn by artists from living dodos, (the dodo sketches of Laerle and the painting of Mansur; see, for instance, Hume, 2006), it appears that the wing of *Raphus* was held in a more extended position than in extant (volant) columbids; hence, the statement by Mundy (1638 [1919]:352) that the dodo had "little hanguing [sic] wings like shortt [sic] sleeves." However, there are no apparent differences in (elbow) joint morphology in *Raphus* that reflect this difference in wing position 'at rest.' The overall shortening of the wing in *Raphus*, combined with increased body size, allows the elbow to be extended without this resulting in the wing dragging on the ground (which would invariably be the case in volant taxa). With wing length reduction, extreme flexion at the elbow joint, as observed in volant columbids, requiring greater energetic expenditure to carry the weight of the antebrachium, is no longer needed. Reduction in wing length likely enabled extension at elbow joint, so that the antebrachium could be carried in an energetically less costly way. Similar extended wing positions are seen in ratites (e.g., *Struthio, Apteryx*). Anatomical specializations associated with extension at the elbow joint are not seen in *Raphus*, likely because the half-extended elbow position in *Raphus* is intermediate between the full flexion and extension of the elbow that would happen during flight; thus, it lies in the middle of the range of motion that was present in the wing morphology of the dodo's volant ancestor.

Despite the reduction of the wing skeleton, muscle insertion scars on the humerus, radius, and ulna are well developed. Amazement regarding the lack of reduction of muscle insertion scars in the non-volant dodo was already voiced early on by, for instance, Owen (1866). The fact that the insertion of the m. latissimus dorsi on the dodo humerus is as pronounced as in *Pezophaps*, which used its wings in intraspecific combat (Hume and Steel, 2013), suggests that the dodo may have been using its wings for another purpose. We can only speculate regarding the use of the dodo wing, but we would like to note that losing one wing function (flight) does not mean that the entire wing becomes vestigial. In extant columbids, the wing functions not solely for flight, but also in display and for balance. Hume and Steel (2013) argued that aggressive behavior and territorial display was present in the ancestral, volant pigeon that colonized the Mascarene Islands. The dodo carpometacarpus lacks the musket ball (carpal knob), which was used as a weapon in the solitaire. The pronounced muscle scars in the dodo wing imply that the wing was not hanging limply alongside the body, but that the wing was frequently used, presumably also in display behavior, which is a widespread phenomenon in birds.

TABLE 23. Measurements of metatarsus I (in mm).

Specimen	Length	Distal lateromedial width
Port Louis R	38	19
Port Louis L	35	19
Durban R	35	17
Durban L	32	16

Pelvis

The stereotypical view of the dodo is that of a clumsy, waddling bird, epitomized by the old Dutch name 'dodaersen,' which specifically refers to its typical large hind quarters (e.g., Owen, 1866; Hachisuka, 1953). Owen (1866) remarked on the dodo's broad, flat pelvis as characteristic for the 'dodaersen.' However, the general proportions of the pelvis of *Raphus* are not very different from those of smaller volant pigeons: postacetabular pelvic width divided by synsacral length falls within the same range as in smaller volant taxa. Differences in pelvic morphology of the dodo in comparison with other columbids are found in the large caudad 'extension' of the pubis and the ala ischia (in

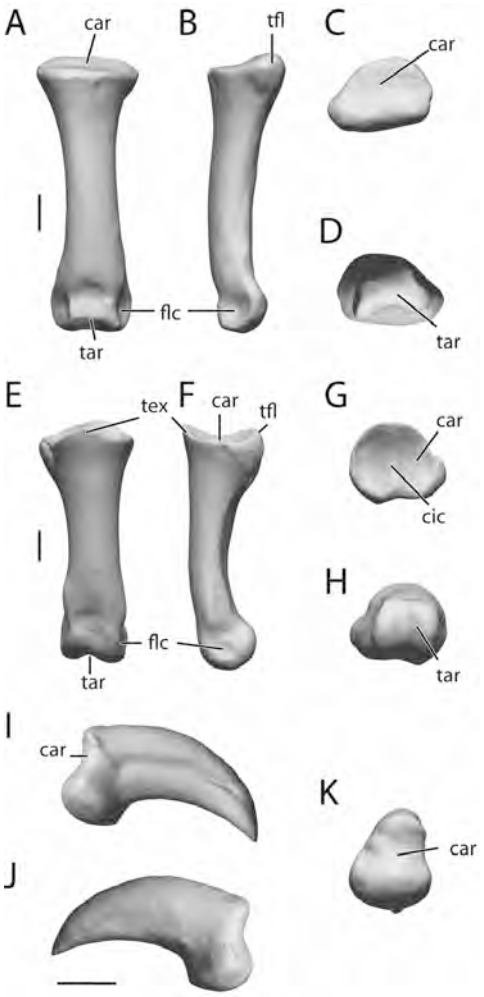

FIGURE 64. 3-D scan images of pedal phalanges from the right foot of the Port Louis dodo. Phalanx I-1 in **A**, dorsal; **B**, lateral; **C**, proximal; and **D**, distal views. Phalanx III-1 in **E**, dorsal; **F**, lateral; **G**, proximal; and **H**, distal views. Ungual phalanx IV-5 in **I**, lateral; **J**, medial; and **K**, proximal views. Ventral surface has been digitally reconstructed by substituting scan data from the Oxford dodo foot skeleton. Anatomical abbreviations as in Appendix 1. Scale bars equal 5 mm.

TABLE 24. Measurements of pedal phalanges, Port Louis specimen, left foot (in mm).

Phalanx	Length	Proximal width	Proximal depth	Mid-shaft width	Mid-shaft depth	Distal width	Distal depth
I-1	38.1	9	4.6	—	—	19	8.2
I-2	37.1	14.3	9.6	7.3	5.5	10.4	6.1
I-3 (ungual)	21.9	8.4	10.3	—	—	—	—
II-1	40	14.3	10.9	7.5	6.6	8.9	6.8
II-2	23.6	8.8	7.4	6.2	6	7.4	4.9
II-3 (ungual)	19.7	7.5	9.5	—	—	—	—
III-1	40	15.3	14.3	8.6	7.8	10.6	10.4
III-2	27	11.3	9.9	8.3	6.1	8.5	6.6
III-3	20.2	8.6	8	7.1	5.5	8	5.1
III-4 (ungual)	23.1	8.1	10.6	—	—	—	—
IV-1	24.5	13.2	10.5	8.4	5.1	8.8	7.4
IV-2	15.9	8.7	8.1	8.8	4.4	7.4	5.3
IV-3	12.7	7.1	7	7.9	4.9	7.2	4.5
IV-4	12.3	6.1	5.6	5.9	4.2	5.7	3.4
IV-5 (ungual)	18.9	6.8	8	—	—	—	—

comparison with the caudad extent of the ilium). These caudad skeletal surfaces would have provided more surface area and greater leverage for the retractor muscles of the hind limb of *Raphus*, and would have likely enabled the dodo be much more efficient in hind limb–propelled ground locomotion. This locomotory efficiency is further supported by the report of the shipwrecked mariner Evertszen in 1662, who stated that the dodo was a fast runner and difficult to catch on open ground (see, e.g., Van Wissen, 1995).

Hind Limb

Despite a highly modified cranium, a reduced wing skeleton, and an increase in body size, the proportions of the dodo's hind limb seem to have undergone little change. The length proportions of the hind limb (femur to tibiotarsus to tarsometatarsus = approximately 30%:44%:26% of the leg) are similar to other columbids, such as *Caloenas, Didunculus*, and *Columba*. Total hind limb length (femur+tibiotarsus +tarsometatarsus) compared with synsacral length in *Raphus* also falls within the range of columbids such as *Caloenas, Didunculus*, and *Columba*. Livezey (1993) claimed that the femur of *Raphus* was unusually long, but we have found no support for this. We only find that robusticity of the hind limb may be slightly greater and measure a 10–15% greater mid-shaft width in *Raphus* compared with our small comparative data set. Livezey (1993) described the pelvic limbs, together with the "huge trunks … and skulls," as overdeveloped, i.e., peramorphic, compared with those of flighted Columbidae (Livezey, 1993:279). Although there is no doubt that the skull is peramorphic, and the pectoral girdle underdeveloped, i.e., paedomorphic, peramorphism of the pelvic girdle in the Thirioux dodos appears to be less than described by Livezey (1993) and mostly reflects an increase in overall robusticity of the hind limb in response to increased body mass.

The range of angles at which the major hind limb joints of the dodo were held do not appear to have differed substantially from that of modern columbids, including the relatively horizontal position of the femur (Table 1), in contrast to the unnatural upright pose in which the Durban specimen was remounted in 1919 (see Claessens and Hume, 2015). The femoral condylus lateralis of *Raphus* does appear to be larger and extend further distad than in other columbids. A larger femoral condylus lateralis is also seen in some ratites and is likely associated with a greater degree of abduction of the distal femur due to increased body size and girth.

The Dodo and Island Evolution

An increase in body size and a reduction of the wing apparatus is a common phenomenon in birds in an insular, predator-free setting (e.g., the anatids of New Zealand and Hawaii; Olson and James, 1991; Worthy and Holdaway, 2002), especially islands such as Mauritius that were devoid of terrestrial mammals. However, flightlessness is not always correlated with increased body size (e.g., McNab, 2002). In columbids outside of the Mascarenes, the only other known examples of giant and flightless pigeons are *Natunaornis gigoura* Worthy, 2001, from Viti Levu, Fiji (Worthy, 2001) and the St. Helena Pigeon *Dysmoropelia dekarchiskos* (Olson, 1975). *Natunaornis gigoura* was only slightly smaller than the dodo and solitaire and more closely related to the crowned pigeons, yet it demonstrates that multiple lineages of pigeons can follow parallel paths towards large body size and flightlessness. Unfortunately, only a few fragmentary skull fragments of *N. gigoura* are known, and a comparison of cranial morphology with that of the dodo will have to wait until more material becomes available.

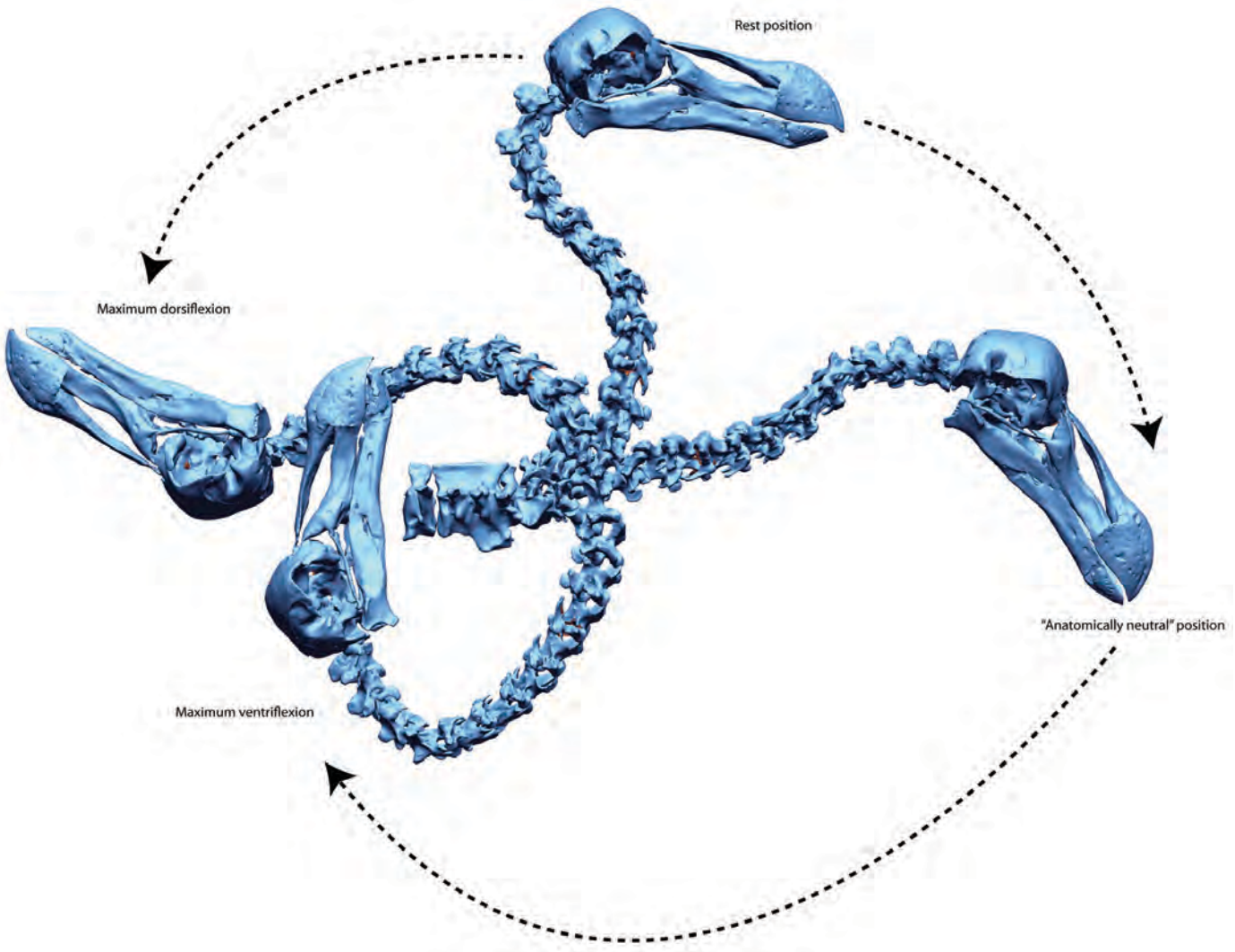

FIGURE 65. Theoretical range of extension in dodo neck in the sagittal plane, showing rest position, 'anatomical neutral' position (where the facies articularis prezygapophyses and postzygapophyses are maximally overlapped at each joint), and maximum dorsiflexion and ventriflexion (modeled as the point before which the cranial and caudal margins of each facies articularis prezygapophysis and postzygapophysis lose contact). The skull is kept in a fixed position with respect to the axis. In order to model maximum extension in the sagittal plane, no lateral displacement or long axis rotation of the neck was modeled. Note that maximally extended positions in the sagittal plane are theoretical; in life, the skull and neck would be impeded by the torso if lateral displacement did not take place. Image composed of Port Louis skull and cervical vertebra 10, and cervical vertebrae 1–9 and 11–17 from the Durban specimen.

CONCLUSIONS

The Thirioux dodos provide, for the first time, accurate skeletal proportions derived from a single, associated and a partially associated dodo, as well as the first descriptions of several previously unknown or hitherto ignored skeletal elements. Our new comprehensive skeletal data and the digital scans (reposited in the Aves 3D database; http://Aves3D.org) will hopefully ensure that the Thirioux specimens play an important role in the future study of the enigmatic and fascinating dodo. A major concept that continues to emerge from our and other recent studies is that, in contrast to popular belief, the dodo was not a clumsy, inadequate bird destined for extinction, but one that was highly adapted to its insular surroundings (e.g., Kitchener, 1993; Livezey, 1993; Rijsdijk et al., 2015). Its skull displays several morphological features that deviate strongly from the pigeon Bauplan and reflect adaptations to the unique ecosystem of Mauritius. The presence of well-developed muscle insertions on the wing bones show that despite a reduction in size, the wings were not entirely vestigial and were likely used in display behavior and other functions such as balance, similar to many other extant columbid genera. The strong, robust hind limbs would have been necessary to support the bulk of a large, terrestrial pigeon, but were equally suited for agile maneuverability (perhaps a necessity in the densely forested and rocky landscape of pre-human Mauritius). The use of the wings for balance would certainly have complemented this. However, although the dodo's skeleton was adapted for increased size and body weight, many aspects of its skeletal anatomy have remained remarkably similar to that of its smaller and volant close relatives in the family Columbidae. The dodo remains an excellent case study for many unexplored evolutionary pathways, and despite more than a century of a plethora of popular books and articles, the dodo remains a true icon of extinction that still holds many secrets and potential insights into the natural world that humans inhabit.

ACKNOWLEDGMENTS

We especially would like to thank G. Beebeejaun and V. Rupear from the Mauritius Institute and all members of the Mauritius Museums Council for providing access to the Port Louis skeleton for 3-D scanning. Similarly, we express much gratitude to D. Allan and the staff of the Durban Natural Science Museum for all their assistance during the 3-D scanning in Durban. We thank P. Sweet and J. Cracraft (AMNH), C. Taylor (Hampshire Museums), G. Beebeejaun and V. Rupear (MI), D. Allan (DNSM), S. Chapman and J. Cooper (NHMUK), M. Nowak-Kemp (OUM), C. Bens, R. Allain, and C. Sagne (MNHN), M. Brooke and M. Taylor (UMZC), S. Olson (NMNH), C. Norris, K. Zyskowski, R. Prum, and J. Gauthier (YPM), J. Trimble and S. Edwards (MCZ), and J. Fjeldså (ZMUC) for providing access to specimens. A. Biedlingmaier and J. Leavitt for assistance with 3-D scanning in Port Louis and Durban, and G. Monfette, A. Randall, and A. Kimelblatt for additional help with 3-D scan processing. We would like to thank K. F. Rijsdijk and Dodo Research Programme members for their assistance during various stages of this project. We thank J. Parish for many helpful discussions and generously sharing materials. We thank R. Prŷs-Jones, E. Fuller, and M. Reindersma for many helpful discussions, L. Schmitz for advice on scleral ossicles, and J. Hutchinson for advice on avian patellar structure. We thank R. Irmis for his careful guidance as the memoir series editor and we thank T. Worthy, J. Parish, and two anonymous reviewers for their constructive comments. Funding for the 3-D scanning project was provided by the National Science Foundation (Aves 3D project, DBI 0743327) and a College of the Holy Cross Research and Publication grant to L.C. Part of L.C.'s work was undertaken during a Temminck sabbatical fellowship at NBC. J.P.H. thanks Special Funds (NHM), Department Investment Fund DIF (NHMUK), and Percy Sladen Centenary Fund. H.J.M.M. received support from the Spanish Ministerio de Economía y Competitividad (CGL2011-28681) and the Generalitat de Catalunya (BP-B-00174).

LITERATURE CITED

Alexander, D. E. 2002. Nature's Flyers: Birds, Insects, and the Biomechanics of Flight. The Johns Hopkins University Press, Baltimore, Maryland.

Angst, D., E. Buffetaut, and A. Abourachid. 2011a. The end of the fat dodo? A new mass estimate for *Raphus cucullatus*. Naturwissenschaften 98:233–236.

Angst, D., E. Buffetaut, and A. Abourachid. 2011b. In defense of slim dodo: a reply to Louchart and Mourer-Chauviré. Naturwissenschaften 98:359–360.

Baumel, J. J., and L. M. Witmer. 1993. Osteologia; pp. 45–132 in J. J. Baumel, A. S. King, J. E. Breazile, H. E. Evans, and J. C. Vanden Berge (eds.), Handbook of Avian Anatomy: Nomina Anatomica Avium, second edition. Publications of the Nuttall Ornithological Club, Cambridge, Massachusetts.

Blainville, H. D. de. 1830. Mémoire sur le Dodo, autrement Dronte. Nouvelles Annales du Muséum d'Histoire Naturelle 4:1–4.

Bock, W. J. 1960. Secondary articulation of the avian mandible. The Auk 77:1–55.

Bock, W. J. 1964. Kinetics of the avian skull. Journal of Morphology 114:1–41.

Butendieck, E. 1980. Die Benennung des Skeletts beim Truthuhn (*Meleagris gallopavo*) unter Berücksichtigung der Nomina Anatomica Avium (1979). Ph.D. dissertation, Tierärztliche Hochschule Hannover, Hannover, Germany, 159 pp.

Cheke, A. S., and J. P. Hume. 2008. Lost Land of the Dodo: The Ecological History of the Mascarene Islands. A. & C. Black Publishers (Poyser Imprint), London.

Chubb, E. C. 1919. A skeleton of the dodo (*Didus ineptus*). Annals of the Durban Museum 2:97–99.

Claessens, L. P. A. M., and J. P. Hume. 2015. The provenance and history of the Thirioux dodos; pp. 21–28 in L. P. A. M. Claessens, H. J. M. Meijer, J. P. Hume, and K. F. Rijsdijk (eds.), Anatomy of the Dodo (*Raphus cucullatus* L., 1758): An Osteological Study of the Thirioux Specimens. Society of Vertebrate Paleontology Memoir 15. Journal of Vertebrate Paleontology 35(6, Supplement).

Cracraft, J. 1968. The lacrimal-ectethmoid bone complex in birds: a single character analysis. American Midland Naturalist 80: 316–359.

Cracraft, J. 1988. The major clades of birds; pp. 339–361 in M. J. Benton (ed.), The Phylogeny and Classification of Tetrapods, Volume 1, Amphibians, Reptiles and Birds. Systematics Association Special Volume 35A. Clarendon Press, Oxford, U.K.

Curtis, E. L., and R. C. Miller. 1938. The sclerotic ring in North American birds. The Auk 55:225–243.

Elzanowski, A., and T. A. Stidham. 2010. Morphology of the quadrate in the Eocene anseriform *Presbyornis* and the extant Galloanserine Birds. Journal of Morphology 271:305–323.

Fürbringer, M. 1888. Untersuchungen zur Morphologie und Systematik der Vögel, zugleich ein Beitrag zur Anatomie der Stütz- und Bewegungsorgane. Bijdragen tot de Dierkunde 15:1–1751.

Gadow, H. 1933. The Evolution of the Vertebral Column. Cambridge University Press, Cambridge, U.K.

Gegenbaur, C. 1871. Beiträge zur Kenntniss des Beckens der Vögel. Jenaische Zeitschrift für Medicin und Naturwissenschaft 6:157–220.

Gmelin, J. F. 1789. Systema Naturae per Regna Tria Naturae, Secundum Classes, Ordines, Genera, Species, Cum Characteribus, Differentiis, Synonymis. Thirteenth Edition. Volume 1, Part 2. G. E. Beer, Leipzig, 531 pp.

Hachisuka, M. 1953. The Dodo and Kindred Birds or the Extinct Birds of the Mascarene Islands. H. F. & G. Witherby, London.

Hume, J. P. 2003. The journal of the flagship *Gelderland*—dodo and other birds on Mauritius 1601. Archives of Natural History 30:13–27.

Hume, J. P. 2005. Contrasting taphofacies in ocean island settings: the fossil record of Mascarene vertebrates. Monografies de la Societat d'Història Natural de les Balears 12:129–144.

Hume, J. P. 2006. The history of the dodo *Raphus cucullatus* and the penguin of Mauritius. Historical Biology 2:65–89.

Hume, J. P. 2011. Systematics, morphology, and ecology of pigeons and doves (Aves: Columbidae) of the Mascarene Islands, with three new species. Zootaxa 3124: 1–62.

Hume, J. P. 2012. The Dodo: from extinction to the fossil record. Geology Today 28:147–151.

Hume, J. P., and L. Steel. 2013. Fight Club: A unique weapon in the wing of the solitaire, *Pezophaps solitaria* (Aves: Columbidae), an extinct flightless bird from Rodrigues, Mascarene Islands. Biological Journal of the Linnean Society 110:32–44.

Hume, J. P., A. S. Cheke, and A. McOran-Campbell. 2009. How Owen 'stole' the Dodo: academic rivalry and disputed rights to a newly-discovered subfossil deposit in nineteenth century Mauritius. Historical Biology 21:33–49.

Hume, J. P., P. G. B. de Louw, and K. F. Rijsdijk. 2015. Rediscovery of a lost Lagerstätte: a comparative analysis of the historical and recent Mare aux Songes dodo excavations on Mauritius. Historical Biology 27: 1127–1140.

Huxley, T. H. 1867. On the classification of birds and on the taxonomic value of the modification of certain cranial bones in that class. Proceedings of the Zoological Society, London, 1867:415–472.

Janoo, A. 1996. On a hitherto undescribed Dodo cranium, *Raphus cucullatus* L., (Aves, Columbiformes), with a brief taxonomical overview of this extinct flightless Mascarene Island bird. Bulletin du Museum national d'Histoire naturelle, Paris, 4e séries 18:57–77.

Jardine, W. 1845. Horae Zoologicae. Annals and Magazine of Natural History 16:174–176.

Johnston, R. F., and M. Janiga. 1995. Feral Pigeons. Oxford University Press, Oxford, U.K., 320 pp.

Kitchener, A. C. 1993. On the external appearance of the dodo, *Raphus cucullatus* (L. 1758). Archives of Natural History 20:279–301.

La Fresnaye, M. de. 1839. Nouvelle classification des oiseaux de proie, ou rapaces. Revue Zoologique par la Société Cuvierienne 2:193–197.

Leguat, F. 1708. Voyage et aventures de François Leguat et des ses compagnons en deux îles désertes des Indes Orientales. 2 vols. J. L. de Lorme, Amsterdam, The Netherlands.

Lima, F. C., L. G. Vieira, A. L. Q. Santos, S. B. S. de Simone, L. Q. L. Hirano, J. M. M. Silva, and M. F. Romão. 2009. Anatomy of the scleral ossicles in Brazilian birds. Brazilian Journal of Morphological Sciences 26:165–169.

Linnaeus, C. 1758. Systema Naturae per Regna Tria Naturae, Secundum Classes, Ordines, Genera, Species, cum Characteribus, Differentiis, Synonymis, Locis. Tenth Edition. Laurentii Salvii, Stockholm, 824 pp.

Livezey, B. C. 1993. An ecomorphological review of the dodo (*Raphus cucullatus*) and solitaire (*Pezophaps solitaria*), flightless Columbiformes of the Mascarene Islands. Journal of Zoology 230:247–292.

Livezey, B. C. 1995. Heterochrony and the evolution of avian flightlessness; pp. 169–194 in K. J. McNamara (ed.), Evolutionary Change and Heterochrony. Wiley, New York.

Livezey, B. C., and R. L. Zusi. 2006. Higher-order phylogeny of modern birds (Theropoda, Aves: Neornithes) based on comparative anatomy: I. Methods and characters. Bulletin of Carnegie Museum of Natural history 37:1–544.

Louchart, A., and C. Mourer-Chauviré. 2011. The dodo was not so slim: leg dimensions and scaling to body mass. Naturwissenschaften 98:357–358.

Martin, R. 1904. Die vergleichende Osteologie der Columbiformes unter besonderer Berücksichtigung von *Didunculus strigirostris*. Zoologische Jahrbücher 20:167–352.

Mayr, G. 2015. Variations in the hypotarsus morphology of birds and their evolutionary significance. Acta Zoologica. doi: 10.1111/azo.12117.

Merz, R. L. 1963. Jaw musculature of the Mourning and White-winged Doves. University of Kansas Publications Museum of Natural History 12:521–551.

Moree, P. 2001. Dodos and galjoenen. De reis van het schip Gelderland naar Oost-Indië, 1601–1603. Walburg Pers, Zutphen, The Netherlands, 348 pp.

Mundy, P. 1638 [1919]. In R. C. Temple (ed.), The Travels of Peter Mundy in Europe and Asia, 1608–1667, Volume 3, Part 2. Hakluyt Society, London.

Newton, E., and H. Gadow. 1893. On additional bones of the dodo and other extinct birds from Mauritius obtained by Mr Théodore Sauzier. Transactions of the Zoological Society of London 13:281–302.

Newton, A., and E. Newton. 1868. On the osteology of the Solitaire or Didine bird of the Island of Rodriguez. Proceedings of the Royal Society 103:428–433.

Olson, S. L. 1975. Paleornithology of St. Helena Island, South Atlantic Ocean. Smithsonian Contributions to Paleobiology 23:1–49.

Owen, R. 1846. Observations on the Dodo. Proceedings of the Zoological Society of London 1846:51–53.

Owen, R. 1866. On the Osteology of the Dodo (*Didus ineptus*, Linn.); pp. 21–55 in R. Owen and W. J. Broderip (eds.), Memoir on the Dodo (*Didus ineptus*), with an Historical Introduction. Taylor and Francis, London.

Owen, R. 1872. On the Dodo (Part II). Notes on the articulated skeleton of the Dodo (*Didus ineptus*, Linn.) in the British Museum. Transactions of the Zoological Society of London 7:513–525.

Pallas, P. S. 1764. Adumbratiunculae. Avium variorum praecedenti Elencho insertarum, sed quae in Systemate Naturae Illustr. Linnaei nondum exant; pp. 1–7 in Addendum to the The Vroeg sale catalogue. Vosmaer, A., 1764 Catalogue raisonné, d'une collection supérieurement belle d'Oiseaux, tant exotiques qu'Européens, de Quadrupedes et d'Insectes. Empaillés, & arrangés avec beaucoup d'art en situations & attitudes extrèmement naturelles, & garantis de la corruption d'une fac, on particulière. Le tout rassemblé & arrangé, pendant une longue suite d'années, avec beaucoup de peines & à grand fraix, par A. Vroeg. Collection qu'on offre aux amateurs entiére & à un prix raisonnable, jusqu'au 22 Septembre de cette année; après l'Echéance duquel terme, elle sera vendue aux plus offrands, le 6 Octobre 1764 à la Haye, dans la Maison de Mr. Coster, au coin du Veenestraat sur le petit Marché aux Herbes, par Pierre van Os. Libraire demeurant sur la Place à la Haye, The Hague, The Netherlands.

Parish, J. C. 2013. The Dodo and the Solitaire: A Natural History. Indiana University Press, Bloomington, Indiana, 406 pp.

Rijsdijk K. F., J. P. Hume, F. Bunnik, V. Florens, C. Baider, B. Shapiro, J. van der Plicht, A. Janoo, O. Griffiths, L. W. van den Hoek Ostende, H. Cremer, T. Vernimmen, P. de Louw, A. Bholah, S. Saumtally, N. Porch, J. Haile, M. Buckley, M. Collins, and E. Gittenberger. 2009. Middle-Holocene Concentration-Lagerstätten on oceanic island Mauritius provides a window into the ecosystem of the dodo (*Raphus cucullatus*). Quaternary Science Reviews 21:14–24.

Rijsdijk, K. F., J. P. Hume, P. G. B. de Louw, H. J. M. Meijer, A. Janoo, E. J. de Boer, L. Steel, J. de Vos, L. G. van der Sluis, H. Hooghiemstra, F. B. V. Florens, C. Baider, T. J. J. Vernimmen, P. Baas, A. H. van Heteren, V. Rupear, G. Beebeejaun, A. Grihault, J. van der Plicht, M. Besselink, J. K. Lubeek, M. Jansen, S. J. Kluiving, H. Hollund, B. Shapiro, M. Collins, M. Buckley, R. M. Jayasena, N. Porch, R. Floore, A. Biedlingmaier, J. Leavitt, G. Monfette, A. Kimelblatt, A. Randall, and L. P. A. M. Claessens. 2015. A review of the dodo and its ecosystem: insights from a vertebrate concentration Lagerstätte in Mauritius; pp. 3–20 in L. P. A. M. Claessens, H. J. M. Meijer, J. P. Hume, and K. F. Rijsdijk (eds.), Anatomy of the Dodo (*Raphus cucullatus* L., 1758): An Osteological Study of the Thirioux Specimens. Society of Vertebrate Paleontology Memoir 15. Journal of Vertebrate Paleontology 35(6, Supplement).

Servaas, A. J. 1887. Hongersnood in Suratta ao 1631, enz. Waarheid of leugen? mag men wel vragen aangaande 'tgeen volgt. De Navorscher 37:4–8.

Shapiro, B., D. Sibthorpe, A. Rambaut, J. Austin, G. M. Wragg, O. R. P. Bininda-Emonds, P. L. M. Lee, and A. Cooper. 2002. Flight of the Dodo. Science 295:1683.

Shufeldt, R. W. 1901. On the osteology of the pigeons (Columbae). Journal of Morphology 17:487–514.

Strickland, H. E., and A. G. Melville. 1848. The Dodo and Its Kindred. Reeve, Benham and Reeve, London.

Van Heteren, A. H., L. P. A. M. Claessens, J. de Vos, and K. F. Rijsdijk. 2014. An investigation of sexual dimorphism and population structure of the dodo (*Raphus cucullatus*) based on the Mare aux Songes fossil remains. Journal of Vertebrate Paleontology, Program and Abstracts, 2014:245.

Van Wissen, B. 1995. Eyewitnesses; pp. 10–43 in B. van Wissen (ed.), Dodo *Raphus cucullatus* [*Didus ineptus*]. ISP/Zoologisch Museum-Universiteit van Amsterdam, Amsterdam, The Netherlands.

Worthy, T. H. 2001. A giant flightless pigeon gen. et sp. nov. and a new species of *Ducula* (Aves: Columbidae), from Quaternary deposits in Fiji. Journal of the Royal Society of New Zealand 31:763–794.

Worthy, T. H., and R. N. Holdaway. 2002. The Lost World of the Moa: Prehistoric Life of New Zealand. Indiana University Press, Bloomington, Indiana, 718 pp.

Zusi, R. L. 1984. A functional and evolutionary analysis of rhynchokinesis in birds. Smithsonian Contributions to Zoology 395:1–38.

Submitted January 10, 2015; revisions received November 3, 2015; accepted November 4, 2015.

APPENDIX 1. Anatomical abbreviations.

a, angular
aat, arcus atlantis
aco, ansa costotransversarium
acr, acromion
ais, ala ischii
ale, area ligamenti elastici
alp, phalanx digiti alulae
am, angulus mandibulae
ame, angulus medialis
apoi, ala postacetabularis ilii
apri, ala preacetabularis ilii
apu, apex pubiis
ar, articular
arc, arcus vertebrae
att, antitrochanter
bic, crista bicipitalis
bp, basitemporal plate
bt, basilar tubercles
c, condylus caudalis
cah, caput humeri
car, cotyla articularis
cas, carina sterni
cat, corpus atlantis
cc, coracoid
ccc, crista cnemialis cranialis
ccl, crista cnemialis lateralis
cco, capitulum costae
cdi, crista dorsolateralis ilii
cdn, crista spinosa dorsalis notarii
cdu, cotyla dorsalis ulnae
cfa, facies articularis coracoidea
cfe, caput femoris
chu, cotyla humeralis
cic, crista intercotylaris
cla, condylus lateralis
cm, crista medialis
cmc, carpometacarpus
cme, condylus medialis
cmf, crista medialis flexor digitorum longus
co, capitulum oticum
coeo, canalis opthalmicus externus ostia
cp, processus coronoideus
cqj, cotyla quadratojugalis
crf, crista fibularis
crp, papillae remigales caudales
crt, crista articularis tibialis
cs, capitulum squamosum
csc, cotyla scapularis
ct, crista tympanica
cte, crista temporalis
ctf, crista transversa fossae
ctl, cotyla lateralis
ctm, cotyla medialis
cto, crista transversa-obliqua
cv, crista ventralis
cvn, crista ventralis notarii
cvu, cotyla ventralis ulnae
d, dentary
dcn, condylus dorsalis
den, dens
dep, epicondylus dorsalis
dhc, condylus dorsalis humeri
dmd, phalanx distalis digiti majoris
dmi, phalanx digiti minoris
dmp, phalanx proximalis digiti majoris
dpc, crista deltopectoralis
dtb, tuberculum dorsale
e, ectethmoid
eca, extremitas caudalis synsacri
ecr, extremitas cranialis synsacri
emc, eminentia costolateralis (parapophysis)
emi, eminentia intercondylaris
epl, epicondylus lateralis
epm, epicondylus medialis
f, frontal
faa, facies articularis axialis
fac, facies articularis caudalis
fact, foramen acetabuli
fah, facies articularis humeralis
fai, facies articularis intercostalis
fam, facies articularis metacarpalis
fap, facies articularis phalangealis
far, facies articularis radialis
farc, facies articularis radiocarpalis
fas, facies articularis sternalis
fat, facies articularis atlantica
fatt, facies articularis antitrochanterica
fau, facies articularis ulnaris
fbm, fossa musculi brachialis
fbo, fossa basiorbitalis
fc, fossa caudalis
fco, fossa condyloidea
fcr, facies articularis cranialis
fcv, fovea cranioventralis
fda, facies articularis digiti alulae
fdl, canal for m. flexor digitorum longus
fdm, facies articularis digiti majoris
ffc, facies articularis condylus lateralis femoris
ffe, facies articularis femoralis
fga, facies gastrocnemialis
fhl, sulcus m. flexor hallucis longus
fic, fenestra intercristalis
fii, foramen ilioischiadicum
fit, foramina intertransversaria
fla, facies lateralis
flc, fovea ligamenti collateralis
flca, fovea ligamenti collateralis atlantoaxialis
fm1, fossa metatarsi I
fmc, facies articularis condylus medialis femoris
fme, facies medialis
fmi, facies articularis digiti minoris
fmp, fovea m. poplitea
fo, foramen opticum
fob, foramen obturatum
fol, fossa olecrani
fpa, foramina pneumaticum articulare
fpm, foramen pneumaticum
fpn, fossa pneumotricipitalis
fpo, facies articularis postzygapophysis
fpp, fossa poplitea
fpr, facies articularis prezygapophysis
fp2, sulcus m. flexor perforans digiti II
fri, fossa renalis, pars ischiadica
frp, fossa renalis, pars pudenda
fso, supraoccipital foramen
fsp, fossa supratrochlearis plantaris
ft, fossa temporalis
fti, facies articularis tibialis
ftr, foramen transversarium
ftro, fossa trochanteris
ful, facies articularis ulnocarpalis
fv, foramen vasculare
fvd, foramen vasculare distale
fve, foramen vertebrale
fvo, foramina venae occipitalis externae
hu, humerus
iac, incisura arcus caudalis
icf, incisura fossae
iic, incisura intercostalis
iico, incisura intercondylaris
iil, incisura intertrochlearis lateralis
iim, incisura intertrochlearis medialis
imb, impressio musculi brachialis
imc, incisura metacarpalis
ims, impressio musculi sternocoracoidei
inc, incisura capitis
int, intumescentia
is, interorbital septum

isc, impressio m. scapulotricipitis
itn, incisura tendinae
j, jugal
l, condylus lateralis
l?, extra lacrimal, not part of specimen
la, lacrimal
lbp, lateral basitemporal process
lc, cotyla lateralis
lca, linea intermuscularis caudalis
lco, condylus lateralis
lcr, linea intermuscularis cranialis
lim, linea intermuscularis
ln, lateral nasal
lp, lamina parasphenoidalis
m, maxilla
mc, cotyla medialis
mco, condylus medialis
mld, impressio m. latissimus dorsi
mpm, medial process of the mandible
mpn, processus maxillaris of the nasal
mpp, processus maxillaris of the premaxillary
mr, maxillary rostrum
msc, impressio m. supracoracoideus
mwi, metal wire impressions
npp, processus frontalis of the premaxillary
o, occipital
oc, occipital condyle
occ, ostium canalis carotici
ocl, ligamentum occipitomandibulare
olc, olecranon
oma, os metacarpale alulare
omi, os metacarpale minus
omm, os metacarpale majus
p, condylus pterygoideus
pa, parietal
pac, processus acromialis
pca, processus caroticus
pcc, processus acrocoracoideus
pcl, processus craniolateralis
pco, processus costalis
pcp, pila cranialis phalangis
pex, processus extensorius
pfx, processus flexorius
pj, processus jugalis
pl, palatine
pmi, impressio musculi pectoralis
po, processus oticus
por, processus orbitalis
ppa, processus paroccipitalis
ppc, processus procoracoideus
ppn, processus premaxillaris of the nasal
ppo, processus postorbitalis
pps, processus pisiformis
prl, processus lateralis
psp, processus spinosus
psu, pons supratendineus
pt, pterygoid
pti, processus terminalis ischii
ptm, processus articularis tarsometatarsalis
ptr, processus transversus
pun, processus uncinatus
pvc, processus ventralis corporis
pz, processus zygomaticus
q, quadrate
ra, radius
rd, radiale
rdo, ramus dorsale
rf, fenestra rostralis mandibulae
rp, rostrum parasphenoidalis
rve, ramus ventrale
sa, supra-angular
sac, sulcus articularis coracoideus
sc, scapula
sca, sulcus caroticus
scp, scapus pubis
sdi, spina dorsolateralis ilii
sfi, spina fibulae
sht, sulcus humerotricipitalis
shy, sulcus m. flexor perforans et perforates digit II
sic, sulcus intercondylaris
sicn, sulcus intercnemialis
sim, spatium intermetacarpalis
sio, sulcus interosseus
spn, sulcus pneumaticus
sst, sulcus scapulotricipitalis
sue, sulcus extensorius
tar, trochlea articularis
tav, tuberculum aponeurosis ventralis
tbc, tuberculum carpale
tbl, tuberculum laterale
tbm, tuberculum mediale
tbr, tuberculum bicipitale radii
tco, tuberculum costae
tct, trochlea cartilaginis tibiales
tdp, tuberculum dorsale postzygapophysis
tex, tuberculum extensorium
tfb, trochlea fibularis
tfe, trochanter femoris
tfl, tuberculum flexorium
til, tuberculum m. iliofibularis
tll, tuberositas ligamenti collateralis lateralis
tm, tomium maxillare
tm2, trochlea metatarsi II
tm3, trochlea metatarsi III
tm4, trochlea metatarsi IV
trl, trabecula lateralis
tro, trochlea
tsc, tuberculum scapulae
ul, ulna
un, ulnare
vcn, condylus ventralis
vep, epicondylus ventralis
vhc, condylus ventralis humeri
vi, incisura intercapitularis
vtb, tuberculum ventrale
X, opening for the n. vagi
XI, foramen n. glossopharyngealis
XII, opening for the n. hypoglossi
zfc, zona flexoria craniofacialis

APPENDIX 2. The Port Louis dodo.

PLATE PL1. Right oblique view of the 3-D scan of the Port Louis dodo as mounted at the Mauritius Institute.

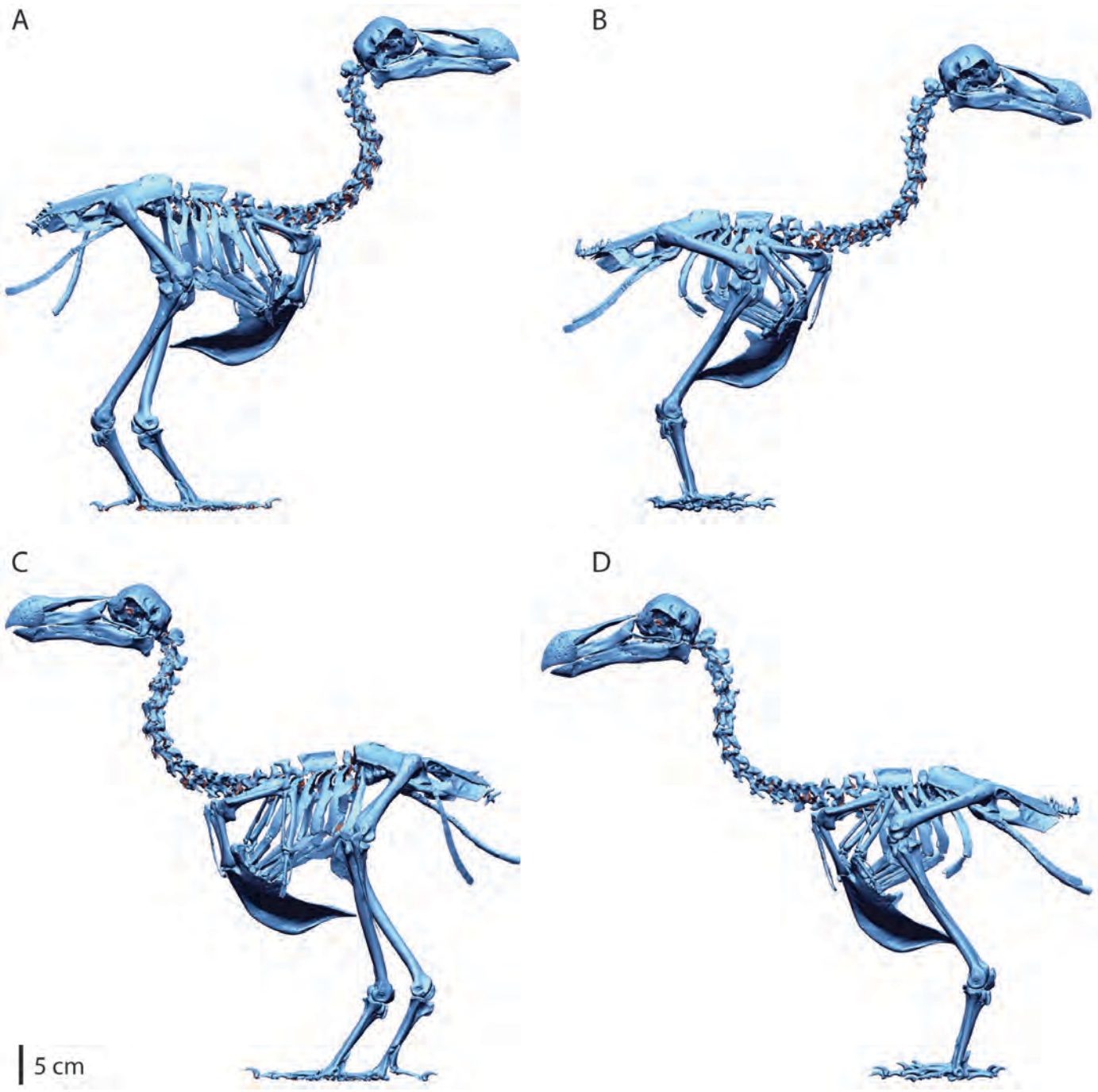

PLATE PL2. 3-D scans of the Port Louis dodo as mounted at the Mauritius Institute (**A**, **C**) and after digital repositioning (**B**, **D**), in right lateral (**A**, **B**) and left lateral (**C**, **D**) views.

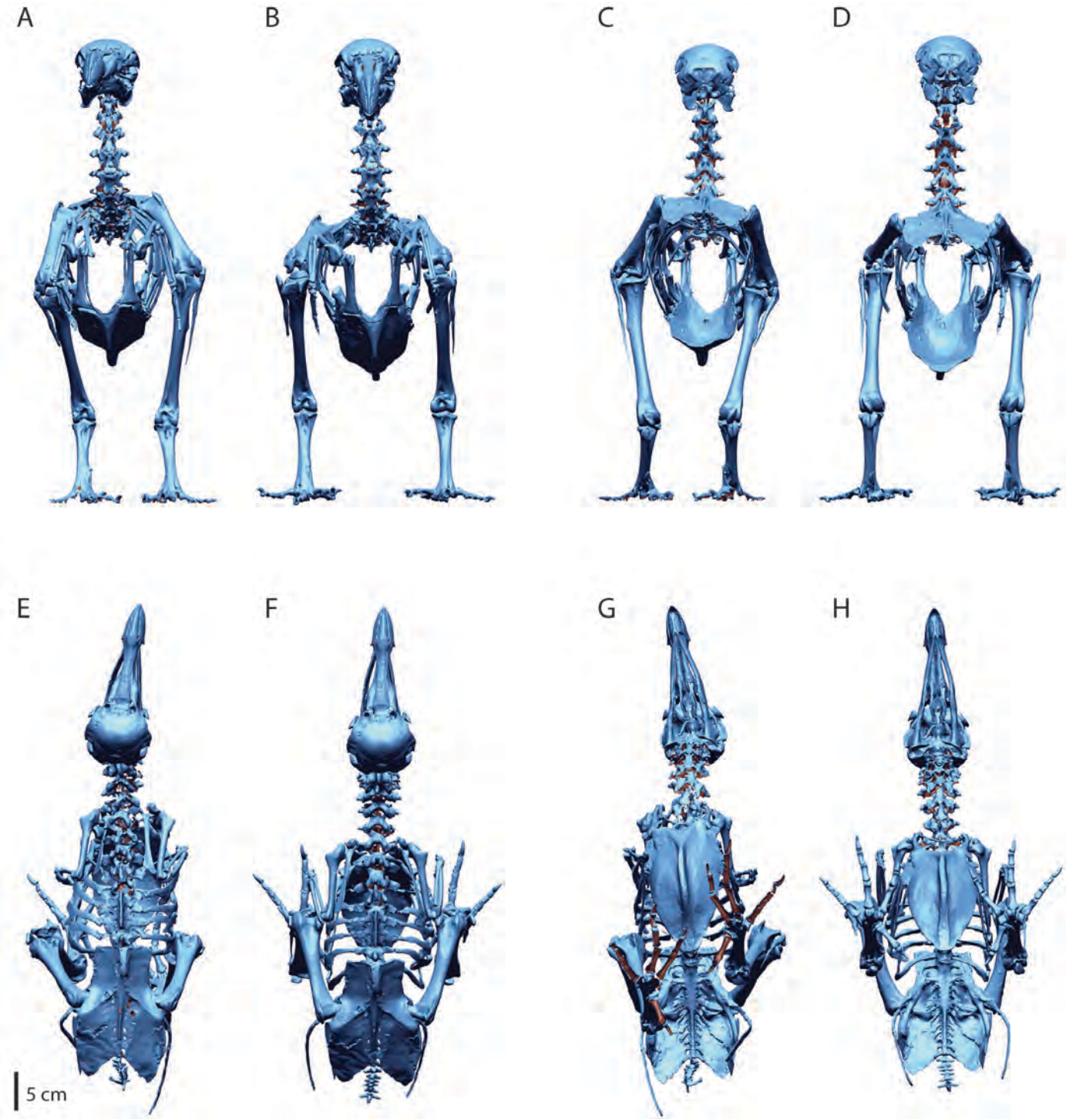

PLATE PL3. 3-D scans of the Port Louis dodo as mounted at the Mauritius Institute (**A**, **C**, **E**, **G**) and after digital repositioning (**B**, **D**, **F**, **H**), in left cranial (**A**, **B**), caudal (**C**, **D**), and dorsal (**E**, **F**), and ventral (**G**, **H**) views.

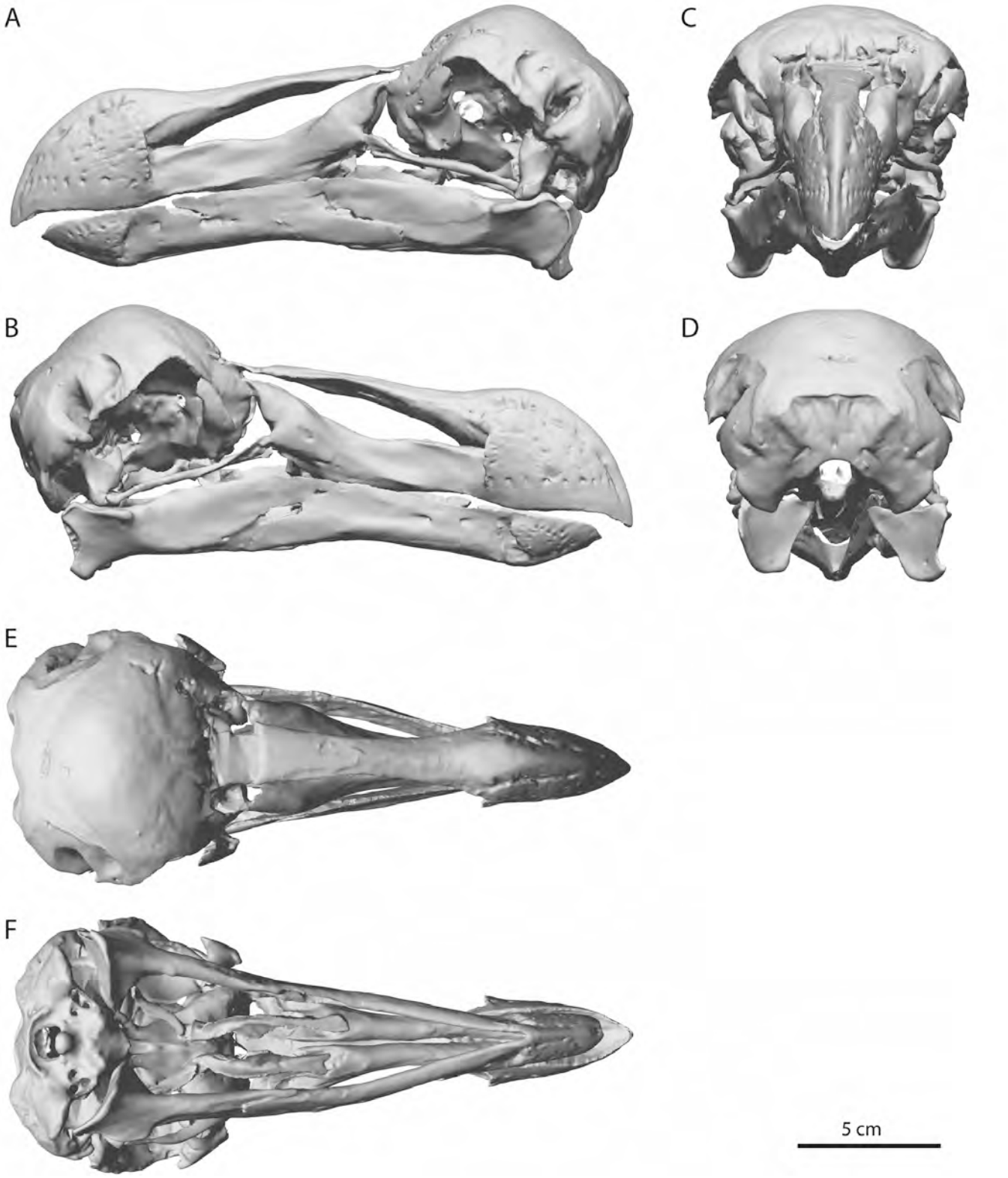

PLATE PL4. 3-D scans of Port Louis dodo skull and mandible in left lateral (**A**), right lateral (**B**), anterior (**C**), posterior (**D**), dorsal (**E**), and ventral (**F**) views.

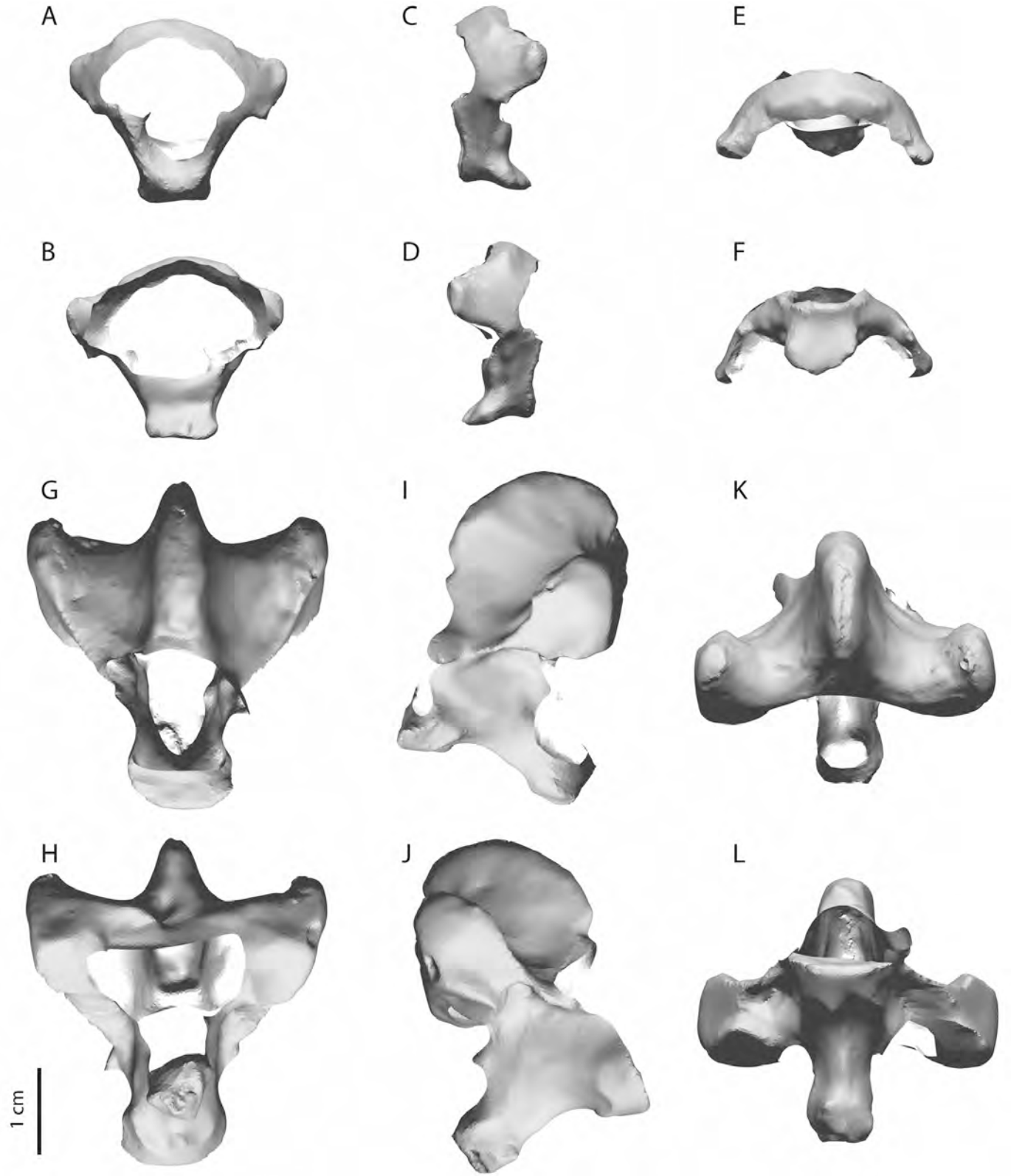

PLATE PL5. 3-D scans of Port Louis dodo atlas (**A**–**F**) and axis (**G**–**L**), in cranial (**A**, **G**), caudal (**B**, **H**), left lateral (**C**, **I**), right lateral (**D**, **J**), dorsal (**E**, **K**), and ventral (**F**, **L**) views. Missing surface data left blank (not reconstructed).

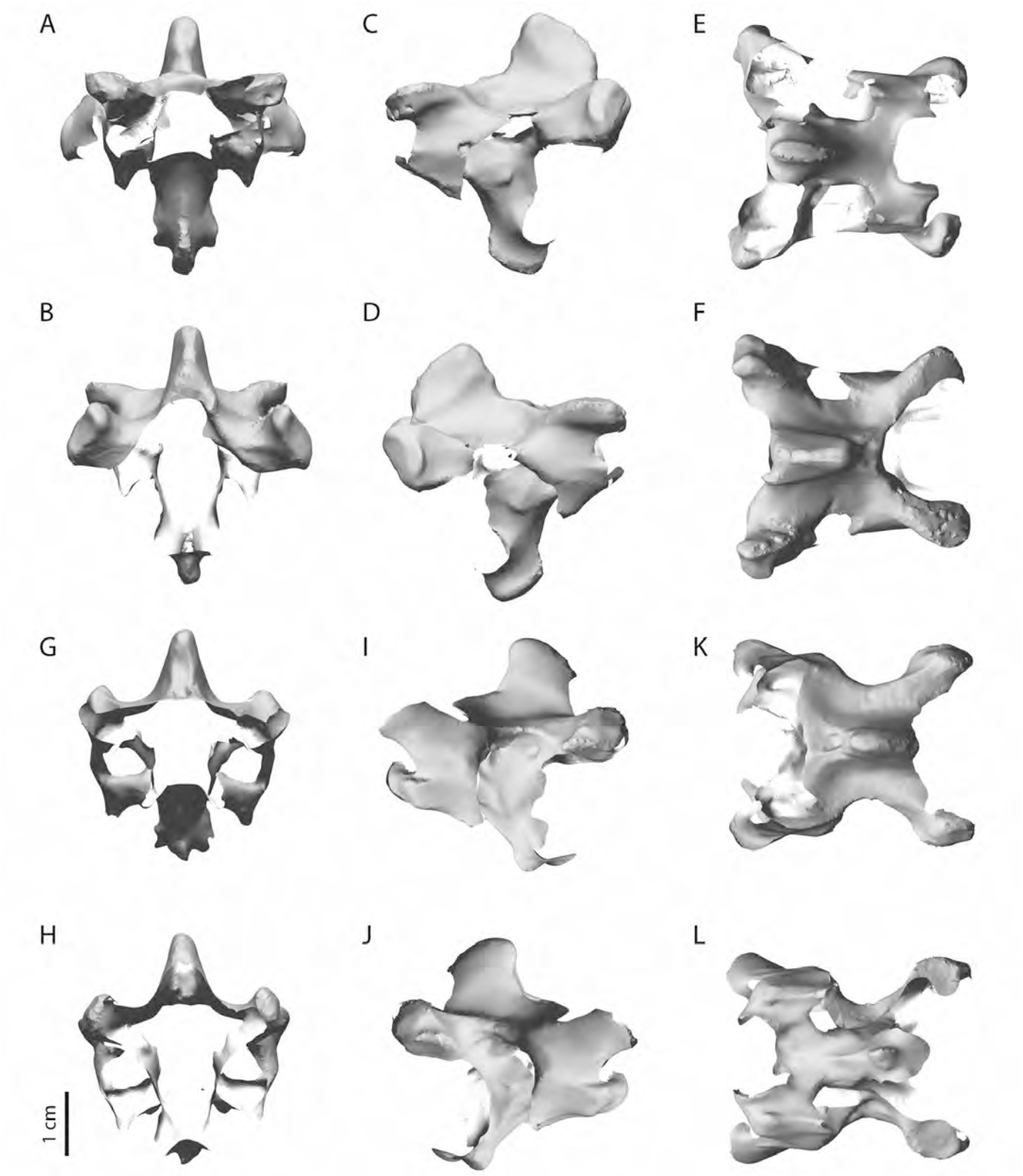

PLATE PL6. 3-D scans of Port Louis dodo cervical vertebra (C) 3 (**A**–**F**) and C4 (**G**–**L**), in cranial (**A**, **G**), caudal (**B**, **H**), left lateral (**C**, **I**), right lateral (**D**, **J**), dorsal (**E**, **K**), and ventral (**F**, **L**) views. Missing surface data left blank (not reconstructed).

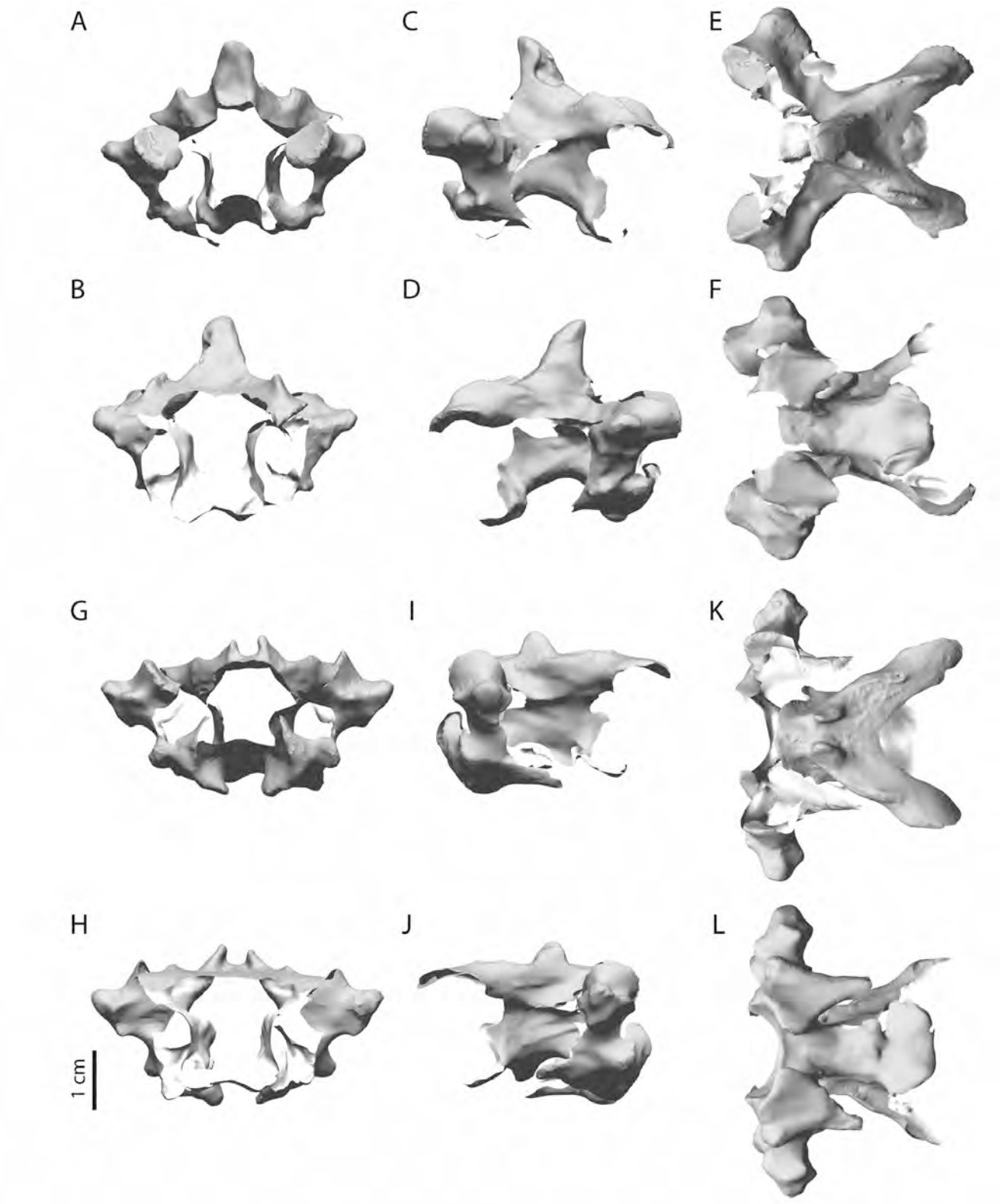

PLATE PL7. 3-D scans of Port Louis dodo C5 (**A**–**F**) and C6 (**G**–**L**), in cranial (**A**, **G**), caudal (**B**, **H**), left lateral (**C**, **I**), right lateral (**D**, **J**), dorsal (**E**, **K**), and ventral (**F**, **L**) views. Missing surface data left blank (not reconstructed).

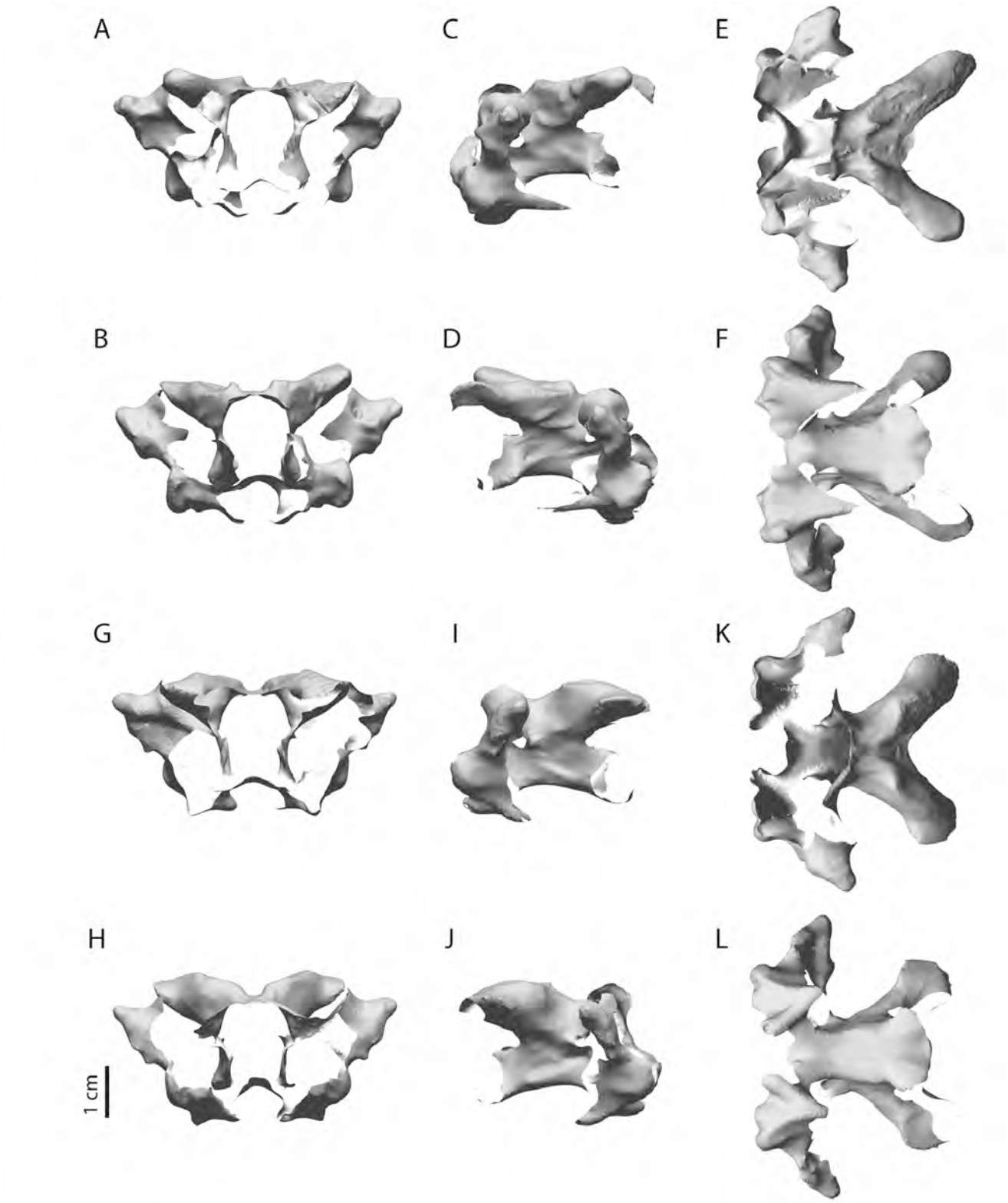

PLATE PL8. 3-D scans of Port Louis dodo C7 (**A**–**F**) and C8 (**G**–**L**), in cranial (**A**, **G**), caudal (**B**, **H**), left lateral (**C**, **I**), right lateral (**D**, **J**), dorsal (**E**, **K**), and ventral (**F**, **L**) views. Missing surface data left blank (not reconstructed).

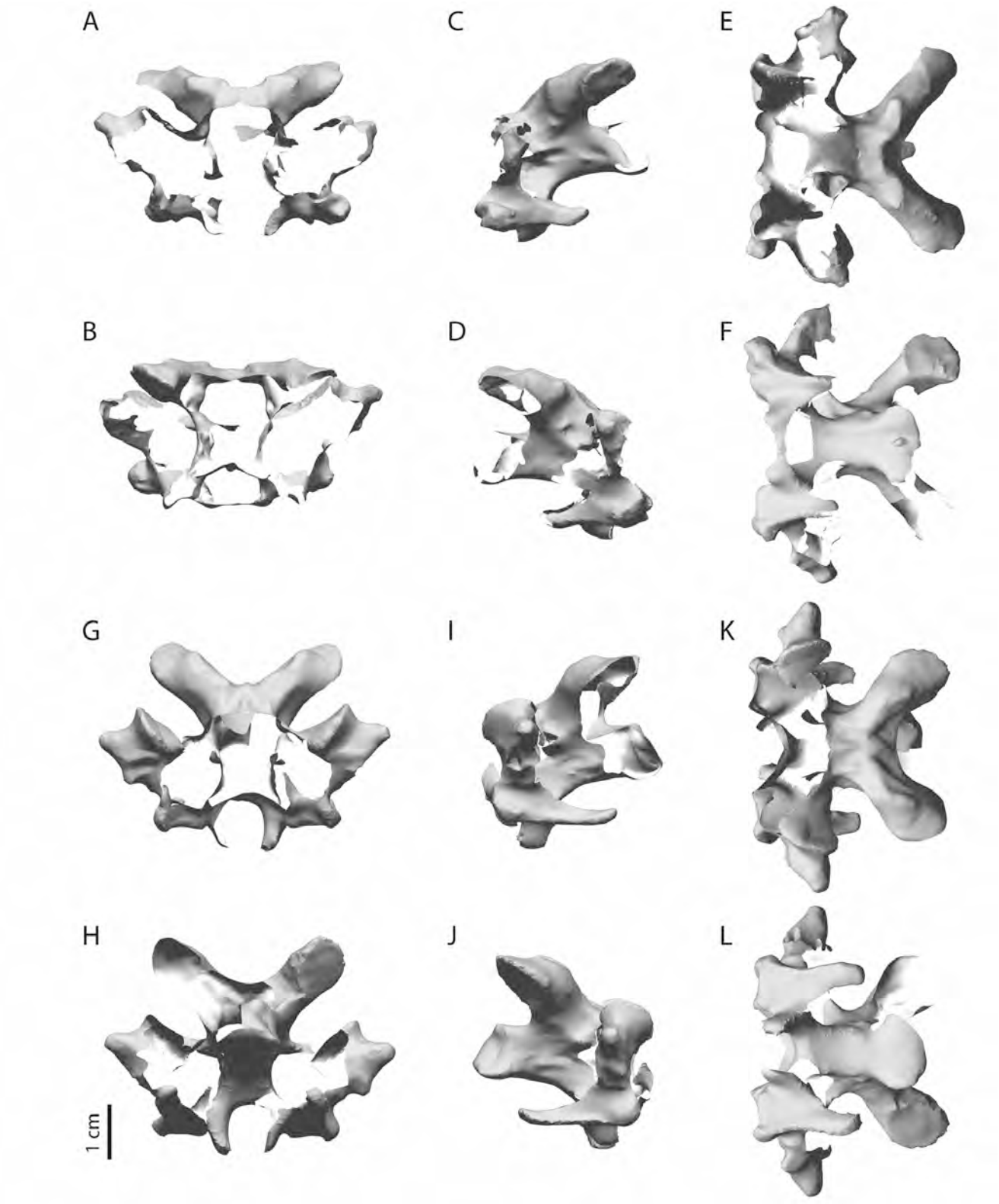

PLATE PL9. 3-D scans of Port Louis dodo C9 (**A**–**F**) and C10 (**G**–**L**), in cranial (**A**, **G**), caudal (**B**, **H**), left lateral (**C**, **I**), right lateral (**D**, **J**), dorsal (**E**, **K**), and ventral (**F**, **L**) views. Missing surface data left blank (not reconstructed).

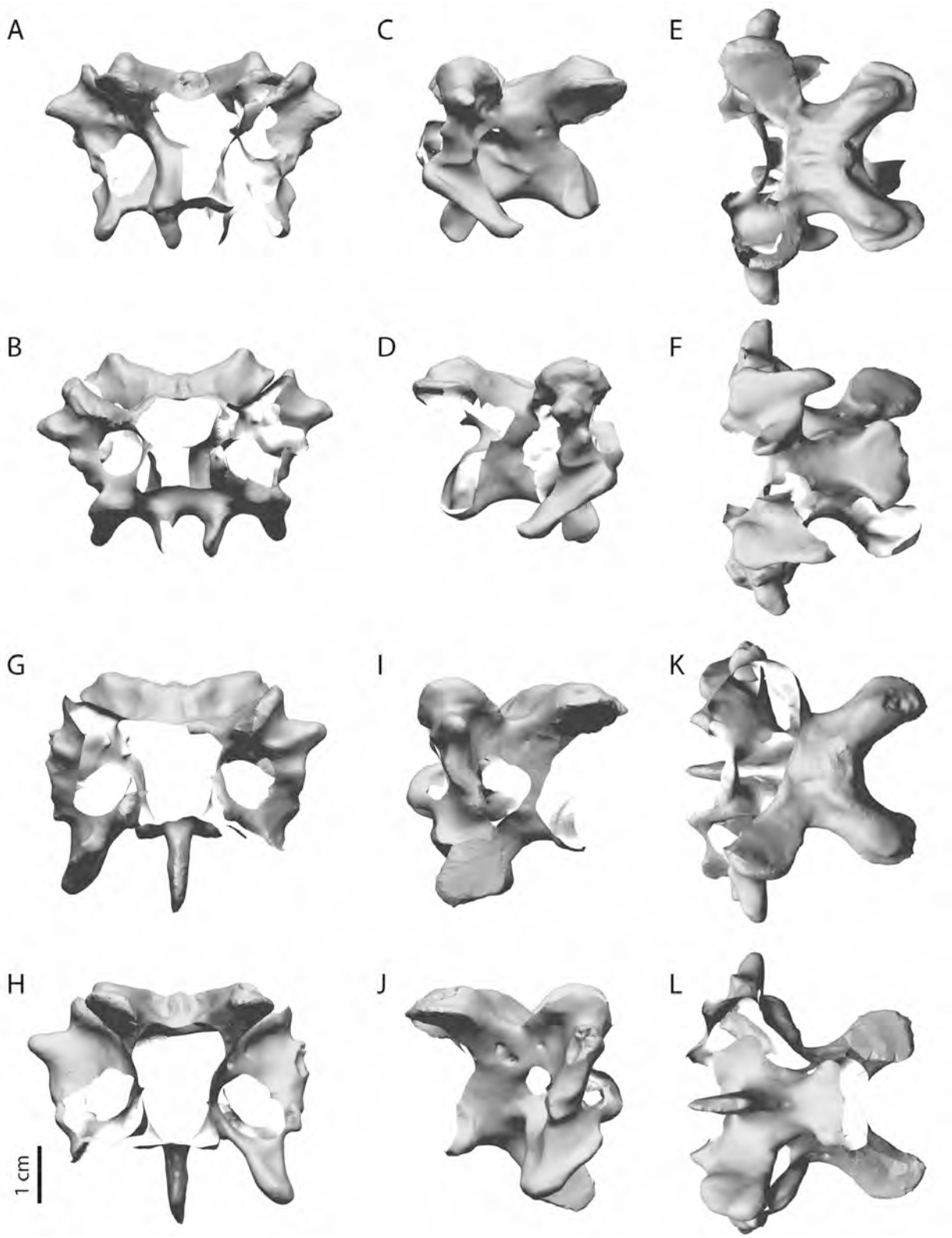

PLATE PL10. 3-D scans of Port Louis dodo C11 (**A**–**F**) and C12 (**G**–**L**), in cranial (**A**, **G**), caudal (**B**, **H**), left lateral (**C**, **I**), right lateral (**D**, **J**), dorsal (**E**, **K**), and ventral (**F**, **L**) views. Missing surface data left blank (not reconstructed).

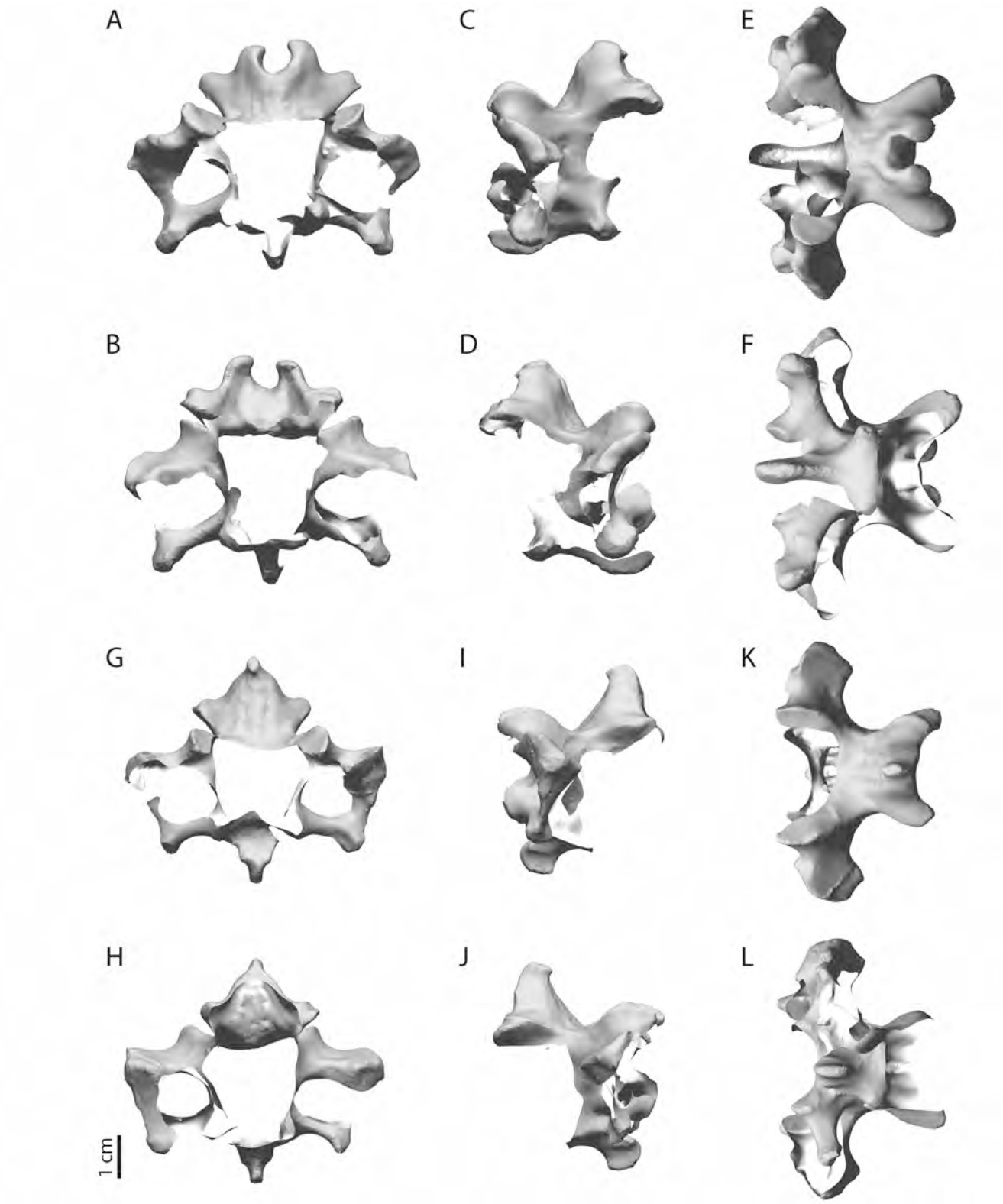

PLATE PL11. 3-D scans of Port Louis dodo C13 (**A**–**F**) and C14 (**G**–**L**), in cranial (**A**, **G**), caudal (**B**, **H**), left lateral (**C**, **I**), right lateral (**D**, **J**), dorsal (**E**, **K**), and ventral (**F**, **L**) views. Missing surface data left blank (not reconstructed).

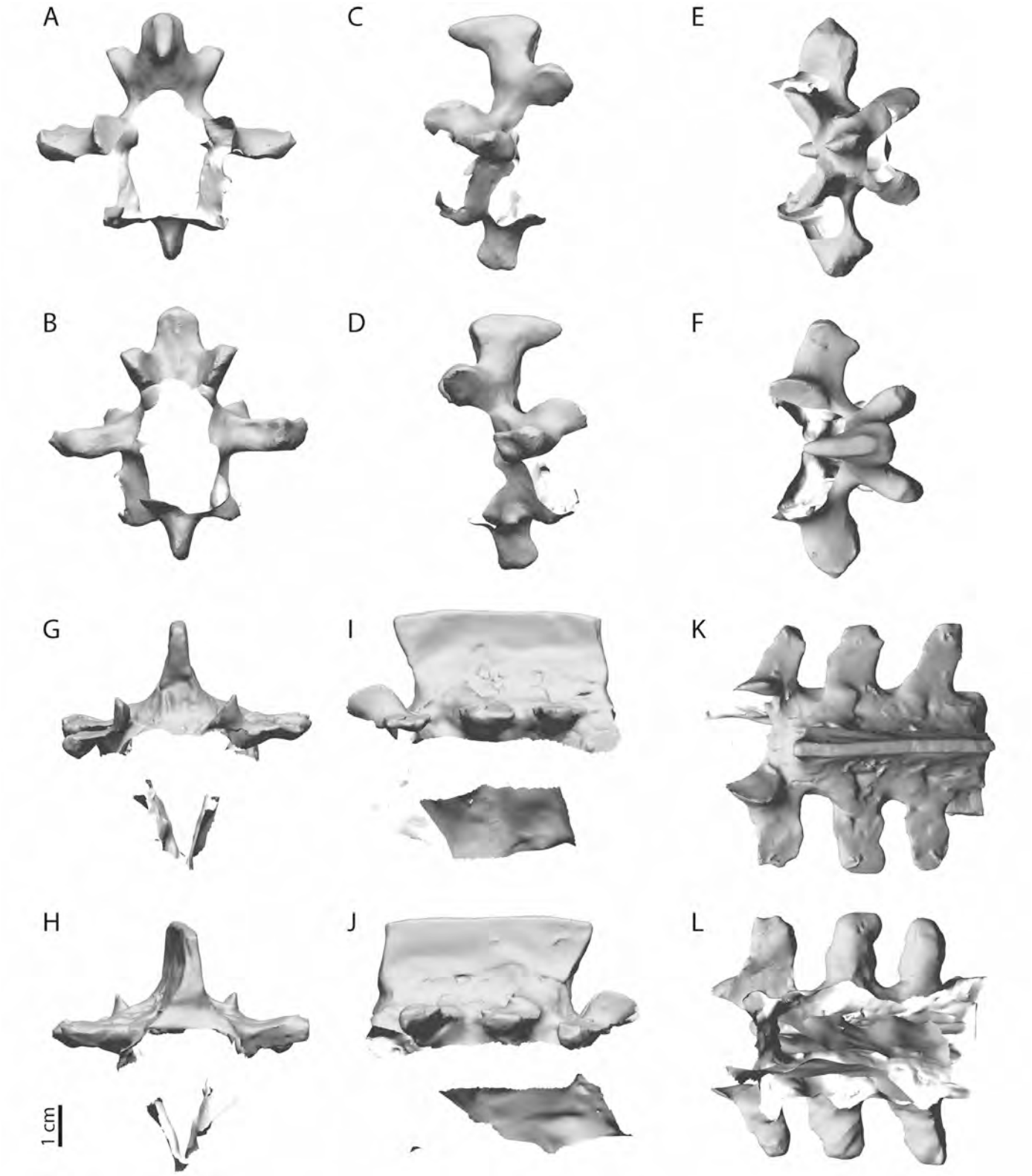

PLATE PL12. 3-D scans of Port Louis dodo cervicodorsal vertebra (C15) (**A**–**F**) and notarium (**G**–**L**), in cranial (**A**, **G**), caudal (**B**, **H**), left lateral (**C**, **I**), right lateral (**D**, **J**), dorsal (**E**, **K**), and ventral (**F**, **L**) views. Missing surface data left blank (not reconstructed).

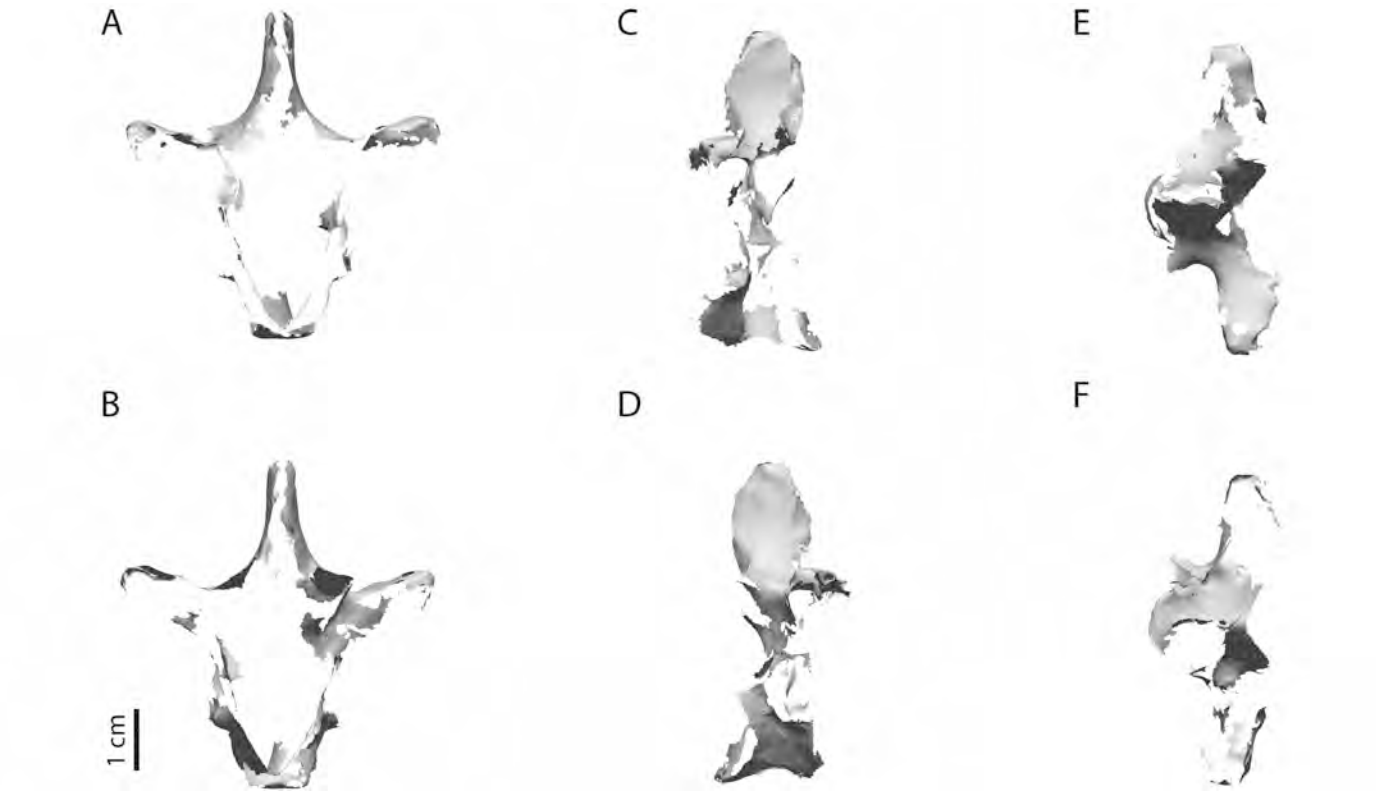

PLATE PL13. Reconstructed 3-D scans of Port Louis dodo presynsacral (thoracic) vertebra 19 (**A**–**F**), in cranial (**A**), caudal (**B**), left lateral (**C**), right lateral (**D**), dorsal (**E**), and ventral (**F**) views. Neural canal and cranial and caudal surfaces digitally reconstructed. Missing surface data left blank (not reconstructed).

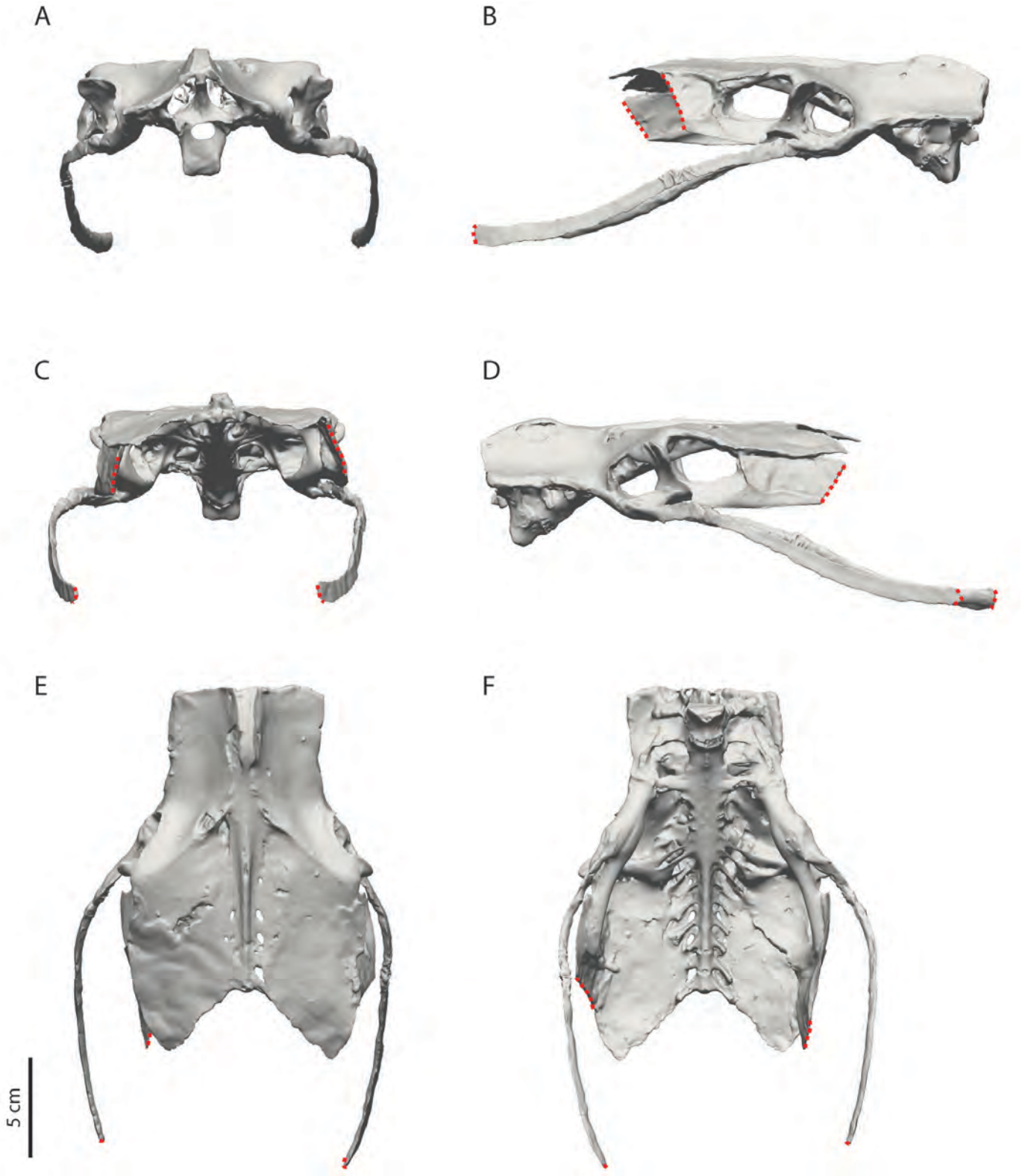

PLATE PL14. 3-D scans of Port Louis dodo pelvis (**A**–**F**), in caudal (**A**), right lateral (**B**), cranial (**C**), left lateral (**D**), dorsal (**E**), and ventral (**F**) views. Location of neural canal reconstructed in **A**. Breaks along right and left processus terminalis ischii and distal scapus pubis are indicated with a stippled line.

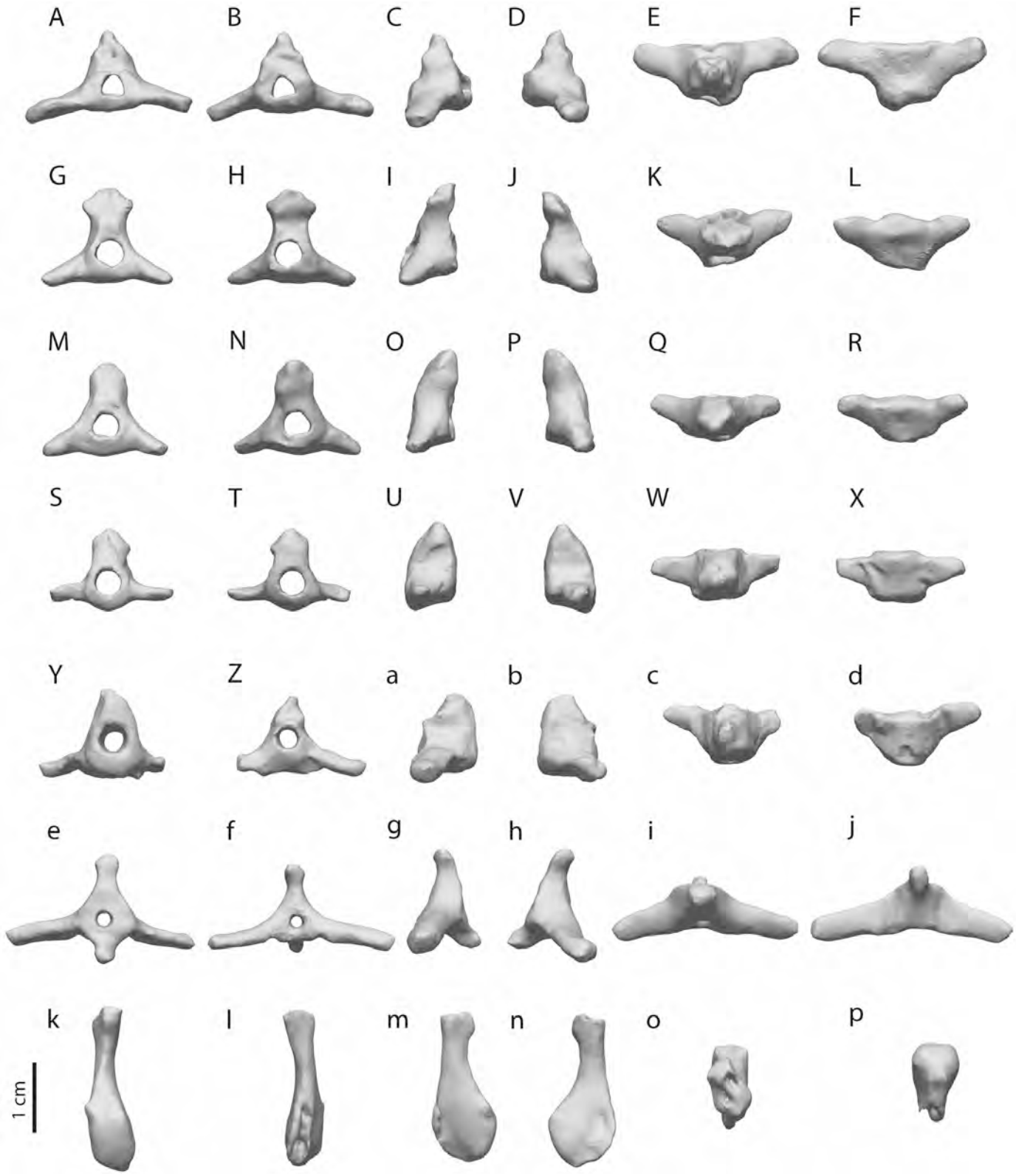

PLATE PL15. 3-D scans of Port Louis free caudal vertebrae 1 (**A**–**F**), 2 (**G**–**L**), 3 (**M**–**R**), 4 (**S**–**X**), 5 (**Y**–**d**), and 6 (**e**–**j**) and pygostyle (**k**–**p**), in cranial (**A**, **G**, **M**, **S**, **Y**, **e**, **k**), caudal (**B**, **H**, **N**, **T**, **Z**, **f**, **l**), left lateral (**C**, **I**, **O**, **U**, **a**, **g**, **m**), right lateral (**D**, **J**, **P**, **V**, **b**, **h**, **n**), dorsal (**E**, **K**, **Q**, **W**, **c**, **i**, **o**), and ventral (**C**, **L**, **R**, **X**, **d**, **j**, **p**) views. Neural canal, obstructed portions of cranial and caudal surfaces and articular facets digitally reconstructed.

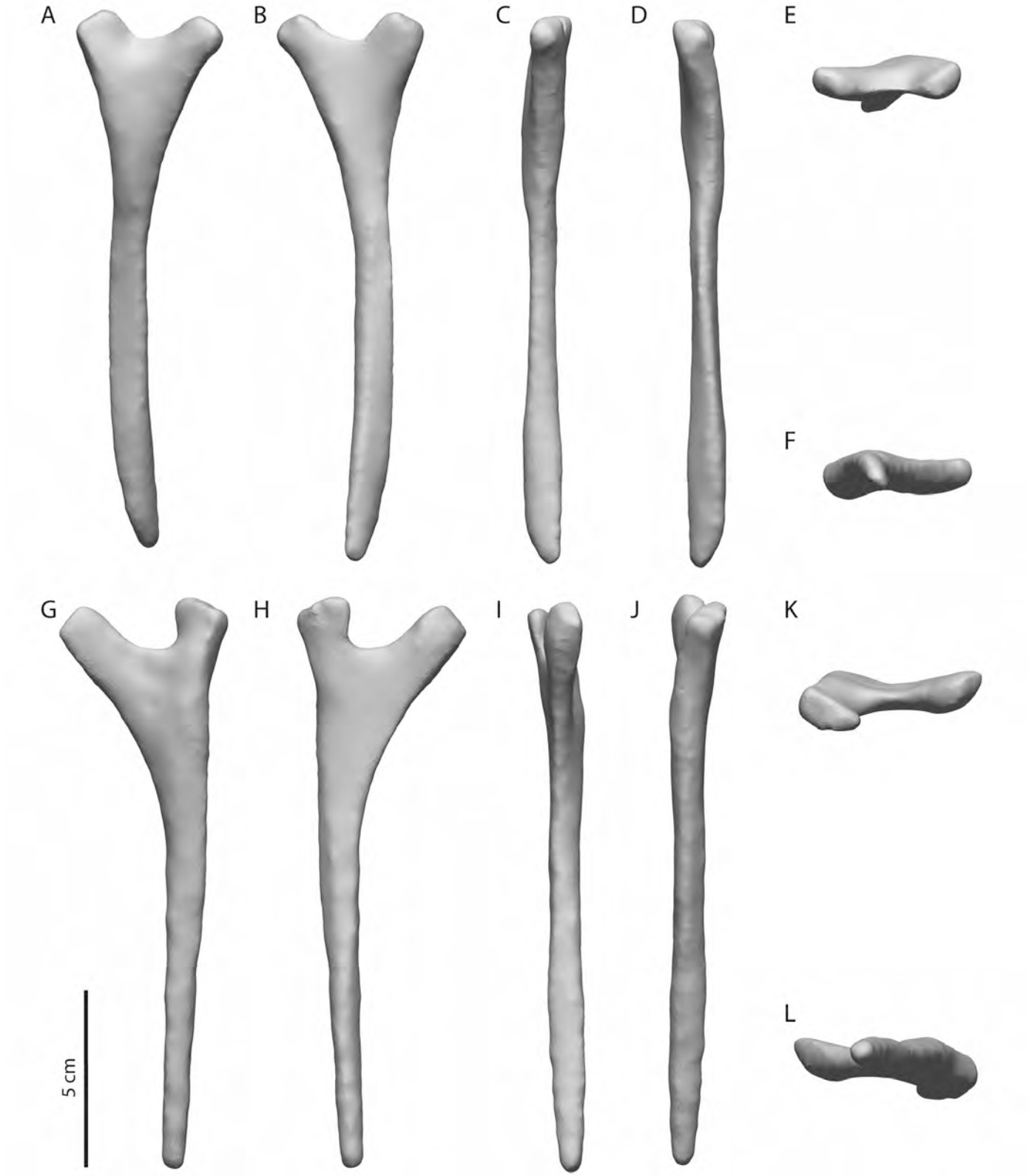

PLATE PL16. 3-D scans of Port Louis right (**A**–**F**) and left (**G**–**L**) vertebral rib Is (presynsacral segment 15, cervicodorsal vertebra), in cranial (**A**, **G**), caudal (**B**, **H**), lateral (**C**, **I**), medial (**D**, **J**), proximal (**E**, **K**), and distal (**F**, **L**) views. Proximal articular facet digitally reconstructed.

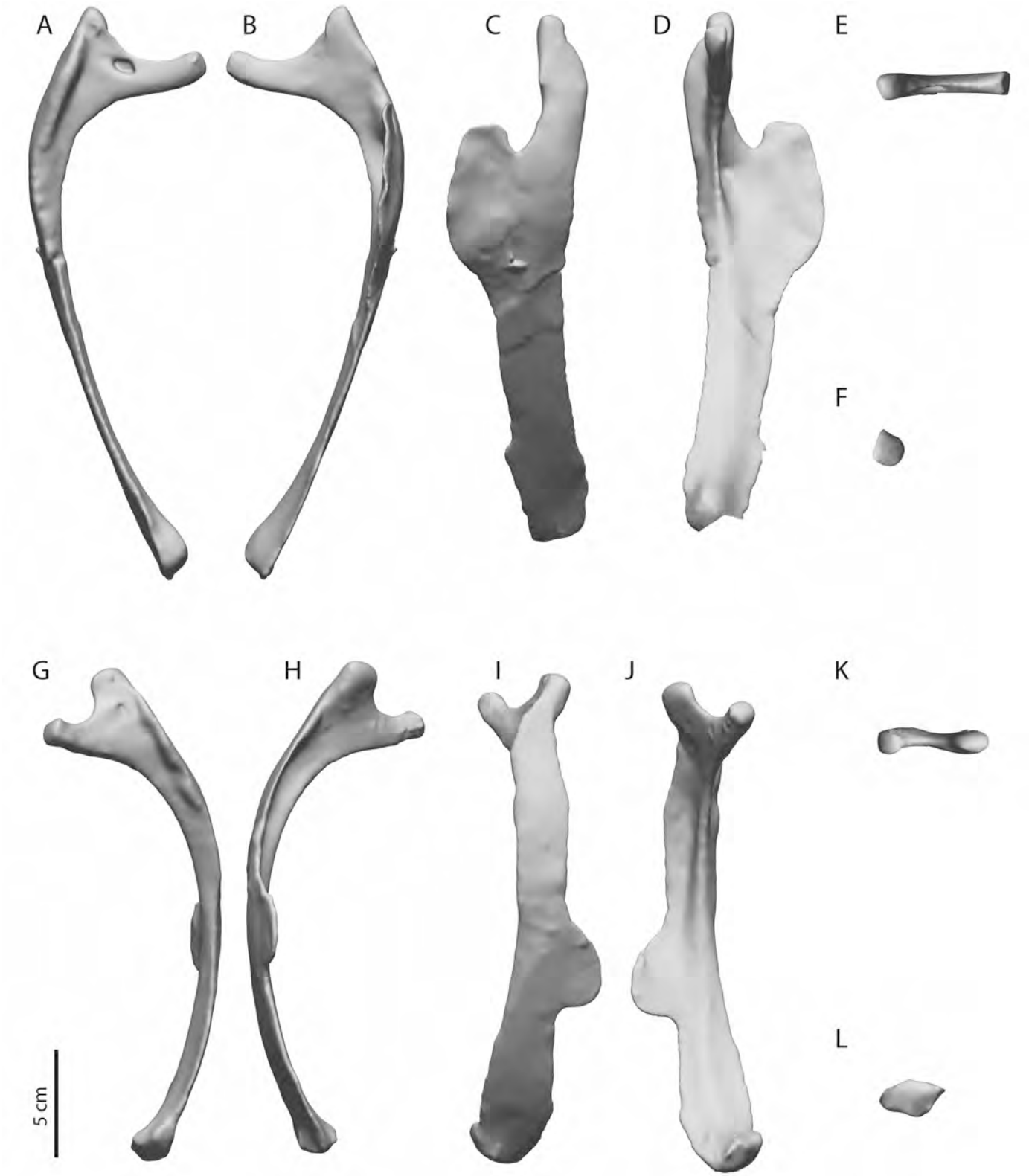

PLATE PL17. 3-D scans of Port Louis right (**A**–**F**) and left (**G**–**L**) vertebral rib IIs (presynsacral segment 16, first notarial segment), in cranial (**A**, **G**), caudal (**B**, **H**), lateral (**C**, **I**), medial (**D**, **J**), proximal (**E**, **K**), and distal (**F**, **L**) views. Obstructed portions of proximal and distal articular facets digitally reconstructed.

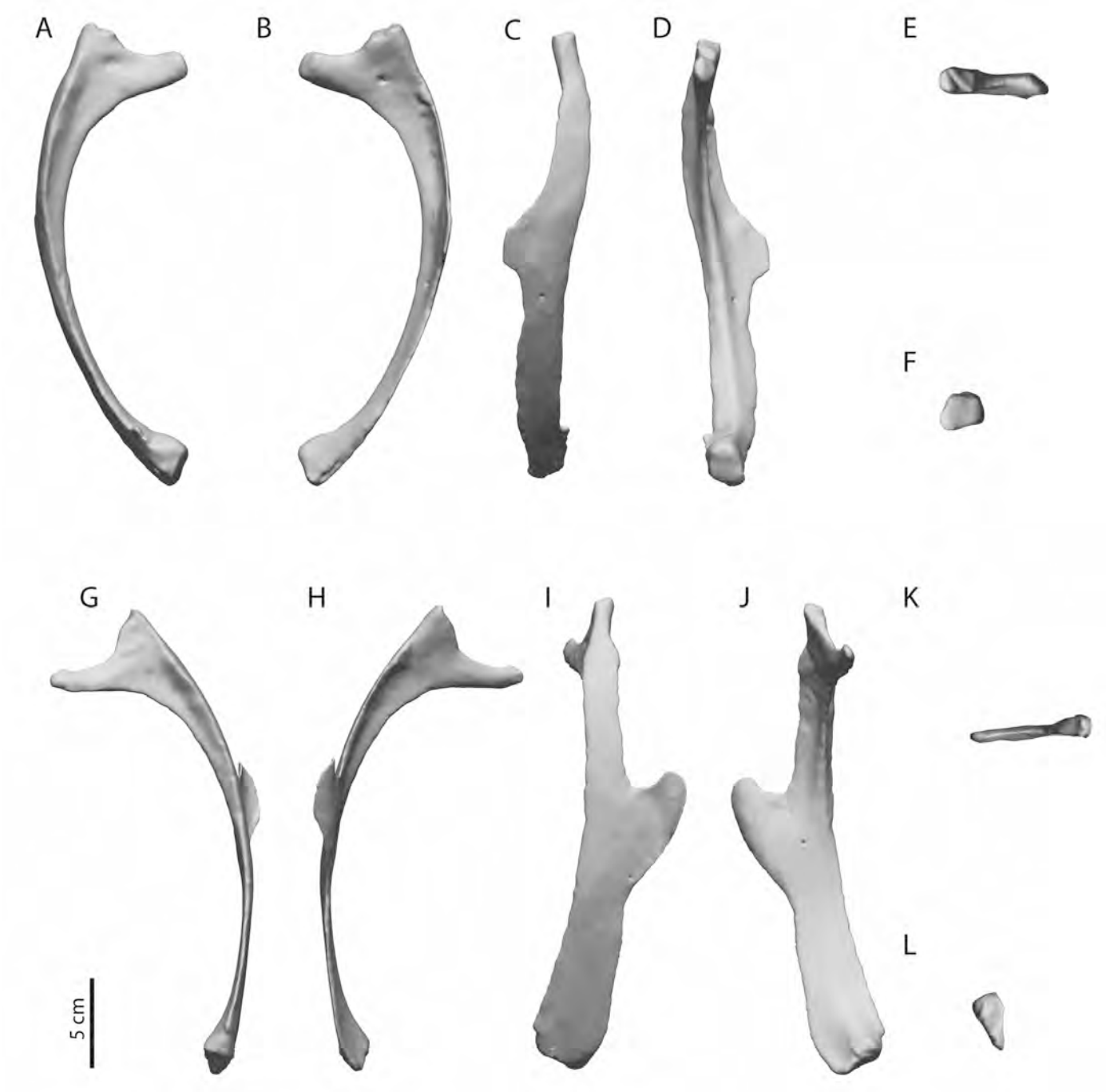

PLATE PL18. 3-D scans of Port Louis right (**A**–**F**) and left (**G**–**L**) vertebral rib IIIs (presynsacral segment 17, second notarial segment), in cranial (**A**, **G**), caudal (**B**, **H**), lateral (**C**, **I**), medial (**D**, **J**), proximal (**E**, **K**), and distal (**F**, **L**) views. Obstructed portions of proximal and distal articular facets digitally reconstructed.

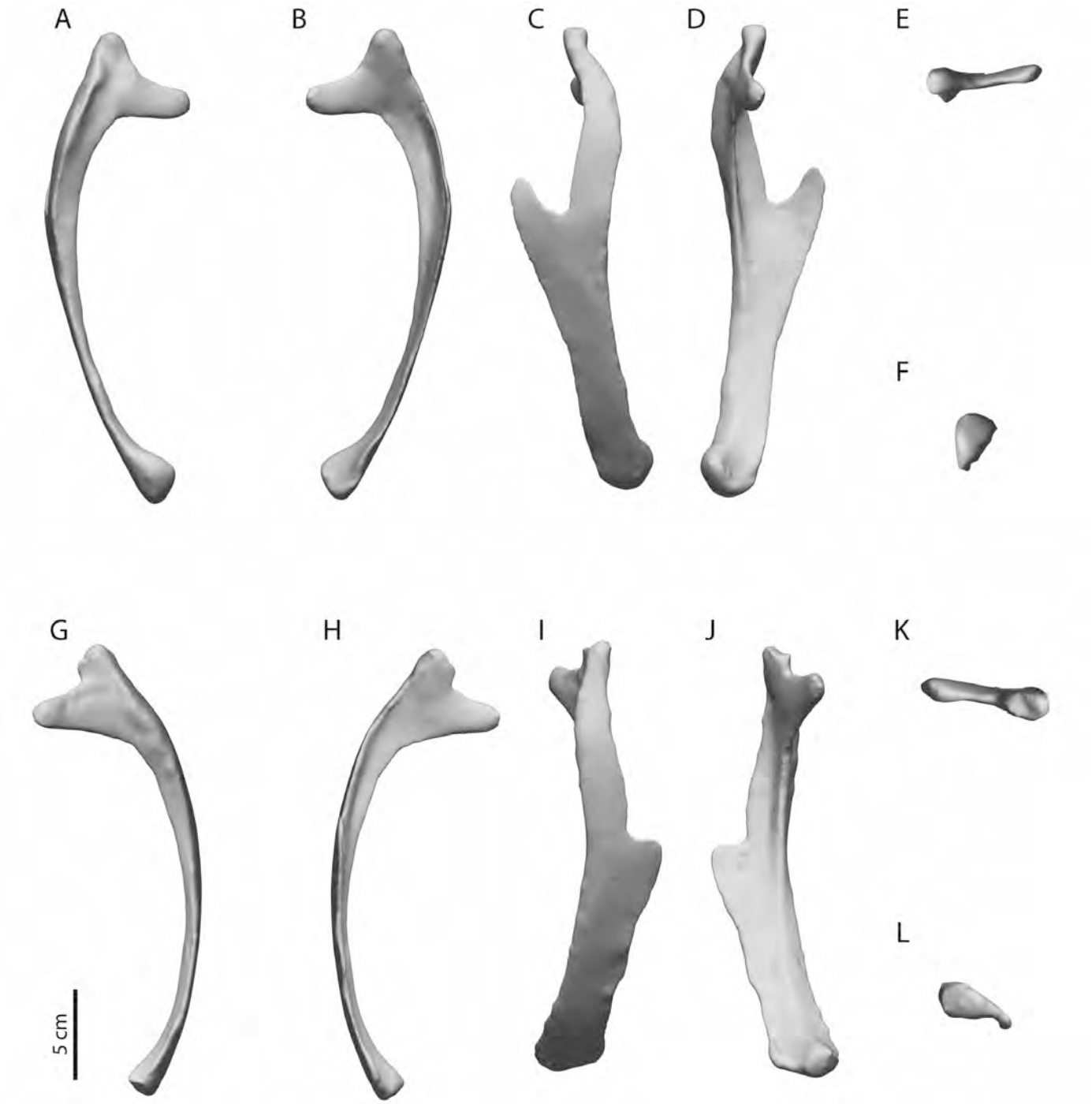

PLATE PL19. 3-D scans of Port Louis right (**A**–**F**) and left (**G**–**L**) vertebral rib IVs (presynsacral segment 18, third notarial segment), in cranial (**A**, **G**), caudal (**B**, **H**), lateral (**C**, **I**), medial (**D**, **J**), proximal (**E**, **K**), and distal (**F**, **L**) views. Obstructed portions of proximal and distal articular facets digitally reconstructed.

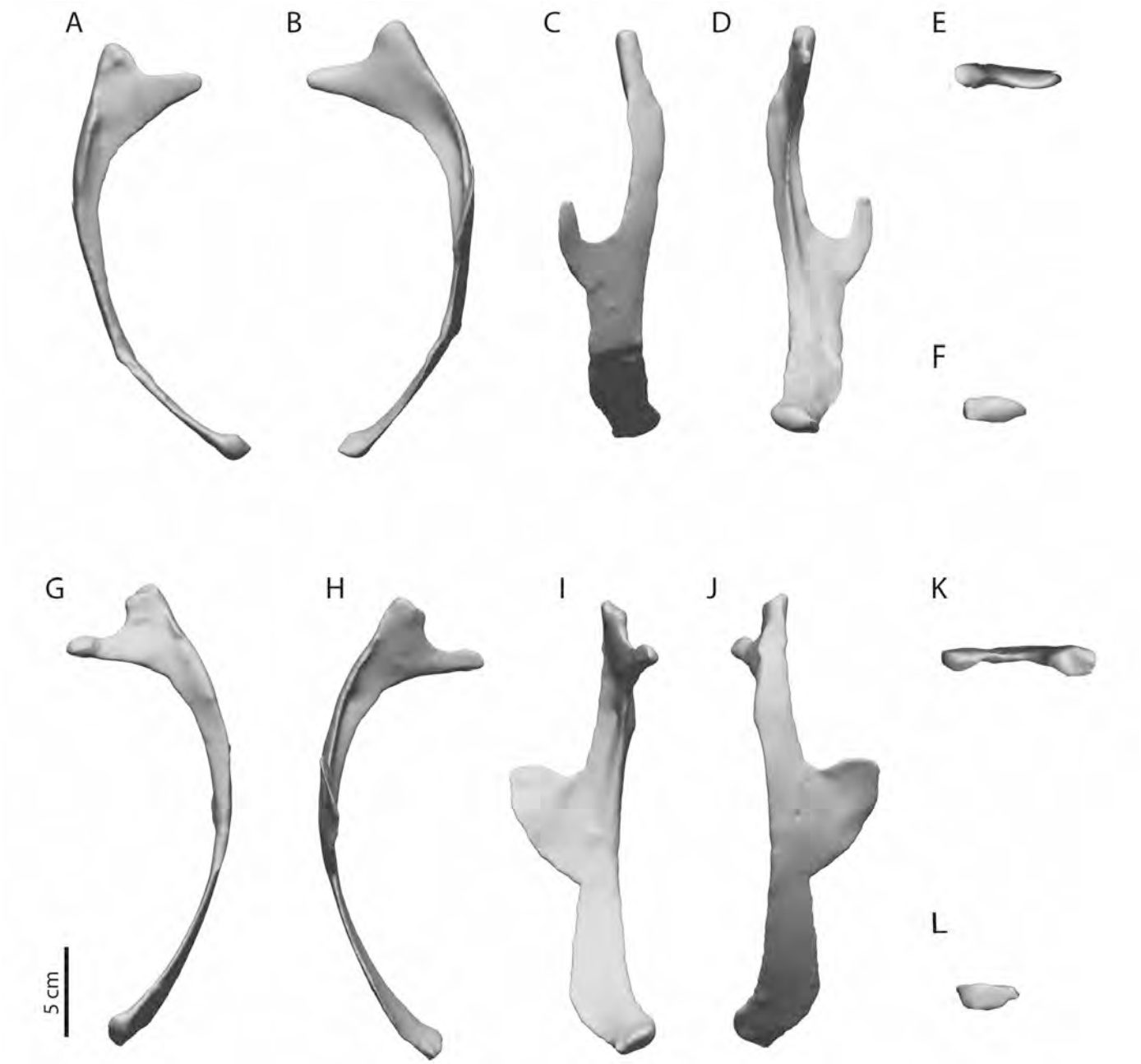

PLATE PL20. 3-D scans of Port Louis right (**A**–**F**) and left (**G**–**L**) vertebral rib Vs (presynsacral segment 19, thoracic), in cranial (**A**, **G**), caudal (**B**, **H**), lateral (**C**, **I**), medial (**D**, **J**), proximal (**E**, **K**), and distal (**F**, **L**) views. Obstructed portions of proximal and distal articular facets digitally reconstructed.

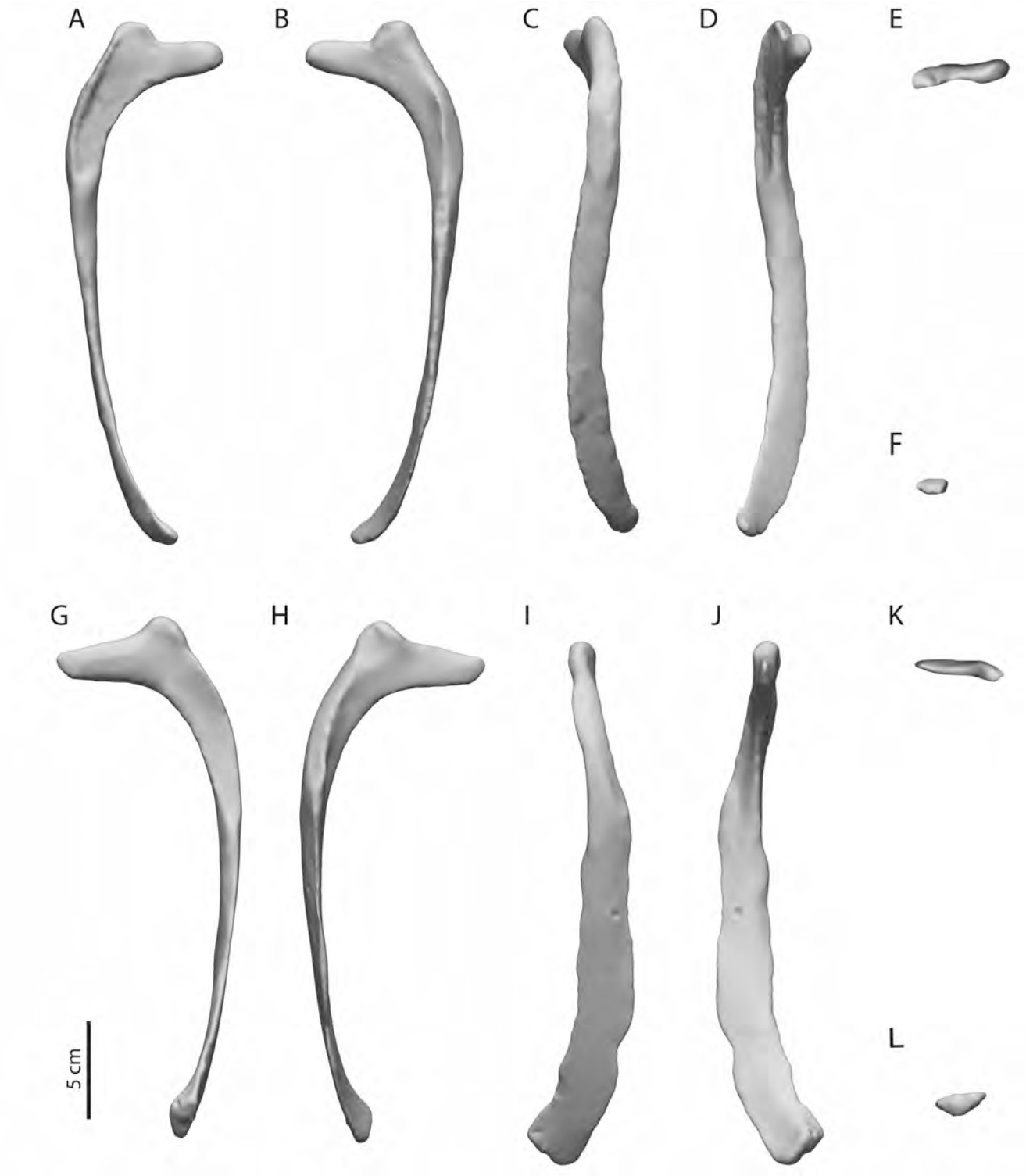

PLATE PL21. 3-D scans of Port Louis right (**A**–**F**) and left (**G**–**L**) vertebral rib VIs (synsacral segment 20), in cranial (**A**, **G**), caudal (**B**, **H**), lateral (**C**, **I**), medial (**D**, **J**), proximal (**E**, **K**), and distal (**F**, **L**) views. Obstructed portions of proximal and distal articular facets digitally reconstructed.

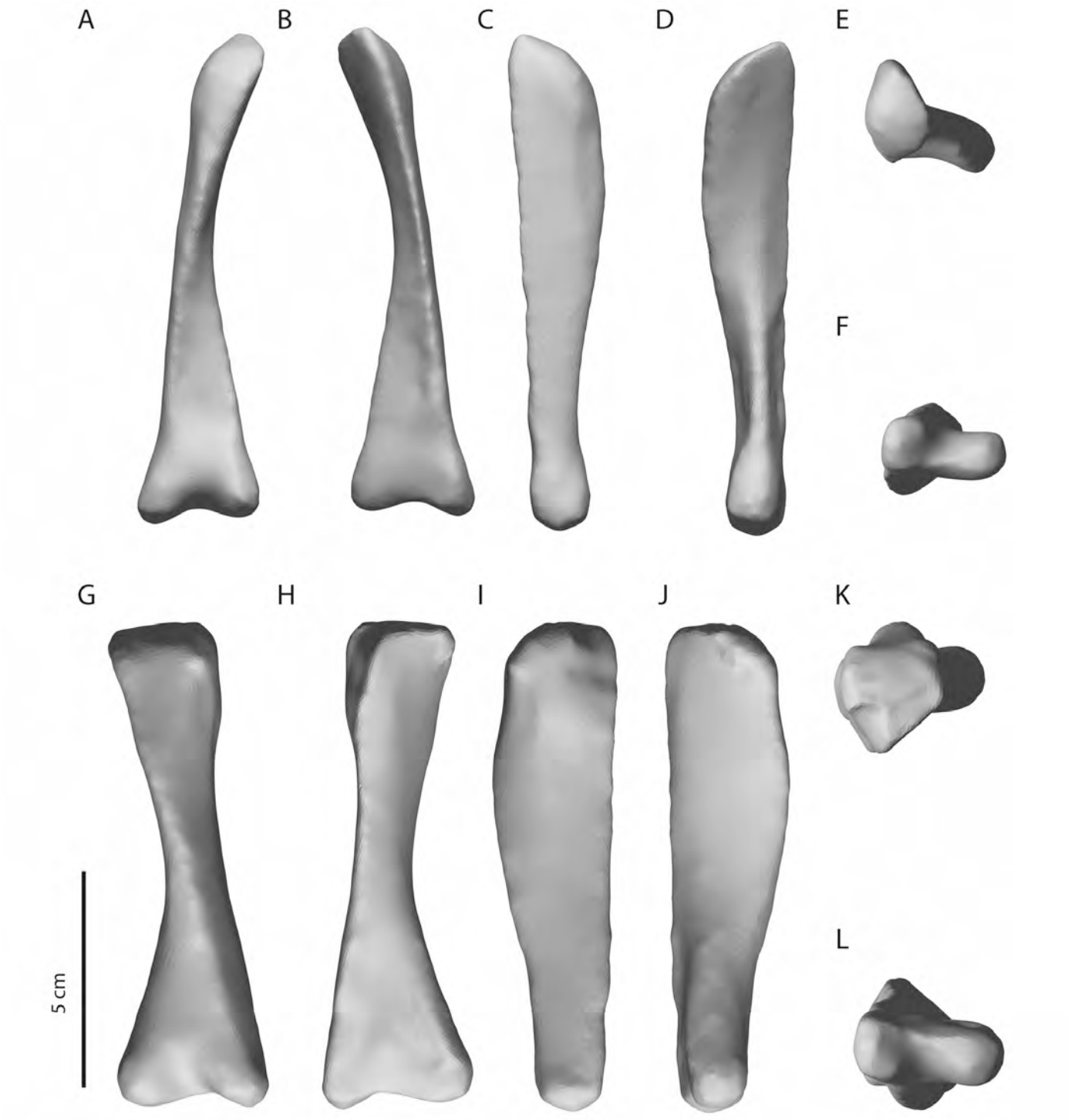

PLATE PL22. 3-D scans of Port Louis right (**A**–**F**) and left (**G**–**L**) sternal rib IIs (thoracic segment 16, thoracic), in cranial (**A**, **G**), caudal (**B**, **H**), lateral (**C**, **I**), medial (**D**, **J**), proximal (**E**, **K**), and distal (**F**, **L**) views. Obstructed portions of proximal and distal articular facets digitally reconstructed.

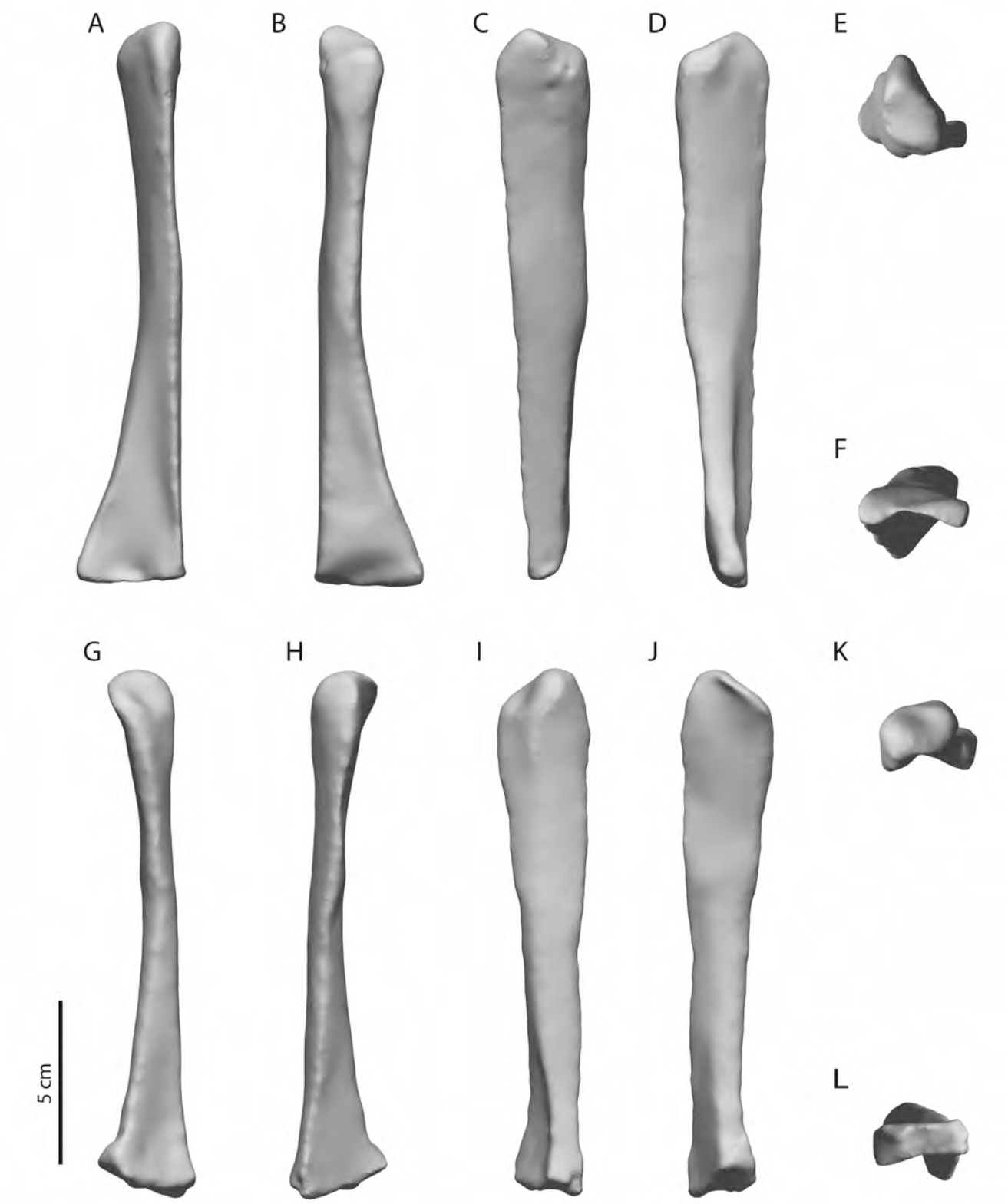

PLATE PL23. 3-D scans of Port Louis right (**A**–**F**) and left (**G**–**L**) sternal rib IIIs (thoracic segment 17, thoracic), in cranial (**A**, **G**), caudal (**B**, **H**), lateral (**C**, **I**), medial (**D**, **J**), proximal (**E**, **K**), and distal (**F**, **L**) views. Obstructed portions of proximal and distal articular facets digitally reconstructed.

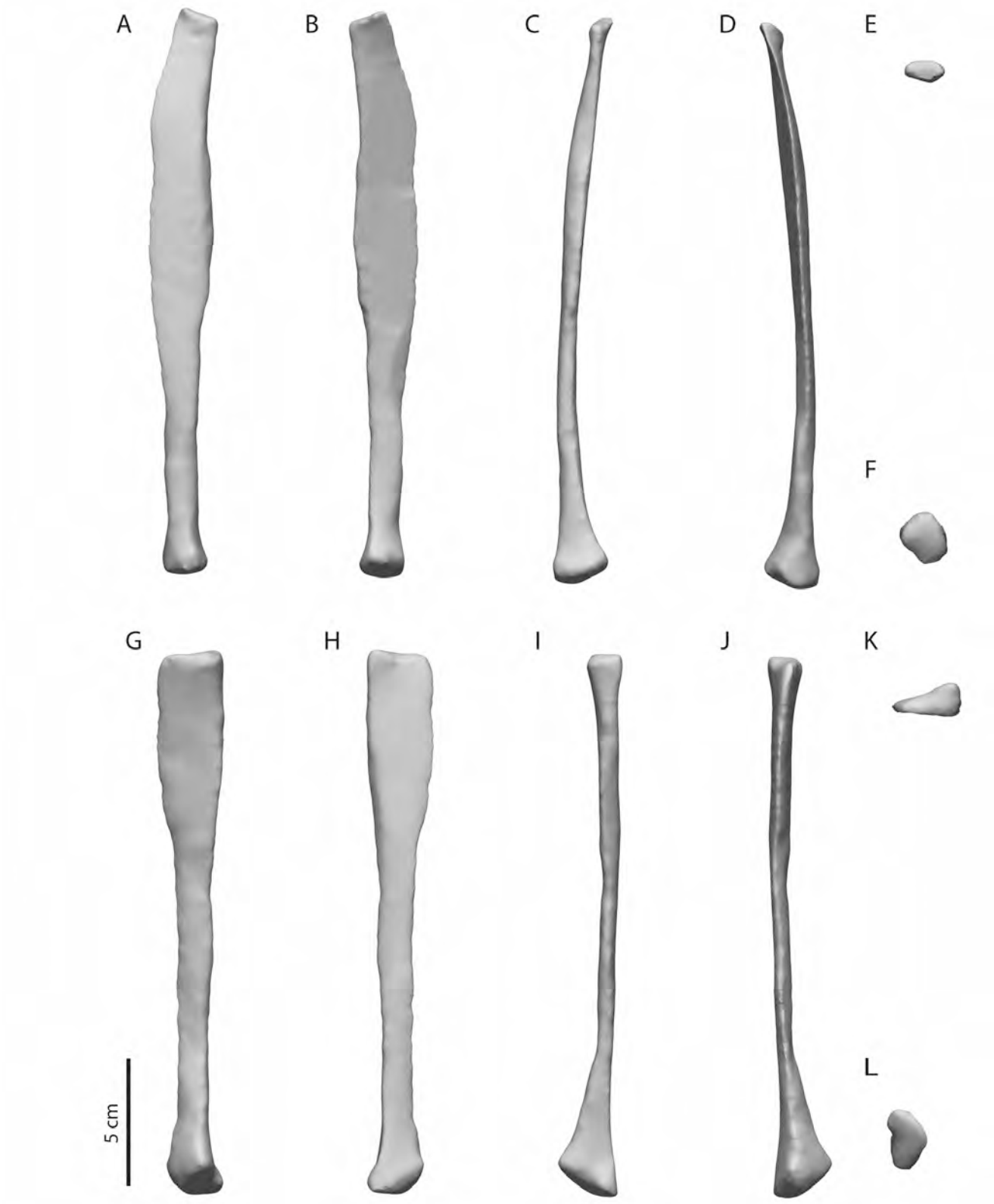

PLATE PL24. 3-D scans of Port Louis right (**A**–**F**) and left (**G**–**L**) sternal rib IVs (thoracic segment 18, thoracic), in cranial (**A**, **G**), caudal (**B**, **H**), lateral (**C**, **I**), medial (**D**, **J**), proximal (**E**, **K**), and distal (**F**, **L**) views. Obstructed portions of proximal and distal articular facets digitally reconstructed.

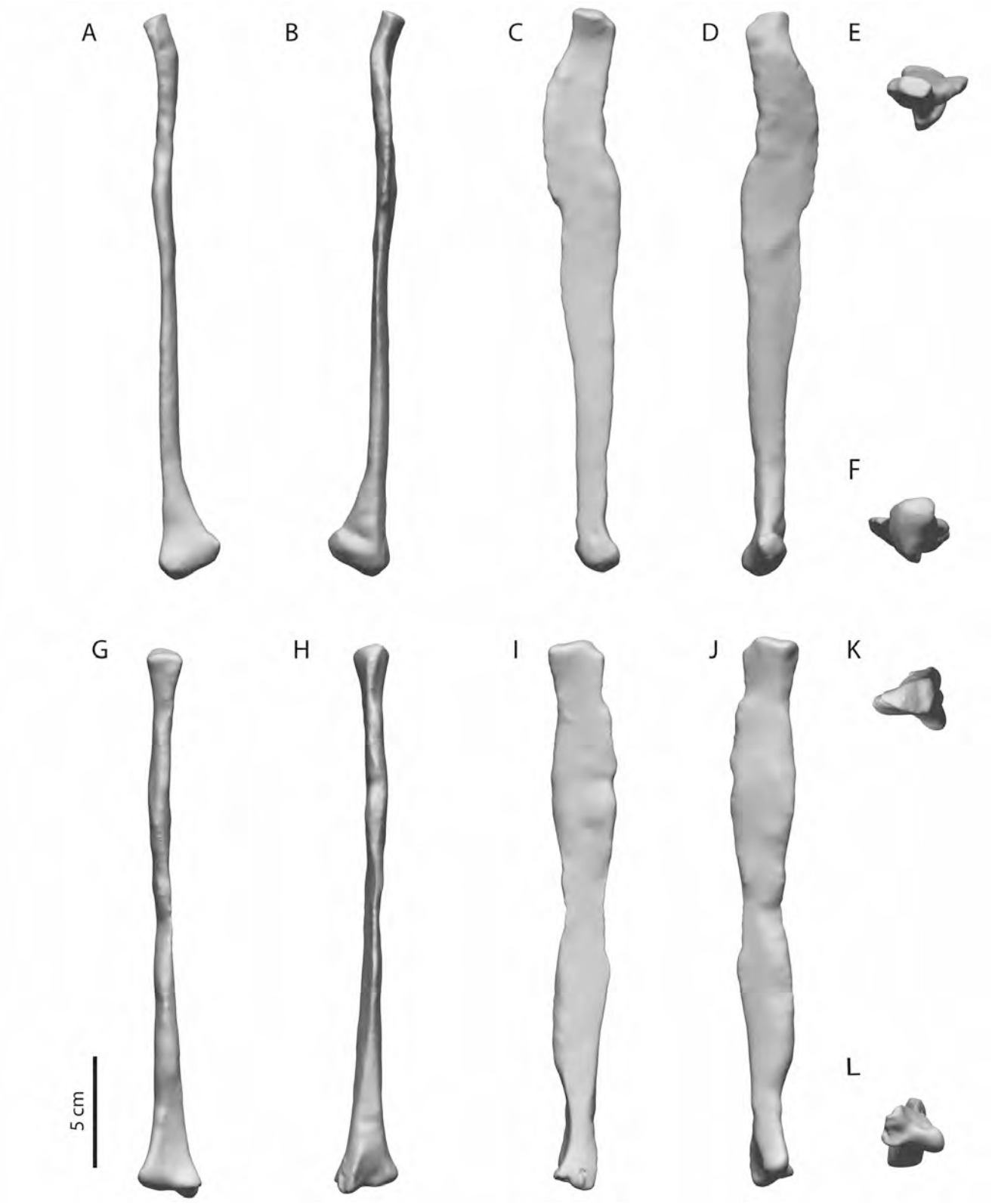

PLATE PL25. 3-D scans of Port Louis right (**A**–**F**) and left (**G**–**L**) sternal rib Vs (thoracic segment 19, thoracic), in cranial (**A**, **G**), caudal (**B**, **H**), lateral (**C**, **I**), medial (**D**, **J**), proximal (**E**, **K**), and distal (**F**, **L**) views. Obstructed portions of proximal and distal articular facets digitally reconstructed.

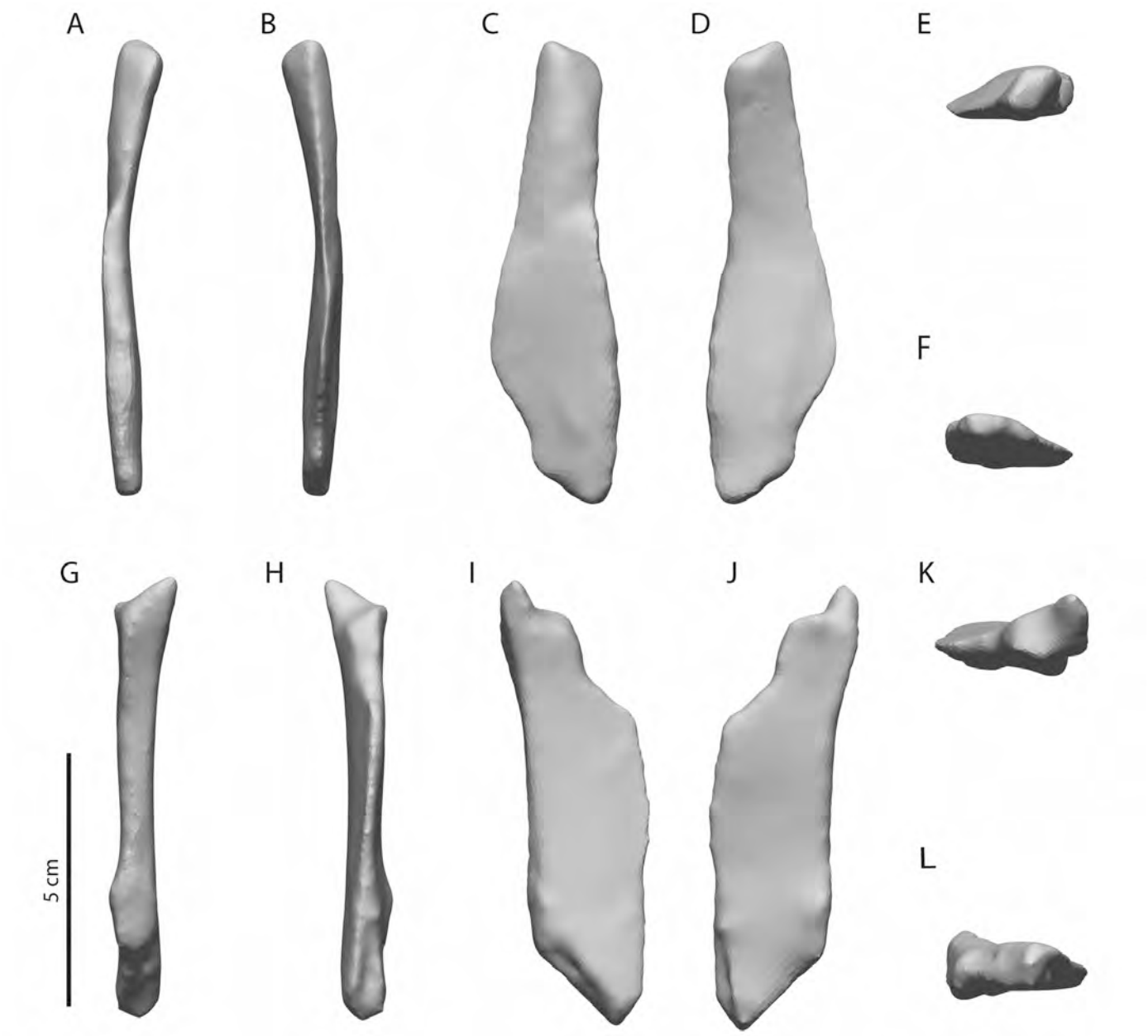

PLATE PL26. 3-D scans of Port Louis right (**A**–**F**) and left (**G**–**L**) sternal rib VIs (synsacral segment 20), in cranial (**A**, **G**), caudal (**B**, **H**), lateral (**C**, **I**), medial (**D**, **J**), proximal (**E**, **K**), and distal (**F**, **L**) views. Obstructed portions of proximal and distal articular facets digitally reconstructed.

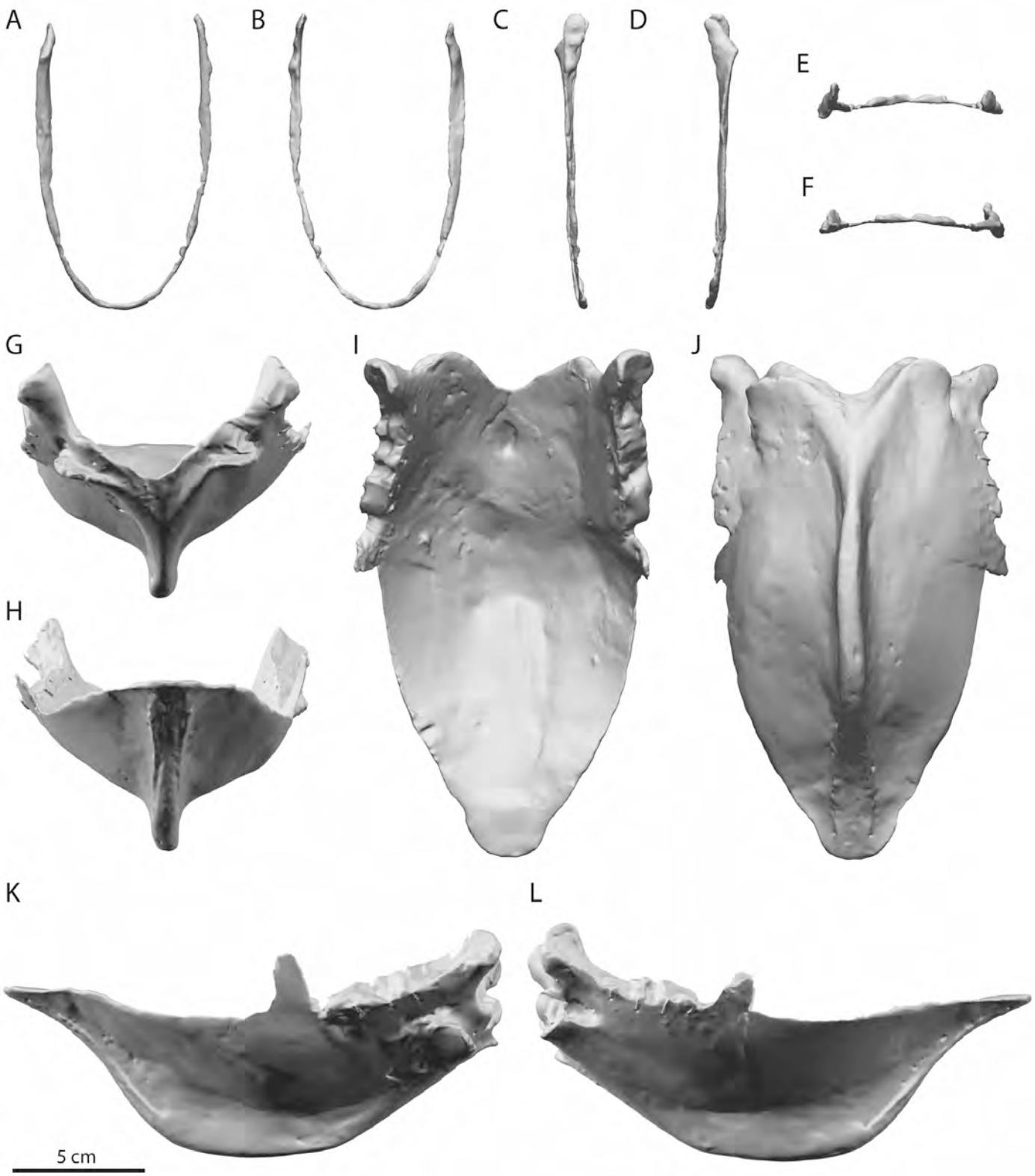

PLATE PL27. 3-D scans of Port Louis furcula (**A**–**F**) and sternum (**G**–**L**), in cranial (**A**, **G**), caudal (**B**, **H**), right lateral (**C**, **K**), left lateral (**D**, **L**), dorsal (**E**, **I**), and ventral (**F**, **J**) views. Obstructed portions of articular facets digitally reconstructed.

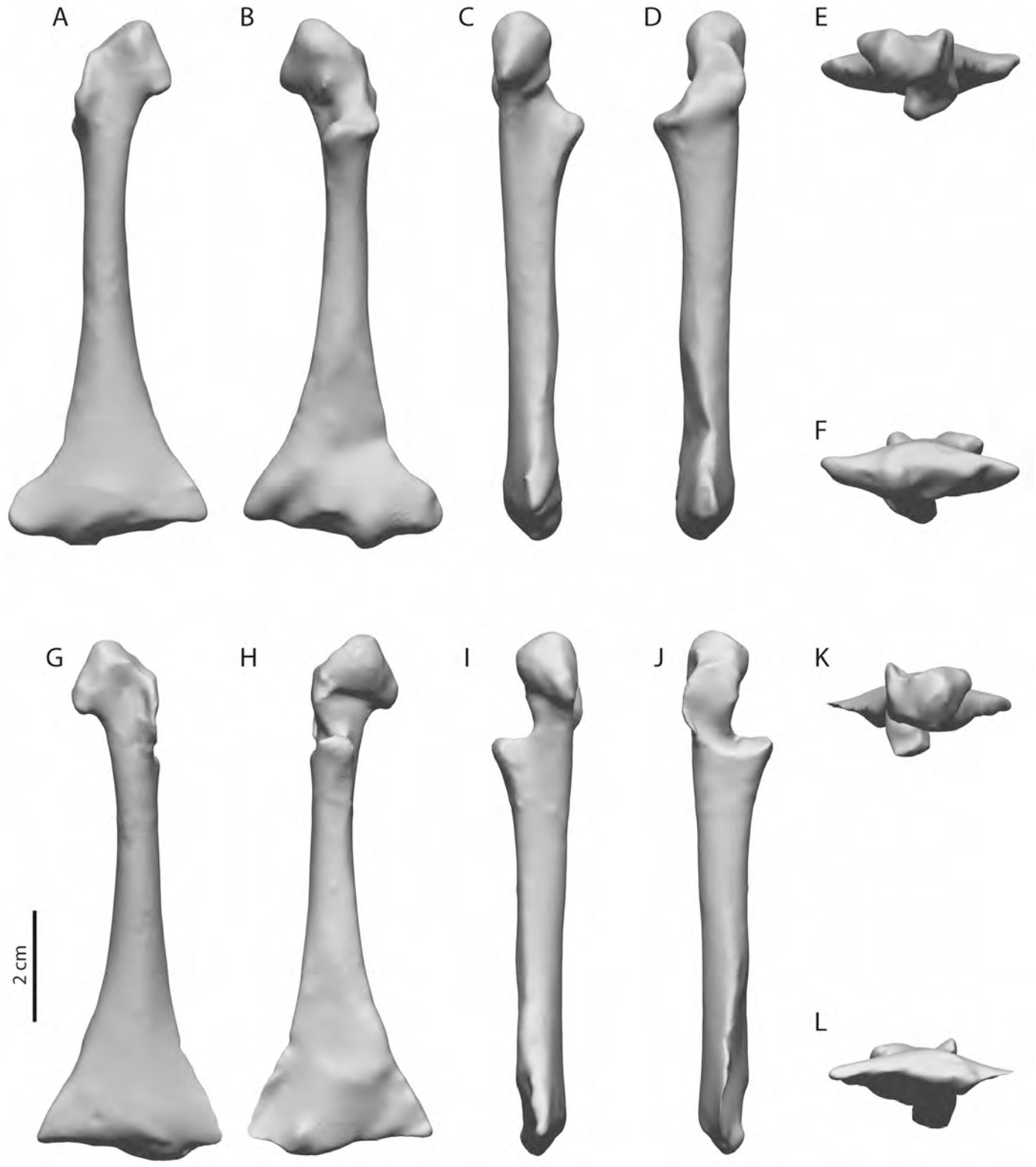

PLATE PL28. 3-D scans of Port Louis right (**A**–**F**) and left (**G**–**L**) coracoids, in ventral (**A**, **G**), dorsal (**B**, **H**), medial (**C**, **I**), lateral (**D**, **J**), proximal (**E**, **K**), and distal (**F**, **L**) views. Obstructed portions of articular facets digitally reconstructed.

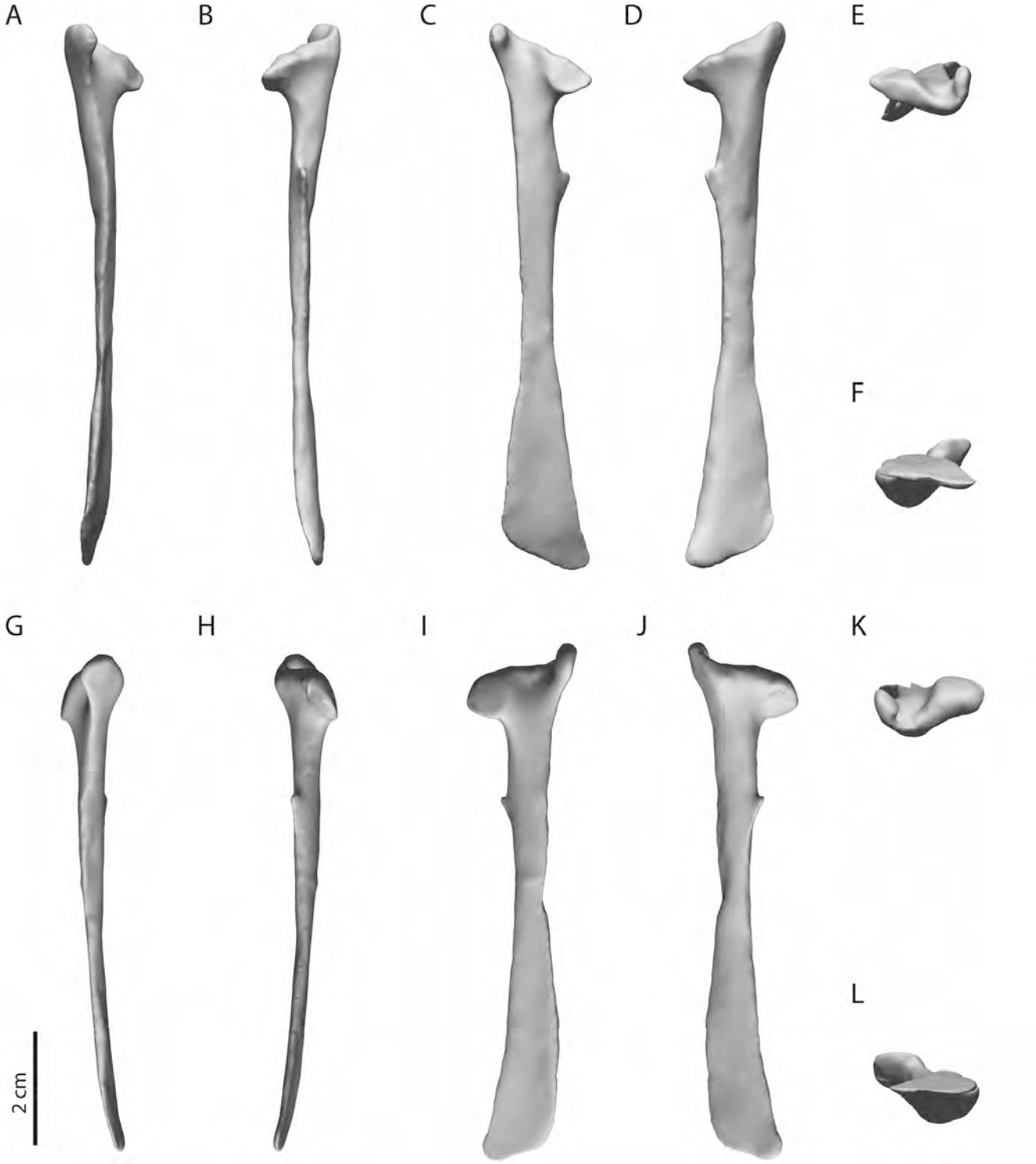

PLATE PL29. 3-D scans of Port Louis right (**A**–**F**) and left (**G**–**L**) scapulae, in dorsal (**A**, **G**), ventral (**B**, **H**), lateral (**C**, **I**), medial (**D**, **J**), cranial (**E**, **K**), and caudal (**F**, **L**) views. Obstructed portions of articular facets digitally reconstructed.

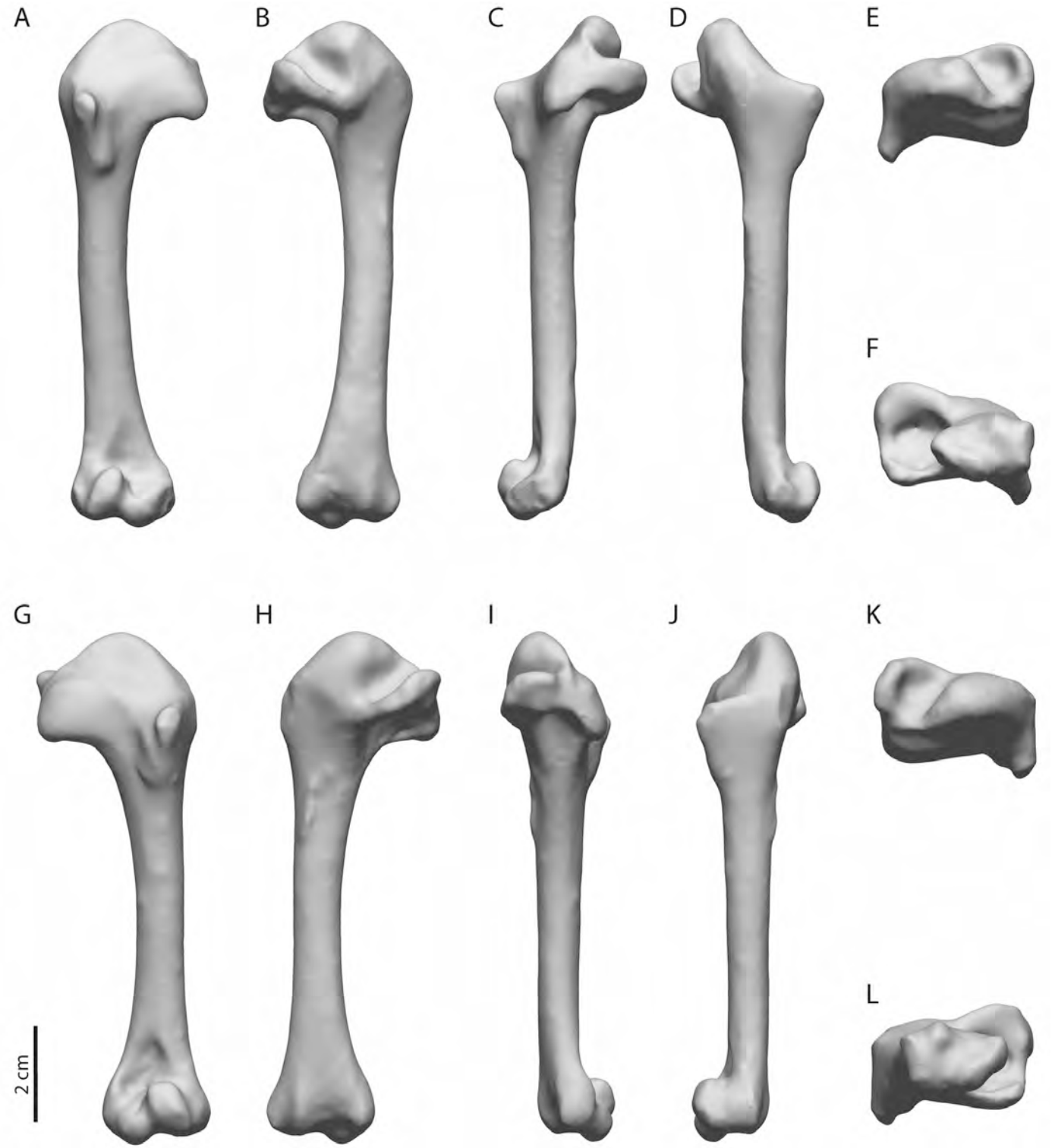

PLATE PL30. 3-D scans of Port Louis right (**A**–**F**) and left (**G**–**L**) humeri, in cranial (**A**, **G**), caudal (**B**, **H**), dorsal (**C**, **I**), ventral (**D**, **J**), proximal (**E**, **K**), and distal (**F**, **L**) views. Obstructed portions of articular facets digitally reconstructed.

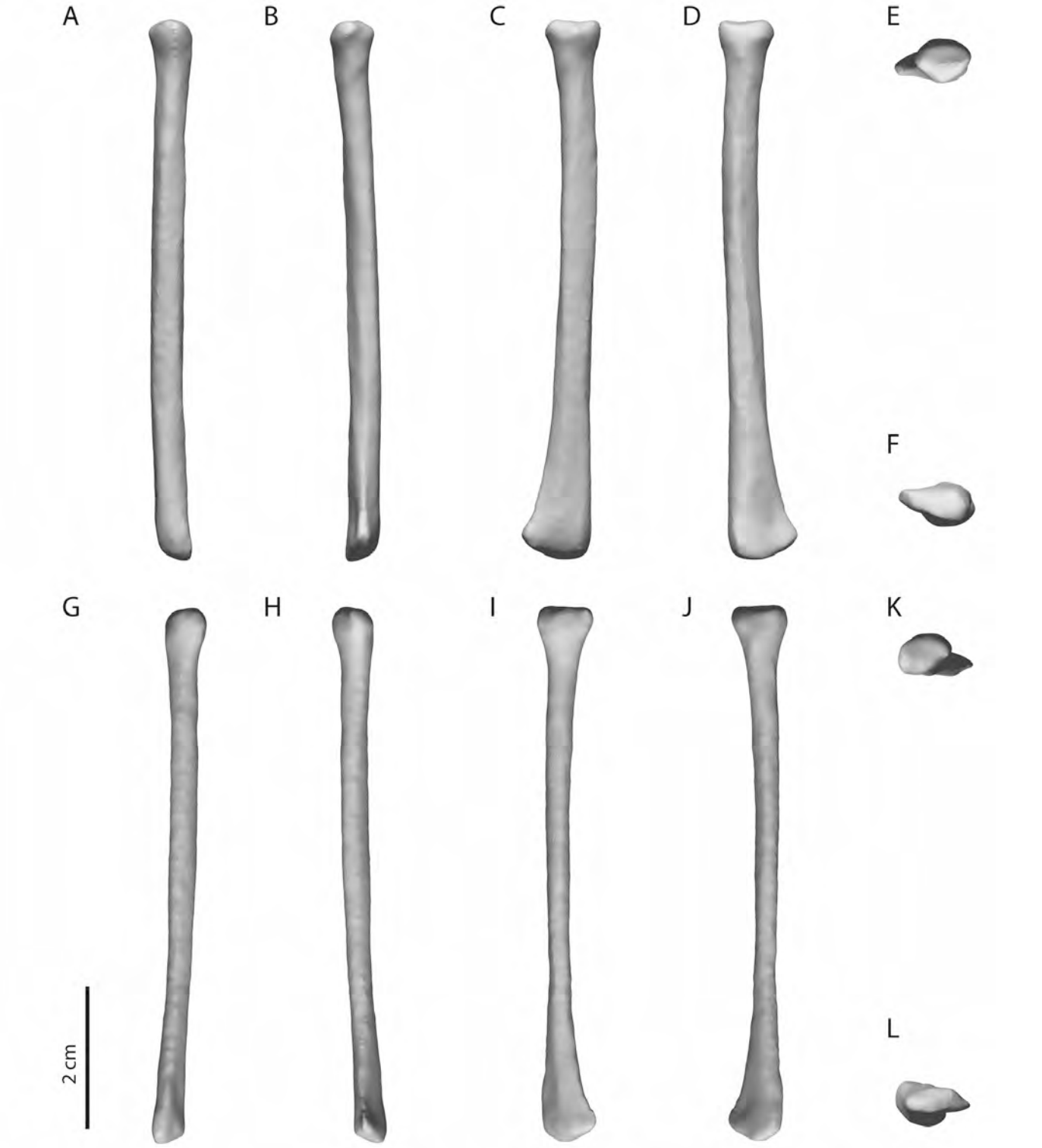

PLATE PL31. 3-D scans of Port Louis right (**A**–**F**) and left (**G**–**L**) radii, in cranial (**A**, **G**), caudal (**B**, **H**), dorsal (**C**, **I**), ventral (**D**, **J**), proximal (**E**, **K**), and distal (**F**, **L**) views. Obstructed portions of articular facets digitally reconstructed.

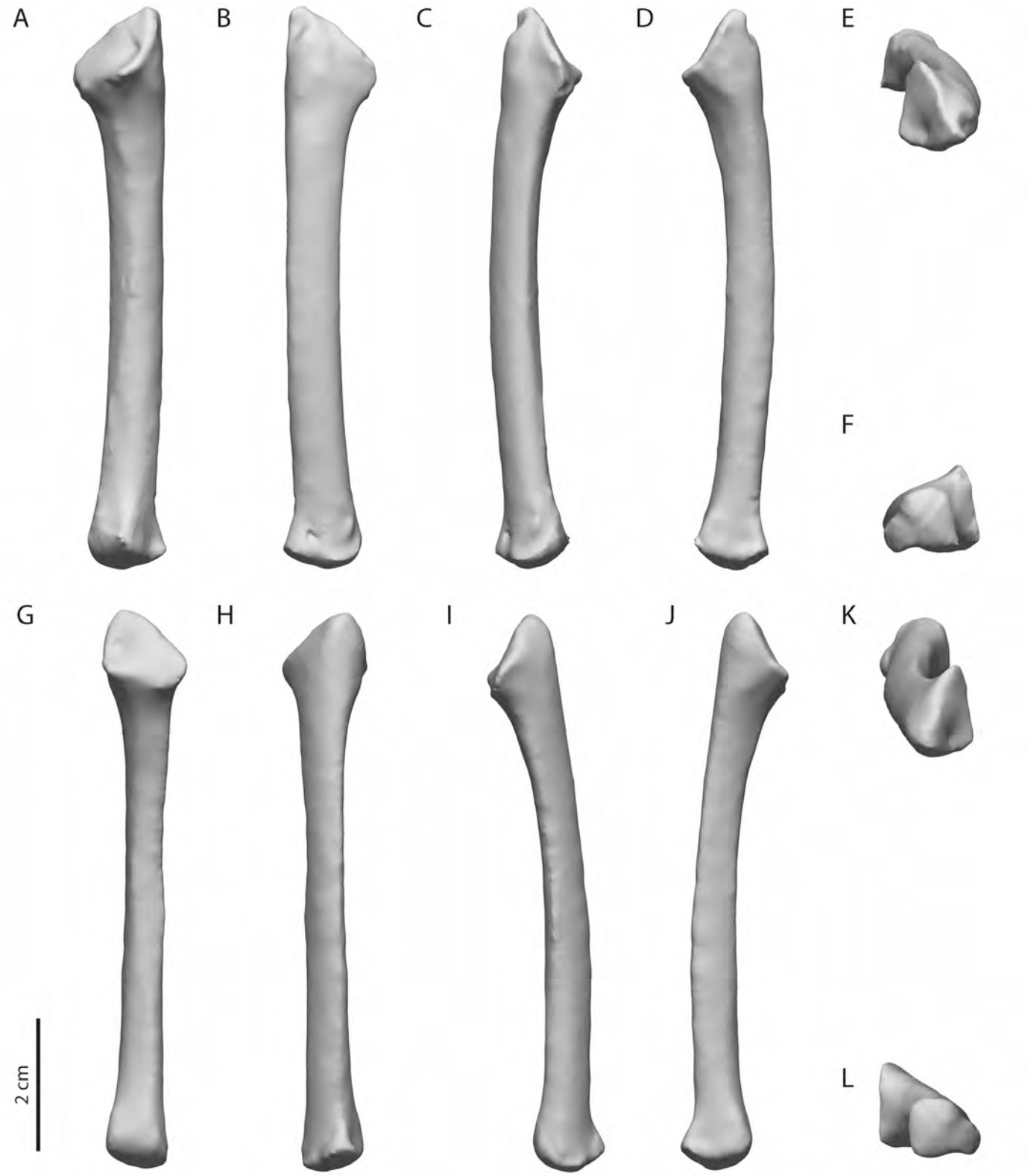

PLATE PL32. 3-D scans of Port Louis right (**A**–**F**) and left (**G**–**L**) ulnae, in cranial (**A**, **G**), caudal (**B**, **H**), dorsal (**C**, **I**), ventral (**D**, **J**), proximal (**E**, **K**), and distal (**F**, **L**) views. Obstructed portions of proximal articular facet digitally reconstructed.

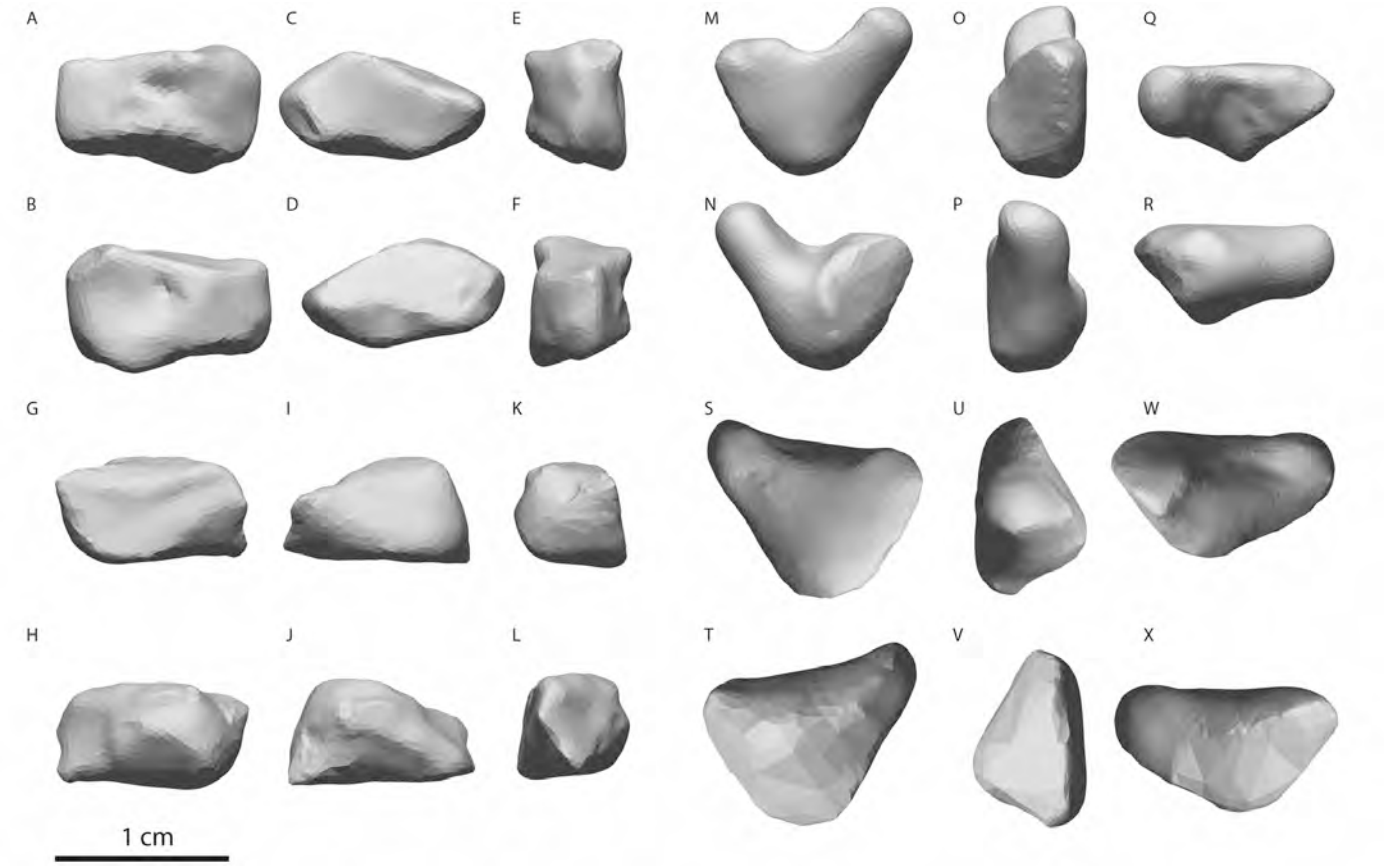

PLATE PL33. 3-D scans of Port Louis right (**A**–**F**) and left (**G**–**L**) radiali and right (**M**–**R**) and left (**S**–**X**) ulnaria, in dorsal (**A**, **G**, **M**, **S**), ventral (**B**, **H**, **N**, **T**), proximal (**C**, **I**, **O**, **U**), distal (**D**, **J**, **P**, **V**), cranial (**E**, **K**, **Q**, **W**), and caudal (**F**, **L**, **R**, **X**) views. Left radiale and ulnare digitally reconstructed.

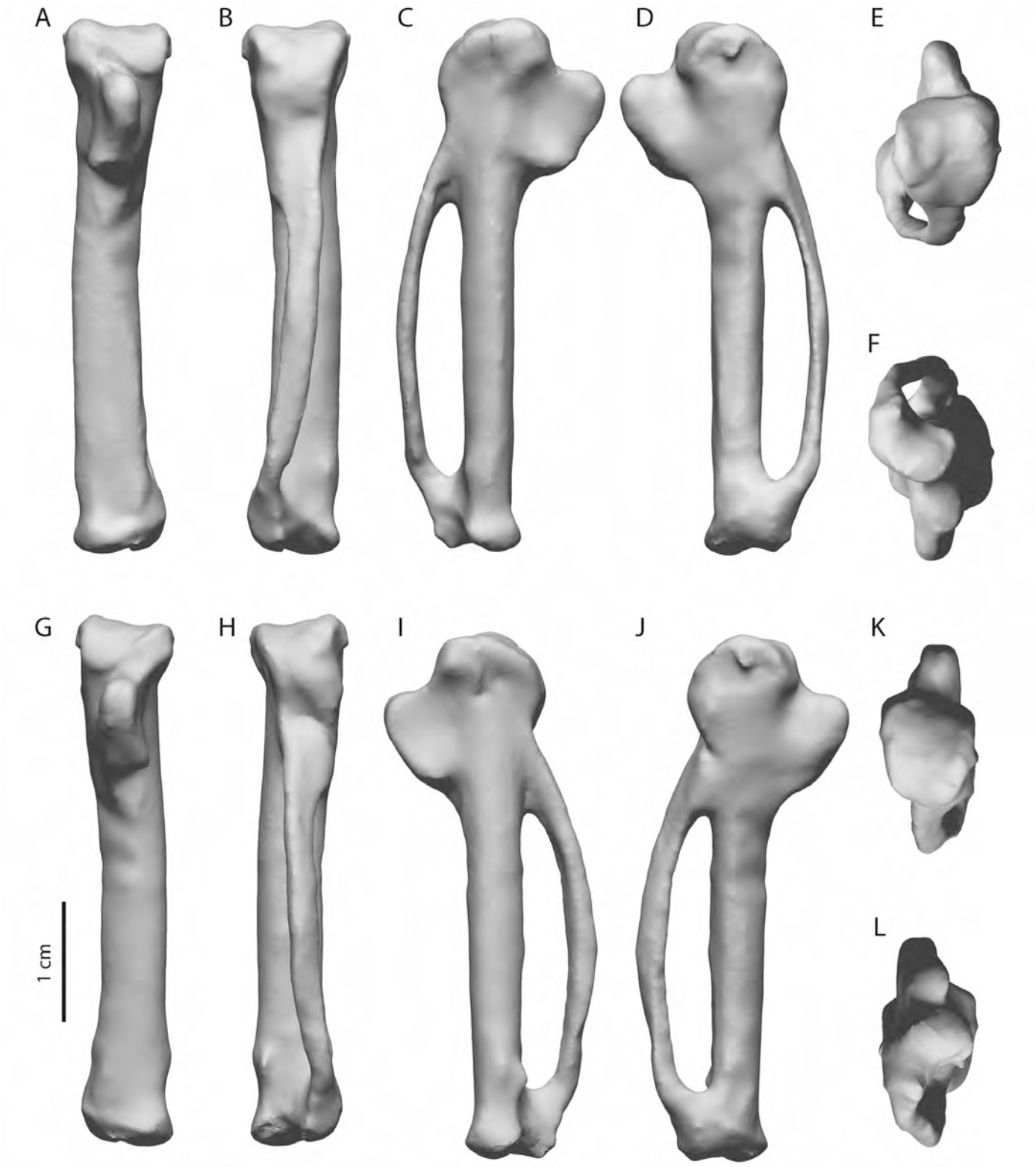

PLATE PL34. 3-D scans of Port Louis right (**A**–**F**) and left (**G**–**L**) carpometacarpi, in cranial (**A**, **G**), caudal (**B**, **H**), dorsal (**C**, **I**), ventral (**D**, **J**), proximal (**E**, **K**), and distal (**F**, **L**) views. Obstructed portions of articular facets digitally reconstructed.

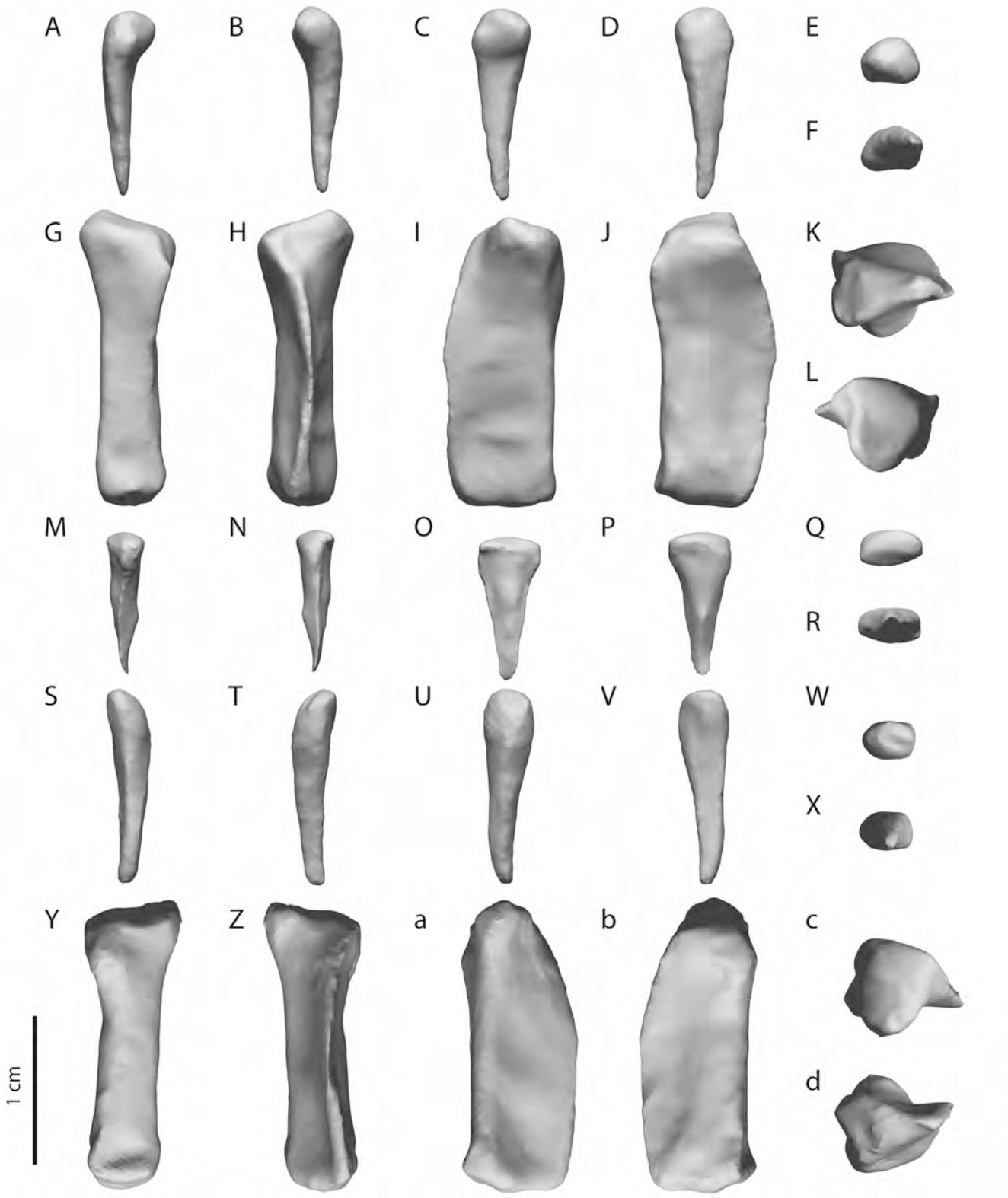

PLATE PL35. 3-D scans of Port Louis left phalanx digiti alulae (**A**–**F**), left phalanx proximalis digiti majoris (**G**–**L**), left phalanx distalis digiti majoris (**M**–**R**), right phalanx digiti alulae (**S**–**X**), and right phalanx proximalis digiti majoris (**Y**–**d**), in dorsal (**A**, **G**, **M**, **S**, **Y**), ventral (**B**, **H**, **N**, **T**, **Z**), cranial (**C**, **I**, **O**, **U**, **a**), caudal (**D**, **J**, **P**, **V**, **b**), proximal (**E**, **K**, **Q**, **W**, **c**), and distal (**F**, **L**, **R**, **X**, **d**) views. Articular facets digitally reconstructed.

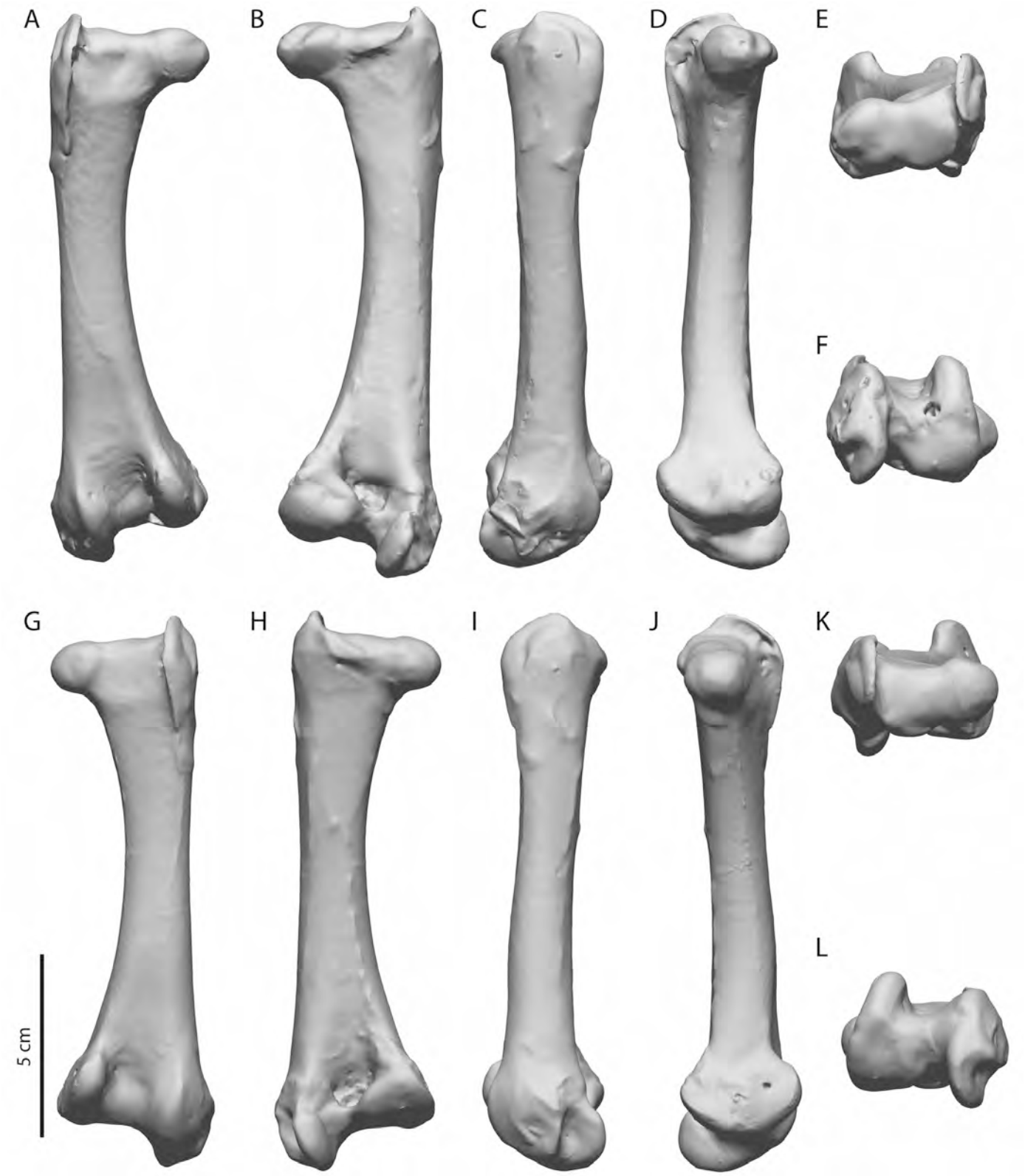

PLATE PL36. 3-D scans of Port Louis right (**A**–**F**) and left (**G**–**L**) femora, in cranial (**A**, **G**), caudal (**B**, **H**), lateral (**C**, **I**), medial (**D**, **J**), proximal (**E**, **K**), and distal (**F**, **L**) views.

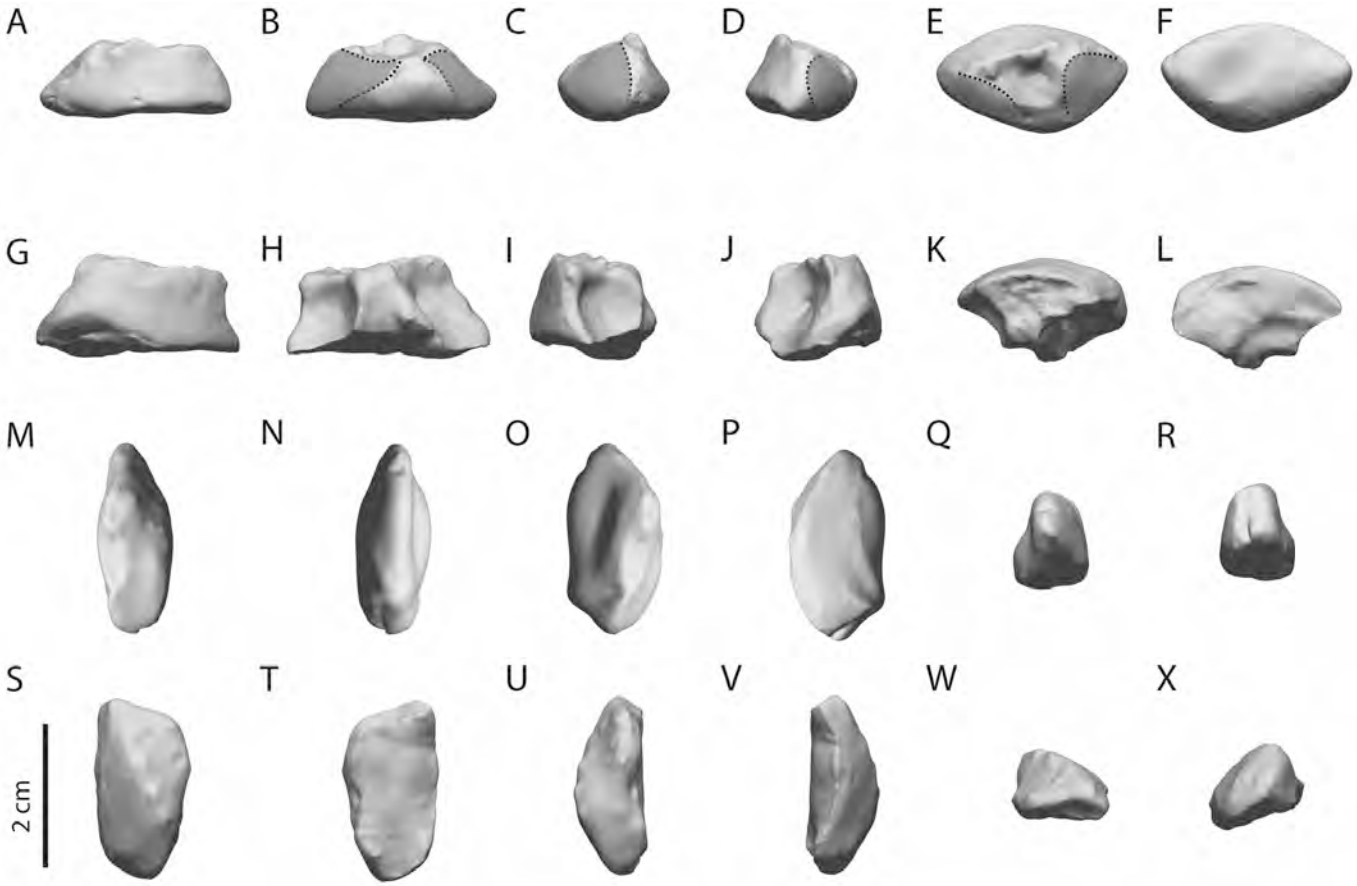

PLATE PL37. 3-D scans of Port Louis right (**A**–**F**) and left (**G**–**L**) patellae, and right (**M**–**R**), and left (**S**–**X**) intertarsal sesamoids, in cranial (**A**, **G**, **M**, **S**), caudal (**B**, **H**, **N**, **T**), lateral (**C**, **I**, **O**, **U**), medial (**D**, **J**, **P**, **V**), dorsal (**E**, **K**, **Q**, **W**), and ventral (**F**, **L**, **R**, **X**) views. Gray areas in **B**–**E** highlight concave articular surfaces filled in during digital editing.

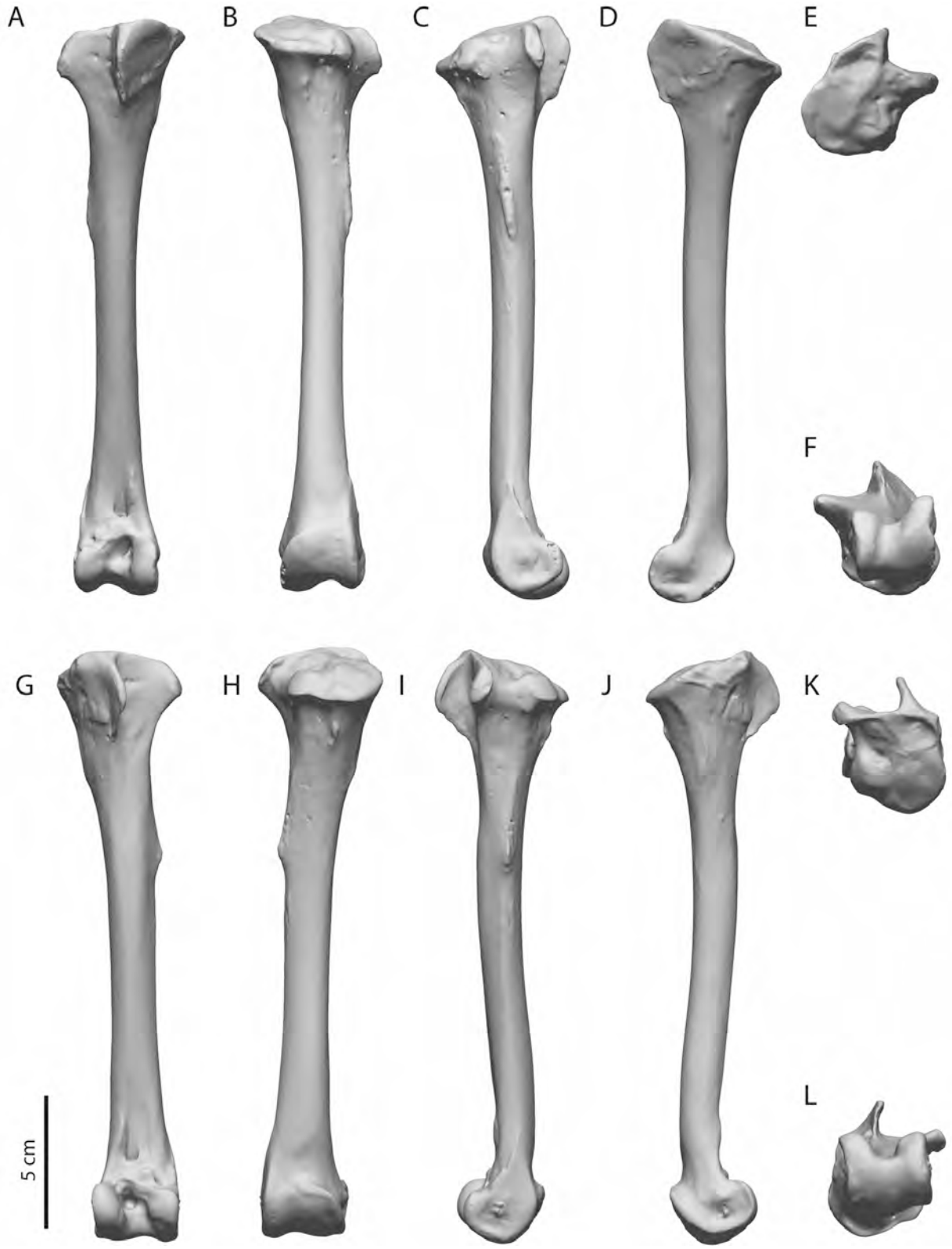

PLATE PL38. 3-D scans of Port Louis right (**A**–**F**) and left (**G**–**L**) tibiotarsi, in cranial (**A**, **G**), caudal (**B**, **H**), lateral (**C**, **I**), medial (**D**, **J**), proximal (**E**, **K**), and distal (**F**, **L**) views. Obstructed area of proximal articular facet digitally reconstructed.

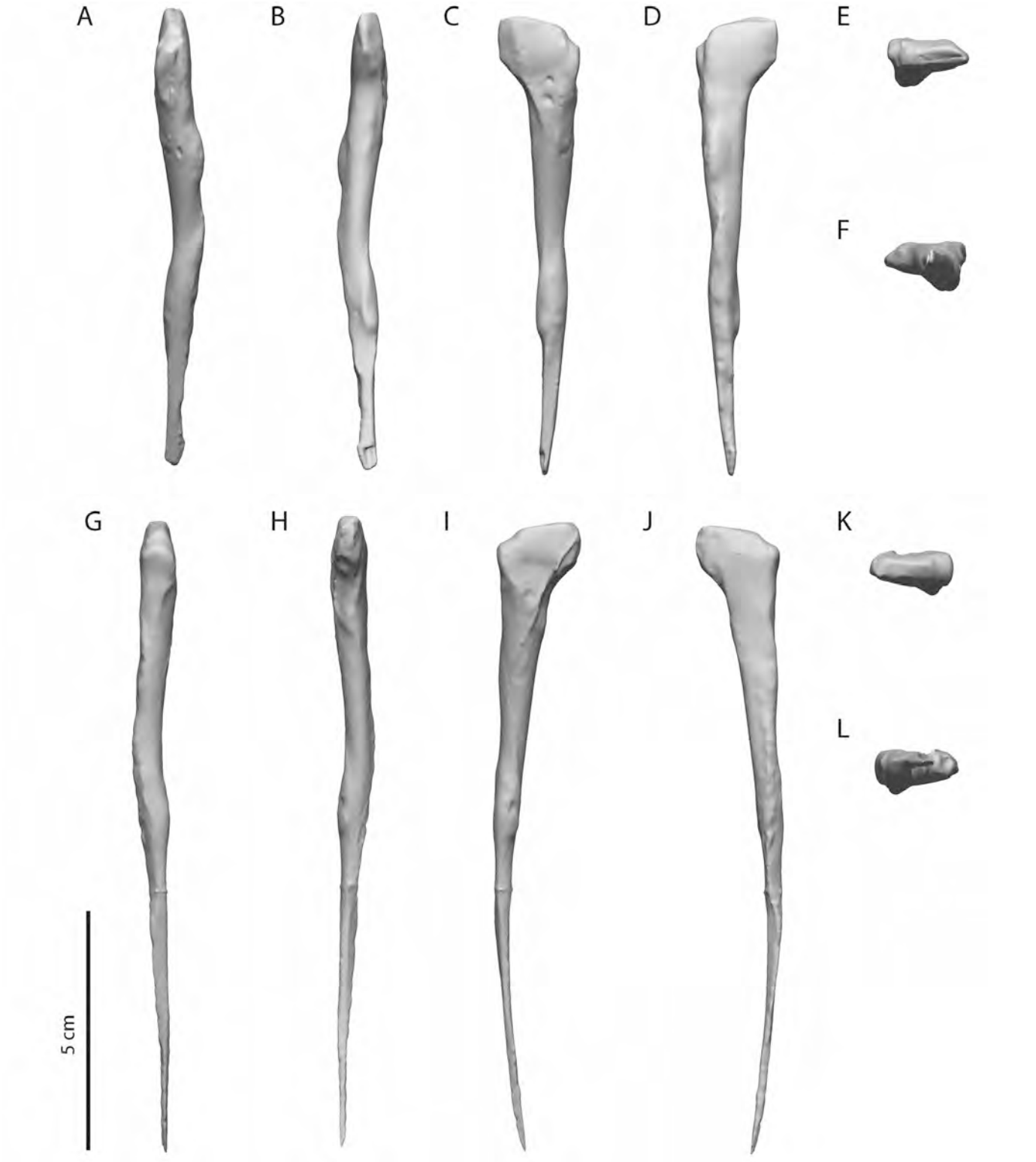

PLATE PL39. 3-D scans of Port Louis right (**A**–**F**) and left (**G**–**L**) fibulae, in cranial (**A**, **G**), caudal (**B**, **H**), lateral (**C**, **I**), medial (**D**, **J**), proximal (**E**, **K**), and distal (**F**, **L**) views. The left fibula is complete; the right distal fibula is broken and incomplete. Proximal medial articular surface with tibiotarsus digitally reconstructed.

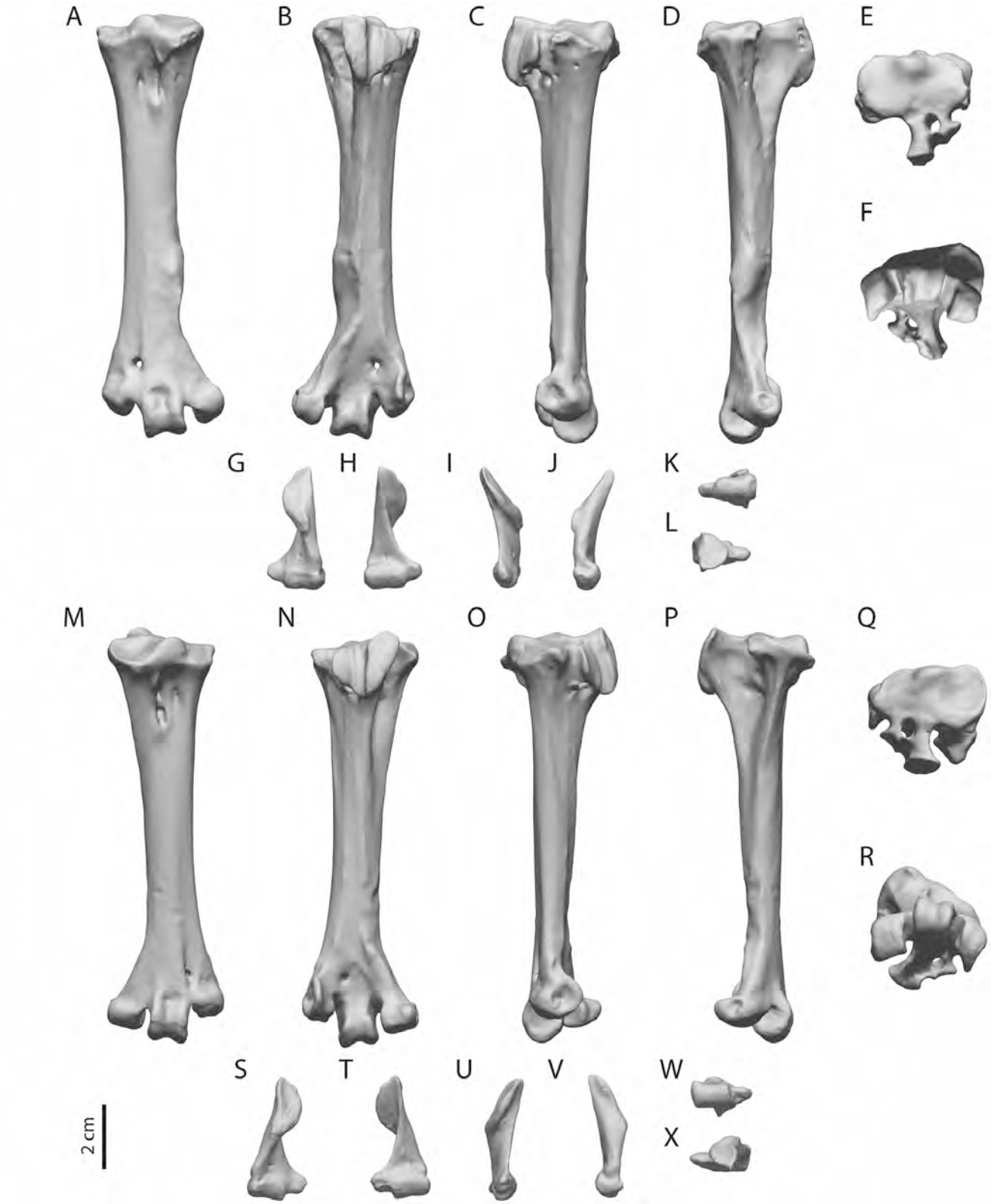

PLATE PL40. 3-D scans of Port Louis right (**A**–**F**) and left (**M**–**R**) tarsometatarsi, and right (**G**–**L**) and left (**S**–**X**) metatarsus Is, in cranial (**A**, **G**, **M**, **S**), caudal (**B**, **H**, **N**, **T**), lateral (**C**, **I**, **O**, **U**), medial (**D**, **J**, **P**, **V**), proximal (**E**, **K**, **Q**, **W**), and distal (**F**, **L**, **R**, **X**) views. Articular facet between tarsometatarsus and metatarsus I digitally reconstructed.

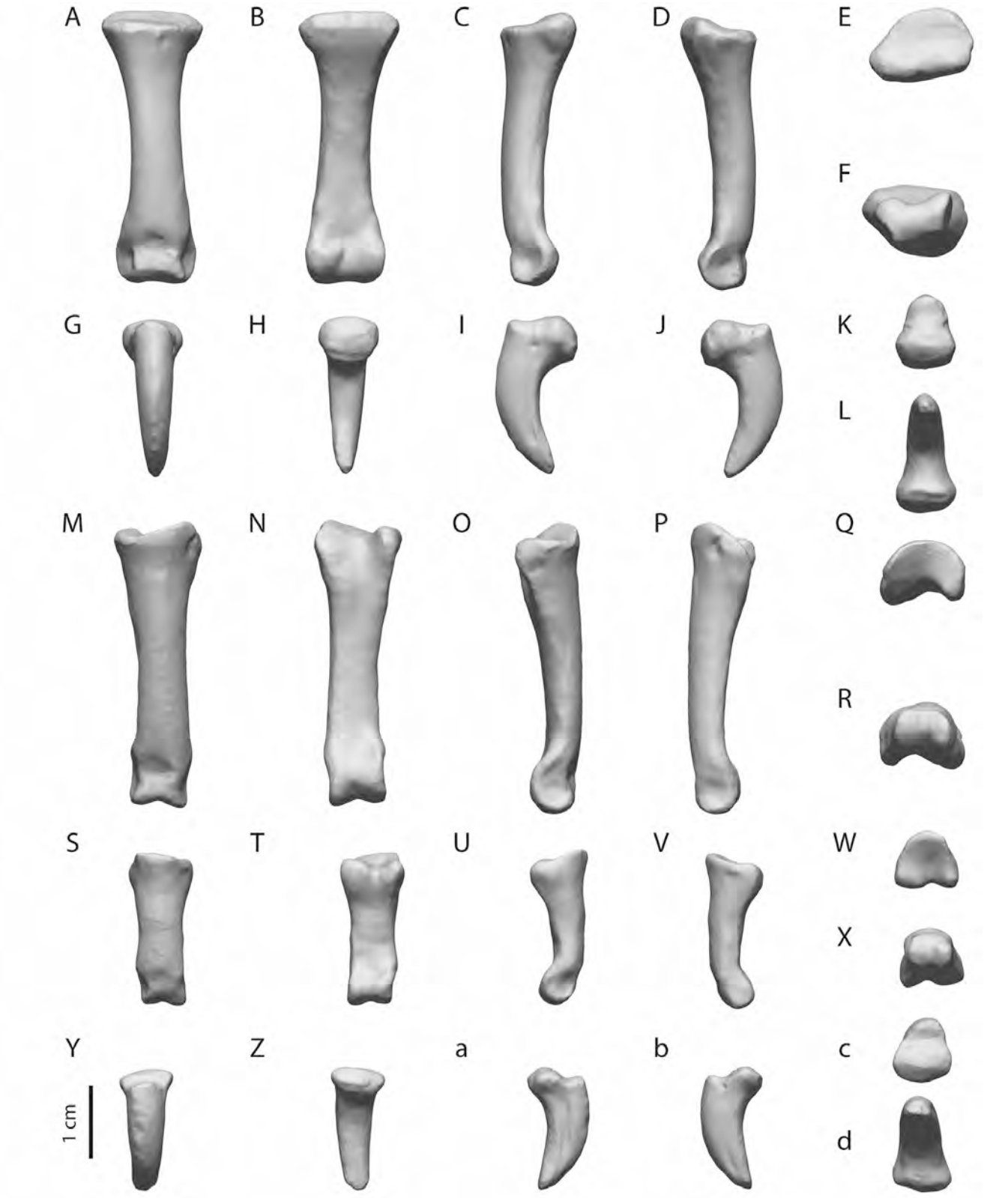

PLATE PL41. 3-D scans of phalanges and unguals of digits I and II of the right foot, Port Louis specimen. Pedal phalanx I-1 (**A**–**F**), phalanx (ungual) I-2 (**G**–**L**), phalanx II-1 (**M**–**R**), phalanx II-2 (**S**–**X**), and phalanx (ungual) II-3 (**Y**–**d**), in dorsal (**A**, **G**, **M**, **S**, **Y**), plantar (**B**, **H**, **N**, **T**, **Z**), lateral (**C**, **I**, **O**, **U**, **a**), medial (**D**, **J**, **P**, **V**, **b**), proximal (**E**, **K**, **Q**, **W**, **c**), and distal (**F**, **L**, **R**, **X**, **d**) views. Obstructed portions of articular facets and plantar surface digitally reconstructed.

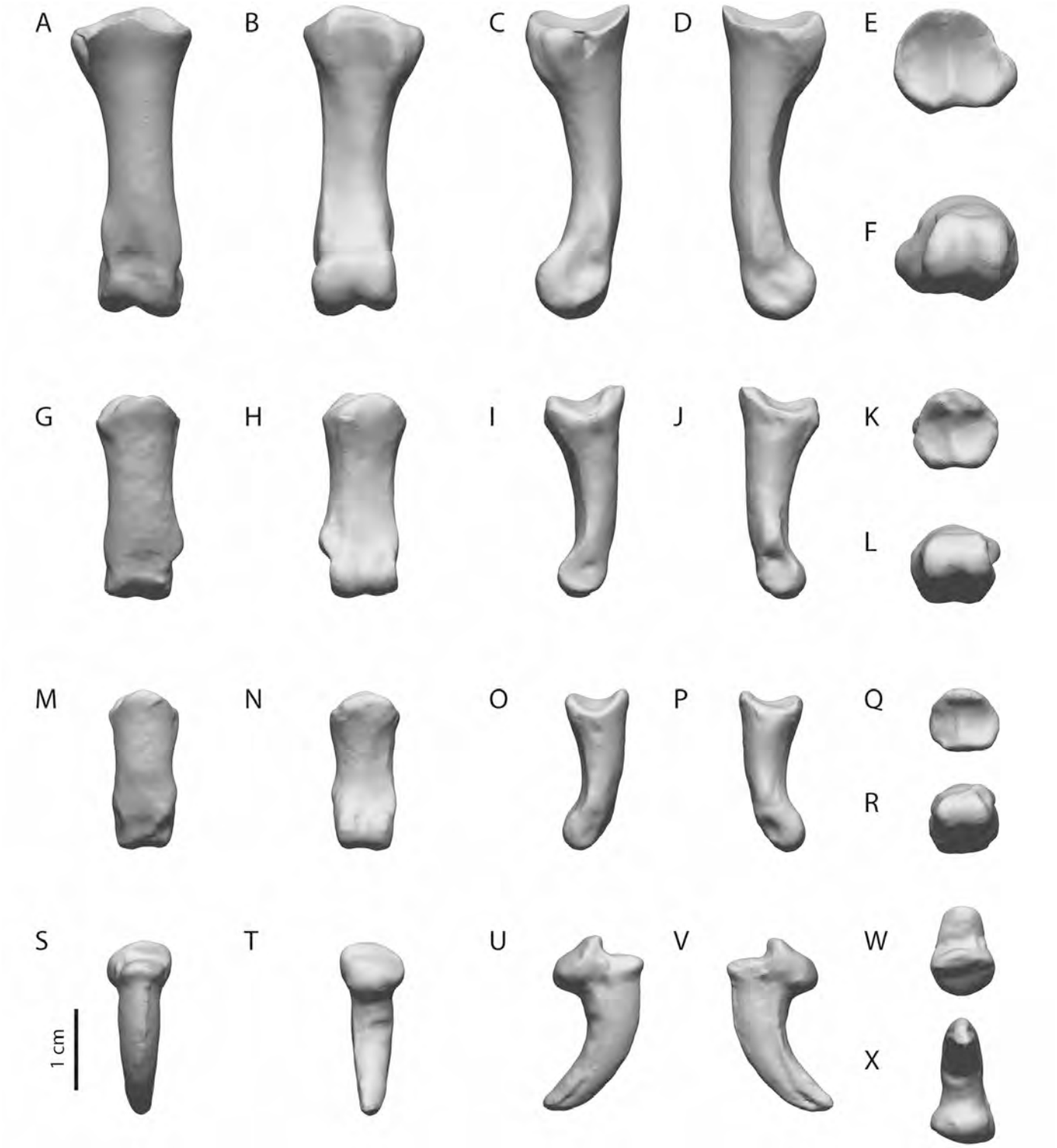

PLATE PL42. 3-D scans of phalanges and unguals of digit III of the right foot, Port Louis specimen. Pedal phalanx III-1 (**A**–**F**), phalanx III-2 (**G**–**L**), phalanx III-3 (**M**–**R**), and phalanx (ungual) III-4 (**S**–**X**), in dorsal (**A**, **G**, **M**, **S**), plantar (**B**, **H**, **N**, **T**), lateral (**C**, **I**, **O**, **U**), medial (**D**, **J**, **P**, **V**), proximal (**E**, **K**, **Q**, **W**), and distal (**F**, **L**, **R**, **X**) views. Obstructed portions of articular facets and plantar surface digitally reconstructed.

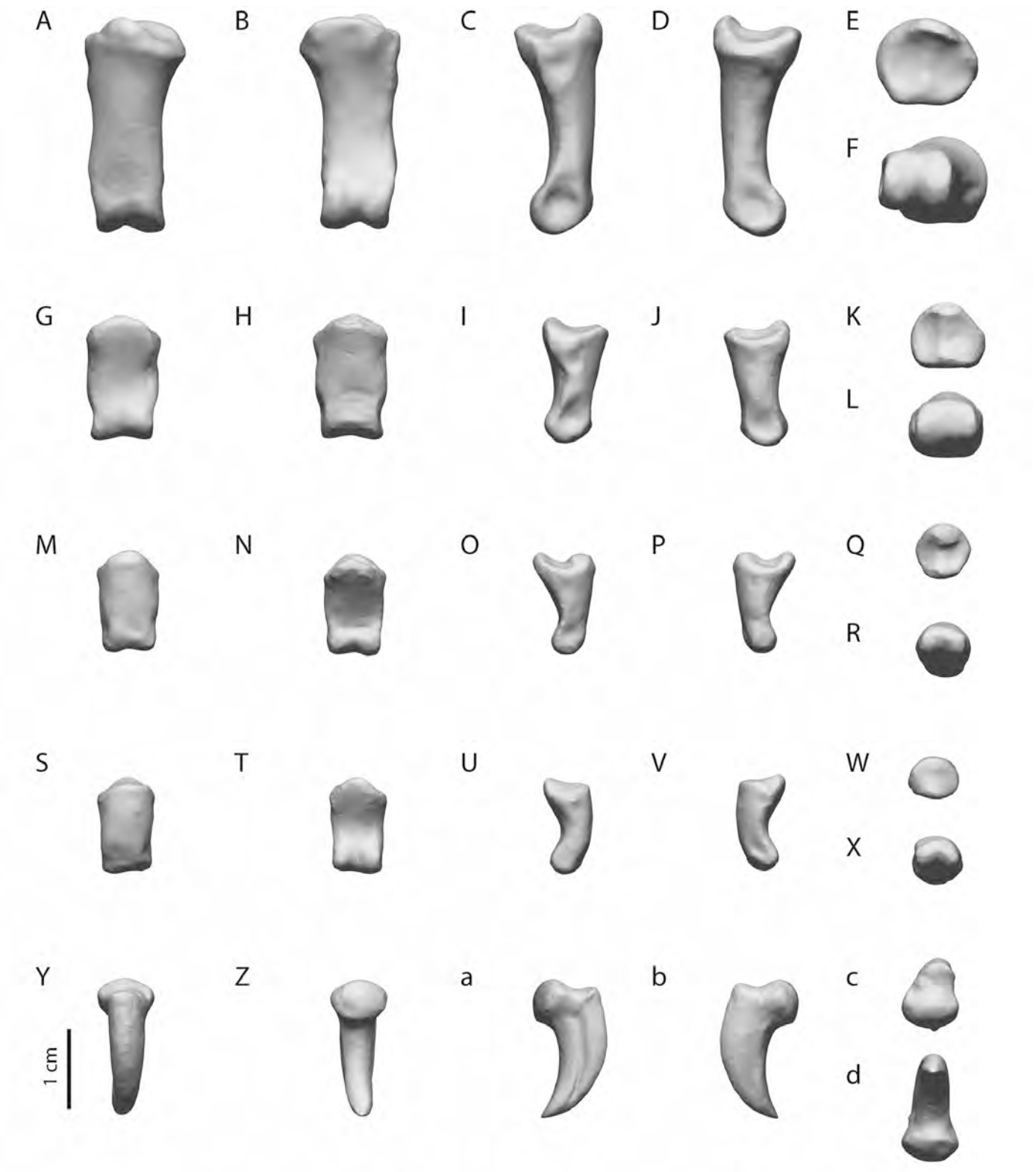

PLATE PL43. 3-D scans of phalanges and unguals of digit IV of the right foot, Port Louis specimen. Pedal phalanx IV-1 (**A**–**F**), phalanx IV-2 (**G**–**L**), phalanx IV-3 (**M**–**R**), phalanx IV-4 (**S**–**X**), and phalanx (ungual) IV-5 (**Y**–**d**), in dorsal (**A**, **G**, **M**, **S**, **Y**), plantar (**B**, **H**, **N**, **T**, **Z**), lateral (**C**, **I**, **O**, **U**, **a**), medial (**D**, **J**, **P**, **V**, **b**), proximal (**E**, **K**, **Q**, **W**, **c**), and distal (**F**, **L**, **R**, **X**, **d**) views. Obstructed portions of articular facets and plantar surface digitally reconstructed.

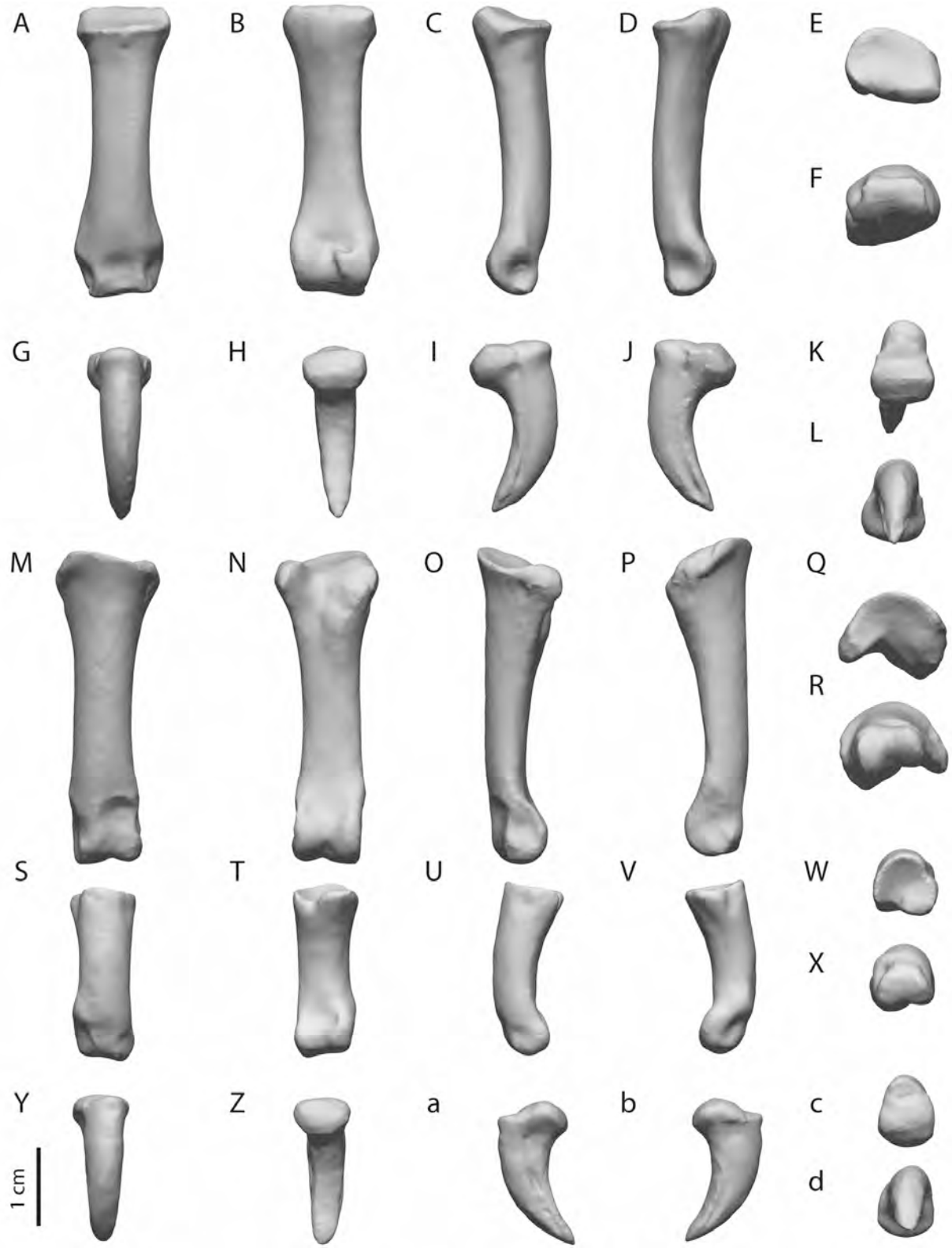

PLATE PL44. 3-D scans of phalanges and unguals of digits I and II of the left foot, Port Louis specimen. Pedal phalanx I-1 (**A**–**F**), phalanx (ungual) I-2 (**G**–**L**), phalanx II-1 (**M**–**R**), phalanx II-2 (**S**–**X**), and phalanx (ungual) II-3 (**Y**–**d**), in dorsal (**A**, **G**, **M**, **S**, **Y**), plantar (**B**, **H**, **N**, **T**, **Z**), lateral (**C**, **I**, **O**, **U**, **a**), medial (**D**, **J**, **P**, **V**, **b**), proximal (**E**, **K**, **Q**, **W**, **c**), and distal (**F**, **L**, **R**, **X**, **d**) views. Obstructed portions of articular facets and plantar surface digitally reconstructed.

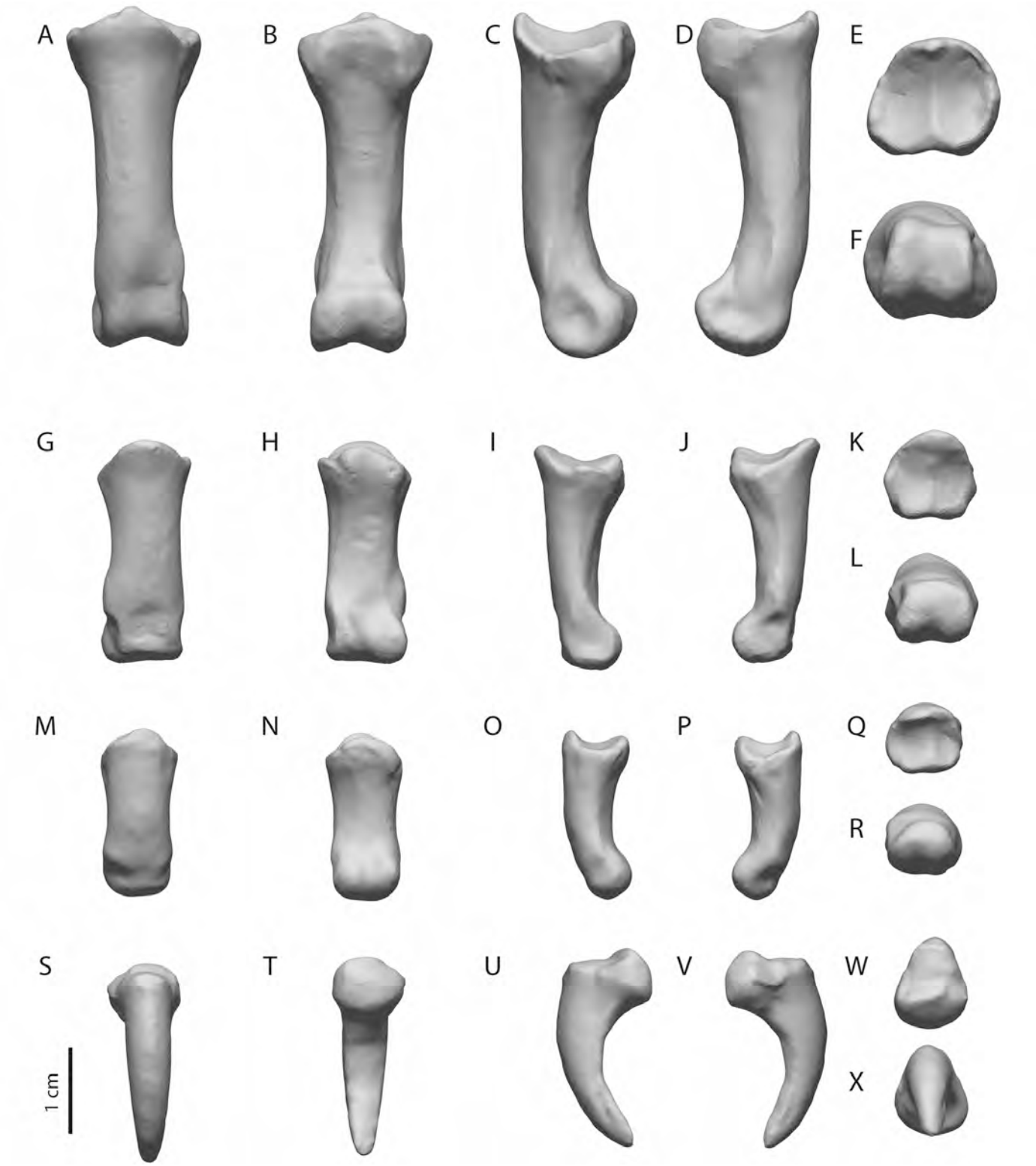

PLATE PL45. 3-D scans of phalanges and unguals of digit III of the left foot, Port Louis specimen. Pedal phalanx III-1 (**A**–**F**), phalanx III-2 (**G**–**L**), phalanx III-3 (**M**–**R**), and phalanx (ungual) III-4 (**S**–**X**), in dorsal (**A**, **G**, **M**, **S**), plantar (**B**, **H**, **N**, **T**), lateral (**C**, **I**, **O**, **U**), medial (**D**, **J**, **P**, **V**), proximal (**E**, **K**, **Q**, **W**), and distal (**F**, **L**, **R**, **X**) views. Obstructed portions of articular facets and plantar surface digitally reconstructed.

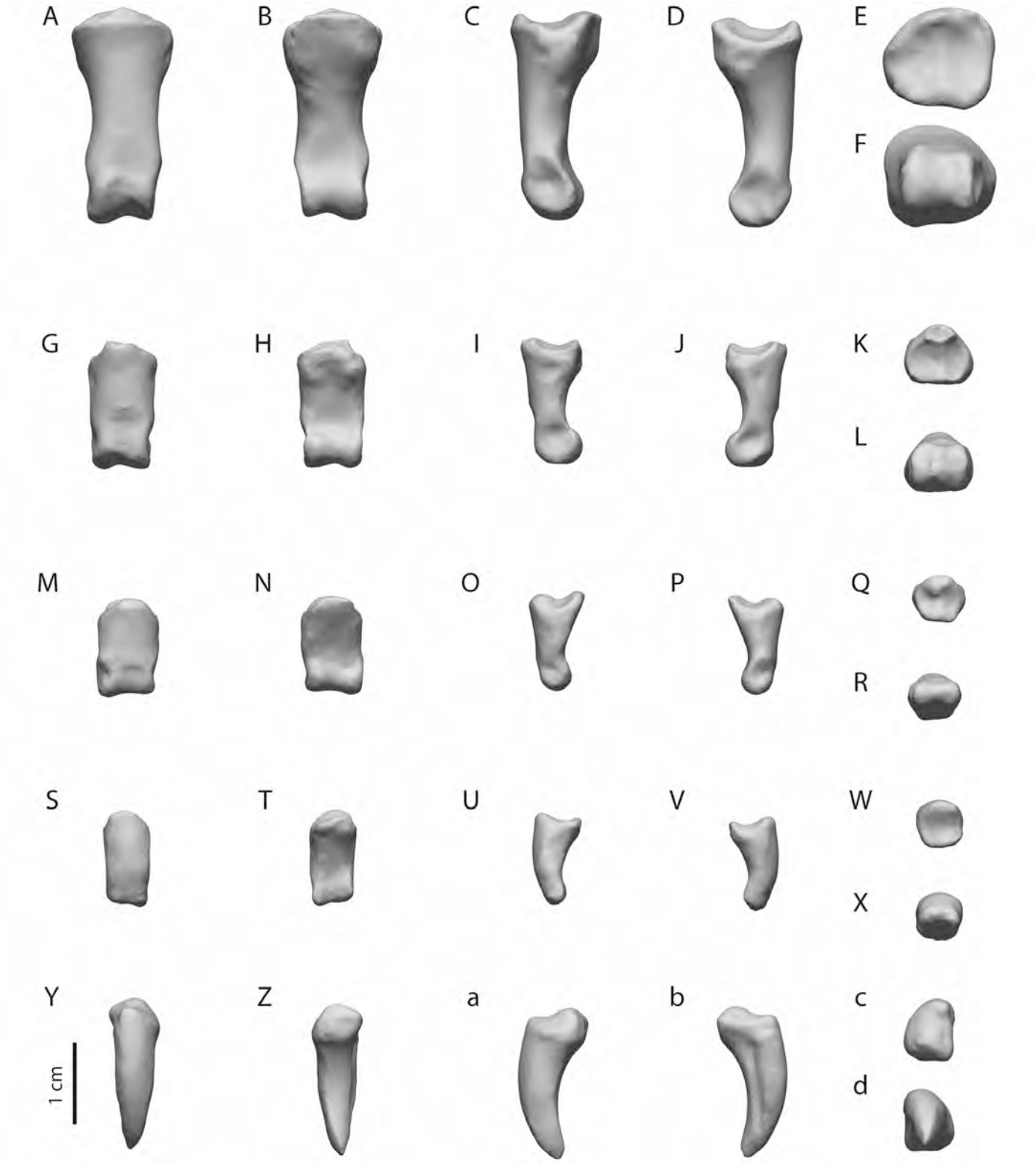

PLATE PL46. 3-D scans of phalanges and unguals of digit IV of the left foot, Port Louis specimen. Pedal phalanx IV-1 (**A**–**F**), phalanx IV-2 (**G**–**L**), phalanx IV-3 (**M**–**R**), phalanx IV-4 (**S**–**X**), and phalanx (ungual) IV-5 (**Y**–**d**), in dorsal (**A**, **G**, **M**, **S**, **Y**), plantar (**B**, **H**, **N**, **T**, **Z**), lateral (**C**, **I**, **O**, **U**, **a**), medial (**D**, **J**, **P**, **V**, **b**), proximal (**E**, **K**, **Q**, **W**, **c**), and distal (**F**, **L**, **R**, **X**, **d**) views. Obstructed portions of articular facets and plantar surface digitally reconstructed.

APPENDIX 3. The Durban dodo.

PLATE D1. Right oblique view of the 3-D scan of the Durban dodo as mounted at the Durban Natural Science Museum.

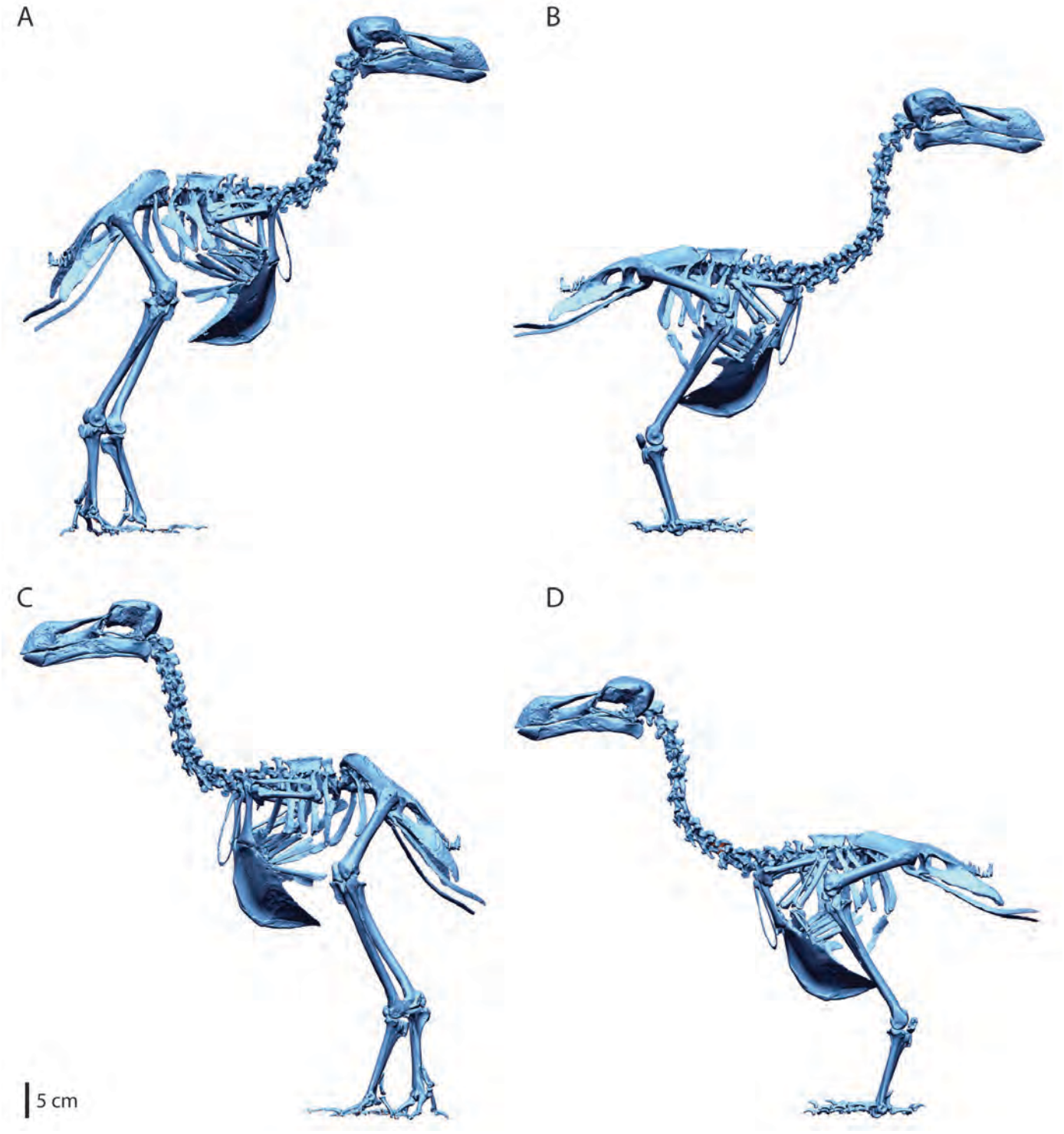

PLATE D2. 3-D scans of the Durban dodo as mounted at the DNSM (**A**, **C**) and after digital repositioning (**B**, **D**), in right lateral (**A**, **B**) and left lateral (**C**, **D**) views.

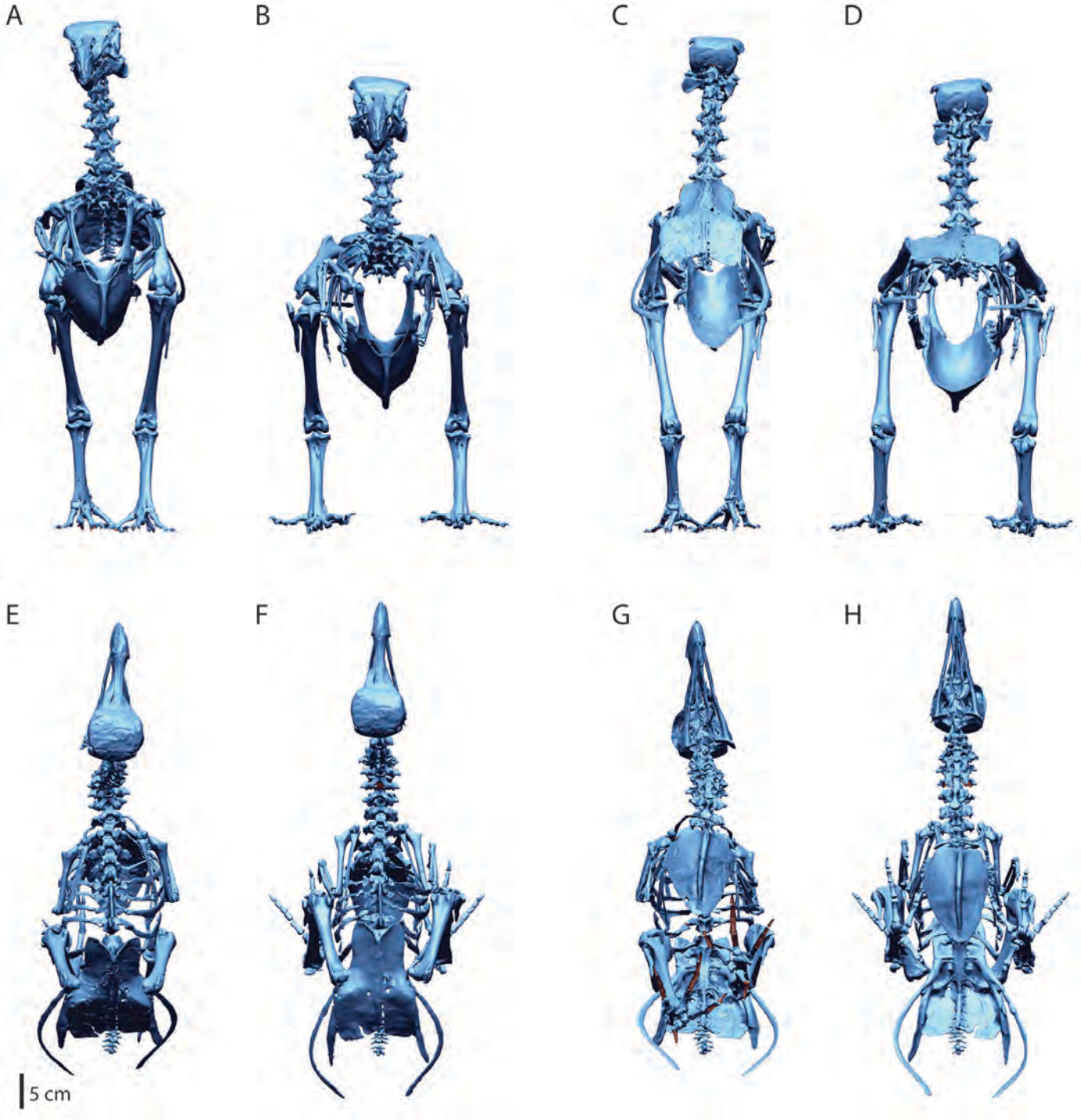

PLATE D3. 3-D scans of the Durban dodo as mounted at the DNSM (**A**, **C**, **E**, **G**) and after digital repositioning (**B**, **D**, **F**, **H**), in left cranial (**A**, **B**), caudal (**C**, **D**), and dorsal (**E**, **F**), and ventral (**G**, **H**) views.

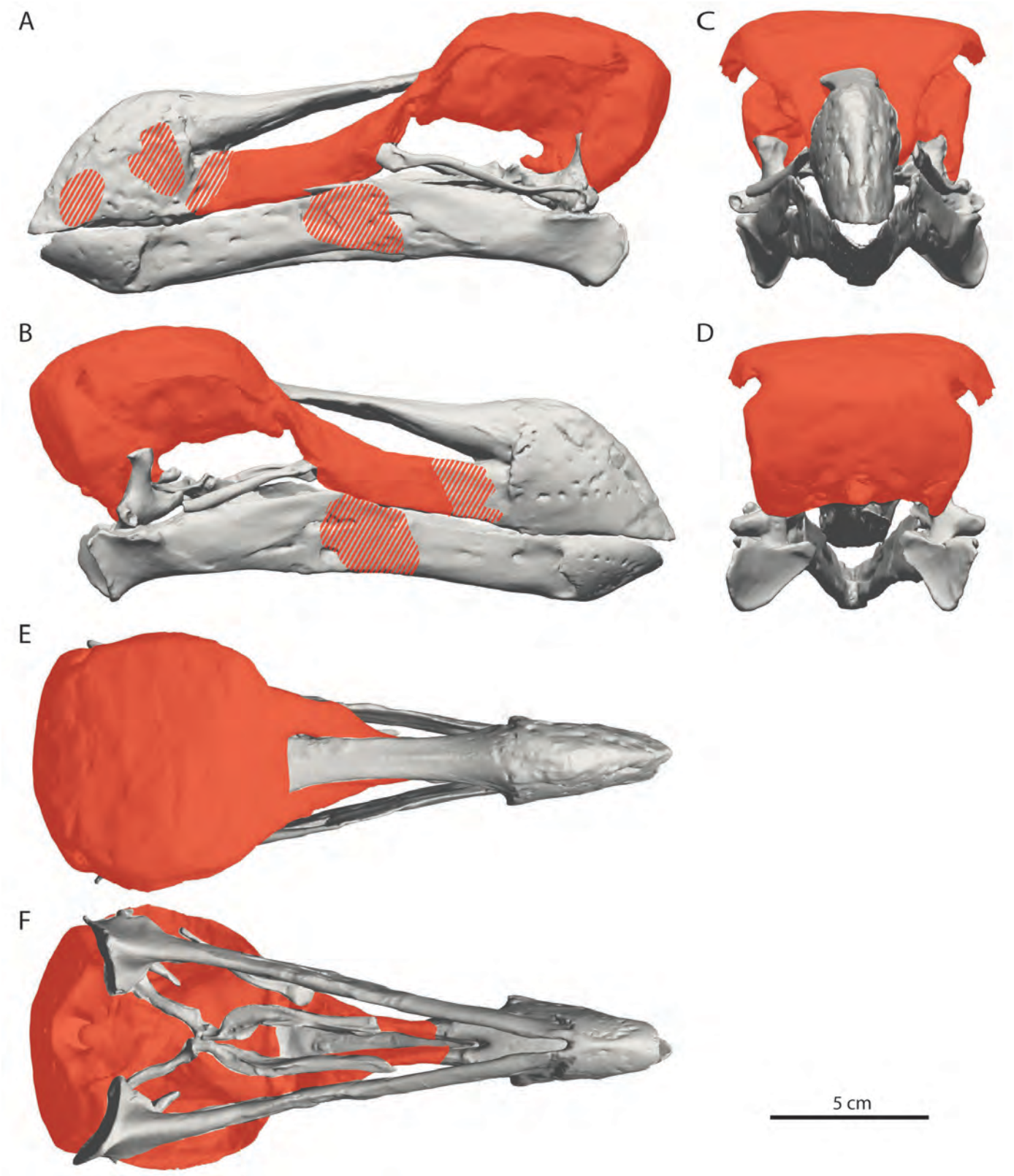

PLATE D4. 3-D scans of Durban dodo skull and mandible in left lateral (**A**), right lateral (**B**), cranial (**C**), caudal (**D**), dorsal (**E**), and ventral (**F**) views. Areas that have been sculpted in plaster are shown in dark gray (red in PDF version). Areas that have plaster covering bone are indicated with a hatched pattern.

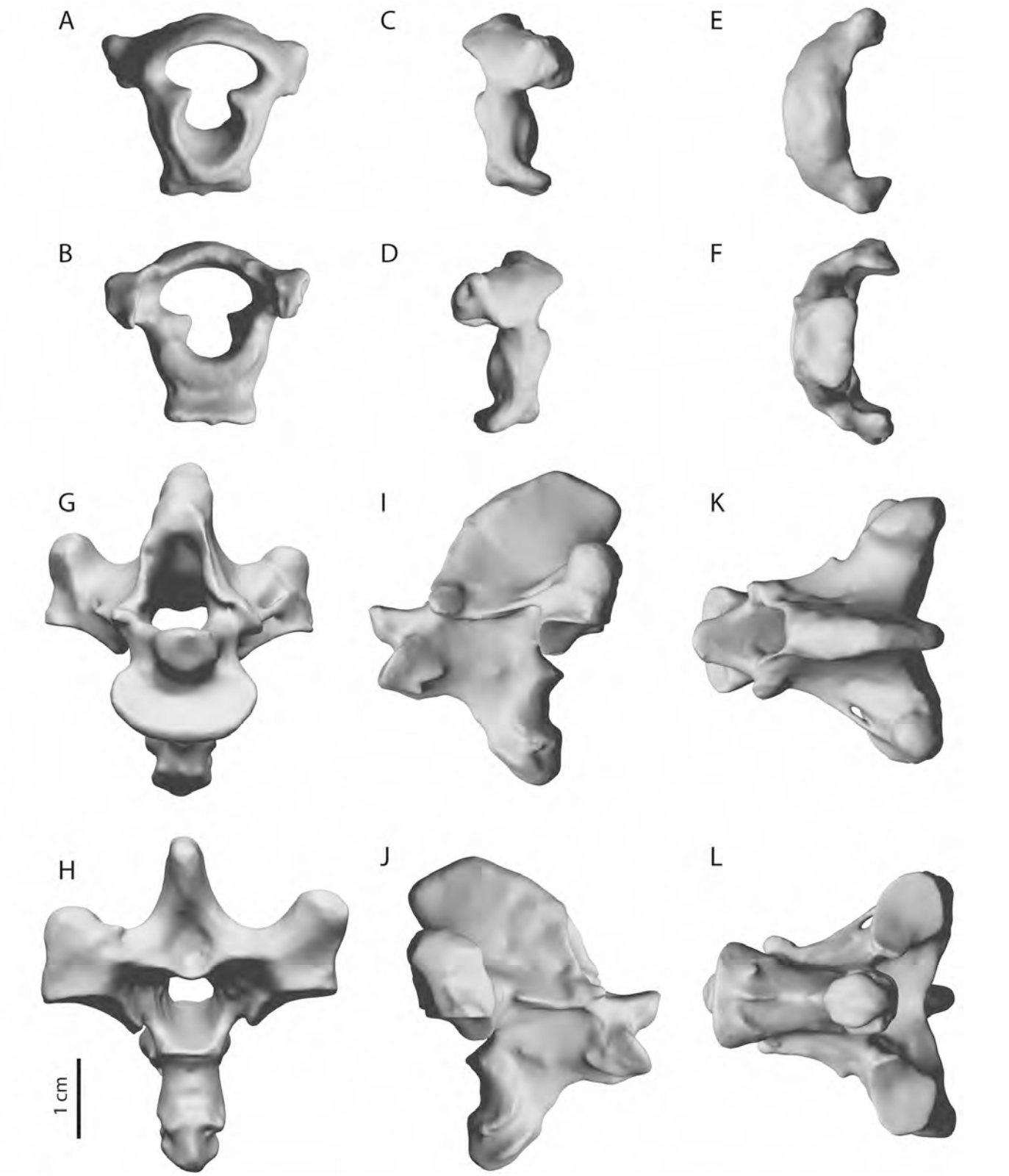

PLATE D5. 3-D scans of Durban dodo atlas (**A**–**F**) and axis (**G**–**L**), in cranial (**A**, **G**), caudal (**B**, **H**), left lateral (**C**, **I**), right lateral (**D**, **J**), dorsal (**E**, **K**), and ventral (**F**, **L**) views. A portion of the cranial margin of the processus spinosus, right facies articularis prezygapophysis, and left tuberculum dorsale postzygapophysis have been reconstructed in plaster (see Figure 18).

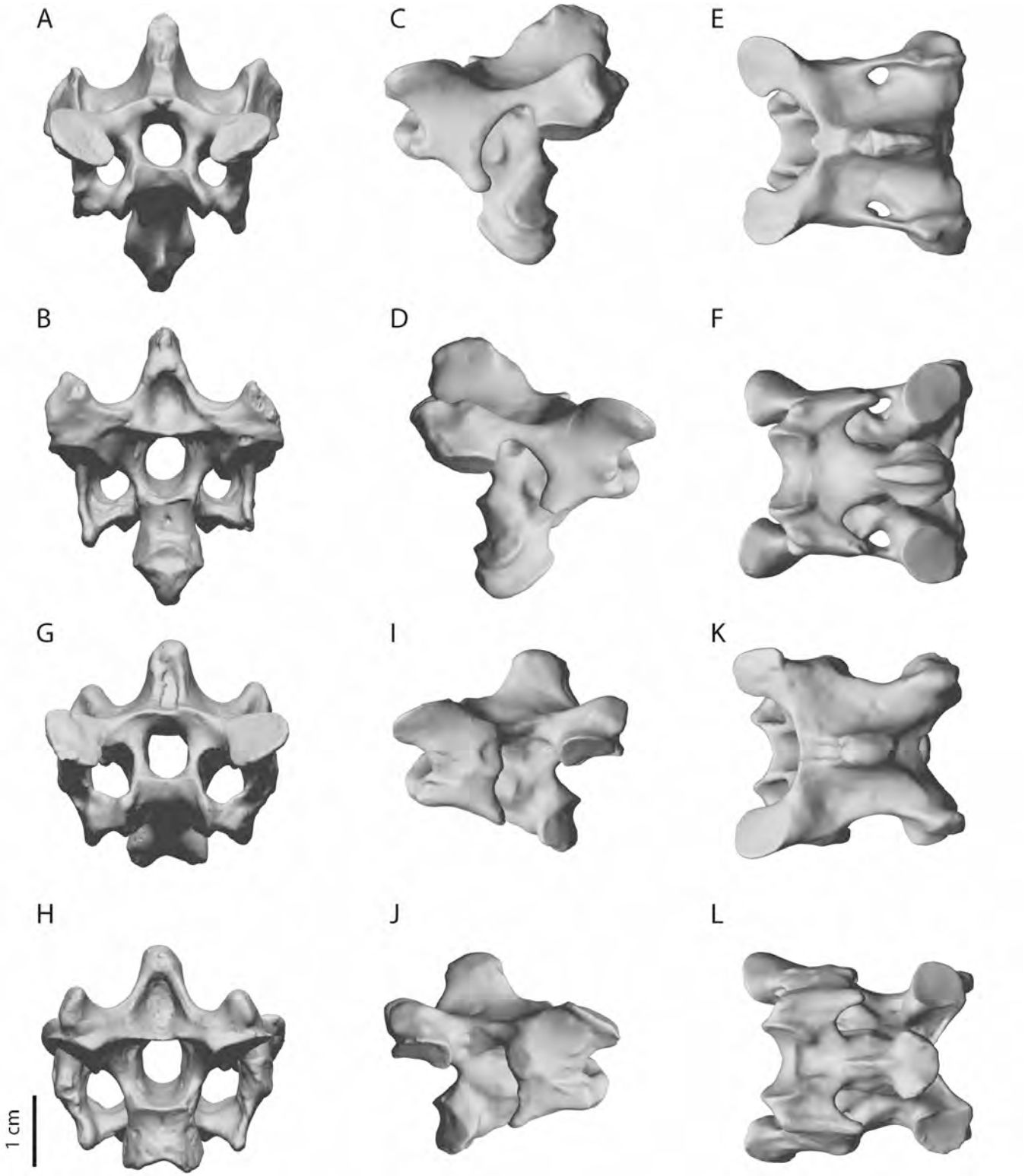

PLATE D6. 3-D scans of Durban dodo cervical vertebra (C) 3 (**A**–**F**) and C4 (**G**–**L**), in cranial (**A**, **G**), caudal (**B**, **H**), left lateral (**C**, **I**), right lateral (**D**, **J**), dorsal (**E**, **K**), and ventral (**F**, **L**) views.

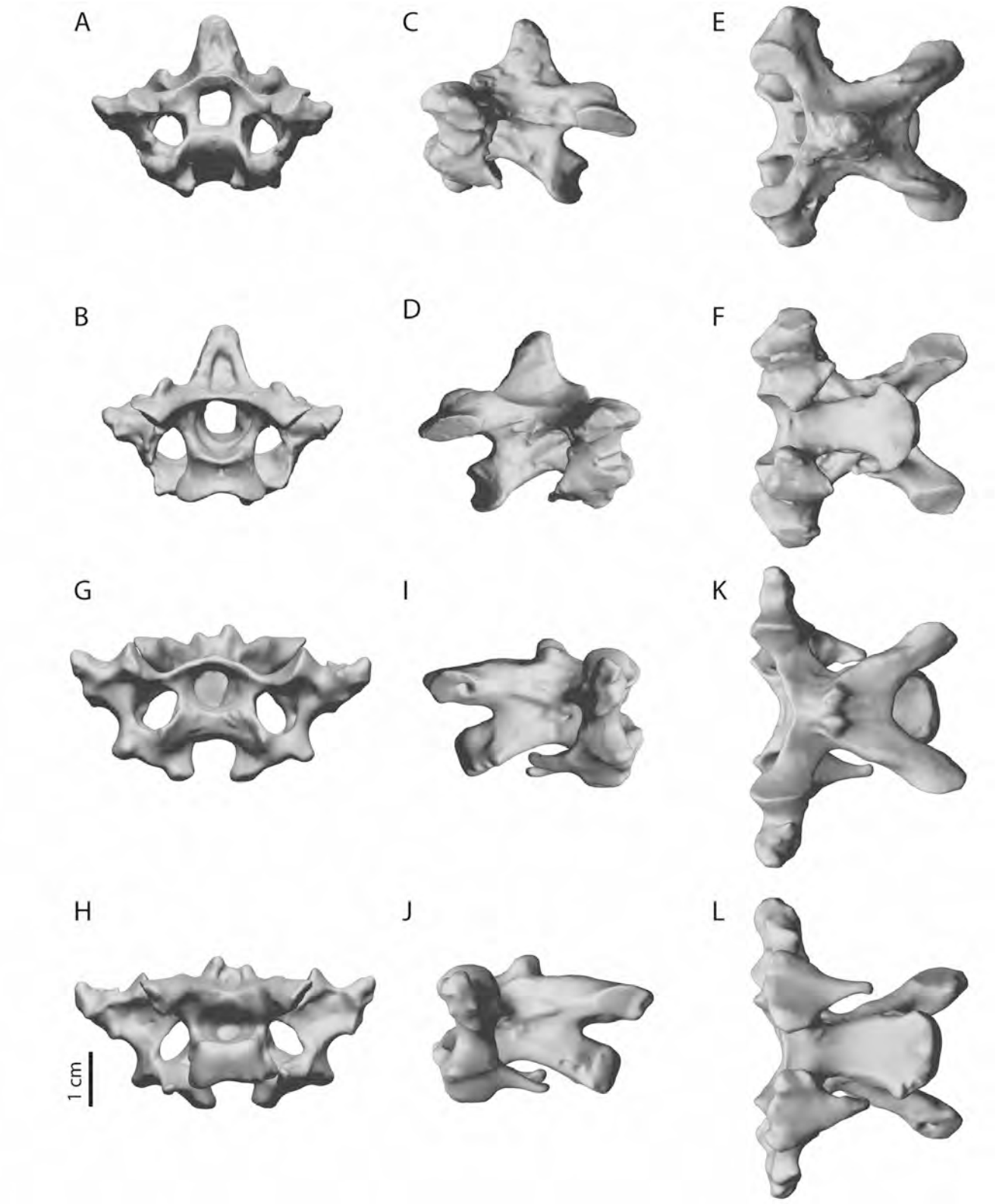

PLATE D7. 3-D scans of Durban dodo C5 (**A**–**F**) and C6 (**G**–**L**), in cranial (**A**, **G**), caudal (**B**, **H**), left lateral (**C**, **I**), right lateral (**D**, **J**), dorsal (**E**, **K**), and ventral (**F**, **L**) views.

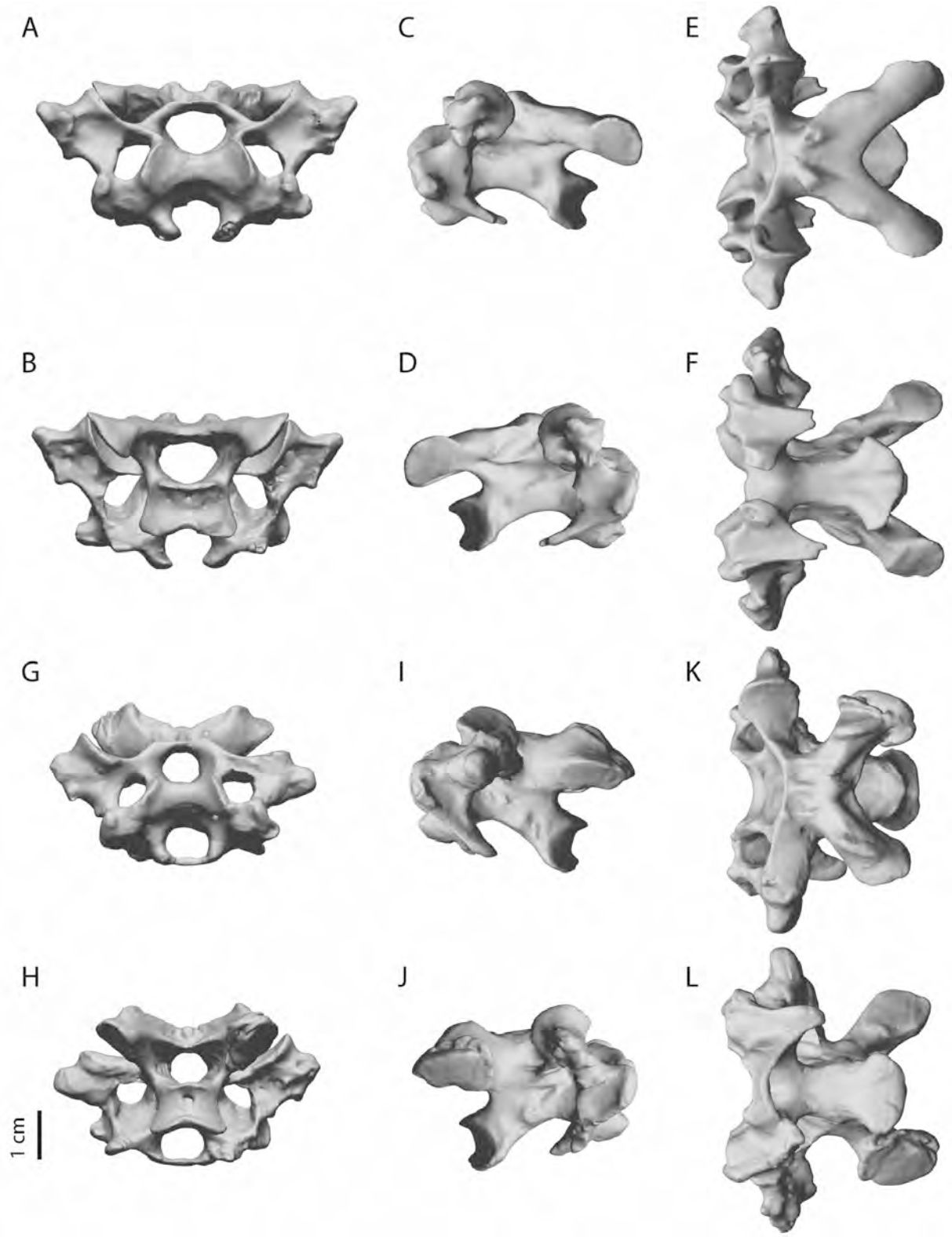

PLATE D8. 3-D scans of Durban dodo C7 (**A**–**F**) and C8 (**G**–**L**), in cranial (**A**, **G**), caudal (**B**, **H**), left lateral (**C**, **I**), right lateral (**D**, **J**), dorsal (**E**, **K**), and ventral (**F**, **L**) views.

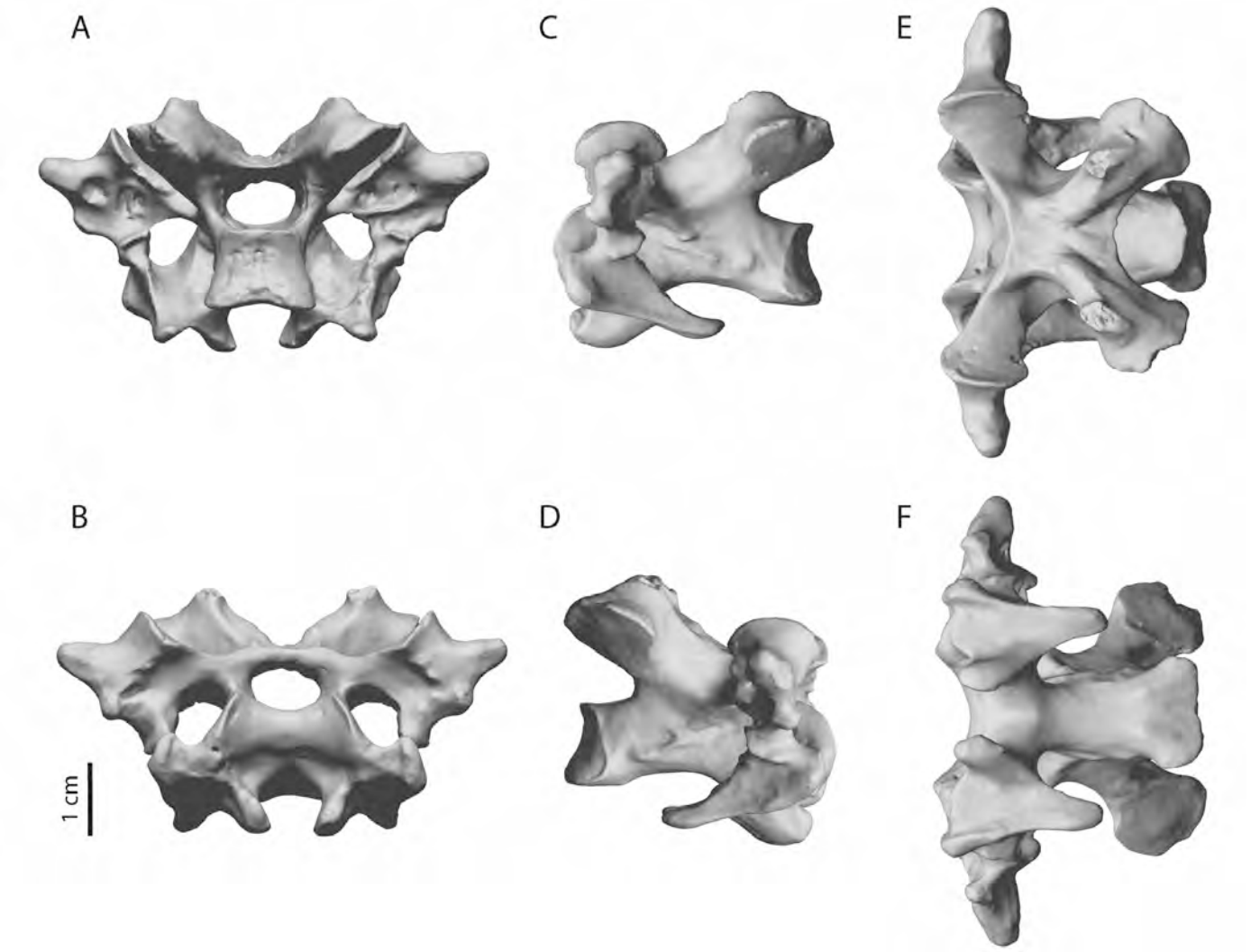

PLATE D9. 3-D scans of Durban dodo C9 (**A**–**F**) in cranial (**A**), caudal (**B**), left lateral (**C**), right lateral (**D**), dorsal (**E**), and ventral (**F**) views.

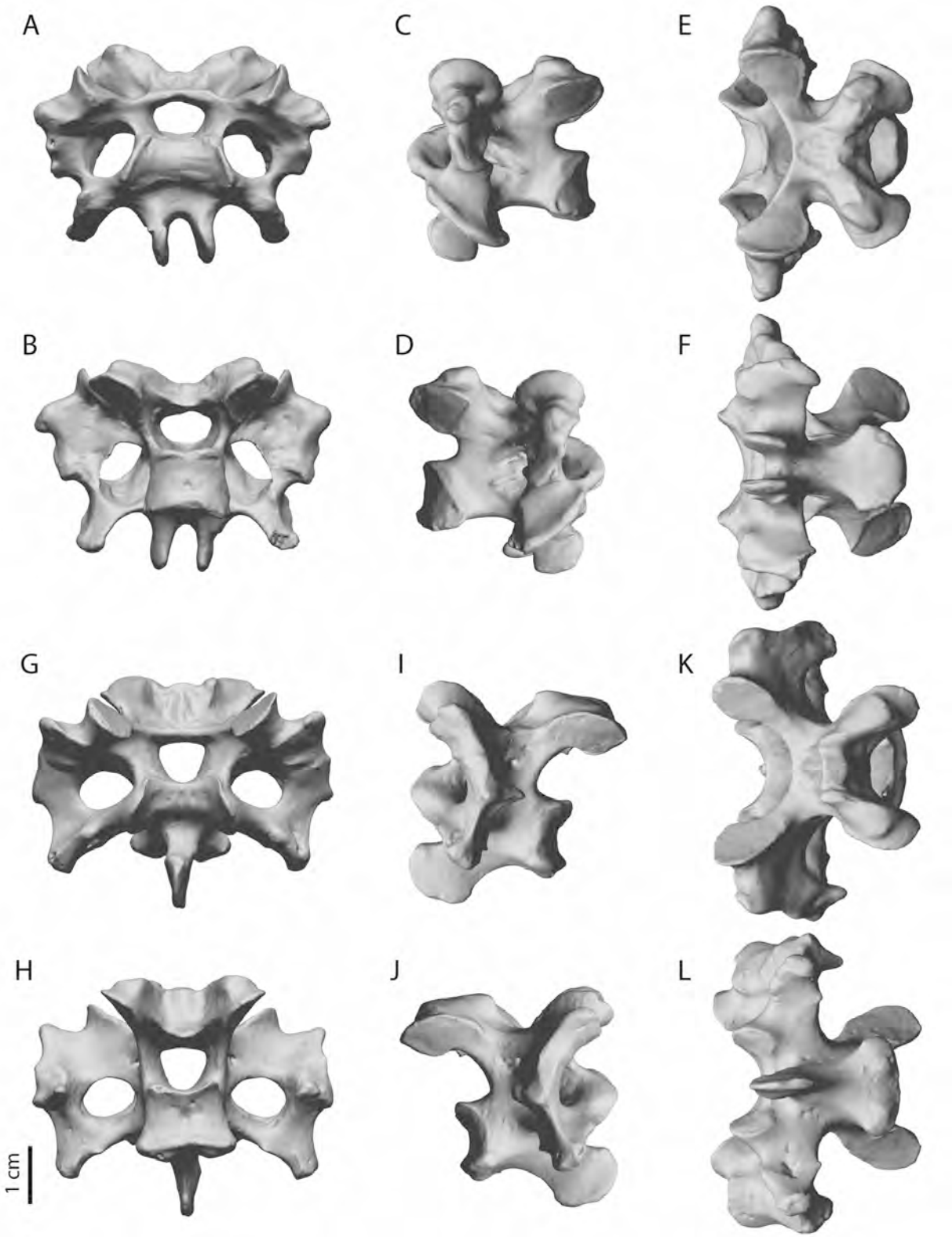

PLATE D10. 3-D scans of Durban dodo C11 (**A**–**F**) and C12 (**G**–**L**), in cranial (**A**, **G**), caudal (**B**, **H**), left lateral (**C**, **I**), right lateral (**D**, **J**), dorsal (**E**, **K**), and ventral (**F**, **L**) views.

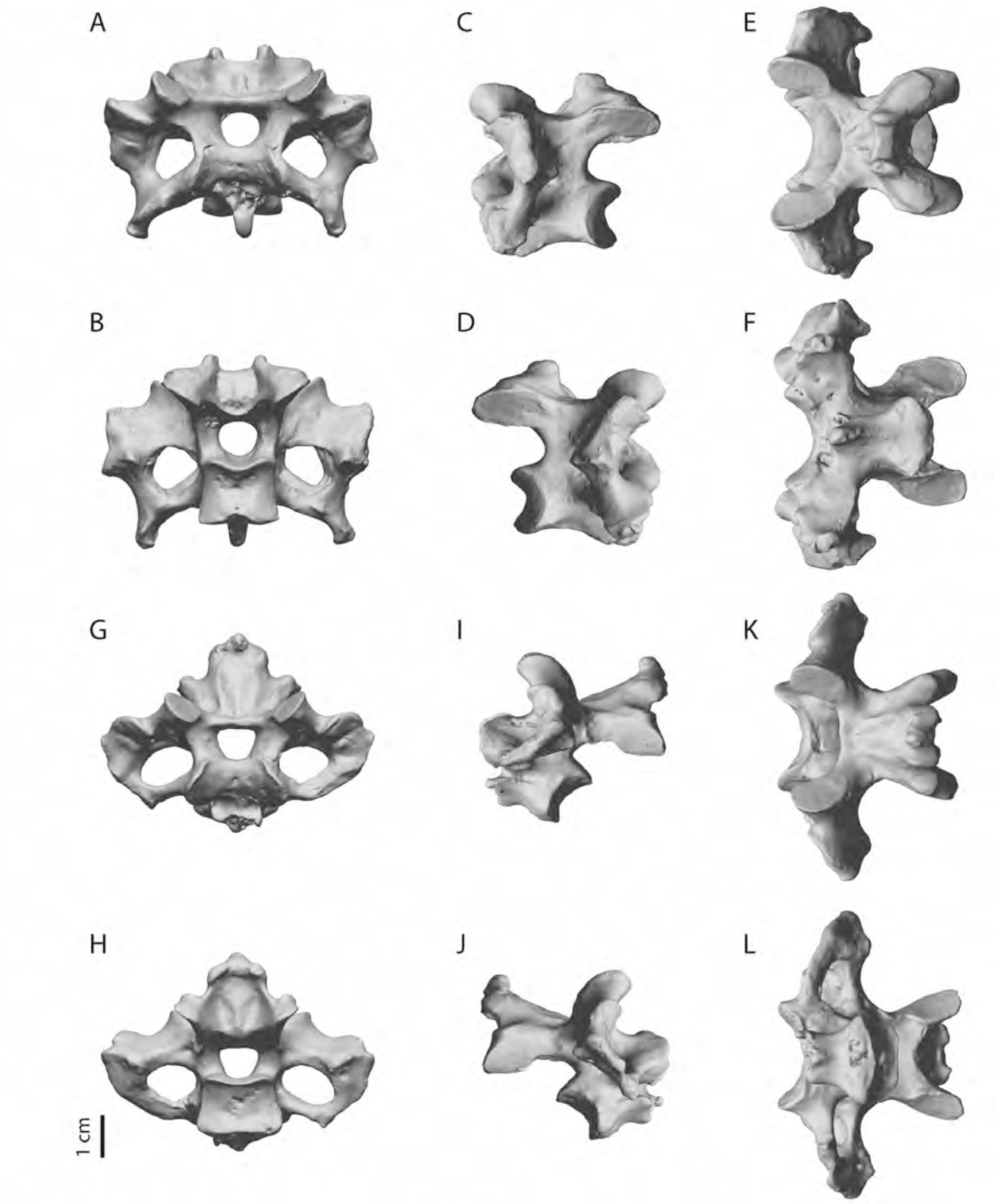

PLATE D11. 3-D scans of Durban dodo C13 (**A**–**F**) and C14 (**G**–**L**), in cranial (**A**, **G**), caudal (**B**, **H**), left lateral (**C**, **I**), right lateral (**D**, **J**), dorsal (**E**, **K**), and ventral (**F**, **L**) views.

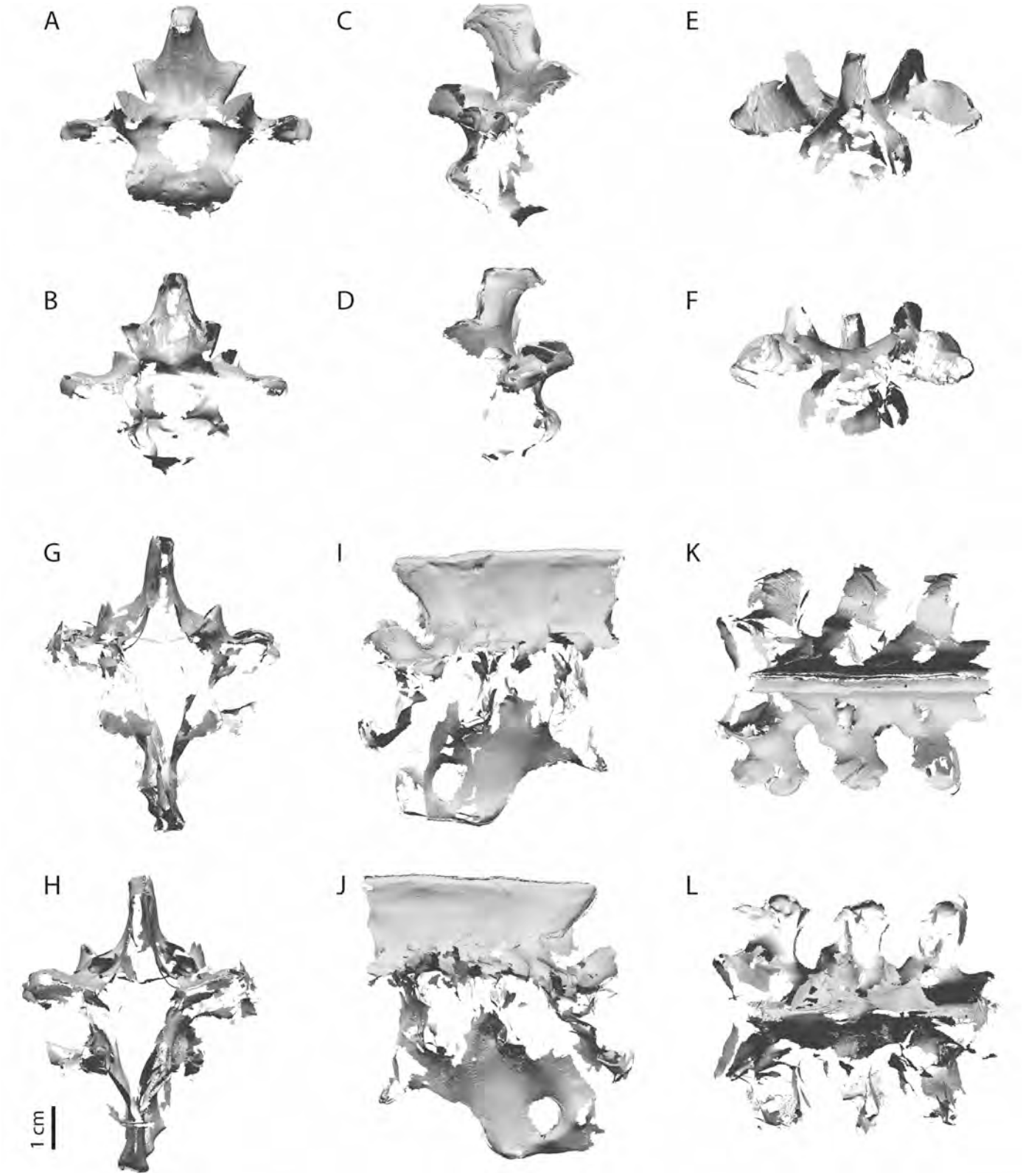

PLATE D12. 3-D scans of Durban dodo cervicodorsal vertebra (C15) (**A**–**F**) and notarium (**G**–**L**), in cranial (**A**, **G**), caudal (**B**, **H**), left lateral (**C**, **I**), right lateral (**D**, **J**), dorsal (**E**, **K**), and ventral (**F**, **L**) views. Missing surface data left blank (not reconstructed).

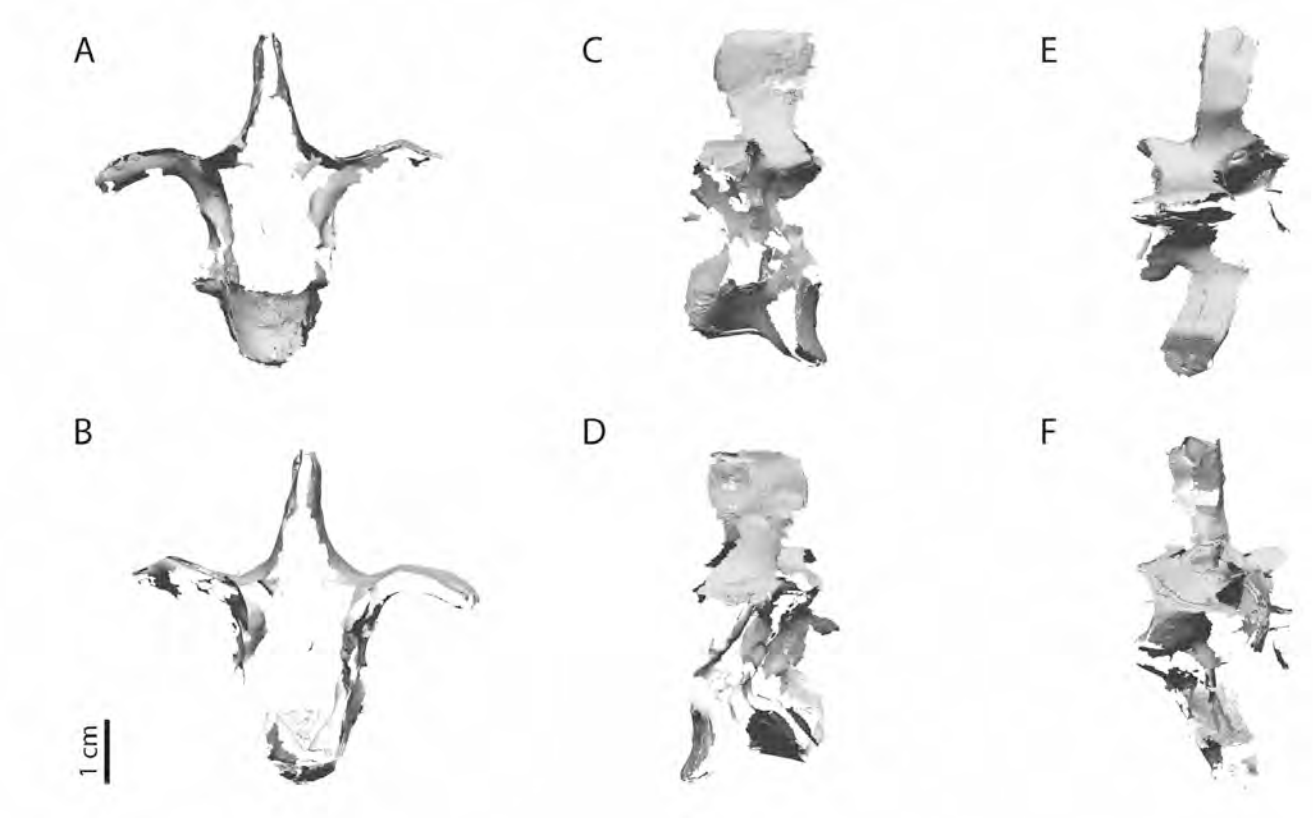

PLATE D13. Reconstructed 3-D scans of Durban dodo presynsacral (thoracic) vertebra 19 (**A**–**F**), in cranial (**A**), caudal (**B**), left lateral (**C**), right lateral (**D**), dorsal (**E**), and ventral (**F**) views. Missing surface data left blank (not reconstructed).

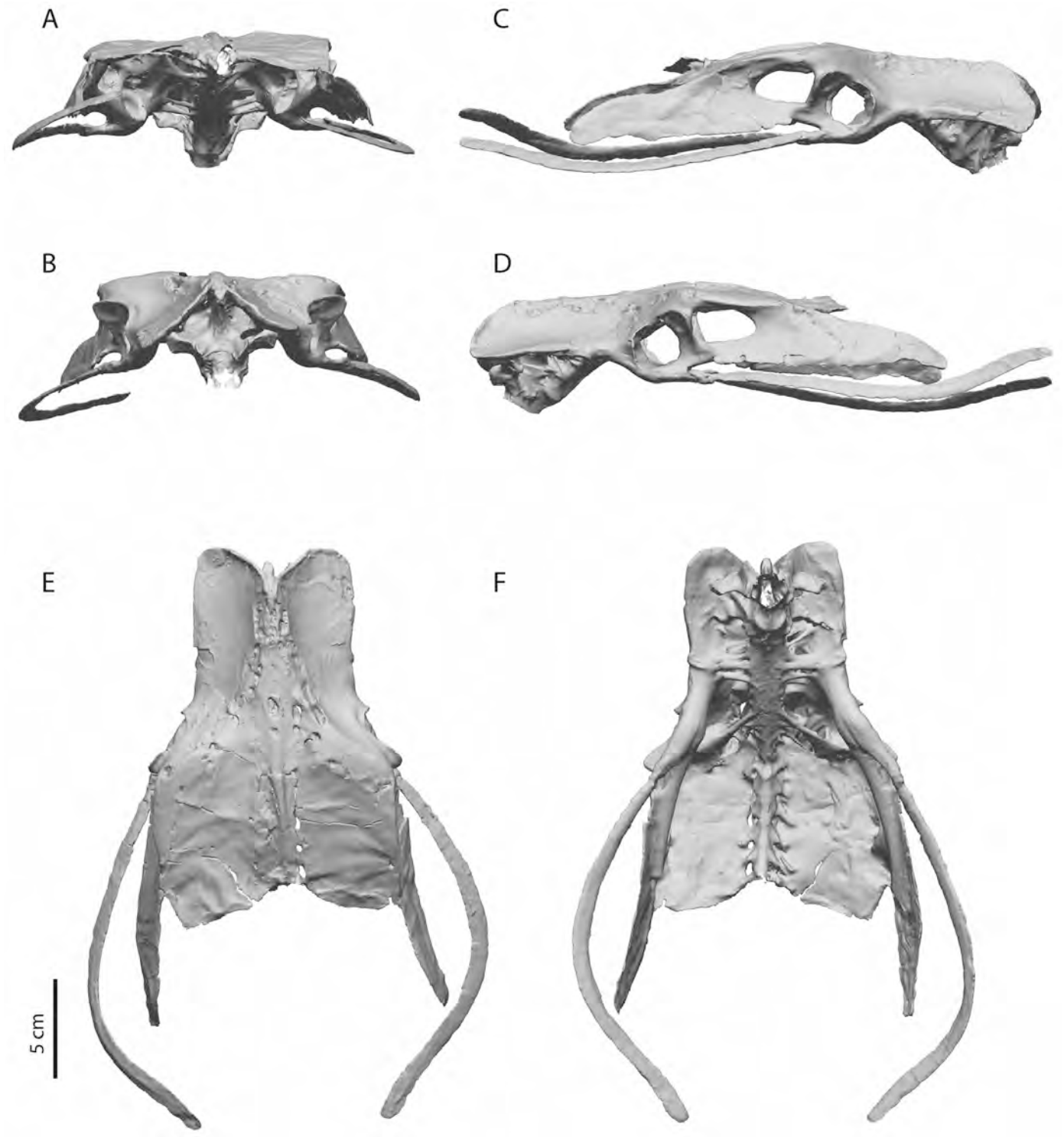

PLATE D14. 3-D scans of Durban dodo pelvis (**A**–**F**), in caudal (**A**), right lateral (**B**), cranial (**C**), left lateral (**D**), dorsal (**E**), and ventral (**F**) views. Processus terminalis ischii and distal scapus pubis are covered in a thick coating of shellac and may have been partially reconstructed.

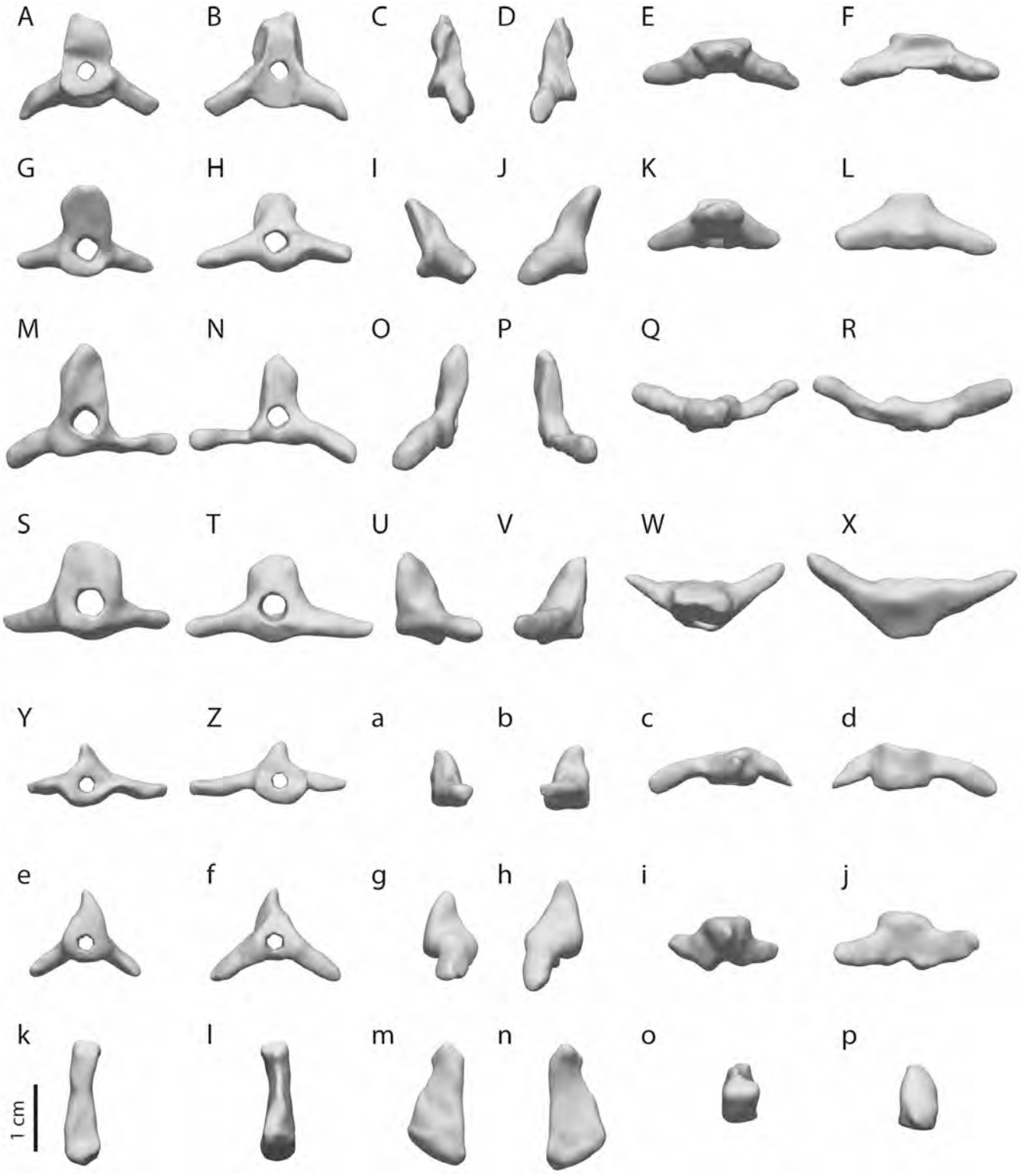

PLATE D15. 3-D scans of Durban free caudal vertebrae 1 (**A**–**F**), 2 (**G**–**L**), 3 (**M**–**R**), 4 (**S**–**X**), 5 (**Y**–**d**), and 6 (**e**–**j**) and pygostyle (**k**–**p**), in cranial (**A**, **G**, **M**, **S**, **Y**, **e**, **k**), caudal (**B**, **H**, **N**, **T**, **Z**, **f**, **l**) left lateral (**C**, **I**, **O**, **U**, **a**, **g**, **m**), right lateral (**D**, **J**, **P**, **V**, **b**, **h**, **n**), dorsal (**E**, **K**, **Q**, **W**, **c**, **i**, **o**), and ventral (**C**, **L**, **R**, **X**, **d**, **j**, **p**) views. Neural canal, obstructed portions of cranial and caudal surfaces and articular facets digitally reconstructed.

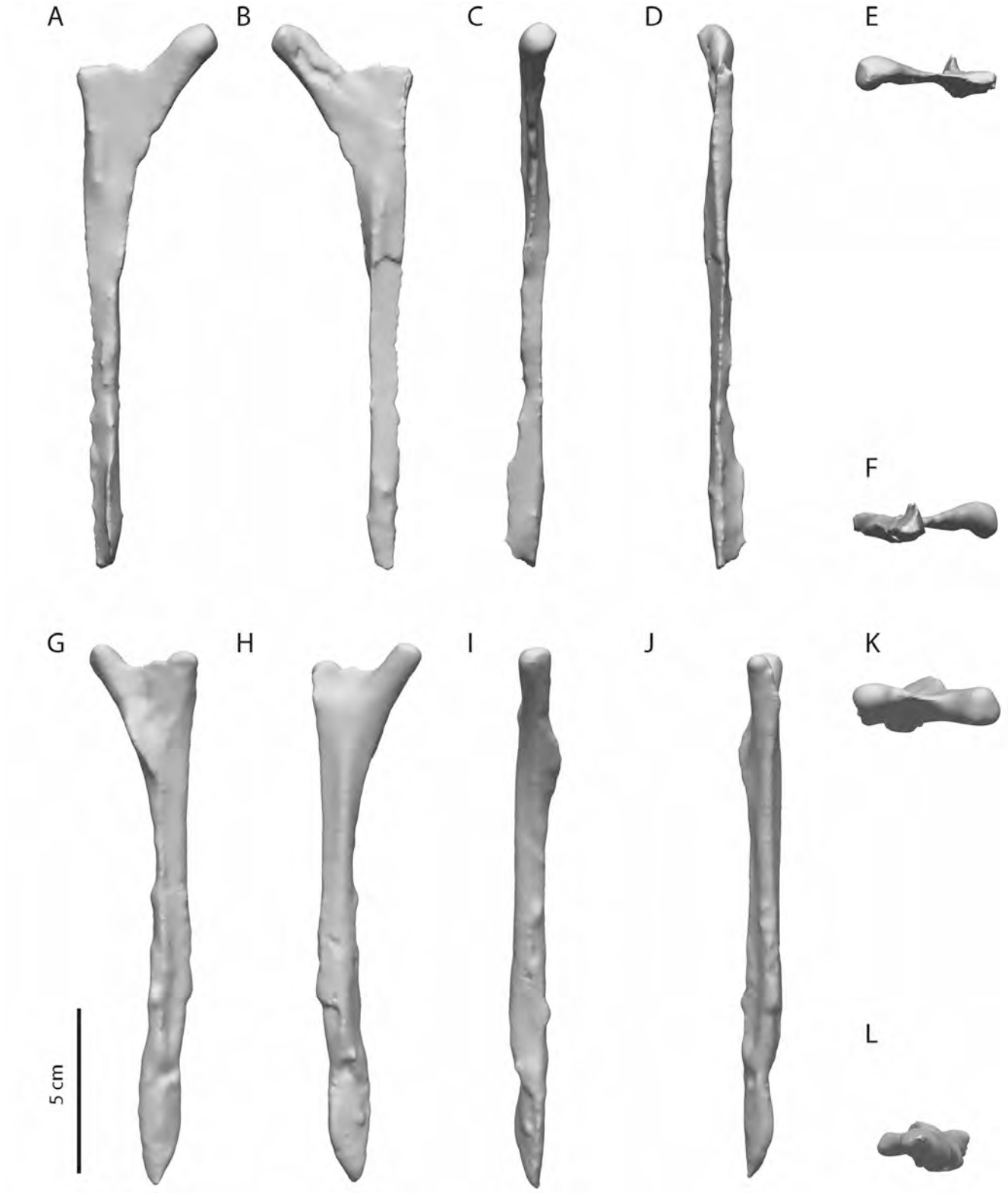

PLATE D16. 3-D scans of Durban right (**A**–**F**) and left (**G**–**L**) vertebral rib Is (presynsacral segment 15, cervicodorsal vertebra), in cranial (**A**, **G**), caudal (**B**, **H**), lateral (**C**, **I**), medial (**D**, **J**), proximal (**E**, **K**), and distal (**F**, **L**) views. Proximal articular facet digitally reconstructed.

PLATE D17. 3-D scans of Durban right (**A**–**F**) and left (**G**–**L**) vertebral rib IIs (presynsacral segment 16, first notarial segment), in cranial (**A**, **G**), caudal (**B**, **H**), lateral (**C**, **I**), medial (**D**, **J**), proximal (**E**, **K**), and distal (**F**, **L**) views. Stippled lines indicate extent of uncinate processes. Obstructed portions of articular facets digitally reconstructed.

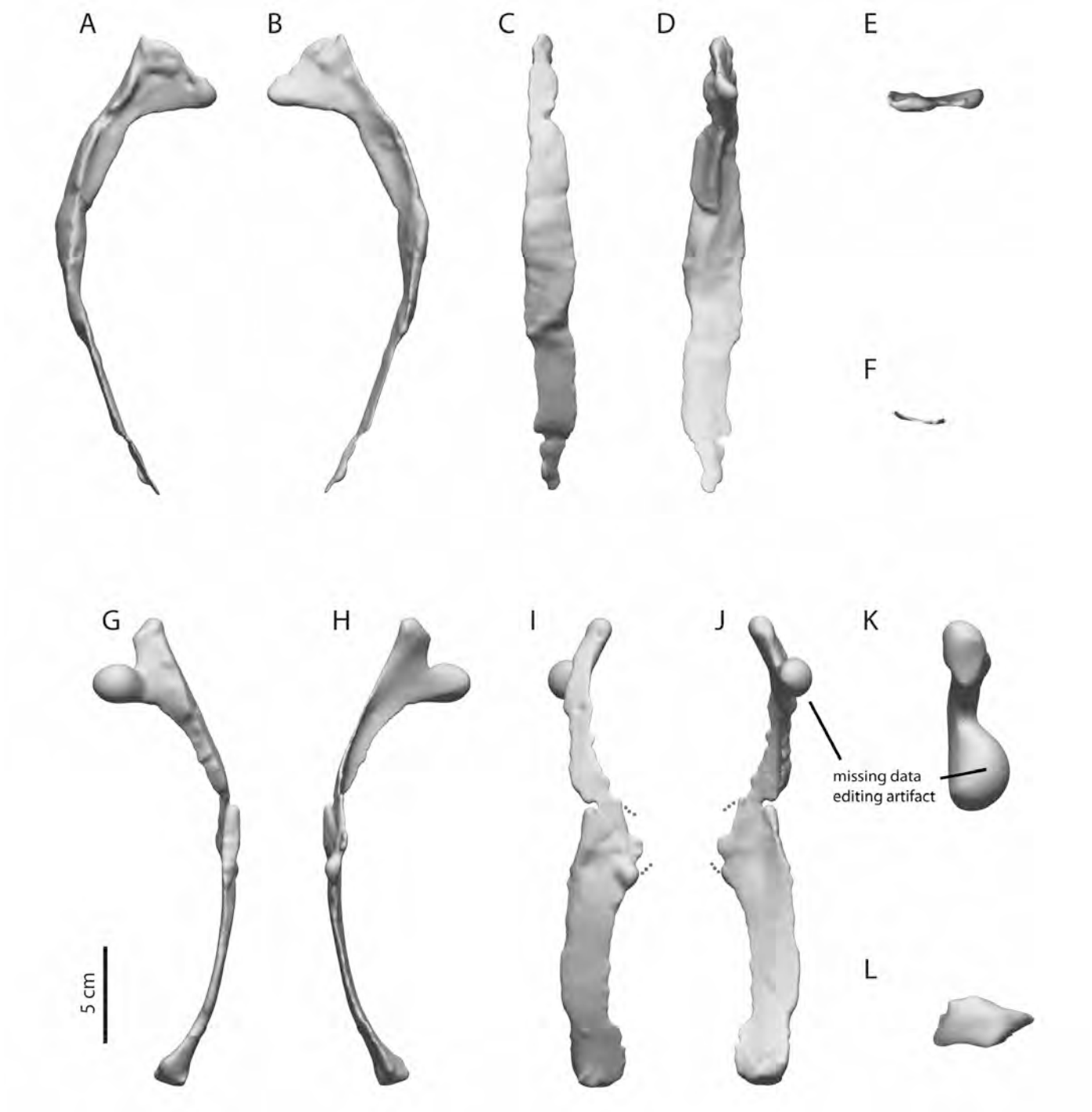

PLATE D18. 3-D scans of Durban right (**A**–**F**) and left (**G**–**L**) vertebral rib IIIs (presynsacral segment 17, second notarial segment), in cranial (**A**, **G**), caudal (**B**, **H**), lateral (**C**, **I**), medial (**D**, **J**), proximal (**E**, **K**), and distal (**F**, **L**) views. Stippled lines indicate extent of uncinate processes. Obstructed portions of articular facets digitally reconstructed.

PLATE D19. 3-D scans of Durban right (**A**–**F**) and left (**G**–**L**) vertebral rib IVs (presynsacral segment 18, third notarial segment), in cranial (**A**, **G**), caudal (**B**, **H**), lateral (**C**, **I**), medial (**D**, **J**), proximal (**E**, **K**), and distal (**F**, **L**) views. Stippled lines indicate extent of uncinate processes. Obstructed portions of articular facets digitally reconstructed.

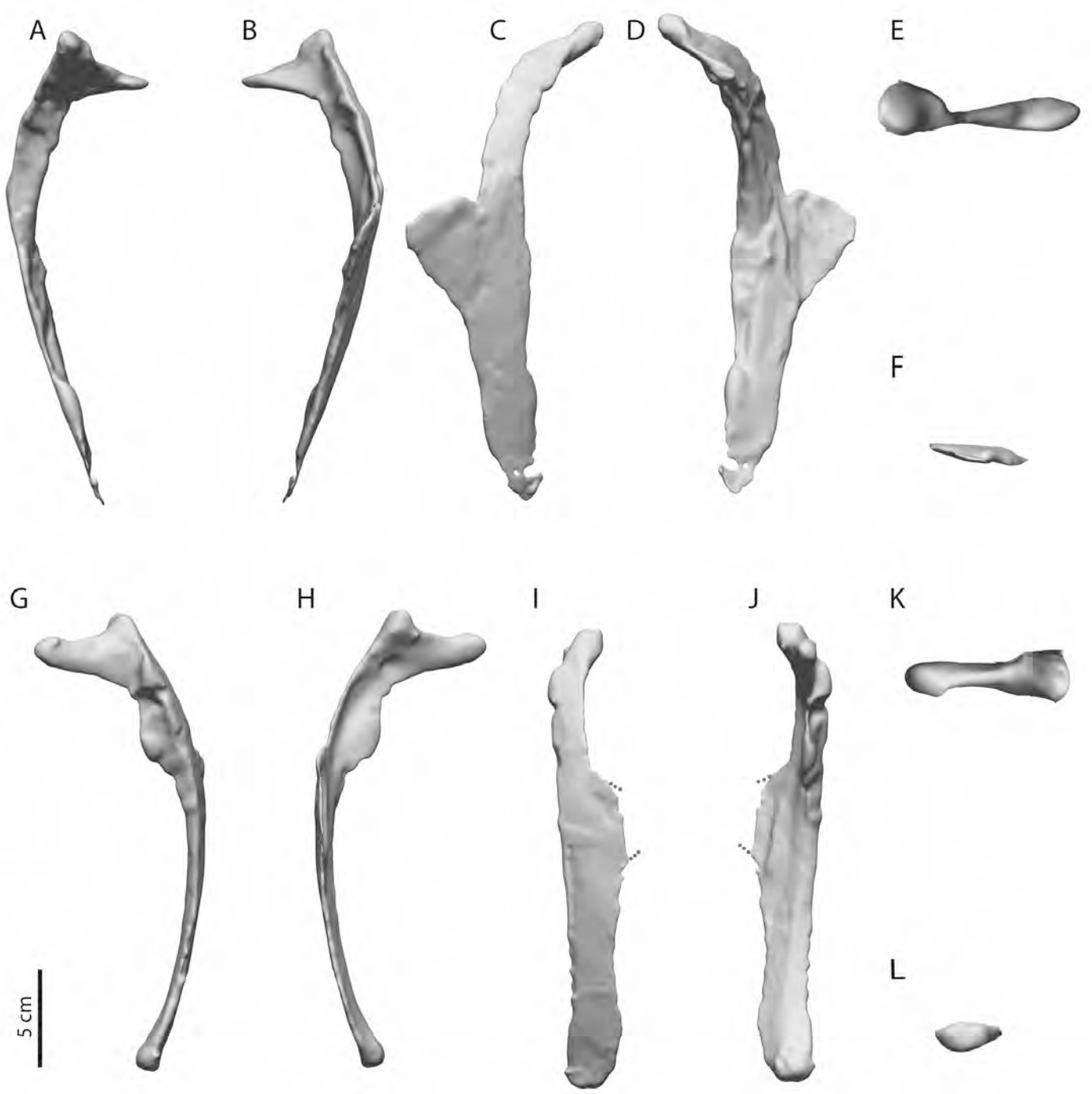

PLATE D20. 3-D scans of Durban right (**A**–**F**) and left (**G**–**L**) vertebral rib Vs (presynsacral segment 19, thoracic), in cranial (**A**, **G**), caudal (**B**, **H**), lateral (**C**, **I**), medial (**D**, **J**), proximal (**E**, **K**), and distal (**F**, **L**) views. Stippled lines indicate extent of uncinate processes. Obstructed portions of articular facets digitally reconstructed.

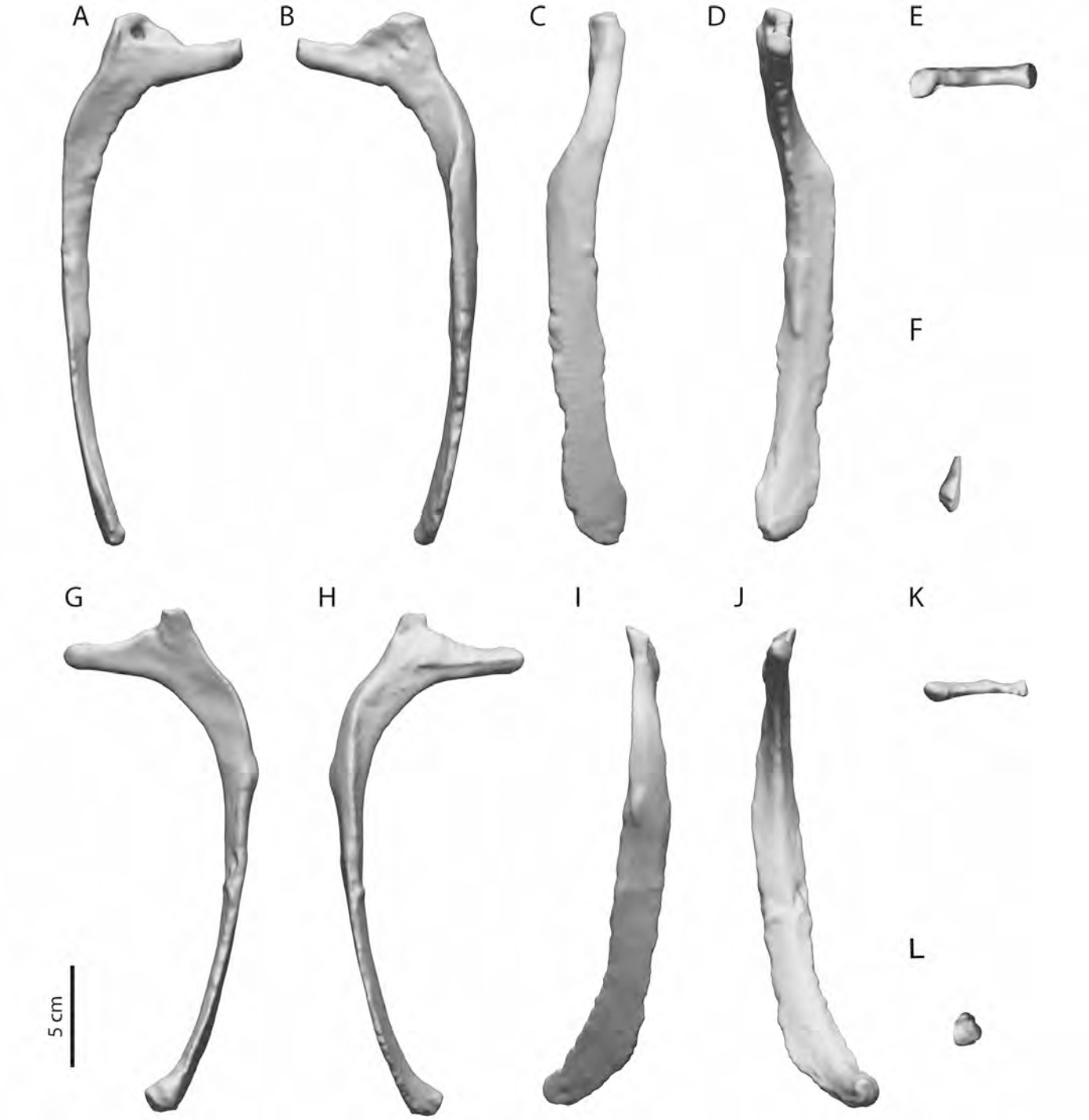

PLATE D21. 3-D scans of Durban right (**A**–**F**) and left (**G**–**L**) vertebral rib VIs (synsacral segment 20), in cranial (**A**, **G**), caudal (**B**, **H**), lateral (**C**, **I**), medial (**D**, **J**), proximal (**E**, **K**), and distal (**F**, **L**) views. Obstructed portions of articular facets digitally reconstructed.

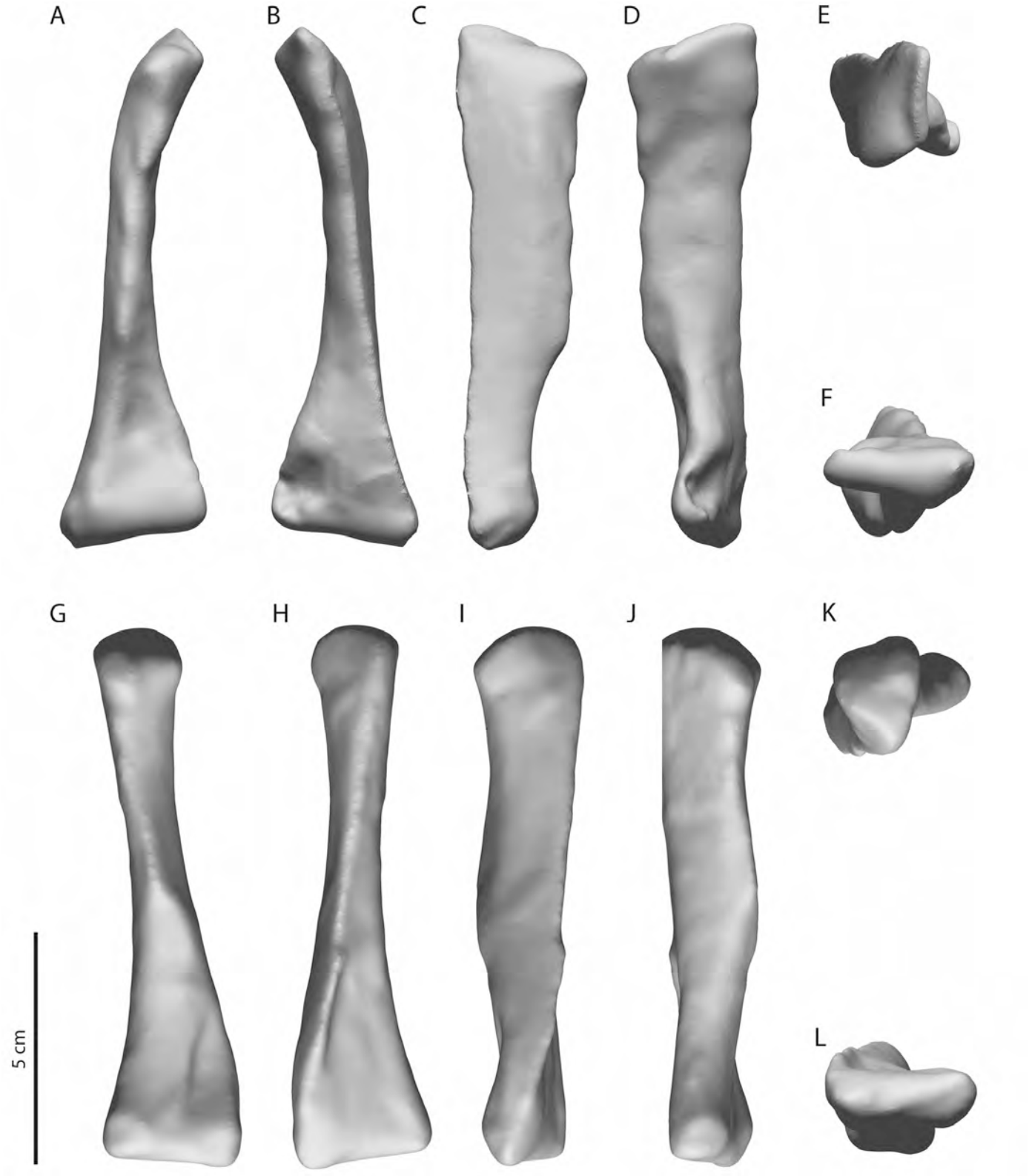

PLATE D22. 3-D scans of Durban right (**A**–**F**) and left (**G**–**L**) sternal rib IIs (thoracic segment 16, thoracic), in cranial (**A**, **G**), caudal (**B**, **H**), lateral (**C**, **I**), medial (**D**, **J**), proximal (**E**, **K**), and distal (**F**, **L**) views. Obstructed portions of articular facets digitally reconstructed.

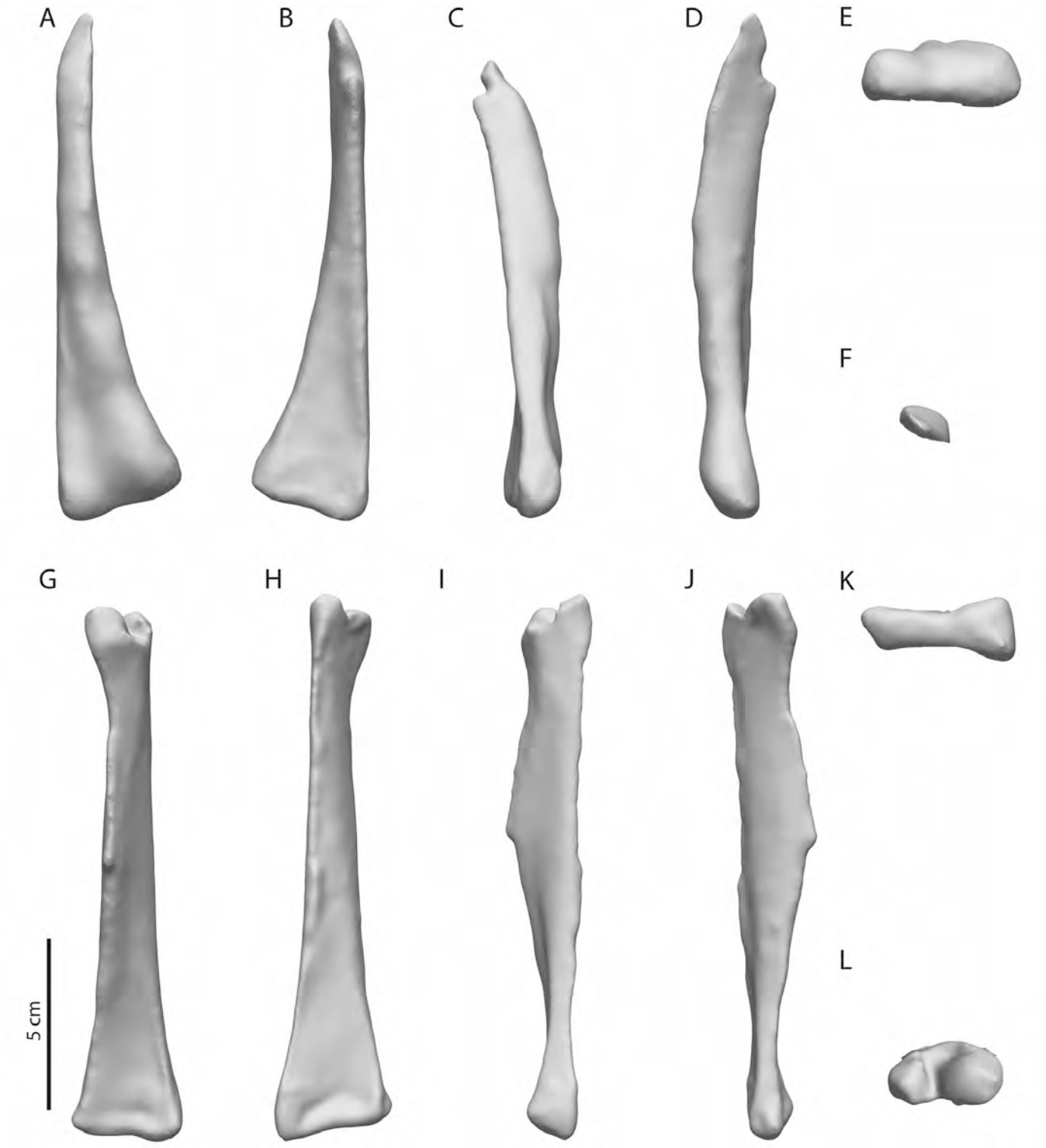

PLATE D23. 3-D scans of Durban right (**A**–**F**) and left (**G**–**L**) sternal rib IIIs (thoracic segment 17, thoracic), in cranial (**A**, **G**), caudal (**B**, **H**), lateral (**C**, **I**), medial (**D**, **J**), proximal (**E**, **K**), and distal (**F**, **L**) views. Obstructed portions of articular facets digitally reconstructed.

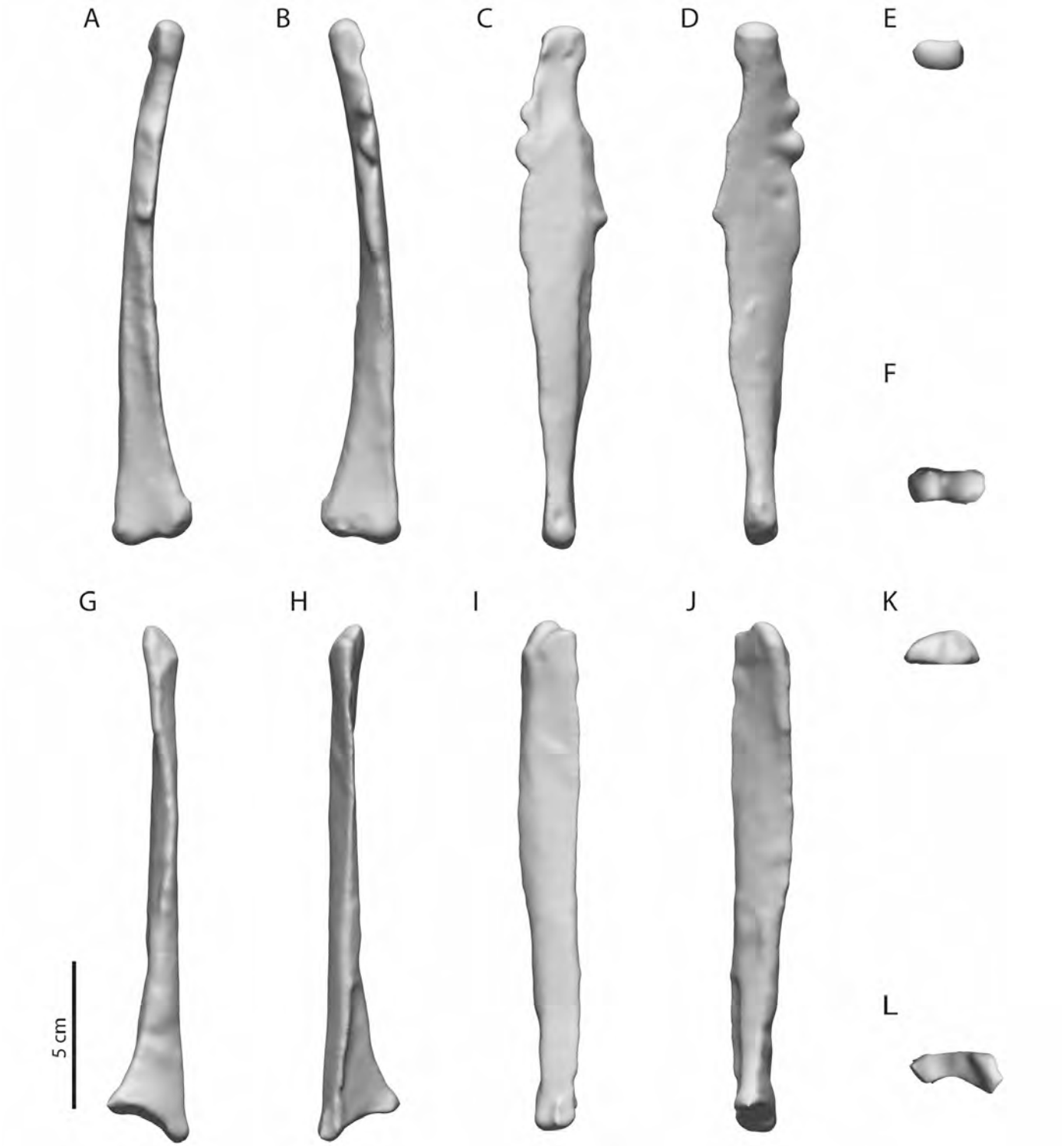

PLATE D24. 3-D scans of Durban right (**A**–**F**) and left (**G**–**L**) sternal rib IVs (thoracic segment 18, thoracic), in cranial (**A**, **G**), caudal (**B**, **H**), lateral (**C**, **I**), medial (**D**, **J**), proximal (**E**, **K**), and distal (**F**, **L**) views. Obstructed portions of articular facets digitally reconstructed.

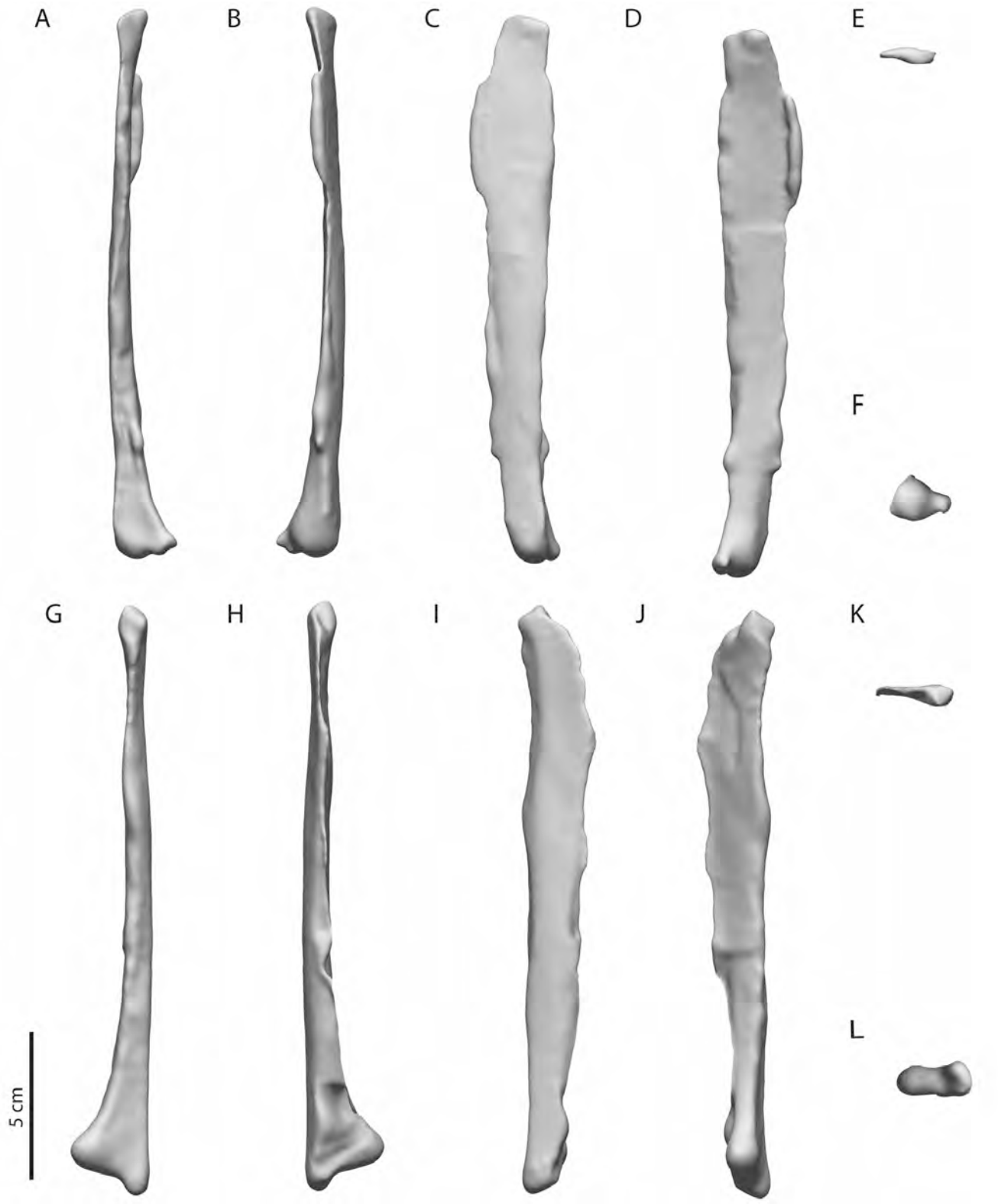

PLATE D25. 3-D scans of Durban right (**A**–**F**) and left (**G**–**L**) sternal rib Vs (thoracic segment 19, thoracic), in cranial (**A**, **G**), caudal (**B**, **H**), lateral (**C**, **I**), medial (**D**, **J**), proximal (**E**, **K**), and distal (**F**, **L**) views. Obstructed portions of articular facets digitally reconstructed.

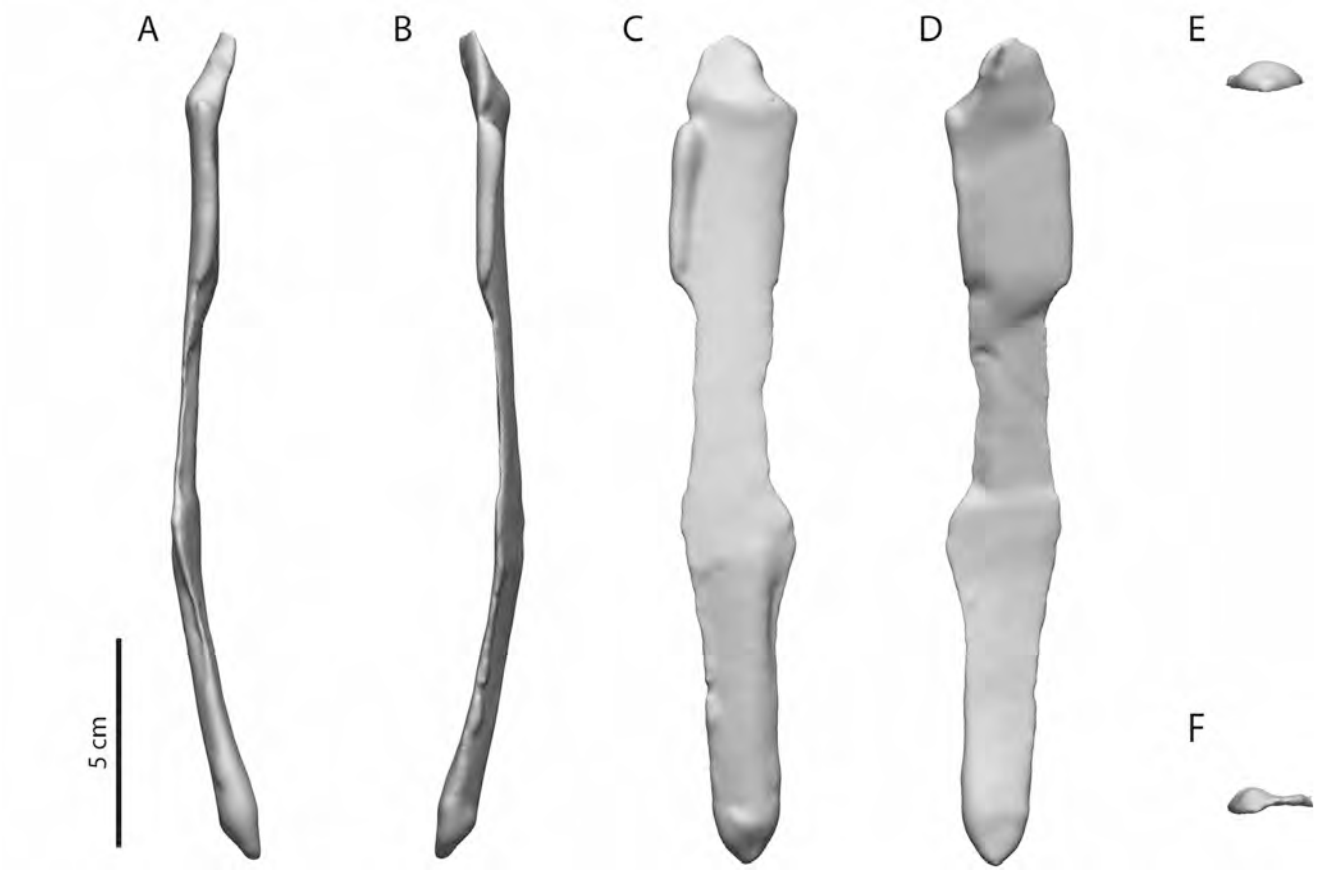

PLATE D26. 3-D scans of Durban right sternal rib VI (synsacral segment 20), in cranial (**A**), caudal (**B**), lateral (**C**), medial (**D**), proximal (**E**), and distal (**F**) views. Obstructed portions of articular facets digitally reconstructed.

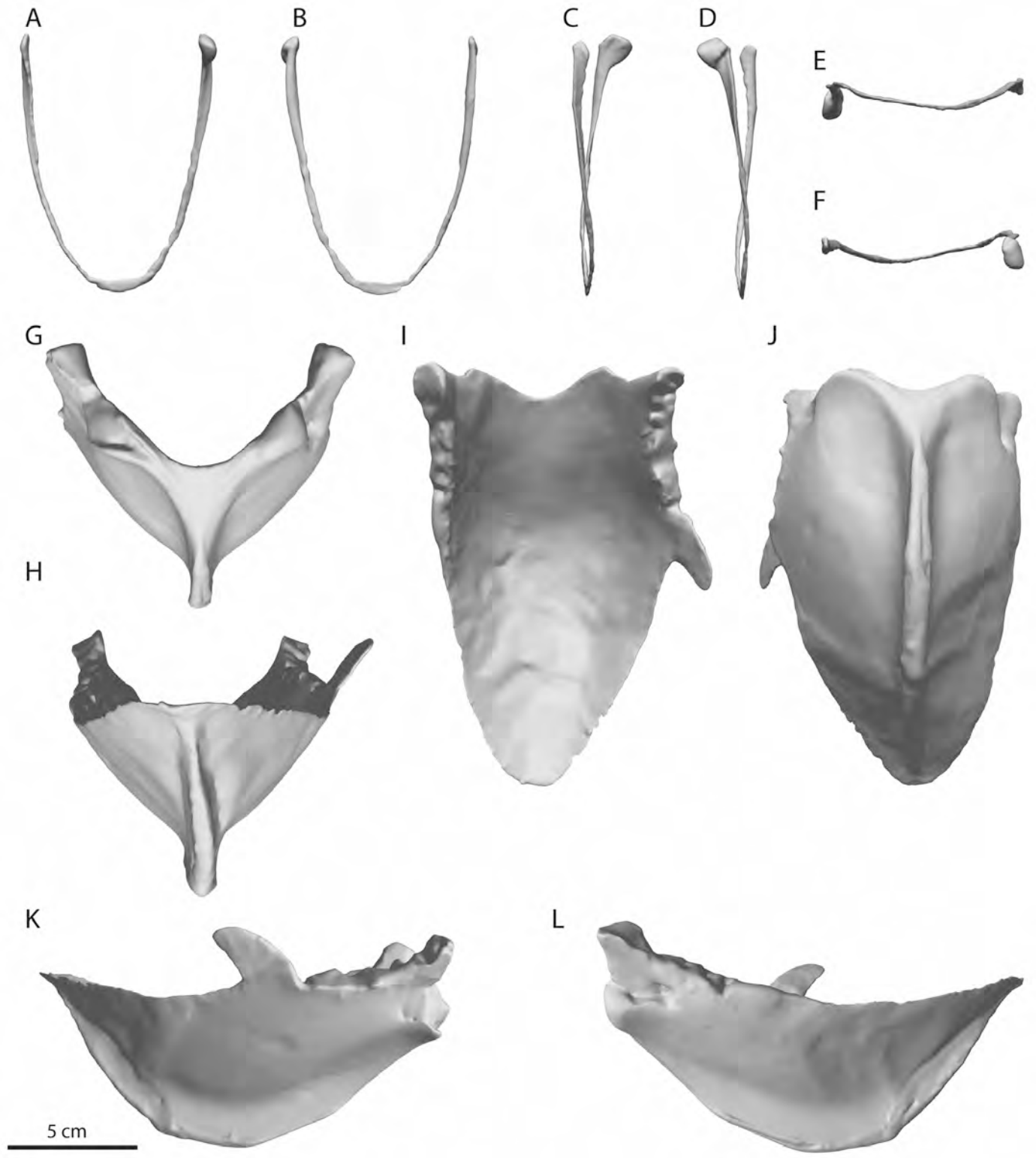

PLATE D27. 3-D scans of Durban furcula (**A**–**F**) and sternum (**G**–**L**), in cranial (**A**, **G**), caudal (**B**, **H**), right lateral (**C**, **K**), left lateral (**D**, **L**), dorsal (**E**, **I**), and ventral (**F**, **J**) views. Obstructed portions of articular facets digitally reconstructed.

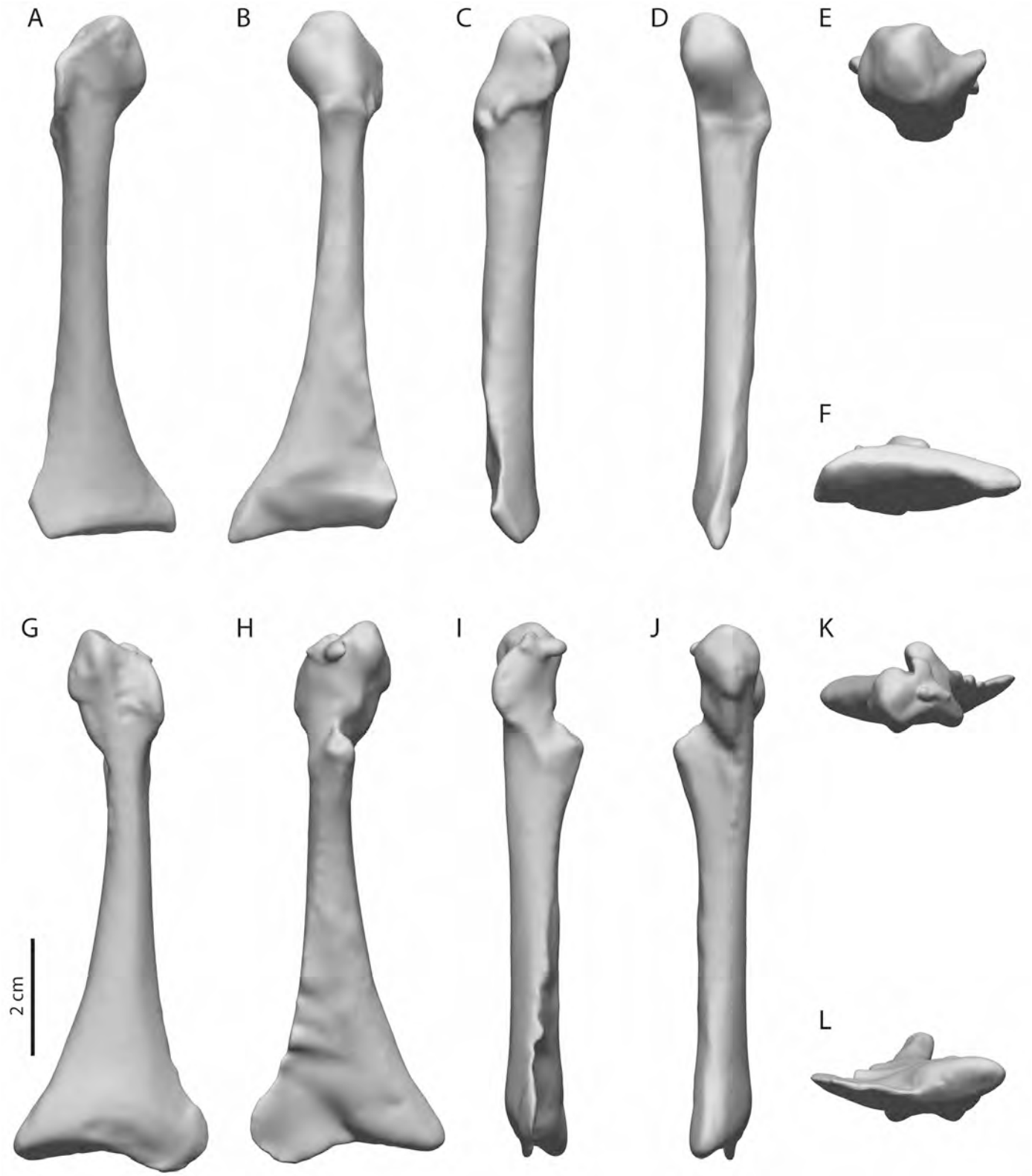

PLATE D28. 3-D scans of Durban right (**A**–**F**) and left (**G**–**L**) coracoids, in ventral (**A**, **G**), dorsal (**B**, **H**), medial (**C**, **I**), lateral (**D**, **J**), proximal (**E**, **K**), and distal (**F**, **L**) views. Obstructed portions of articular facets digitally reconstructed.

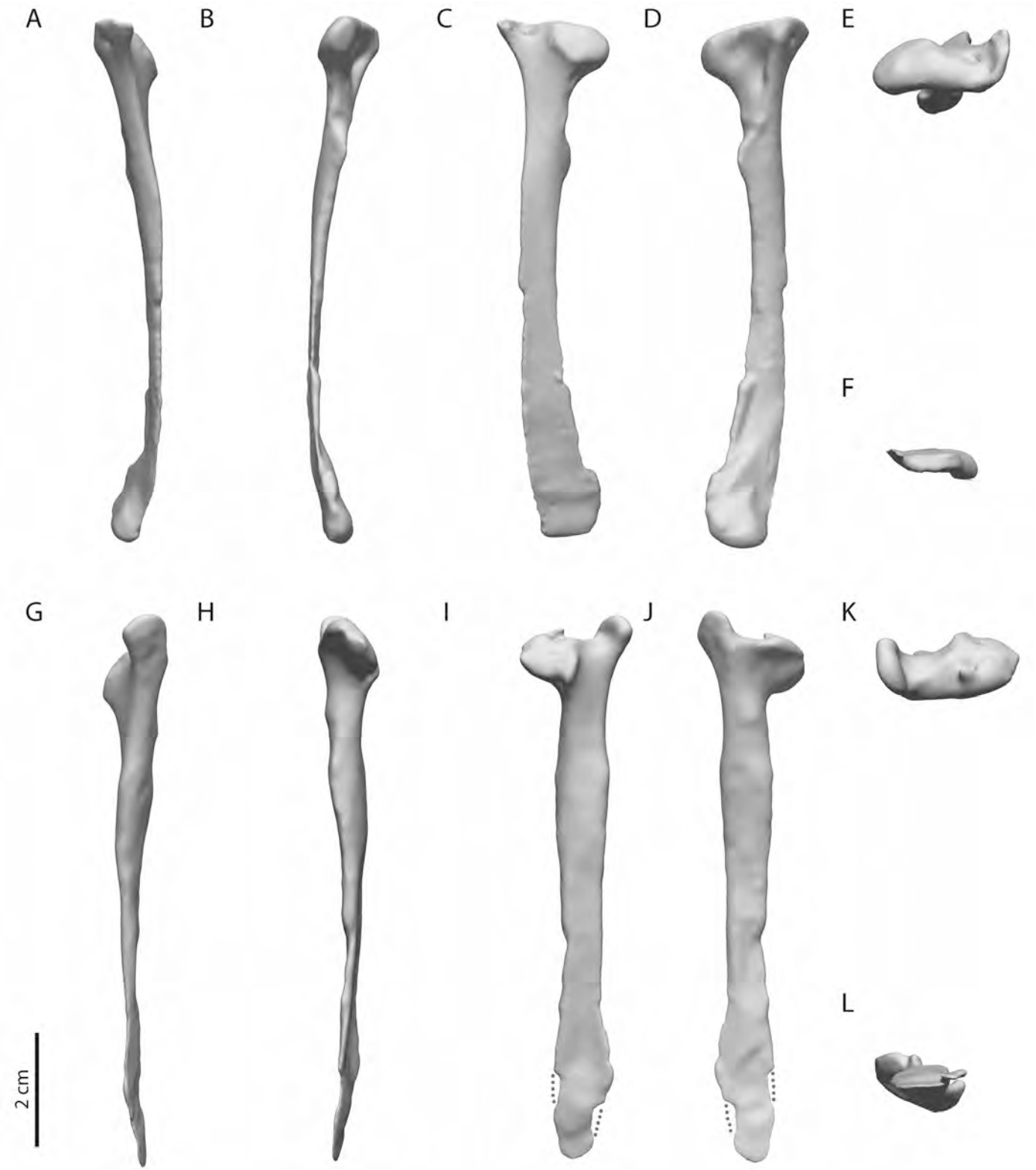

PLATE D29. 3-D scans of Durban right (**A**–**F**) and left (**G**–**L**) scapulae, in medial (**A**, **G**), lateral (**B**, **H**), dorsal (**C**, **I**), ventral surface (**D**, **J**), cranial (**E**, **K**), and caudal extremity (**F**, **L**) views. Obstructed portions of articular facets digitally reconstructed.

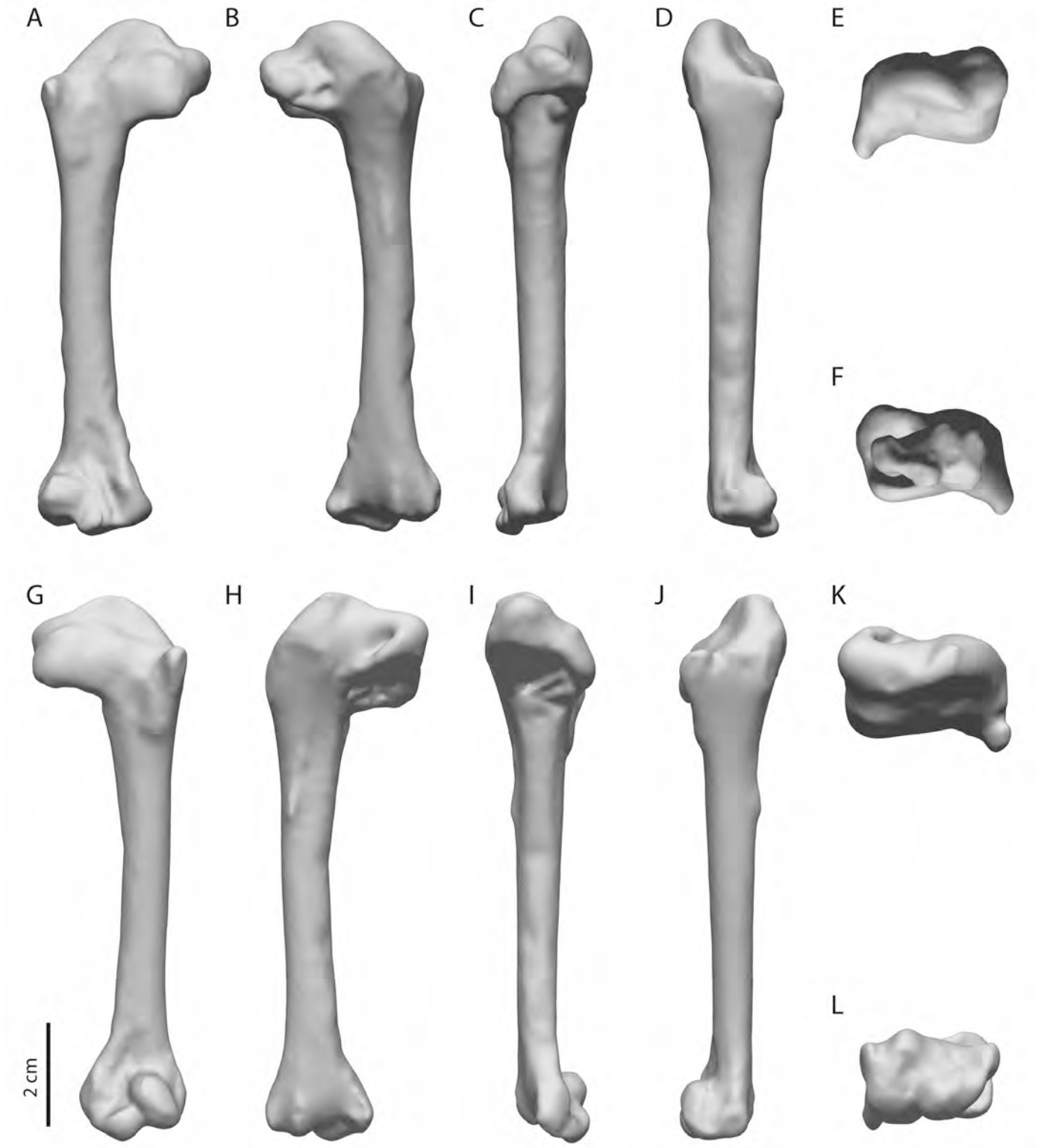

PLATE D30. 3-D scans of Durban right (**A**–**F**) and left (**G**–**L**) humeri, in cranial (**A**, **G**), caudal (**B**, **H**), dorsal (**C**, **I**), ventral (**D**, **J**), proximal (**E**, **K**), and distal (**F**, **L**) views. Obstructed portions of articular facets digitally reconstructed.

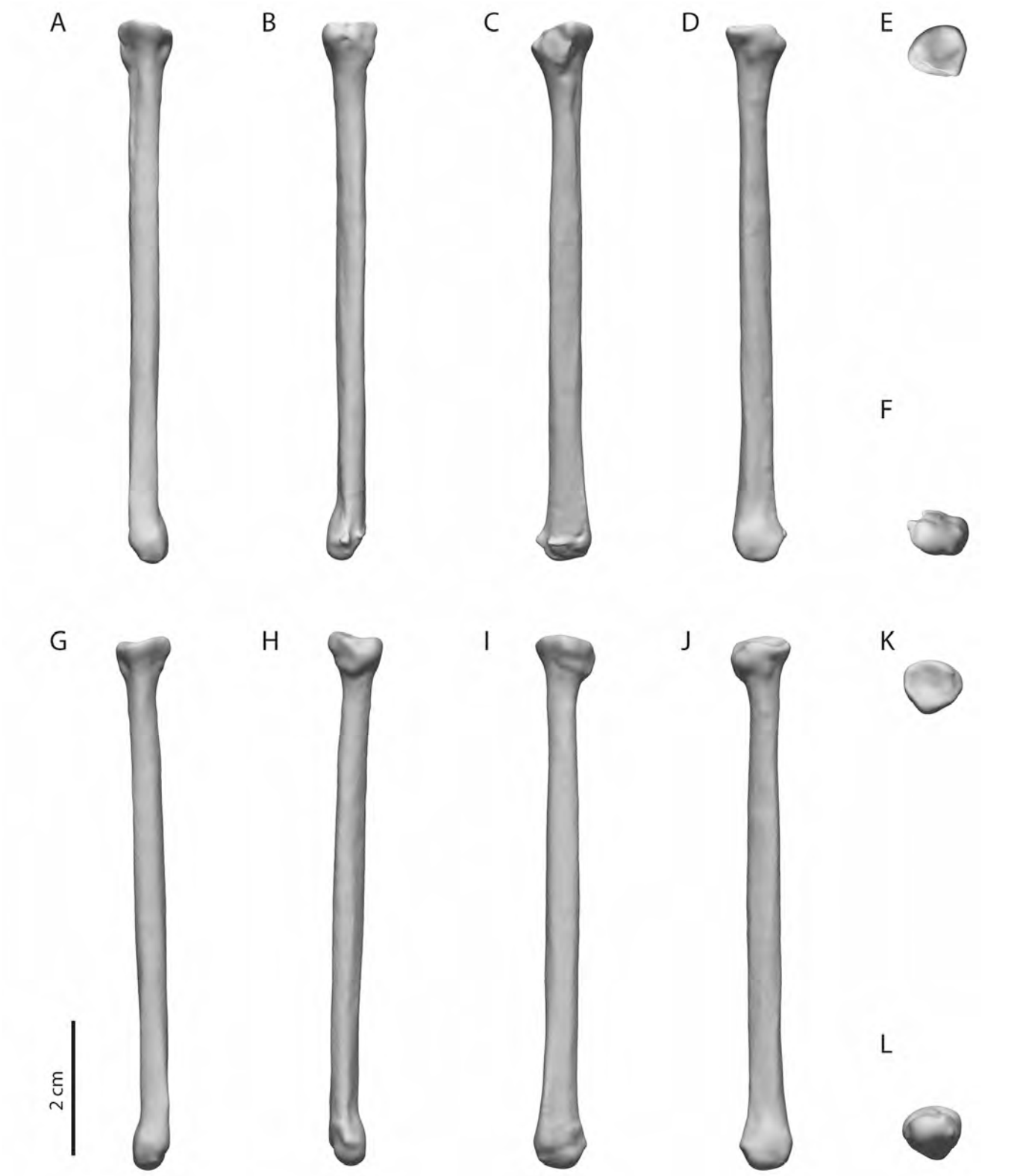

PLATE D31. 3-D scans of Durban right (**A**–**F**) and left (**G**–**L**) radii, in cranial (**A**, **G**), caudal (**B**, **H**), dorsal (**C**, **I**), ventral (**D**, **J**), proximal (**E**, **K**), and distal (**F**, **L**) views. Obstructed portions of articular facets digitally reconstructed.

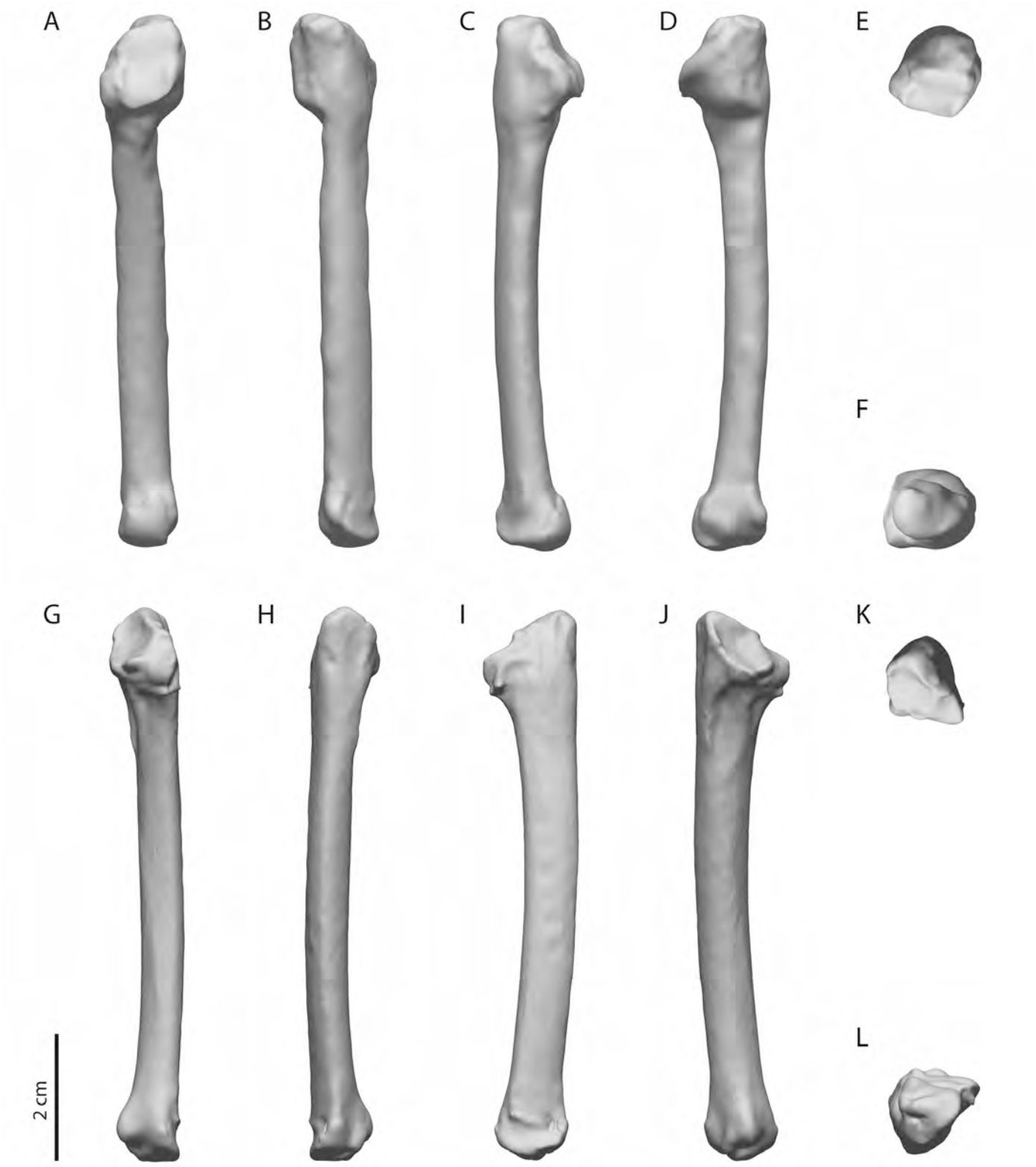

PLATE D32. 3-D scans of Durban right (**A**–**F**) and left (**G**–**L**) ulnae, in cranial (**A**, **G**), caudal (**B**, **H**), dorsal (**C**, **I**), ventral (**D**, **J**), proximal (**E**, **K**), and distal (**F**, **L**) views. Obstructed portions of articular facets digitally reconstructed.

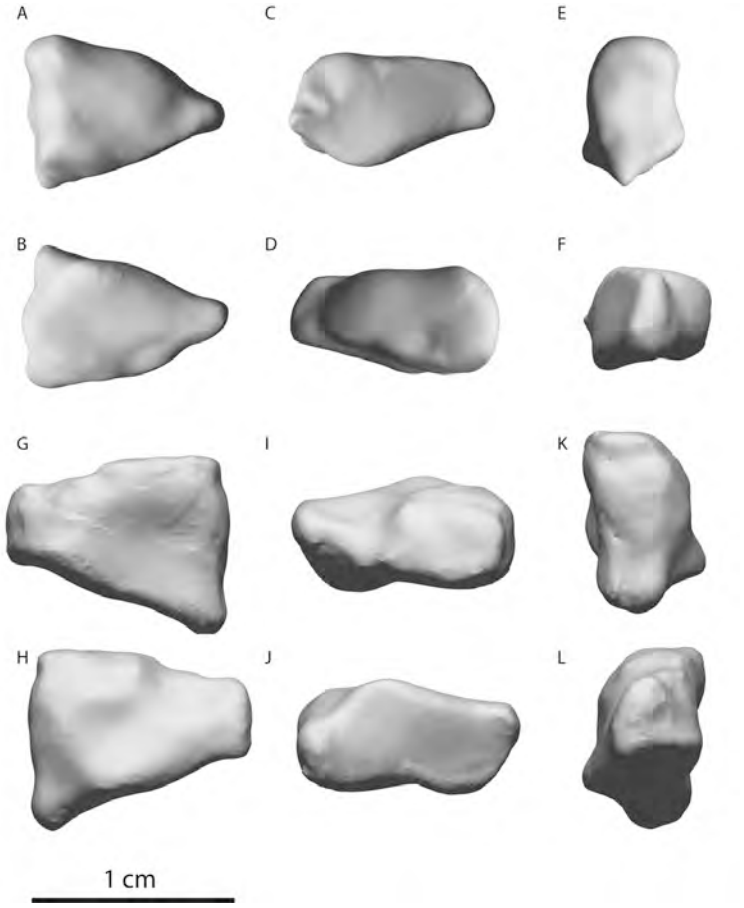

PLATE D33. 3-D scans of Durban right (**A**–**F**) and left (**G**–**L**) radiali, in dorsal (**A**, **G**), ventral (**B**, **H**), proximal (**C**, **I**), distal (**D**, **J**), cranial (**E**, **K**), and caudal (**F**, **L**) views. Proximal articular facet digitally reconstructed.

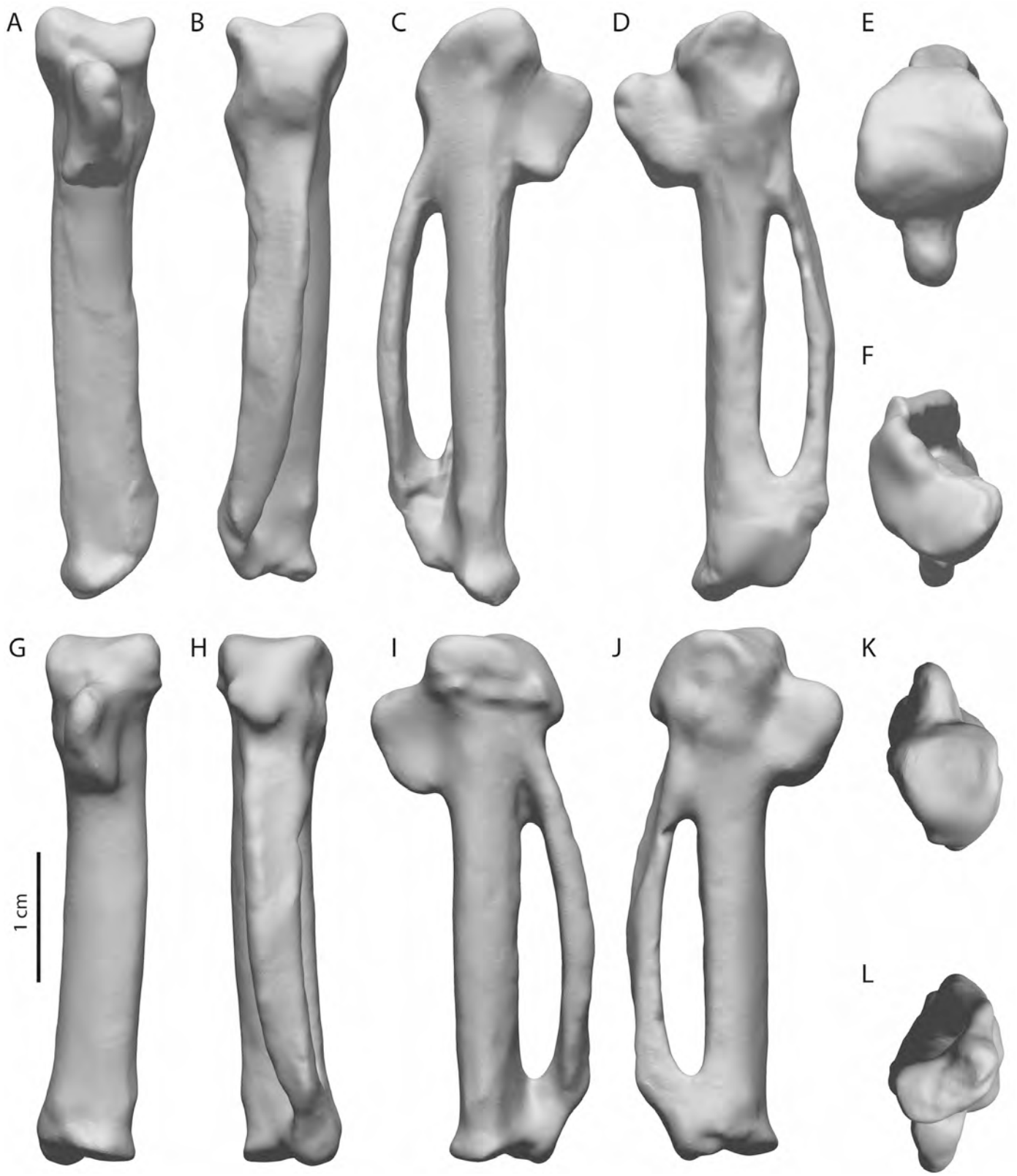

PLATE D34. 3-D scans of Durban right (**A**–**F**) and left (**G**–**L**) carpometacarpi, in cranial (**A**, **G**), caudal (**B**, **H**), dorsal (**C**, **I**), ventral (**D**, **J**), proximal (**E**, **K**), and distal (**F**, **L**) views. Obstructed portions of articular facets digitally reconstructed.

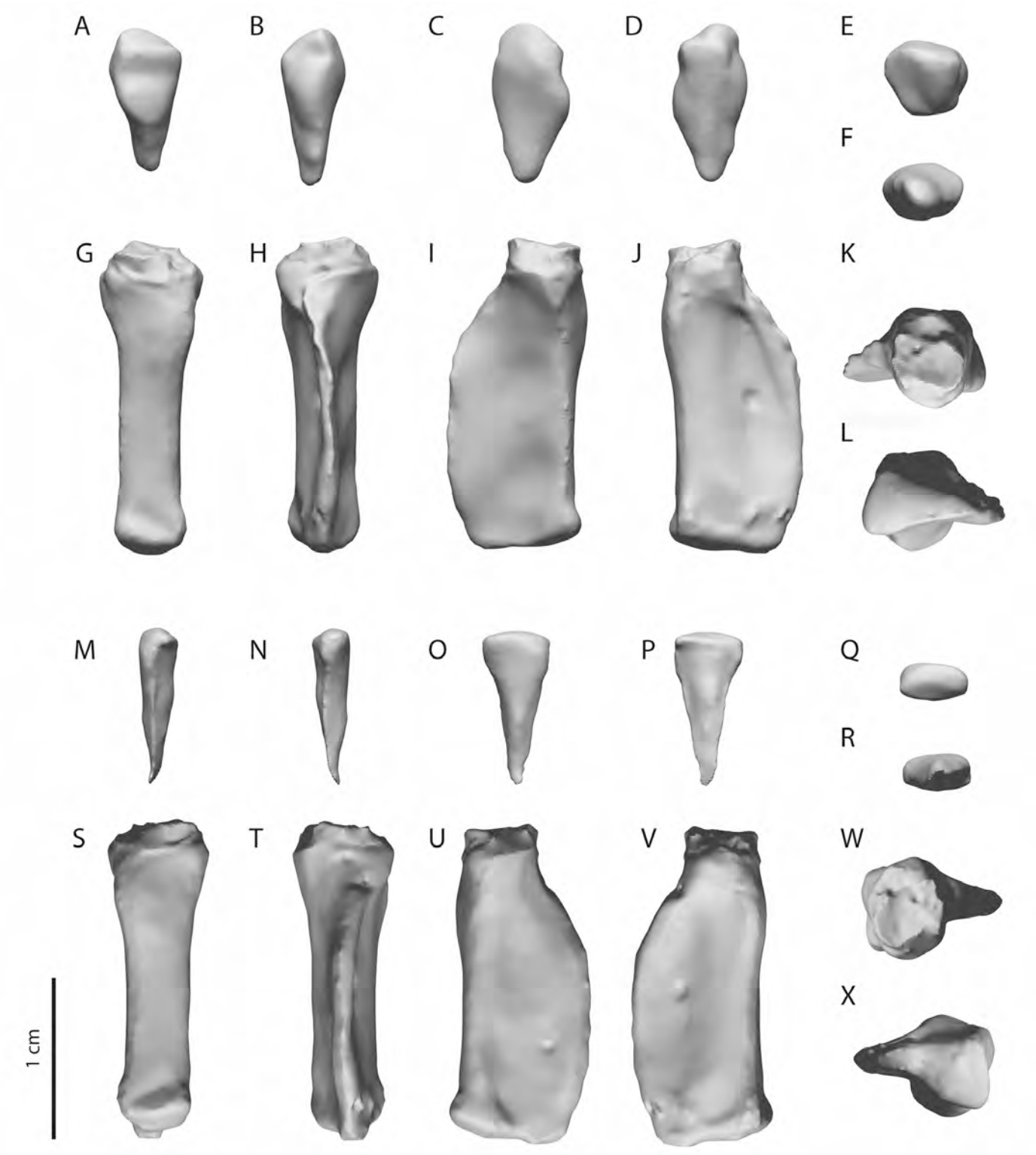

PLATE D35. 3-D scans of Durban right phalanx digiti minoris (**A**–**F**), left phalanx proximalis digiti majoris (**G**–**L**), right phalanx distalis digiti majoris (**M**–**R**), and left phalanx proximalis digiti majoris (**S**–**X**), in cranial (**A**, **G**, **M**, **S**), caudal (**B**, **H**, **N**, **T**), dorsal (**C**, **I**, **O**, **U**), ventral (**D**, **J**, **P**, **V**), proximal (**E**, **K**, **Q**, **W**), and distal (**F**, **L**, **R**, **X**) views. Articular facets digitally reconstructed on (**A**–**R**).

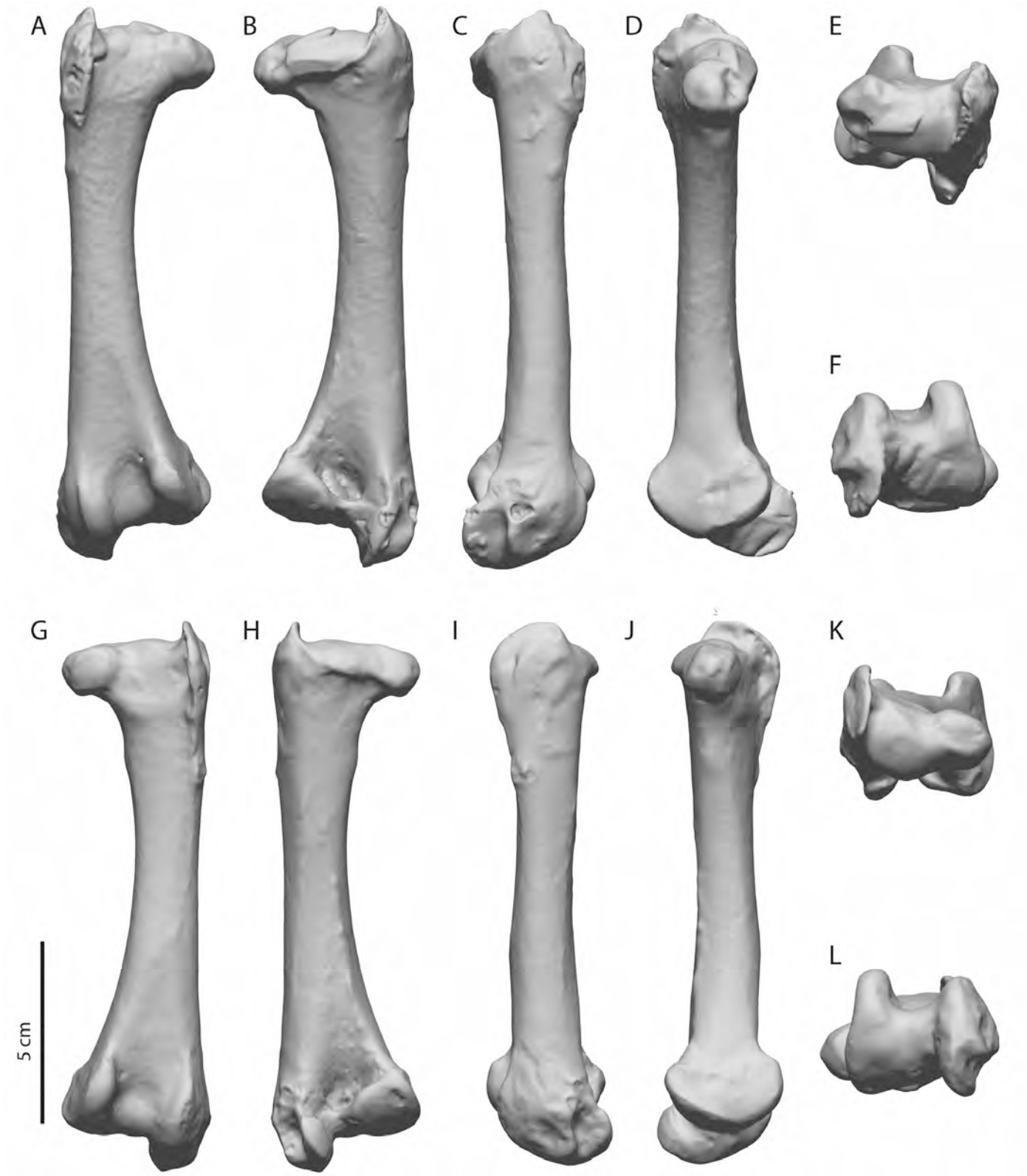

PLATE D36. 3-D scans of Durban left (**A**–**F**) and right (**G**–**L**) femora, in cranial (**A**, **G**), caudal (**B**, **H**), lateral (**C**, **I**), medial (**D**, **J**), proximal (**E**, **K**), and distal (**F**, **L**) views.

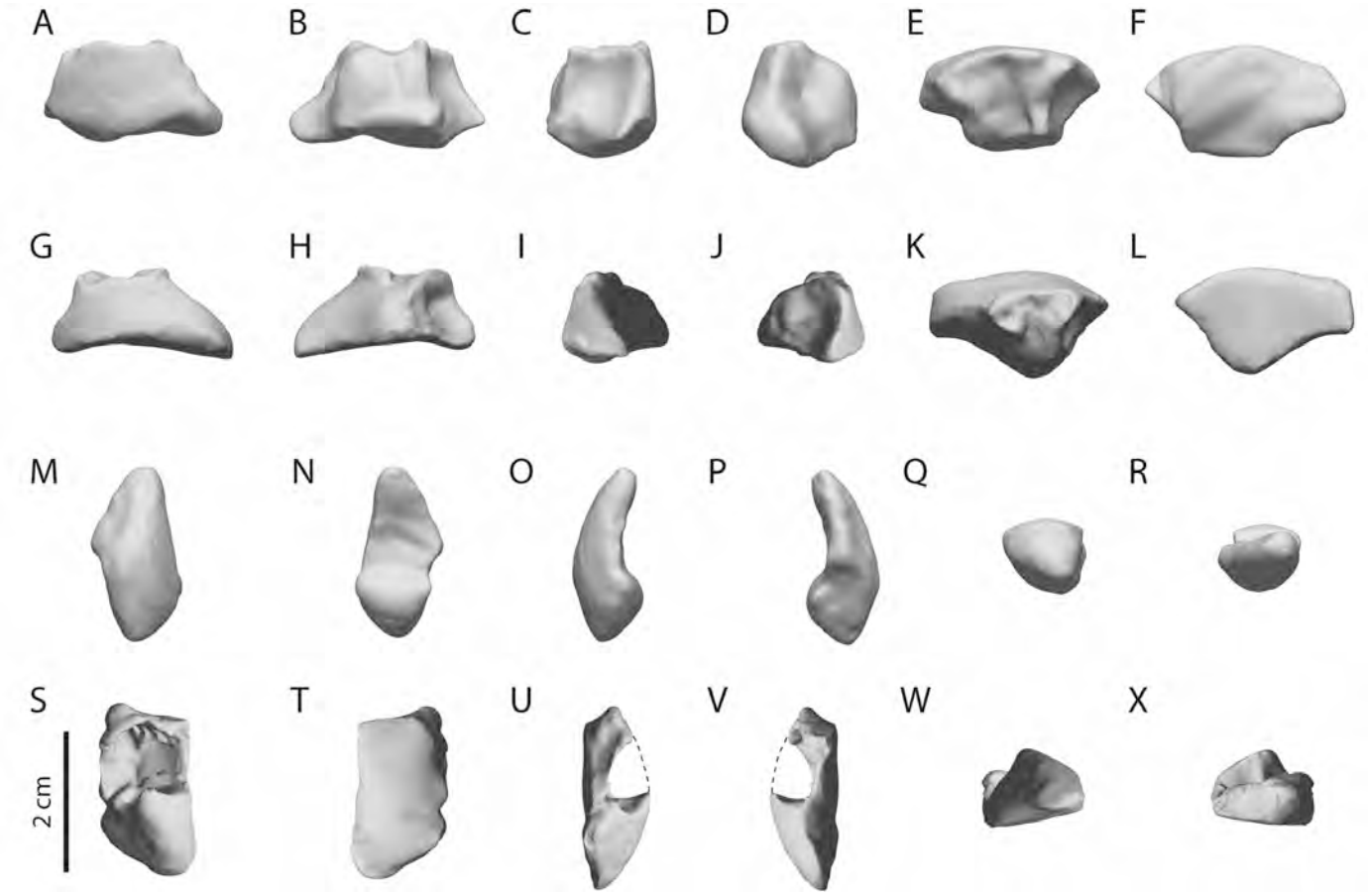

PLATE D37. 3-D scans of Durban right (**A**–**F**) and left (**G**–**L**) patellae, and right (**M**–**R**), and left (**S**–**X**) intertarsal sesamoids, in cranial (**A**, **G**, **M**, **S**), caudal (**B**, **H**, **N**, **T**), lateral (**C**, **I**, **O**, **U**), medial (**D**, **J**, **P**, **V**), dorsal (**E**, **K**, **Q**, **W**), and ventral (**F**, **L**, **R**, **X**) views. Obstructed portions of articular facets digitally reconstructed.

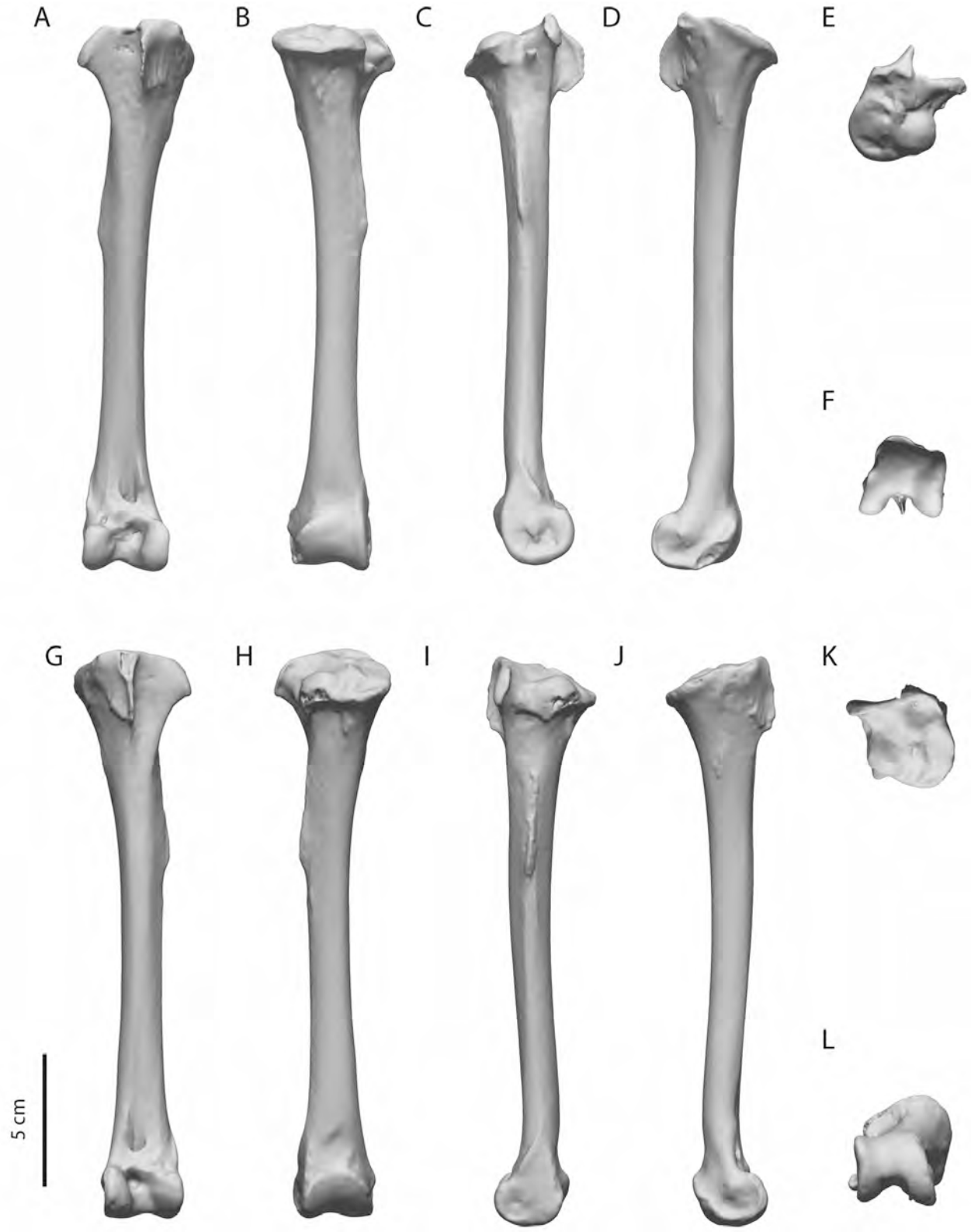

PLATE D38. 3-D scans of Durban right (**A**–**F**) and left (**G**–**L**) tibiotarsi, in cranial (**A**, **G**), caudal (**B**, **H**), lateral (**C**, **I**), medial (**D**, **J**), proximal (**E**, **K**), and distal (**F**, **L**) views. Obstructed portion of proximal articular facet digitally reconstructed.

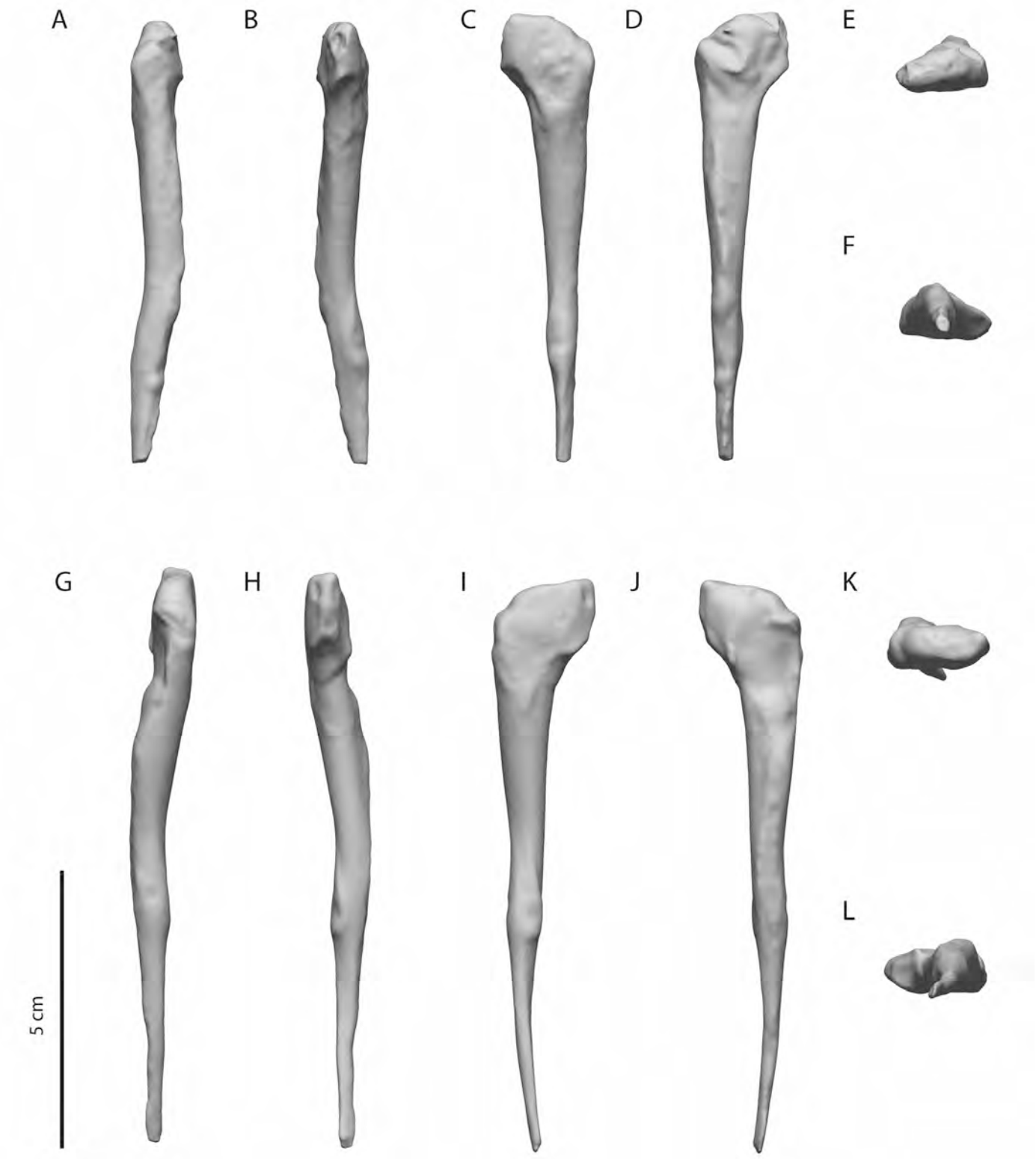

PLATE D39. 3-D scans of Durban right (**A**–**F**) and left (**G**–**L**) fibulae, in cranial (**A**, **G**), caudal (**B**, **H**), lateral (**C**, **I**), medial (**D**, **J**), proximal (**E**, **K**), and distal (**F**, **L**) views. Both fibulae are broken and incomplete distally. Proximal medial articular surface with tibiotarsus digitally reconstructed.

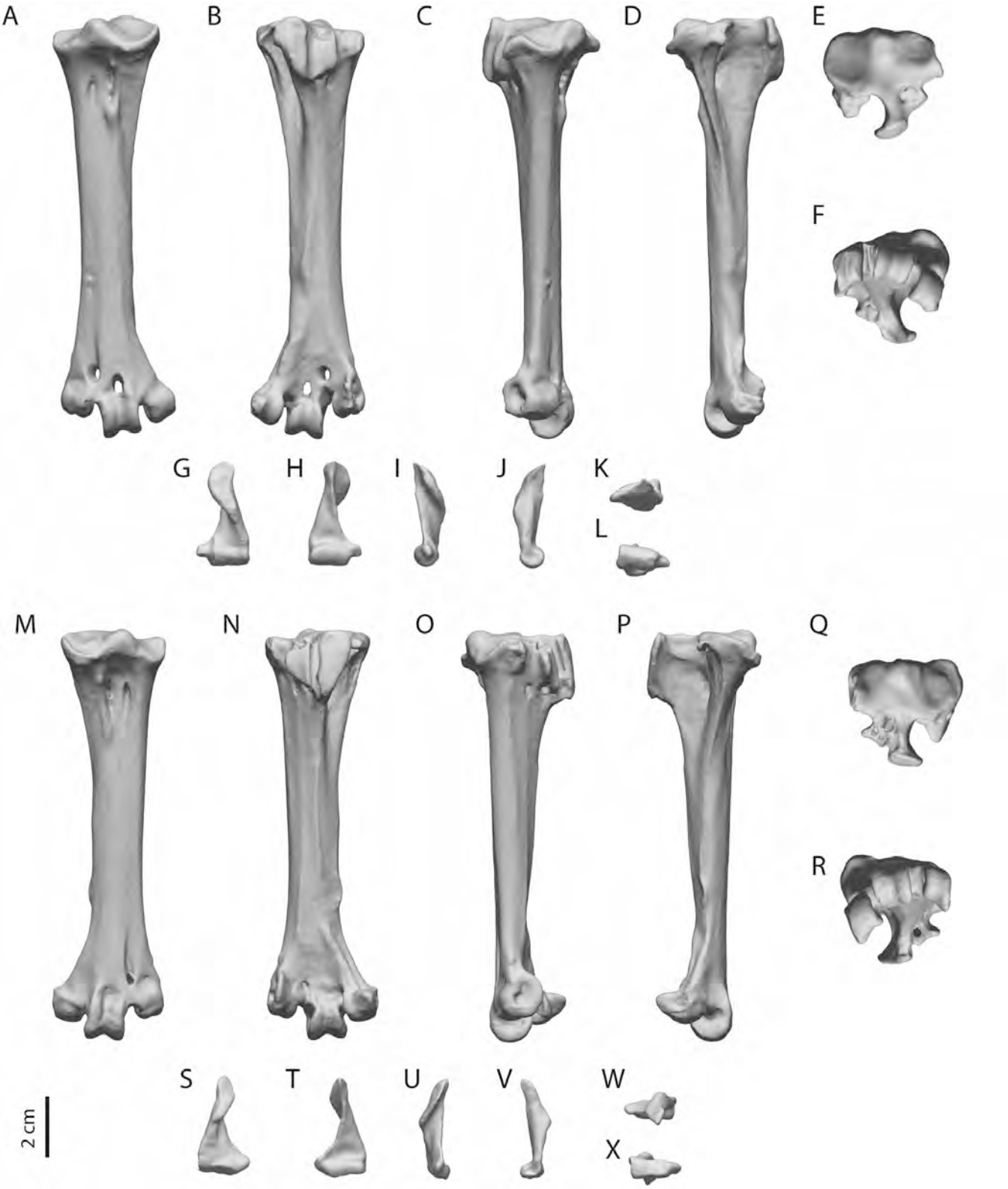

PLATE D40. 3-D scans of Durban right (**A**–**F**) and left (**M**–**R**) tarsometatarsi, and right (**G**–**L**) and left (**S**–**X**) metatarsus Is, in cranial (**A**, **G**, **M**, **S**), caudal (**B**, **H**, **N**, **T**), lateral (**C**, **I**, **O**, **U**), medial (**D**, **J**, **P**, **V**), proximal (**E**, **K**, **Q**, **W**), and distal (**F**, **L**, **R**, **X**) views. Articular facet between tarsometatarsus and metatarsus I digitally reconstructed.

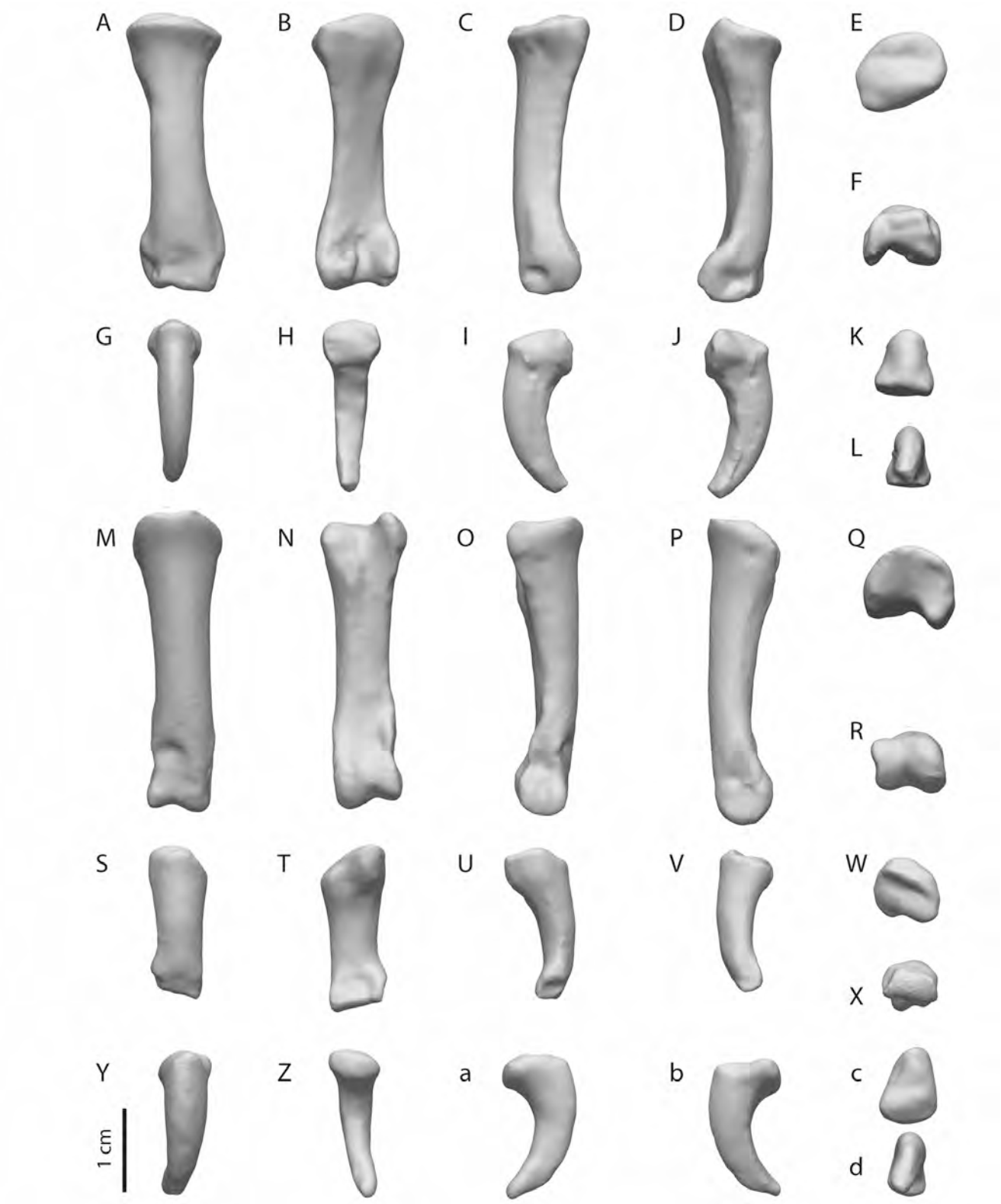

PLATE D41. 3-D scans of phalanges and unguals of digits I and II of the right foot, Durban specimen. Pedal phalanx I-1 (**A**–**F**), phalanx (ungual) I-2 (**G**–**L**), phalanx II-1 (**M**–**R**), phalanx II-2 (**S**–**X**), and phalanx (ungual) II-3 (**Y**–**d**), in dorsal (**A**, **G**, **M**, **S**, **Y**), plantar (**B**, **H**, **N**, **T**, **Z**), lateral (**C**, **I**, **O**, **U**, **a**), medial (**D**, **J**, **P**, **V**, **b**), proximal (**E**, **K**, **Q**, **W**, **c**), and distal (**F**, **L**, **R**, **X**, **d**) views. Obstructed portions of articular facets and plantar surface digitally reconstructed.

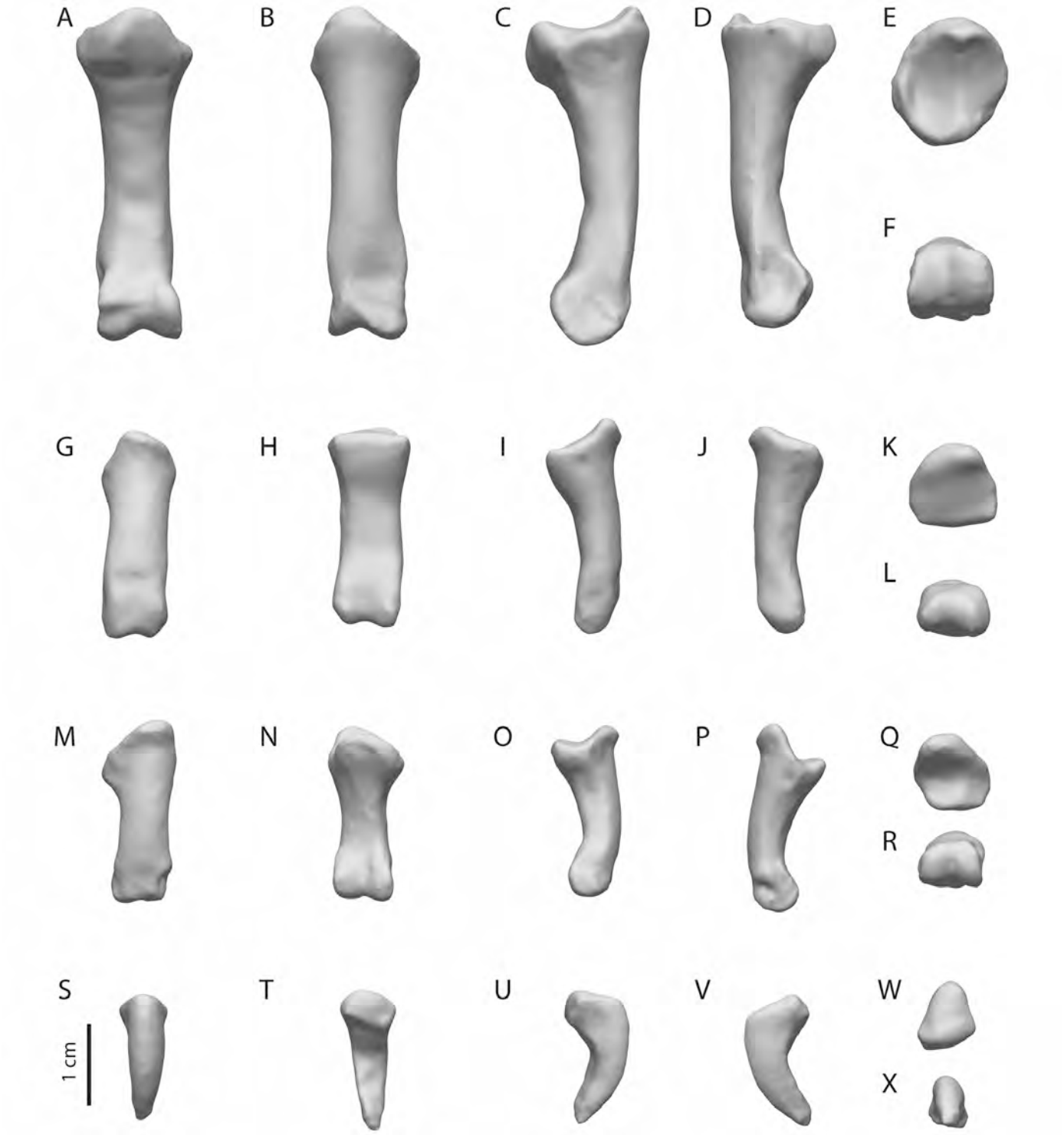

PLATE D42. 3-D scans of phalanges and unguals of digit III of the right foot, Durban specimen. Pedal phalanx III-1 (**A**–**F**), phalanx III-2 (**G**–**L**), phalanx III-3 (**M**–**R**), and phalanx (ungual) III-4 (**S**–**X**), in dorsal (**A**, **G**, **M**, **S**), plantar (**B**, **H**, **N**, **T**), lateral (**C**, **I**, **O**, **U**), medial (**D**, **J**, **P**, **V**), proximal (**E**, **K**, **Q**, **W**), and distal (**F**, **L**, **R**, **X**) views. Obstructed portions of articular facets and plantar surface digitally reconstructed.

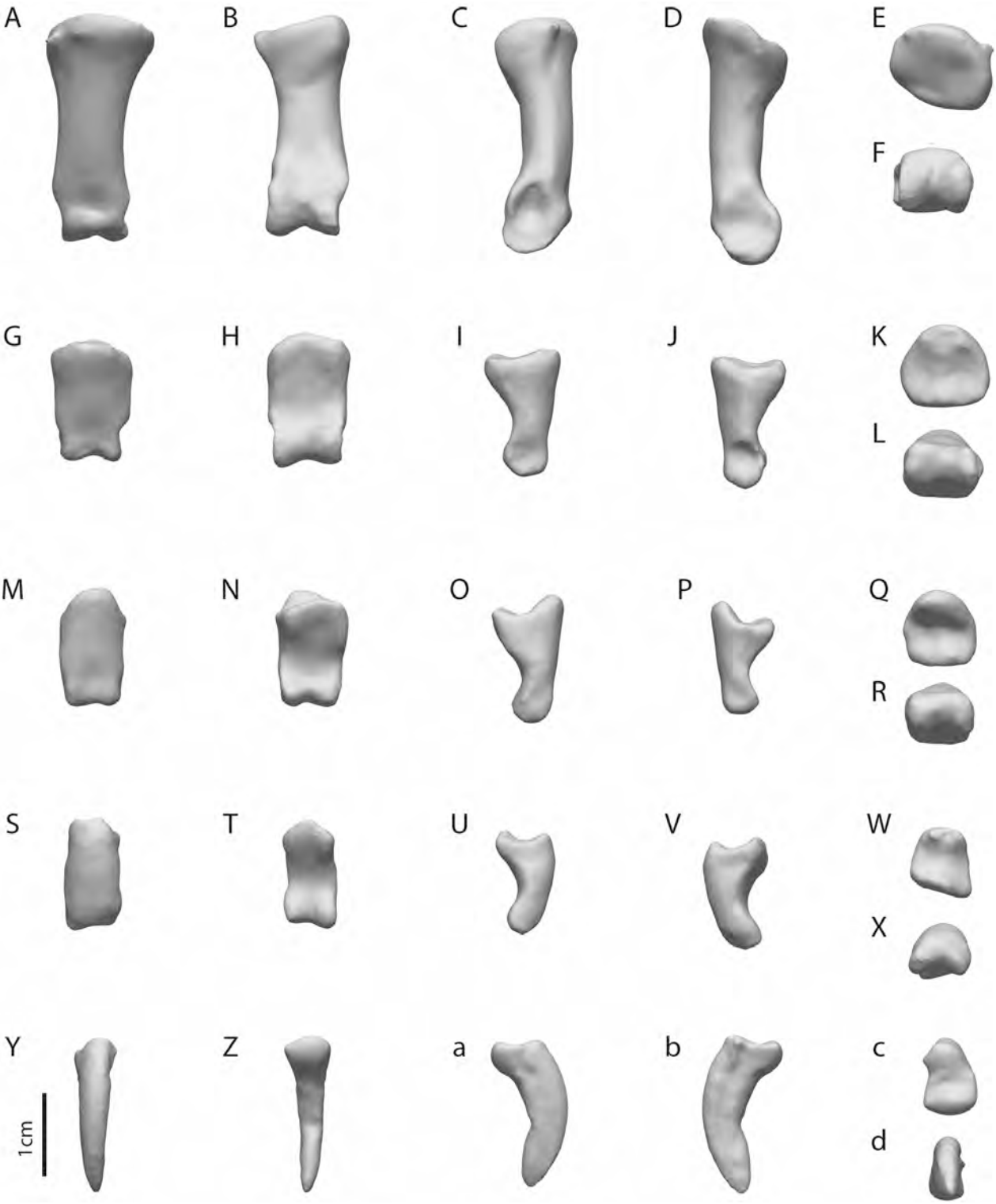

PLATE D43. 3-D scans of phalanges and unguals of digit IV of the right foot, Durban specimen. Pedal phalanx IV-1 (**A**–**F**), phalanx IV-2 (**G**–**L**), phalanx IV-3 (**M**–**R**), phalanx IV-4 (**S**–**X**), and phalanx (ungual) IV-5 (**Y**–**d**), in dorsal (**A**, **G**, **M**, **S**, **Y**), plantar (**B**, **H**, **N**, **T**, **Z**), lateral (**C**, **I**, **O**, **U**, **a**), medial (**D**, **J**, **P**, **V**, **b**), proximal (**E**, **K**, **Q**, **W**, **c**), and distal (**F**, **L**, **R**, **X**, **d**) views. Obstructed portions of articular facets and plantar surface digitally reconstructed.

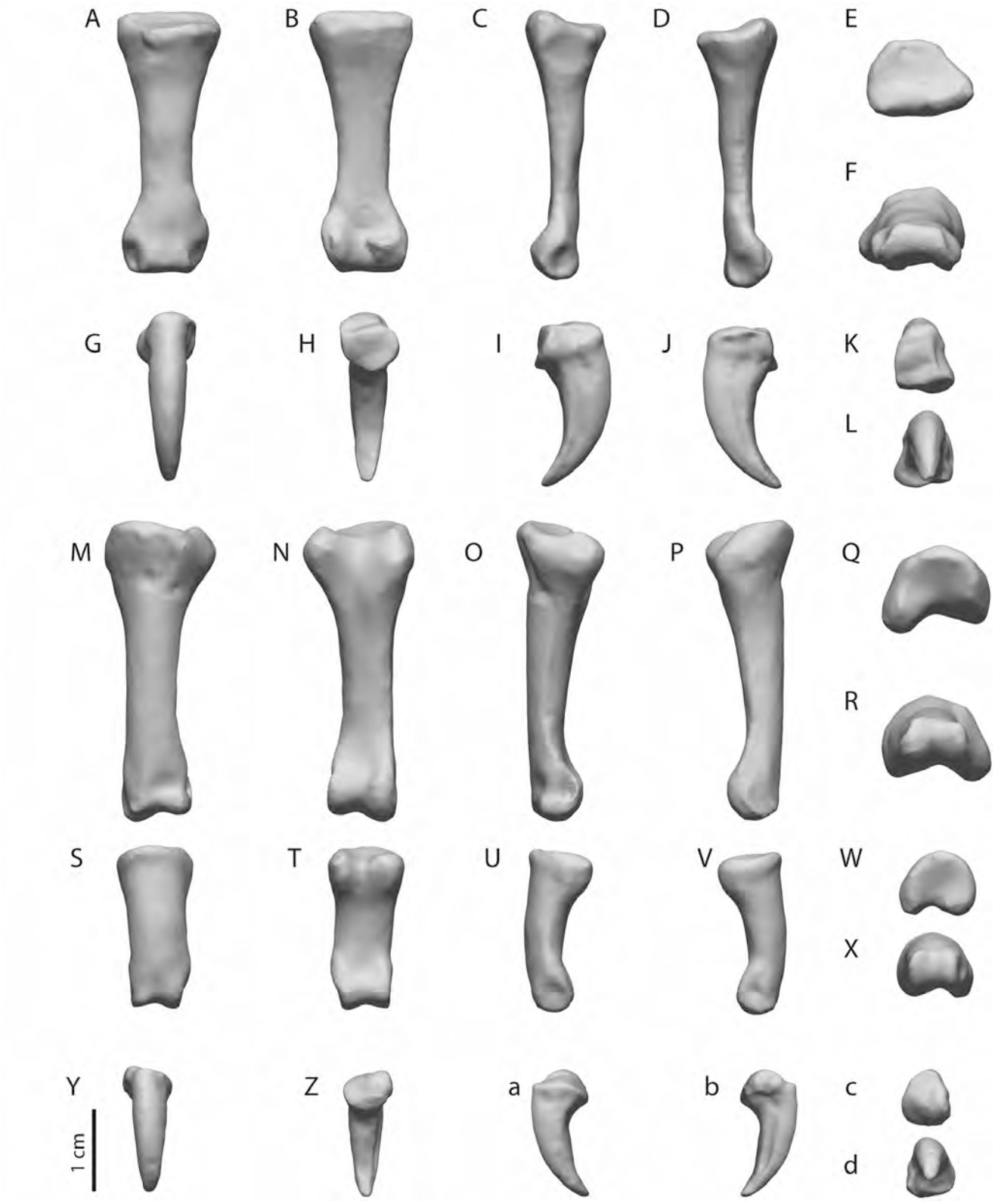

PLATE D44. 3-D scans of phalanges and unguals of digits I and II of the left foot, Durban specimen. Pedal phalanx I-1 (**A**–**F**), phalanx (ungual) I-2 (**G**–**L**), phalanx II-1 (**M**–**R**), phalanx II-2 (**S**–**X**), and phalanx (ungual) II-3 (**Y**–**d**), in dorsal (**A**, **G**, **M**, **S**, **Y**), plantar (**B**, **H**, **N**, **T**, **Z**), lateral (**C**, **I**, **O**, **U**, **a**), medial (**D**, **J**, **P**, **V**, **b**), proximal (**E**, **K**, **Q**, **W**, **c**), and distal (**F**, **L**, **R**, **X**, **d**) views. Obstructed portions of articular facets and plantar surface digitally reconstructed.

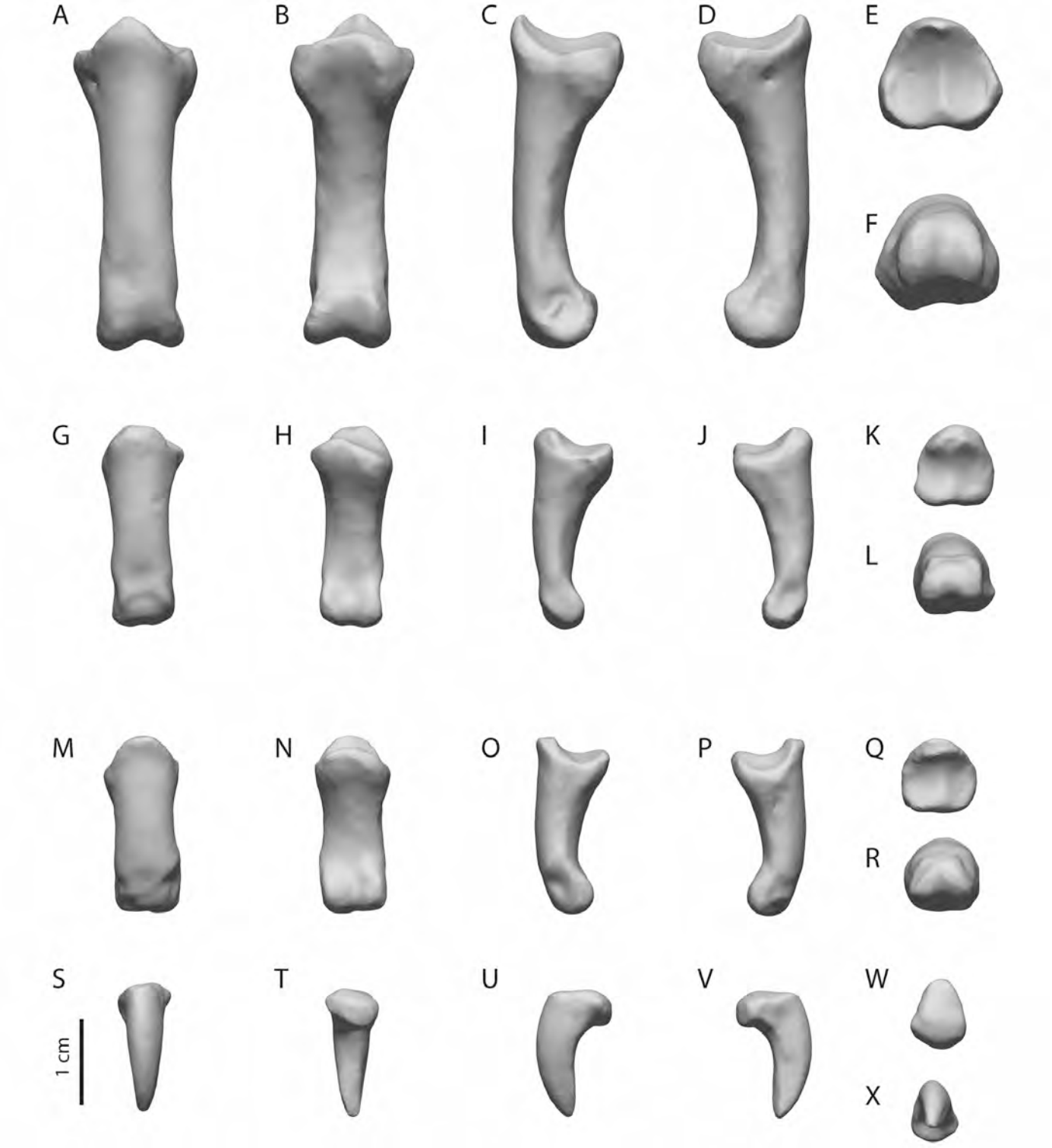

PLATE D45. 3-D scans of phalanges and unguals of digit III of the left foot, Durban specimen. Pedal phalanx III-1 (**A**–**F**), phalanx III-2 (**G**–**L**), phalanx III-3 (**M**–**R**), and phalanx (ungual) III-4 (**S**–**X**), in dorsal (**A**, **G**, **M**, **S**), plantar (**B**, **H**, **N**, **T**), lateral (**C**, **I**, **O**, **U**), medial (**D**, **J**, **P**, **V**), proximal (**E**, **K**, **Q**, **W**), and distal (**F**, **L**, **R**, **X**) views. Obstructed portions of articular facets and plantar surface digitally reconstructed.

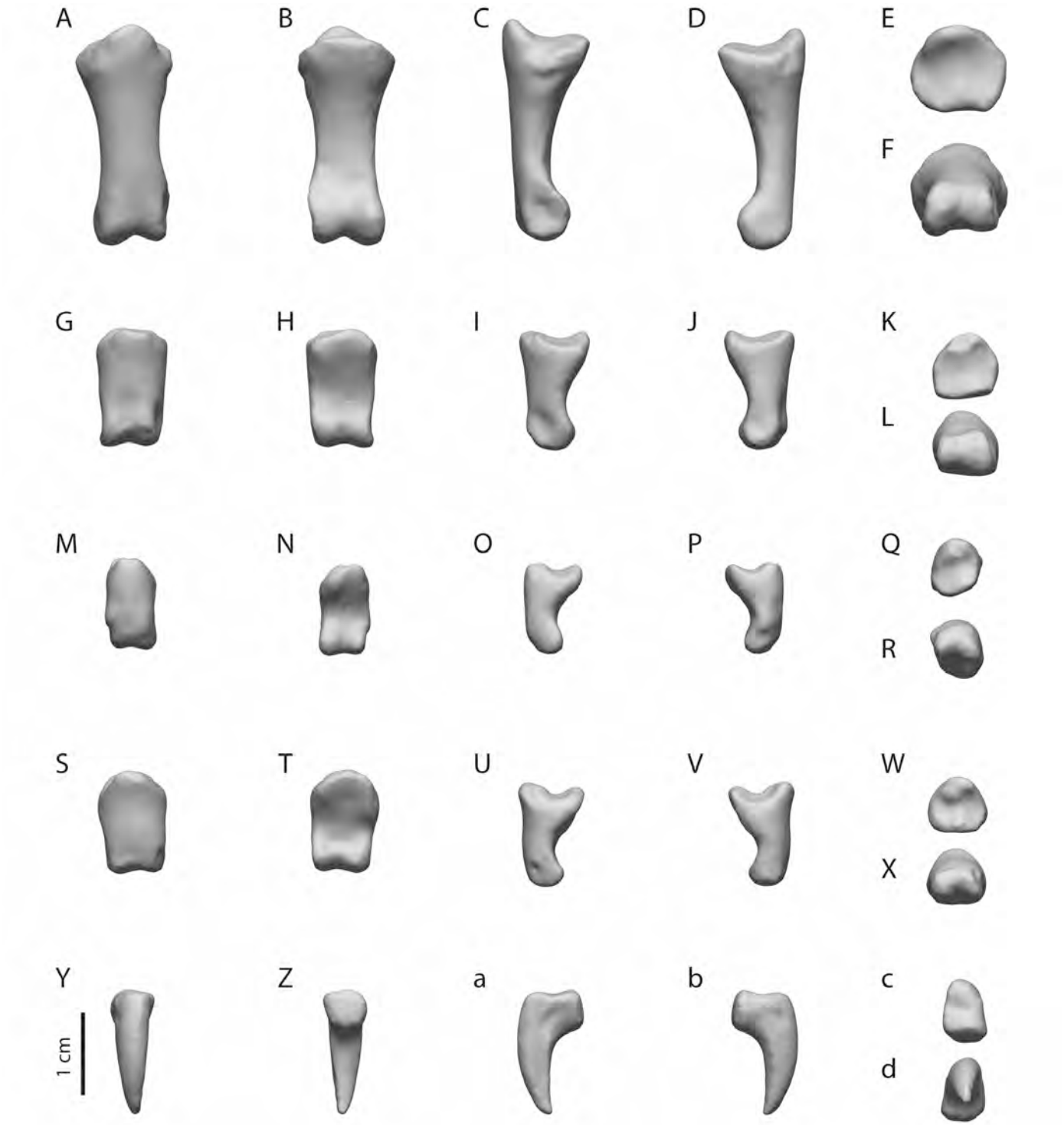

PLATE D46. 3-D scans of phalanges and unguals of digit IV of the left foot, Durban specimen. Pedal phalanx IV-1 (**A**–**F**), phalanx IV-2 (**G**–**L**), phalanx IV-3 (**M**–**R**), phalanx IV-4 (**S**–**X**), and phalanx (ungual) IV-5 (**Y**–**d**), in dorsal (**A**, **G**, **M**, **S**, **Y**), plantar (**B**, **H**, **N**, **T**, **Z**), lateral (**C**, **I**, **O**, **U**, **a**), medial (**D**, **J**, **P**, **V**, **b**), proximal (**E**, **K**, **Q**, **W**, **c**), and distal (**F**, **L**, **R**, **X**, **d**) views. Obstructed portions of articular facets and plantar surface digitally reconstructed.

APPENDIX 4. Comparative measurements of comparison taxa.

Cranial Measurements

TABLE A1. Cranial measurements of columbiform taxa in millimeters (mm).

Dimension	*Caloenas nicobarica* 10573	*Caloenas nicobarica* 7677	*Caloenas nicobarica* 8475	*Goura victoria* 6330	*Goura cristata* 1688	*Goura cristata* 1667	*Didunculus strigirostris* 6344
Skull							
Length of from tip of maxilla to parietal (note that in other Columbids, the prominentia cerebellaris forms the caudal part of the skull)	69*	70*	71.1*	91.4	88.9	102.4*	51
Length of rostrum (from tip to nasofrontal hinge, along central axis of the skull)	29.1*	32*	34*	43.8	44.6	51*	16.5
Length of rostrum diagonally	34.8*	37.5*	40.5*	49.2	50.8	59*	19.4
Length of cranium (from nasofrontal hinge to parietal, along central axis)	40.2	38	37	45.4	42.8	52.0	35.6
Length of maxillary rostrum	5.1	13*	7.4*	9	7.4	11.2*	10.8
Maximum height of maxilla	8	8.2	7.2	10.2	10.0		8.3
Maximum width of maxilla	11.4	11.9	11.6	13.6	13.1	15.0	6.7
Length of nasal opening (diagonally)	27.5	26.6	28.2	40.3	40.7	47.7	7.2
Width across nasofrontal hinge	12.6	13.2	14	22.3	17.7	19.1	14.8
Maximum width of cranium	22.8	22.3	22.7	32.9	30.6	33.9	21.4
Width between temporal fossae	20.9	21.1	21.4	28.4	28.1	30.0	20.5
Length of jugal	25	25.1	24.6	30.1	29.0	33.8	22.6
Width across paroccipital processes	19.3	19.2	19.3	24.1	23.8	28.0	17.6
Length of occipital condyle to rostral tip of basitemporal plate	11.7	12	11.9	14.2	11.1	15.4	9.4
Minimum width of rostrum parasphenoidale		3.4	3.7			5.6	
Length of sphenoid (tip of basitemporal plate to anterior end of sphenoid)		10.1	11		14.0	12.6	
Width of ethmoid		16	18.6		17.7	19.2	
Length of pterygoids	7.4	7.4	7.6	9	9.3	9.2	
Length of palatines		19.9	20.8		21.9	26.1	
Mandible							
Length of ramus from tip of mandible to caudal fossa	51.6*	54.9*	54.9*	72.1	70.4*	80.4*	43.1
Maximum height of ramus (at angulus mandibulae)	5.8	6.1	6	9.1	7.5	8.3	6.2
Length of rostral symphysis along ventral side	7*	7.4	7.4	6.7	9.6*	9.5*	7.8
Width of mandible across posterior fossae	19.1	20.5	20.7	26.8	25.8	28.1	21.1
Depth of posterior fossa		4.5	4.4		6.1	6.4	
Width of posterior fossa		6.1	7.1		8.5	9.0	

*Value is underestimated due to damage and/or reconstructive work.

Postcranial Measurements

All measurements were made using dial calipers and rounded to the nearest 0.1 mm.

TL = total length; sternum, from anterior tip of spina externa to margo caudalis in a median plane; coracoid, measured on the medial side; humerus, measured in dorsal aspect; ulna, measured in dorsal aspect.
TLH = total length of hypotarsus; from crista medialis hypotarsi to distal tip of trochlea metatarsi III.
PD = proximal depth; taken in a dorsoventral plane.
GW = greatest width; sternum, taken between the posterior most processus costalis.
LW = least width, in lateromedial plane; sternum, taken between the anterior-most processus costalis.
PW = proximal width, in lateromedial plane; carpometacarpus, proximal end from processus extensorius to facies articularis ulnacarpalis; femur, from the acetabulum through mid-depth point of the neck to lateral side.
SW = shaft width, in lateromedial plane.
SD = shaft depth, in dorsoventral plane.
DW = distal width, in lateromedial plane; coracoid, taken from angulus medialis to processus lateralis; ulna, taken in dorsal aspect.
DWP = distal width of coracoid including processus lateralis.
DD = distal depth, in dorsoventral plane.
LC = greatest length of carina sterni; from apex carinae to margo caudalis of sternum.
DK = greatest depth of keel; taken from facies muscularis sterni to apex carinae.

Measurements of the male NHMUK A3505 and female NHMUK A3506 *Pezophaps solitaria* are taken from associated individuals.

TABLE A2. Measurements (mm) of columbiforms mentioned in the text: sternum.

Species	TL (n) range	TL (M) (SD)	GW (n) range	GW (M) (SD)	LC (n) range	LC (M) (SD)	DK (n) range	DK (M) (SD)
Columba livia	(12) 58.5–71.7	(65.8) (3.91)	(12) 22.4–30.4)	(26.6) (2.53)	(12) 58.5–76.1	(68.9) (4.93)	(12) 20.3–28.0)	(23.7) (1.91)
Caloenas nicobarica	(1) 71.5	(71.5)	(1) 27.8	(27.8)	(1) 77.1	(77.1)	(1) 31.2	(31.2)
Didunculus strigirostris								
Pezophaps solitaria (male)	(1) 170.0	(170.0)	(1) 101.4	(101.4)	(1) 130.4	(130.4)	(1) 29.8	(29.8)
Pezophaps solitaria (female)	(1) 141.2	(141.2)	(1) 84.0	(84.0)	(1) 111.9	(111.9)	(1) 24.3	(24.3)
Raphus cucullatus	(3) 167.0–172.5	(175.1) (9.77)	(3) 102.0–110.0	(105.9) (4.00)	(3) 130.0–142.0	(137.3) (6.42)	(4) 14.3–19.3	(16.1) (2.32)

TABLE A3. Measurements (mm) of columbiforms mentioned in the text: coracoid.

Species	TL (n) range	TL (M) (SD)	SW (n) range	SW (M) (SD)	SD (n) range	SD (M) (SD)	DW (n) range	DW (M) (SD)
Columba livia	(11) t31.7–37.7	(34.7) (1.96)	(11) 3.4–4.9	(4.1) (0.43)	(11) 2.7–3.4	(2.96) (0.91)	(10) 11.7–16.9	(14.7) (1.62)
Caloenas nicobarica	(1) 44.3	(44.3)	(1) 4.4	(4.4)	(1) 3.7	(3.7)	(1) 11.2	(11.2)
Didunculus strigirostris								
Pezophaps solitaria (male)	(1) 91.5	(91.5)	(1) 9.6	(9.6)	(1) 8.8	(8.8)	(1) 32.6	(32.6)
Pezophaps solitaria (female)	(1) 71.8	(71.8)	(1) 8.5	(8.5)	(1) 6.0	(6.0)	(1) 24.9	(24.9)
Raphus cucullatus	(14) 76.8–93.0	(85.1) (4.80)	(14) 6.9–9.5	(7.9) (0.75)	(14) 6.5–8.5	(7.4) (0.69)	(13) 22.9–32.1	(26.0) (2.72)

TABLE A4. Measurements (mm) of columbiforms mentioned in the text: humerus.

Species	TL (n) range	TL (M) (SD)	PW (n) range	PW (M) (SD)	PD (n) range	PD (M) (SD)	SW (n) range	SW (M) (SD)	SD (n) range	SD (M) (SD)	DW (n) range	DW (M) (SD)	DD (n) range	DD (M) (SD)
Columba livia	(11) 44.7–50.0	(47.0) (1.88)	(11) 13.1–14.7	(13.7) (0.60)	(11) 7.6–9.1	(8.4) (0.44)	(11) 4.8–5.7	(5.2) (0.31)	(11) 3.6–4.6	(4.1) (0.28)	(11) 10.2–12.1	(11.1) (0.54)	(11) 6.7–8.3)	(7.2) (0.57)
Caloenas nicobarica	(1) 60.0	(60.0)	(1) 17.0	(17.0)	(1) 8.3	(8.3)	(1) 6.6	(6.6)	(1) 5.3	(5.3)	(1) 3.5	(3.5)	(1) 9.0	(9.0)
Didunculus strigirostris														
Pezophaps solitaria (male)	(1) 123.8	(123.8)	(1) 33.6	(33.6)	(1) 20.4	(20.4)	(1) 12.3	(12.3)	(1) 11.1	(11.1)	(1) 23.4	(23.4)	(1) 17.0	(17.0)
Pezophaps solitaria (female)	(1) 95.8	(95.8)	(1) 27.2	(27.2)	(1) 14.2	(14.2)	(1) 9.8	(9.8)	(1) 9.5	(9.5)	(1) 18.7	(18.7)	(1) 14.8	(14.8)
Raphus cucullatus	(2) 91.1–107.2	(99.1) (11.38)	(2) 24.5–27.4	(25.9) (2.05)	(2) 15.7–19.5	(17.6) (2.68)	(3) 8.0–9.8	(8.9) (0.90)	(3) 7.1–9.2	(8.1) (1.05)	(3) 19.1–22.7	(20.3) (2.02)	(3) 13.3–15.3	(14.2) (1.00)

TABLE A5. Measurements (mm) of columbiforms mentioned in the text: radius.

Species	TL (n) range	TL (M) (SD)	PW (n) range	PW (M) (SD)	SW (n) range	SW (M) (SD)	SD (n) range	SD (M) (SD)	DW (n) range	DW (M) (SD)
Columba livia	(11) 44.8–53.6	(49.2) (2.81)	(11) 4.3–5.6	(4.9) (0.43)	(11) 1.9–2.4	(2.1) (0.18)	(11) 2.0–2.5	(2.3) (0.18)	(11) 3.3–4.4	(4.0) (0.34)
Caloenas nicobarica										
Didunculus strigirostris										
Pezophaps solitaria (male)	(1) 87.9	(87.9)	(1) 11.0	(11.0)	(1) 8.6	(8.6)	(1) 7.7	(7.7)	(1) 11.7	(11.7)
Pezophaps solitaria (female)	(1) 65.4	(65.4)	(1) 8.1	(8.1)	(1) 5.4	(5.4)	(1) 5.9	(5.9)	(1) 9.4	(9.4)
Raphus cucullatus	(1) 75.1	(75.1)	(1) 8.4	(8.4)	(1) 4.7	(4.7)	(1) 3.6	(3.6)	(1) 8.2	(8.2)

TABLE A6. Measurements (mm) of columbiforms mentioned in the text: ulna.

Species	TL (n) range	TL (M) (SD)	PW (n) range	PW (M) (SD)	SW (n) range	SW (M) (SD)	SD (n) range	SD (M) (SD)	DW (n) range	DW (M) (SD)
Columba livia	(10) 48.9–58.9	(54.7) (3.37)	(10) 6.8–8.8	(7.7) (0.72)	(10) 3.2–3.8	(3.5) (0.22)	(10) 3.9–4.9	(4.2) (0.33)	(10) 6.3–7.9	(7.1) (0.44)
Caloenas nicobarica	(1) 72.7	(72.7)	(1) 8.3	(8.3)	(1) 4.7	(4.7)	(1) 5.0	(5.0)	(1) 8.2	(8.2)
Didunculus strigirostris										
Pezophaps solitaria (male)	(1) 93.6	(93.6)	(1) 17.1	(17.1)	(1) 9.5	(9.5)	(1) 9.6	(9.6)	(1) 11.8	(11.8)
Pezophaps solitaria (female)	(1) 73.3	(73.3)	(1) 13.2	(1) 13.2	(1) 6.3	(6.3)	(1) 6.7	(1) 6.7	(1) 10.1	(1) 10.1
Raphus cucullatus	(2) 81.3–83.8	(82.5) (1.76)	(2) 12.5–13.2	(12.8) (0.49)	(2) 6.5–7.4	(6.9) (0.63)	(2) 6.1–7.0	(6.5) (0.63)	(2) 10.9–12.5	(11.7) (1.13)

TABLE A7. Measurements (mm) of columbiforms mentioned in the text: carpometacarpus.

Species	TL (n) range	TL (M) (SD)	PW (n) range	PW (M) (SD)	PD (n) range	PD (M) (SD)	SW (n) range	SW (M) (SD)	SD (n) range	SD (M) (SD)	DW (n) range	DW (M) (SD)	DD (n) range	DD (M) (SD)
Columba livia														
Caloenas nicobarica														
Didunculus strigirostris														
Pezophaps solitaria (Male)	(13) 41.0–49.9	(45.3) 3.27	(11) 13.5–18.3	(15.3) 1.72	(13) 7.5–15	(10.7) 2.26	(13) 4.4–9.3	(6.52) 1.62	(13) 5.5–10.1	(7.7) 1.39	(13) 7.7–14.9	(10.2) 2.02	(13) 5.1–10.2	(7.3) 1.76
Pezophaps solitaria (Female)	(11) 37.0–40.5	(38.6) 1.07	(11) 12.8–15.7	(14.0) 1.03	(11) 8.1–11.8	(9.23) 1.04	(11) 4.5–5.6	(4.86) 0.34	(11) 5.4–6.7	(6.1) 0.47	(11) 7.5–10.5	(8.6) 0.90	(11) 4.8–7.1	(5.83) 0.76
Raphus cucullatus	(3) 41.5–47.0	(43.5) 3.04	(3) 13.5–14.7	(13.9) 0.64	(3) 8.6–10.4	(9.3) 0.21	(4) 4.3–4.8	(4.5) 0.21	(4) 5.6–6.2	(5.9) 0.25	(4) 8.6–9.7	(9.0) 0.49	(4) 5.3–5.9	(5.5) 0.32

TABLE A8a. Measurements (mm) of columbiforms mentioned in the text: femur.

Species	TL (n) range	TL (M) (SD)	PW (n) range	PW (M) (SD)	PD (n) range	PD (M) (SD)	SW (n) range	SW (M) (SD)	SD (n) range	SD (M) (SD)	DW (n) range	DW (M) (SD)	DD (n) range	DD (M) (SD)
Columba livia	(11) 40.9–45.3	(42.6) (2.02)	(11) 8.5–9.8	(9.0) (0.46)	(11) 5.0–6.3	(5.4) (0.38)	(11) 3.1–3.9	(3.4) (0.26)	(11) 3.0–3.7	(3.3) (0.23)	(11) 7.2–8.7	(7.9) (0.39)	(11) 5.9–7.4	(6.5) (0.45)
Caloenas nicobarica	(1) 49.4	(49.4)	(1) 11.2	(11.2)	(1) 11.6	(11.6)	(1) 4.5	(4.5)	(1) 4.5	(4.5)	(1) 9.8	(9.8)	(1) 12.5	(12.5)
Didunculus strigirostris														
Pezophaps solitaria (male)	(1) 182.0	(182.0)	(1) 48.8	(48.8)	(1) 27.6	(27.6)	(1) 21.5	(21.5)	(1) 15.7	(15.7)	(1) 45.2	(45.2)	(1) 35.0	(35.0)
Pezophaps solitaria (female)	(1) 142.6	(142.6)	(1) 40.5	(40.5)	(1) 22.8	(22.8)	(1) 17.3	(17.3)	(1) 13.2	(13.2)	(1) 34.9	(34.9)	(1) 28.7	(28.7)
Raphus cucullatus	(2) 150.0–157.0	(153.5) (4.94)	(2) 43.5–44.3	(43.9) (0.56)	(2) 24.6–25.6	(25.1) (0.70)	(2) 17.8–18.5	(18.1) (0.49)	(2) 16.0–16.5	(16.2) (0.35)	(2) 41.5–44.0	(42.7) (1.76)	(2) 33.2–35.2	(34.2) (1.41)

TABLE A8b. Measurements (mm) of columbiforms mentioned in the text: patella.

Species	TL (n) range	TL (M) (SD)	GW (n) range	GW (M) (SD)	GD (n) range	GD (M) (SD)
Pezophaps solitaria (male)	(1) 13.3	(13.3)	(1) 25.2	(25.2)	(1) 17.3	(17.3)
Pezophaps solitaria (female)	(1) 10.2	(10.2)	(1) 18.3	(18.3)	(1) 11.7	(11.7)
Raphus cucullatus	(1) 14.9	(14.9)	(1) 27.1	(27.1)	(1) 12.0	(12.0)

TABLE A8c. Measurements (mm) of columbiforms mentioned in the text: intertarsal sesamoid.

Species	TL (n) range	TL (M) (SD)	GW (n) range	GW (M) (SD)	GD (n) range	GD (M) (SD)
Pezophaps solitaria (female)	(1) 16.8	(16.8)	(1) 7.6	(7.6)	(1) 6.7	(6.7)
Raphus cucullatus	(1) 26.9	(26.9)	(1) 12.0	(12.0)	(1) 8.2	(8.2)

TABLE A9. Measurements (mm) of columbiforms mentioned in the text: tibiotarsus

Species	TL (n) range	TL (M) (SD)	PW (n) range	PW (M) (SD)	PD (n) range	PD (M) (SD)	SW (n) range	SW (M) (SD)	SD (n) range	SD (M) (SD)	DW (n) range	DW (M) (SD)	DD (n) range	DD (M) (SD)
Columba livia	(10) 53.4–63.7	(58.5) (3.56)	(10) 5.6–8.3	(7.0) (0.86)	(10) 7.2–9.1	(8.4) (0.62)	(10) 2.9–3.6	(3.2) (0.26)	(10) 2.9–3.3	(2.9) (0.22)	(10) 5.9–7.5	(6.9) (0.45)	(10) 5.8–6.8	(6.4) (0.31)
Caloenas nicobarica	(1) 75.0	(75.0)	(1) 8.9	(8.9)	(1) 10.5	(10.5)	(1) 4.0	(4.0)	(1) 3.6	(3.6)	(1) 8.5	(8.5)	(1) 8.7	(8.7)
Didunculus strigirostris														
Pezophaps solitaria (male)	(1) 265.0	(265.0)	(1) 39.5	(39.5)	(1) 54.7	(54.7)	(1) 17.2	(17.2)	(1) 14.2	(14.2)	(1) 32.3	(32.3)	(1) 31.4	(31.4)
Pezophaps solitaria (female)	(1) 213.0	(213.0)	(1) 28.2	(28.2)	(1) 42.8	(42.8)	(1) 13.9	(13.9)	(1) 11.8	(11.8)	(1) 26.1	(26.1)	(1) 25.6	(25.6)
Raphus cucullatus	(2) 230.0–232.0	(231.0) (1.41)	(2) 36.2–37.2	(36.7) (0.70)	(2) 46.6–47.0	(46.8) (0.28)	(2) 15.8–16.6	(16.2) (0.56)	(2) 14.6–15.3	(14.9) (0.49)	(2) 33.0–34.2	(33.6) (0.84)	(2) 32.3–32.6	(32.4) (0.21)

TABLE A10. Measurements (mm) of columbiforms mentioned in the text: tarsometatarsus.

Species	TL (n) range	TL (M) (SD)	PW (n) range	PW (M) (SD)	PD (n) range	PD (M) (SD)	SW (n) range	SW (M) (SD)	SD (n) range	SD (M) (SD)	DW (n) range	DW (M) (SD)	DD (n) range	DD (M) (SD)
Columba livia	(11) 29.1–34.3	(31.7) (1.62)	(11) 7.0–8.3	(7.6) (0.40)	(11) 6.1–7.5	(6.9) (0.38)	(11) 2.7–3.6	(3.1) (0.31)	(11) 2.1–3.0	(2.5) (0.34)	(11) 7.2–8.5	(8.0) (0.38)	(11) 4.1–5.2	(4.6) (0.36)
Caloenas nicobarica	(1) 43.3	(43.3)	(1) 9.5	(9.5)	(1) 9.1	(9.1)	(1) 4.3	(4.3)	(1) 4.1	(4.1)	(1) 10.3	(10.3)	(1) 5.9	(5.9)
Didunculus strigirostris														
Pezophaps solitaria (male)	(1) 178.0	(178.0)	(1) 36.4	(36.4)	(1) 31.1	(31.1)	(1) 15.1	(15.1)	(1) 12.8	(12.8)	(1) 38.1	(38.1)	(1) 25.9	(25.9)
Pezophaps solitaria (female)	(1) 138.9	(138.9)	(1) 29.7	(29.7)	(1) 25.4	(25.4)	(1) 12.2	(12.2)	(1) 10.2	(10.2)	(1) 32.2	(32.2)	(1) 19.1	(19.1)
Raphus cucullatus	(2) 129.0–129.3	(129.1) (0.21)	(2) 33.9–38.0	(35.9) (2.89)	(2) 30.6–33.5	(32.0) (2.05)	(2) 15.2–15.3	(15.2) (0.07)	(2) 11.2–11.8	(11.5) (0.42)	(2) 36.0–36.6	(36.3) (0.42)	(2) 19.5–21.8	(20.6) (1.62)